# LA-UR-21-32376

**Approved for public release; distribution is unlimited.**

| | |
|---|---|
| **Title:** | 2021 Virtual Theoretical Division Lightning Talk Series |
| **Author(s):** | Ramsey, Marilyn Leann; Adams, Claire Leeanne; Archer, Emma Marie; Arzola Roig, Angelic Marie; Banerjee, Sneha; Bellante, Armando; Bhati, Manav; Cengil, Muhammet Fatih; Coker, Abigail Allison; Eidenbenz, Tayra J.; Hehl, Rebecca Lynn; Herndon, Liam Kai; Ikuyajolu, Olawale James; Kang, Shinwoo; Khan, Noor Md Shahriar; Kolade, Beauty Ayomide; Kulchenko, Maksim; Lalonde, Jessica Nicole; Larocca, Martin; Liu, Yanhua; Miller, Brendan J; et al. |
| **Intended for:** | Report |
| **Issued:** | 2021-12-20 |



2021 Virtual Theoretical Division Lightning Talk Series
Marilyn L. Ramsey

Adams, Claire
Archer, Emma
Arzola Roig, Angelic
Banerjee, Sneha
Bellante, Armando
Bhati, Manav
Cengil, Faith
Coker, Ablgail
Eidenbenz, Tayra
Hehl, Rebecca
Herndon, Liam
Ikuyajolu, Olawale
Kang, Shiwoo (Chris)
Khan, Shahriar
Kolade, Beauty
Kulchenko, Maksim
Lalonde, Jessica
Larocca, Martin
Liu, Yanhu
Miller, Brendan
Montez, Christopher
Mora Perez, Carlos
Park, Ryan
Parker, Quinn
Pereiro, Felipe
Perez, Kyle
Petersen, Lillian
Phillip, Aaron
Roat, Gabriela (Abby)
Romero, Elena
Sachdeva, Geeta
Spurlock, Jacob
Touil, Arkam
Weight, Braden

# 2021 Virtual Theoretical Division Lightning Talk Series

Meeting Information
Meeting number:177 689 9045
Password: cSBDBdep757
Meeting link: https://lanl-us.webex.com/lanl-us/j.php?MTID=me7d1bdea59975e2c49673d7813b90b60

Tuesday, July 27, 2021
10:00 a.m. - 11:00 a.m.

Student Speaker: Claire Adams
Group: T-3, Fluid Dynamics and Solid Mechanics
Mentor(s): Richard Lebensohn
Student Status: GRA
School Affiliation: Washington Student University

*Fast Fourier Transform (FFT)-based modelling of microstructural effects in additively manufactured (AM) metals*

Abstract: Additive manufacturing is becoming a very popular processing method for metallic parts in fields such as aerospace or biomedical. However, standardization of this process is still needed to reduce variance in properties. Using an FFT-based micromechanical model, the overall goal of this project is to study process-structure-property relationships in AM metals. This talk aims at showing my understanding of LANL's elasto-viscoplastic FFT-based (EVPFFT) model and code, and explain how it could be applied to model AM processing. Conceptual understanding of EVPFFT is provided, and predictions

Student Speaker: Manav Bhati
Group: T-1, Physics and Chemistry of Materials
Mentor(s): Sergei Tretiak
Student Status: GRA
School Affiliation: Rice University

*Investigating electronic excitations in non-stoichiometric quantum dots*

Abstract: Quantum dots (QDs) that exhibit tunable optoelectronic properties find applications in numerous fields (solar cells, LEDs, quantum communication, photocatalysis). While most of the experimentally synthesized QDs are non-stoichiometric, the theoretical exploration has mostly focused on stoichiometric QDs. Here, we aim to understand the optoelectronic properties of non-stoichiometric QDs using atomistic simulations. We find a distinct nature of low-energy electronic excitations in non-stoichiometric QDs, that corresponds to a charge transfer (CT)

phenomenon between QD core and surface. Such CT arises due to the inequivalent number of anionic and cationic atoms on the QD surface. Understanding CT phenomenon is crucial for emission characteristics and the insights can be utilized to manipulate QDs for various applications, such as photocatalysis.

Student Speaker: Martin Larocca
Group: T-4, Physics and Condensed Matter and Complex Systems
Mentor(s): Patrick Coles and Marco Cerezo
Student Status: GRA
School Affiliation: Departamento de Física "J. J. Giambiagi" and IFIBA, FCEyN, Universidad de Buenos Aires, 1428 Buenos Aires, Argentina

*Diagnosing barren plateaus with tools from quantum optimal control*

Abstract: Variational Quantum Algorithms (VQAs) have received considerable attention due to their potential for achieving near-term quantum advantage. However, more work is needed to understand their scalability. One known scaling result for VQAs is barren plateaus, where certain circumstances lead to exponentially vanishing gradients. It is common folklore that problem-inspired ansatzes avoid barren plateaus, but in fact, very little is known about their gradient scaling. In this work we employ tools from quantum optimal control to develop a framework that can diagnose the presence or absence of barren plateaus for problem-inspired ansatzes. Such ansatzes include the Quantum Alternating Operator Ansatz (QAOA), the Hamiltonian Variational Ansatz (HVA), and others. With our framework, we prove that avoiding barren plateaus for these ansatzes is not always guaranteed. Specifically, we show that the gradient scaling of the VQA depends on the controllability of the system, and hence can be diagnosed through the dynamical Lie algebra obtained from the generators of the ansatz. We analyze the existence of barren plateaus in QAOA and HVA ansatzes, and we highlight the role of the input state, as different initial states can lead to the presence or absence of barren plateaus. Taken together, our results provide a framework for trainability-aware ansatz design strategies that do not come at the cost of extra quantum resources. Moreover, we prove no-go results for obtaining ground states with variational ansatzes for controllable system such as spin glasses. We finally provide evidence that barren plateaus can be linked to dimension of dynamical lie algebra.

Wednesday, August 4, 2021
10:00 a.m. - 11:00 a.m.

Student Speaker: Sneha Banerjee
Group: T-CNLS Center for Nonlinear Studies
T-5 Applied Mathematics and Plasma Physics
Mentor(s): Chengkun Huang, Andrei Piryatinski, Anna Marie Alexander
Student Status: GRA

School Affiliation: Michigan State University

*Theory and modeling of quantum mechanical transport for electron and negative-ion sources*

Abstract: Electron and negative-ion sources are critical for applications such as fusion, high-energy particle accelerators, neutron generation, and mass spectroscopy. Electron field emission, which relies on quantum mechanical tunneling of electrons from surfaces under a strong bias electric field, plays a crucial role in the development of coherent electron sources. Similar quantum tunneling principles are also important to negative-ion sources. In this work, we first investigate the transverse properties of the electron beam emitted from a high aspect ratio semiconductor nanotip. We use Monte Carlo approach combined with scattering and emission models to simulate the electron transport and emission through a diamond nanotip. Our model includes the effects of conduction band quantization and electron-phonon scattering. We study the divergence ratio of the emitted beam for different input parameters, such as, externally applied field, temperature, and initial quantum states of the particles. Next, we develop simple analytical and numerical models to characterize charge capture phenomenon in a negative ion source. We found that the surface-to-atom charge transfer probability and the negative ion yield strongly depends upon the surface to atom distance, applied electric field, work function of the cathode, and the electron affinity of the atom.

Student Speaker: Brendan Miller
Group: T-1 Physics and Chemistry of Materials
Mentors: Christian Negre, Joshua Finkelstein
Student Status: GRA
School Affiliation: Northern Illinois University

*A Three-Dimensional Graph-Based Model for Porous Media Fluid Flow*

Abstract: The understanding and modeling of the flow of fluid in porous media remains a significant theoretical and computational challenge. Previous work has demonstrated a successful computational model in two spatial dimensions which models the flow of fluid using a graph-based approach to represent the pore network. In this talk, we describe our recent efforts to build on this two-dimensional model and extend this graph-based approach to three dimensions. We will present two new approaches of building a pore network in two-dimensions which generalize to three-dimensional porous media. We will conclude with a simple example of a three-dimensional porous medium and the associated centrality computation.

Thursday, August 5, 2021
10:00 a.m. - 11:00 a.m.

Student Speaker: Gabriela (Abby) Roat
Group: T3, Fluid Dynamics and Solid Mechanics
Mentor's name: Trevor Hillebrand and Matthew Hoffman
Student Status: UGS
School Affiliation: Colorado College

*Characterizing changes in 21st century subglacial hydrology at Humboldt Glacier, north Greenland*

Abstract: Located in northern Greenland, Humboldt glacier (HG) has experienced accelerated retreat since the 1990s. With the potential to contribute 19 cm to global sea-level rise, understanding the systems which drive HG's retreat is imperative to quantifying how it will change in the next century. Here, we examine the impact of the subglacial hydrologic system, which is comprised of inefficient, distributed 'sheet' drainage that can evolve to efficient subglacial channels when water flux is large. The character of subglacial hydrology impacts subglacial water pressure and thus basal friction determining, in part, the speed at which the glacier will flow. Currently, many ice sheet models do not take seasonal changes in the subglacial hydrologic system into account when determining basal friction. We use the subglacial hydrology component of the MPAS Albany Land Ice (MALI) ice sheet model to characterize subglacial hydrology at HG during the 21st century, specifically investigating how increases in surface melt draining to the bed change the character of drainage and impact ice effective pressure and associated basal traction. A projected four-fold increase in summer surface melt draining to the glacier bed late in the 21st century causes a substantial change in the character of drainage, with the proportion of total subglacial meltwater conveyed by the channelized system during the late summer nearly doubling. However, this increased channelization has only a slight moderating effect on seasonally-averaged effective pressure as surface melt increases. This suggests that while subglacial channelization can offset some of the impacts of increasing surface melt on ice dynamics, it is insufficient to prevent meltwater-induced speedup of HG in the coming decades.

Tuesday, August 10, 2021
10:00 a.m. - 11:00 a.m.

Student Speaker: Shahriar Khan
Group: T-1, Physics and Chemistry of Materials
Mentor's name: Sergei Tretiak, Brendan Gifford
Student Status: GRA
School Affiliation: Auburn University, Department of Chemistry and Biochemistry

Characterization of Graphene Quantum Dots in terms of Their Optical Properties

Graphene Quantum Dots (GQDs) are promising materials for their possible application as semi-conductors. Based on the size, shape, and functionalization of GQDs, the electronic and optical properties are tunable. The goal of this project is the theoretical investigation

of the optical properties of GQDs using electronic structure theory. We have studied hexagonal, square and rhombus shape of two-dimensional $sp^2$-hybridized graphene flakes and their edge functionalized species. For the square $C_{118}$ graphene sheet, two and four methylene substitution at the edge is probed and the change of optical properties of these species (including isomers) is reported. Also, a comparison between $C_{96}$ hexagon, and $C_{96}$ rhombus shape graphene flakes is studied, and we found that the optical properties vary depending on the shape of the edge (zigzag or armchair) of GQDs. Finally, the effect of the substituent groups ($CH_3$, F, Cl, Br) functionalized at the edge of the graphene sheet is presented.

Student Speaker: Quinn Parker
Group: T-1, Physics and Chemistry of Materials
Mentor(s): Thomas Vogel, Danny Perez
Student Status: UGS
School Affiliation: University of North Georgia

*Simulating the Thermodynamic properties of Tungsten Grain Boundaries*

The boundaries between grains of a material play a key role in the mechanical strength of the material and affect its response to irradiation. The ability to investigate such grain boundaries (GB), in particular phase transitions and GB structures, are critical in the search for finding new ground- and low-energy states and multiple phases within the system. Current methods of analysis typically consider one structure that minimizes the energy in a γ-surface search at a finite temperature, leaving out the possibility that multiple structures could coexist. In our work, the interfacial structure of two body-centered cubic (bcc) Tungsten GBs is determined; one Σ5[001] (310)-twist GB and a [100] tilt GB. We do so by sampling from the grand-canonical ensemble, that is, considering atomic relaxation in systems with variable particle numbers, along with multicanonical adaptive biasing force sampling methods. We report the full entropic information of the GB, and the relevant minimum free-energy GB structures with respect to total particle number and temperature.

Student Speaker: Jacob Spurlock
Group: T-1, Physics and Chemistry of Materials
Mentor(s): Danny Perez
Student Status: UGS
School Affiliation: North Carolina University

*Unraveling the Thermodynamics of Copper Grain Boundaries in the Grand-Multi-Canonical Ensemble via Adaptive Biasing Force Simulations*

The boundaries between grains of materials at an atomic level play a critical role in the properties of these materials. Changing grain structure and grain boundaries (GB) can allow for optimization of the system's properties, such as increasing the overall strength

and resistance of the system. However, current conventional models typically consider only one structure at a finite temperature, which ignores the possibility of multiple structures of the GB. Using a 11 asymmetric tilt and a 45 asymmetric tilt/twist copper GB, we systematically study their structures in multi-canonical and grand-canonical ensembles that allow for a more complete analysis of the GB. This allows us to locate relevant structures at different temperatures and conduct simulations that more extensively sample these complex systems. Extensive simulations and analysis of simulation data resulted in obtaining the full thermodynamic functions of the system and the identification of configurations that form low-energy structures.

Wednesday, August 11, 2021
10:00 a.m. - 11:00 a.m.

Student Speaker: Emma M. Archer
Mentors: Ping Yang, Enrique Batista, Dan Burrill
Group: T-1, Physics and Chemistry of Materials
Student Status: GRA
School Affiliation: Colorado School of Mines

## *Exploring of Electronic Structures of Dipicolinic Acid Derivatives with $Am^{3+}$ and $Nd^{3+}$*

The separation of trivalent lanthanides from trivalent actinides is crucial to the nuclear fuel cycle, particularly in steps of waste reprocessing, remediation, and long-term storage. However, trivalent lanthanides and actinides have similar chemical and physical characteristics posing serious challenges to the chemical separation of these species. To tackle these separations, the exploration of the fundamental chemistry of the An(III) and Ln(III) must be understood leading to molecular species that preferentially bind one of the two. The contraction of the ionic radii of the actinide series would lead one to anticipate the interaction of these ions to be ionic. However, recent studies have explored ligand systems with the trivalent actinides from Am-Cf and found increasing 5f orbital participation in bonding with the 2p ligand orbitals resulting in covalent bonding. This was reported in studies of heavy actinides coordinated by dipicolinic acid (DPA), a well-studied ligand for separations. Due to the open functionalization points on the DPA pyridine ring, the ligand can be modified to change its electronic structure. Computational methods are being used to focus on $Am^{3+}$ and its lanthanide size analog $Nd^{3+}$ to unravel the effects on the metal-ligand interactions as function of the substituents in a DPA derivative series. The derivatives were chosen for their electron withdrawing or donating character in the para position include the hydroxymethyl, methylpiperizine, morpholine, or trimethylamine substituents. Utilizing density functional theory, it is observed that there are more metal to ligand interactions in the $Am^{3+}$ complexes compared to the $Nd^{3+}$ complexes. In addition, the 4f orbitals of the $Nd^{3+}$ complexes reveal more contribution to the frontier orbitals than the 5f orbitals of the $Am^{3+}$ complexes. These results support the hypothesis that covalent interactions in actinide complexes can be probed and tune

Student Speaker: Christopher Montez
Group: A-1, Information and Modeling and T-CNLS, Center for Nonlinear Studies
Mentor: Kaarthik Sundar
Student Status: GRA
School Affiliation: Texas A&M University

*Post-Optimality Sensitivity Analysis of Routing Problems Solved Using Branch-and-Price*

Vehicle routing problems (VRPs) are combinatorial optimization problems that occur in a wide array of applications such as operations research, crew scheduling, logistics, robotics, and many more. As a result, VRPs are of great importance and have been intensely studied by researchers. For some applications, it may be beneficial to consider how removing vertices or changing the fleet size will affect the solution to a VRP. We show how to compute an upper bound on the objective value of a VRP when performing either of these changes. This upper bound is computed using the branch-and-bound tree used to solve the original VRP. As a result, an upper bound is immediately available for little computational cost. As an example we solve the well-known team orienteering problem and show the computed upper bounds are relatively tight and quick to compute.

Student Speaker: Felipe Pereiro
Group: T-1, Physics and Chemistry of Materials
Mentor: Ping Yang, Enrique Batista, Daniel Burrill
Student Status: GRA
School Affiliation: Colorado School of Mines

*Eu Redox Modulation through Ligand Functionalization: A DFT Study*

Felipe Pereiro*, Ping Yang, Enrique Batista, Daniel Burrill

Nuclear power supplies the United States with 20% of its energy economy, while supplying countries like France with as high as 80% of energy needs. Despite the high energy density and low carbon footprint of nuclear power plants, high level waste (HLW) remediation and management remains a concern for existing and future power plants. Chemical separations between lanthanides (Ln) and actinides (An) in HLW have proven to be one of the most difficult chemical challenges to date as a result overlapping ionic radii, core-like behavior of f-electrons, and the dominance of the trivalent oxidation state among both series. Building off the widely-used redox-based PUREX process, the obstacle of similar ionic radii and oxidation states can be overcome by stabilizing divalent and tetravalent redox states of Ln/An, which would alter the ionic radii and access different chemical behaviors apart from that of the trivalent state. In addition to the aforementioned redox separation, previous work on transition metals and select lanthanides show that metal-ligand orbital interactions and reduction potentials can be shifted with the appropriate choice of ligand and functional group. In this study, density

functional theory is employed to screen a series of dipicolinic acid (DPA) derivatives functionalized with different substituents in order to promote metal-ligand interactions that allow for modulation the $Eu^{III/II}$ reduction potential. DPA was specifically chosen for its tunability, relevance to f-element separations, and ability to saturate f-element coordination spheres. The $Eu^{III/II}$ reduction was chosen as a model redox couple because of its experimental accessibility and availability of reported experimental ligand-functionalization work on the couple. This talk will focus on highlighting the change in bonding character of the functionalized ligands in Eu(III/II) complexes. Ongoing and future work are focused on obtaining reproducible geometric and thermodynamic data on the Eu-DPA systems of interest.

Thursday, August 12, 2021
10:00 a.m. - 11:00 a.m.

Student Speaker: Ryan Park
Group: T-1 Physics and Chemistry of Materials
Mentor:Mark C. Zammit
Student Status: UGS
School Affiliation: Tulane Unversity, Department of Chemical and Biomolecular

*Comparison of transport coefficients derived from electron-neutral scattering angular distribution functions via two-term Boltzmann solversimulations*.

Ryan Park,[1, 2] Willem Kupets,[1] Mark C. Zammit,[1, a)] James Colgan,[1] Christopher J. Fontes,[3] Xian-Zhu Tang,[1] Liam H. Scarlett,[4] Dmitry V. Fursa,[4] Igor Bray,[4] and Nathan A. Garland[1, 5, 6, b)]

[1)] *Theoretical Division, Los Alamos National Laboratory, Los Alamos, NM 87545, USA*
[2)] *Tulane Department of Chemical and Biomolecular Engineering, Tulane University, New Orleans, LA 70118, USA*
[3)] *Computational Physics Division, Los Alamos National Laboratory, Los Alamos, NM 87545, USA*
[4)] *Curtin Institute for Computation and Department of Physics, Astronomy and Medical Radiation Sciences, Curtin University, Perth, Western Australia 6102, Australia*
[5)] *School of Environment, Science & Engineering, Southern Cross University, Lismore, NSW 2480, Australia*
[6)] *School of Environment & Science, Griffith University, Brisbane, QLD 4111, Australia* (Dated: 19 July 2021)
[7)]

State-of-the-art Monte Carlo plasma simulations use statistical methods to account for collisional behavior of parti- cles and require accurate angular distribution functions to describe scattering events during runtime. In light of new angular distribution models developed for H, $H_2$, and He here at LANL, we sought to investigate the impact of the present work in the calculation of plasma transport parameters, as opposed to previously utilized angular distribution functions. After deriving He elastic momentum transfer cross sections corresponding to each angular distribution function, we tested these models using a popular Boltzmann equation solver, BOLSIG, to obtain transport coef- ficients. It is shown that our present model is significantly more accurate than previous

approaches in describing collisional anisotropies, and is more consistent with benchmark convergent close-coupling (CCC) collision models and swarm experiment measurements than other commonly used angular distribution models. Utilizing the new angular distribution functions resulted in error reduction of the calculated mobility and diffusion coefficients by as much as 50-100%.

Student Speaker: Braden M. Weight
Group: T-1, Physics and Chemistry of Materials; CINT, Center for Integrated Nanotechnologies
Mentor(s): Sergei Tretiak, Brendan Gifford
Student Status: GRA
School: University of Rochester (PhD)

## *Non-adiabatic Dynamics Simulations of Single-Walled Carbon Nanotubes with Topological $sp^3$-defects: An On-the-fly NEXMD Study*

Braden M. Weight[1,2], Andrew Sifain[3], Brendan Gifford[2], Sergei Tretiak[2]
*[1]Department of Physics and Astronomy, University of Rochester, Rochester, NY 14627, U.S.A.*
*[2]Center for Integrated Nanotechnologies, Center for Nonlinear Studies, and Theoretical Division Los Alamos National Laboratory, Los Alamos, NM 87545, U.S.A.*
*[3]Department of Chemistry, Princeton University, Princeton, NJ, 08540, USA*

Single walled carbon nanotubes (SWCNTs) functionalized with $sp^3$-hybridized defects are a promising material for many optical applications, including single-photon emission at telecommunication wavelengths, photoluminescent sensing in biological applications, and in spintronics. These surface-bound defects increase the photoluminescence yield compared to pristine SWCNTs by forming low-energy, defect-localized bright states.[1] *In this work, we present non-adiabatic dynamics simulations of $sp^3$-defected SWCNTs of varying chirality, defect morphology, and defect chemical composition*. We include excitonic effects at the configuration interaction singles (CIS) level utilizing the collective electronic oscillator (CEO) method to provide solutions for the single-electron density matrices. We propagate the electronic wavefunction by means of Tully's fewest switches surface hopping (FSSH) trajectory-based algorithm with decoherence corrections. The ground state is solved self-consistently using the semi-empirical Austin Model 1 (AM1) parameterized Hamiltonian.[2] The time-dependent population of the initially excited $S_2$ state is tracked and shows *strong dependence (* lifetime around *$\approx$ 50 – 450 fs ) on the chemical composition* of the $sp^3$-defect *as well as its morphology*, which impacts the utility of these materials for optical applications.

(1) Gifford, B. J.; Kilina, S.; Htoon, H.; Doorn, S. K.; Tretiak, S. Controlling Defect-State Photophysics in Covalently Functionalized Single-Walled Carbon Nanotubes. *Acc. Chem. Res.* 2020, *53* (9), 1791–1801.
(2) Malone, W.; Nebgen, B.; White, A.; Zhang, Y.; Song, H.; Bjorgaard, J. A.; Sifain, A. E.; Rodriguez-Hernandez, B.; Freixas, V. M.; Fernandez-Alberti, S.; Roitberg, A. E.; Nelson, T. R.; Tretiak, S. NEXMD Software Package for Nonadiabatic Excited State Molecular Dynamics Simulations. *J. Chem. Theory Comput.* 2020, *16* (9), 5771–5783.

Tuesday, August 17, 2021
10:00 a.m. - 11:00 a.m.

Student Speaker: Kyle Perez
Group: T3, Fluid Dynamics and Solid Mechanics
Mentor's name: Duan Zhang
Student Status: GRA
School Affiliation: Rice University

*Modelling Continua with the Discontinuous Galerkin Method*

Abstract: The Discontinuous Galerkin (DG) Method is a method of numerically solving differential equations. This scheme can be applied to the equations of motion of continuous systems; those of solids and fluids. We present a basic overview of the differential equations we are looking to model, and then visit the update rules of the DG Method. Finally we look some details of the computation of terms in the update rules.

Wednesday, August 18, 2021
10:00 a.m. - 11:00 a.m.

Student Speaker: Chris Kang
Group: T-CNLS, Center for Nonlinear Studies
Mentor's name: Yen Ting Lin, William Hlavacek
Student Status: GRA
School Affiliation: Washington State University

*Efficient Bayesian Inference with MCMC Samplers*
*Chris Kang, Zachary Fox, Yen Ting Lin, William Hlavacek*

Abstract: When applying the Bayesian inference approach to quantify parameter estimates of given data, one requires the use of Markov Chain Monte Carlo (MCMC) methods to sample the posterior. While traditional MCMC choices, such as the Metropolis-Hastings algorithm, may be sufficientfor modeling low-dimensional data, the performance of the sampler is not scalable as the parameter dimensions grow. Alternative MCMC samplers such as the Hamiltonian Monte Carlo(HMC) and No-U-Turn Sampler (NUTS) are promising in that they utilize gradient information (sensitivity of the likelihood with respect to parameters) to effectively span the parameter space.The current state of these samplers in probabilistic programming languages such as Stan, however, resort to Automatic Differentiation (AD) to compute the sensitivity. While AD is excellent in gradient computation when the likelihood function is analytical, in most cases of modeling, analyticity should not be assumed, nor should it be guaranteed. Here, we propose to perform a shallow survey of sensitivity methods, including Adjoint Sensitivity Analysis, and implement these in HMC and NUTS in the context of fitting an

SIR-model and its derivatives. Our long-term goal is to qualitatively characterize the computational improvements of the MCMC samplers with different sensitivity methods and provide an informed decision matrix formodelers.

Thursday, August 19, 2021
10:00 a.m. - 11:00 a.m.

Student Speaker: Liam Herndon
Group: T-6, Theoretical Biology and Biophysics
Mentor's name: S. Gnanakaran
Student Status: GRA
School Affiliation: Stanford University

*Machine Learning to Guide Design of Novel Antibiotics*

Abstract: The outer membrane (OM) and efflux pumps are key to antibiotic resistance in gram-negative bacteria. The OM acts as a barrier to drug entry, and efflux pumps expel compounds from the cytoplasm. These mechanisms allow gram-negative bacteria to be resistant to numerous antibiotics by preventing them from reaching targets in the cytoplasm. A key focus of antibiotic development is therefore to design compounds that can permeate the OM and avoid efflux pumps. In recent years, significant progress has been made in this field. Recent research has identified key physico-chemical properties of OM permeators and efflux avoiders. Many of these properties are broad and can be achieved through a range of structures. We present an algorithm that provides more specific guidance in the design of OM permeator and efflux avoiders. This algorithm uses a nonlinear machine learning model to compare compounds based on structural motifs. This software can accurately identify the stronger OM permeator and efflux avoider from pairs of highly analogous compounds, meaning that it could predict how potential modifications to antibiotics would affect OM permeation and efflux avoidance.

Student Speaker: Elena Violeta Romero
School Affiliation: University of Washington
Group Name: T-6, Theoretical Biology and Biophysics
Mentor: Brian Foley
Student Status: GRA
School Affiliation: University of Washington

*Creating a genome browser for SARS-CoV-2 visualization.*

Abstract: Recently, SARS-CoV-2 has had an extensive impact on the health and ways of life of people across the globe. While enormous progress has been made with the development of several vaccines for the virus, cataloging its diversity remains important as new variants arise. A subset of these variants, such as the well-known "Delta" or B.1.617.2. variant, bring with them new challenges and concerns in our fight against the virus. Due to this, researchers find themselves in need of bioinformatics tools that

help visualize SARS-CoV-2 diversity and features of specific variants. The SARS-CoV-2 Genome Browser is one such tool that aids researchers by providing information on the locations of genomic changes carried by variants. It then maps these changes to domains of interest. This can provide clues as to what newly arising variants are likely to allow the virus to evade current vaccines and thus should be monitored further.

Thursday, August 26, 2021
10:00 a.m. - 11:00 a.m.

Student Speaker: Abigail Coker
Group: T-4/T-CNLS: Physics and Condensed Matter and Complex Systems and Center for Nonlinear Studies
Mentor: Jian-Xin Zhu
Student Status: GRA
School Affiliation: University of Utah

*Spin Dynamics in the Kagome Lattice*

Abstract: The Kagome lattice is attracting a multitude of research interest as a result of its recently discovered ability to host the elusive quantum spin liquid state and topologically protected bands. The ability to harness control of these intriguing states of matter presents potential avenues for significant technological advancement. To do this, it is necessary to understand the spin dynamics and underlying microscopic processes within this family of materials. In this study, we consider a Heisenberg Hamiltonian to elucidate the effect of the exchange interaction on the ground state and spin dynamics, and proceed to study the effects of an applied magnetic field, on-site anisotropy, and Dzyaloshinskii-Moriya exchange interaction. Competition between these interactions drives the system to exhibit a rich phase diagram consisting of interesting spin configurations and textures. By evaluating our model numerically, we explore the spin waves of these configurations with varying parameters associated with each of the considered interactions. This allows us to thoroughly inspect the form of the spin waves, including the ability to determine whether or not spin excitations are gapless. Such examination has the potential to provide key insights to the promising nature of Kagome materials in development of spintronics and other quantum information systems

Student Speaker: Lillian Petersen
Group: T-CNLS: Center for Nonlinear Studies
Mentor: Christina Steadman
Student Status: UGS
School Affiliation: Harvard University

*Genome-Wide Association Study for Female Infertility*

Abstract: Polycystic ovarian syndrome (PCOS) is the largest cause of infertility, affecting approximately 10% of the population. PCOS is highly heritable (about 70%), but current research has been largely unable to find the genetic basis for this heritability.The goal of my research is to conduct a genome-wide association study (GWAS) to find the biological pathways behind PCOS and determine a female's genetic risk for developing it. Previous GWAS for PCOS had limited power for two primary reasons: small databases and underreporting of PCOS. This study aims to improve on previous research on both of these fronts. First, I use data from the UK Biobank, a database housing the genotypes and phenotypes of over 250,000 females in the UK. However, underreporting remains a problem: the UK biobank reports a mere 330 cases of PCOS. To address this, I collaborated with GWAS and infertility experts Dr. Liang and Dr. Mahalingaiah of Harvard Medical School to create a model that predicts whether an individual has PCOS based on their existing medical records. This model raised the number of PCOS individuals to about 1500. I am currently in the process of conducting the PCOS GWAS using this new PCOS diagnostic criteria. Next, I plan to find the genetic overlap between PCOS and other heritable diseases such as diabetes and asthma, which will illuminate their biological relationships. In the future, I hope to further this research by extending to whole exome or whole genome sequences. These richer sequencing data have only become available at scale in the last year and hold huge potential to advance the field of genetic association studies.

Student Speaker: Aaron Phillip
Group: T-1: Physics and Chemistry of Materials
Mentors: Benjamin Nebgen, Guoqing Zhou
Student Status: High School Co-op
School Affiliation: Los Alamos High School

*Transition Path Search for Light-Driven Molecular Motor*

Abstract: Molecular machines are molecules that convert energy into dynamic function; proteins in living organisms are a result of specific combinations of several molecular machines. A subset of molecular machines, molecular motors, have the specific role of producing repetitive rotation. Dr. Ben Feringa et. al. at the University of Groningen developed a light-driven molecular motor and its cycle of rotation takes place over four distinct reaction steps. With controlled external stimulus like heat or light, the motor will rotate with cycles of photochemical and thermal isomerizations. Due to the complex geometries of these motor molecules, traditional methods for finding the transition path fail with unrealistic intermediate states. To study the dynamics, this project will find a realistic transition path between isomers by generating intermediate geometries and optimizing them. We explore various constraints and implement a trained machine learning model based on semi-empirical theory to obtain atomization energies of each geometry in order to assess the viability of the generated transition path. The reaction cycle of the motor has provided evidence that the motor can serve as a molecular propeller, so study of intermediate geometries is valuable in

determining ways to further optimize the rotation rate.

Tuesday, August 31, 2021
10:00 a.m. - 11:00 a.m.

Student Speaker: Armando Bellante
Group: T-4, Physics and Condensed Matter and Complex Systems
Mentors: Rolando D. Somma, Gopikrishnan Muraleedharan
Student Status: GRA
School Affiliation: Politecnico di Milano
*Solving the quantum simulation problem via signal analysis*

Abstract: The computation of scattering amplitudes soon becomes an intractable problem for a classical computer as the size of the quantum system and the evolution time grows. Nevertheless, this problem is in the class BQP, where a quantum computer can offer an efficient solution in time polynomial in both the system size and evolution time. The currently available quantum devices (NISQ) have enough qubits to represent challenging instances of this problem. However, because of errors, they can not run the simulations for long times. Our research frames the quantum simulation problem as a signal analysis one to combine NISQ devices' power and classical computation. The goal is to devise an algorithm that can forecast the expectation values at longer times with bounded error, given the outcome of short-time simulations. Using a Matrix Pencil approach, we conduct numerical experiments that suggest that the predictions can be accurate under certain conditions. At the same time, we are aware of adversarial problem instances that can make the prediction hard.

Student Speaker: Maksim Kuichenko
Group: T-1, Physics and Chemistry of Materials
Mentors: Justin S. Smith, Sergei Tretiak
Student Status: GRA
School: Utah State University

*Diversification of ML Datasets Using Bias Potentials as Functions of "Uncertainty"*

Abstract: One of the central issues in machine learning is a dataset. Its diversity, size, and preparation time are the variables which researchers always aim to optimize. The purpose of this work is to capture as much chemical space as possible using active learning and biased potentials embedded in the molecular dynamics.
Active learning is the technique which allows to keep the dataset as diverse as possible using the ensemble of neural networks. Within MD framework this means augmentation of dataset with only those MD steps where ensemble of neural networks feels uncertain. By constructing biased potentials which are functions of the "uncertainty", we want to make poorly sampled regions more energetically favorable. Thus, artificially forcing the MD to avoid well sampled regions, bias potentials within active learning may significantly accelerate datasets preparation time while increasing the data diversity.

Wednesday, September 1, 2021
10:00 a.m. - 11:00 a.m.

Student Speaker: Jessica Lalonde
Group: B-11, T-CNLS: Bioenergy and Biome Sciences, Center for Nonlinear Studies
Mentors: Babetta Marrone , Ghanshyam Pilania
Student Status: GRA
School Affiliation: Duke University
*A Machine Learning Approach for Polymeric Degradation Prediction*

Abstract: The environmental impacts of plastic degradation affect all aspects of the global ecosystem for many generations. Bio-based plastic alternatives have emerged as an important materials solution in the transition towards a future sustainability-focused economy. Poly(hydroxyalkanoates) (PHAs) are one large class of naturally derived bioplastics that have been extensively studied since the 1970s as replacement materials for food and commercial packaging. While PHAs offer a large chemical space for design, their degradation is currently not well understood or modeled. Machine learning can be employed to predict and better understand how these materials break down in a wide variety of environments by learning from trends in previously published, open-access degradation data. Previous studies have examined the critical factors affecting degradation rate for traditional plastics but have often been limited to specific environmental conditions or restricted to one or two classes of materials. In this talk, I will describe the development of a machine learning model to predict polymer degradation behavior in a variety of environmental conditions (hydrolytic, enzymatic, water- and soil-based environments). Employing a manually-accumulated database of over 1,600 data points and 195 samples of traditional plastics and conventional biopolymers, containing both monomers and copolymers of PHAs, here we train a random forest model to predict specific parameters which physically represent the long- and short-term degradation factors affecting the breakdown of the material. The validated and tested model is then employed to predict chemical trends over a wide range of multicomponent polymer chemistries to understand their degradation behavior and the relative importance of the factors affecting it.
Thursday, September 2, 2021
10:00 a.m. - 11:00 a.m.

Student Speaker: Faith Cengil
Group: T-5: Applied Mathematics and Plasma Physics
Mentors: Harsha Nagarajan, Russell Bent
Student Status: GRA
School Affiliation: University of Arkansas

*Learning to Accelerate Globally Optimal Solutions to the AC Optimal Power Flow Problem*

Abstract: In this work, we propose to use ML to accelerate global solutions by effectively extracting information from previously solved ACOPF instances. We will also replace ad-hoc heuristics with ML-based policies, which can aid in predicting better greedy steps towards global optimality on similar instances with different parameters. Further, we will present numerical results on a diverse set of realistic and large-scale IEEE benchmarks to empirically show the efficacy of ML-based acceleration methods. We will also provide out-of-distribution experiments to study the robustness of proposed methods.

Student Speaker: Olawale Ikuyajolu
Group: T-3, Fluid Dynamics and Solid Mechanics
Mentors: Luke Van Roekel, Steven R. Brus (ANL)
Student Status: GRA
School Affiliation: Georgia Institute of Technology

*Porting Wave Action Source Terms to GPU on WaveWatch III*

Abstract: Present and future simulations of extreme events by Earth system models (ESMs) are of fundamental importance in guiding policy decisions on climate change. Consequently, effective climate change policies heavily depend on the continuous development and improvement of ESMs. Accurate representation of small-scale physical processes such as ocean surface gravity waves and their impact on ocean mixing and surface fluxes is still missing in most state-of-the-art ESMs. Despite the growing literature on the importance of ocean surface waves in modulating air-sea fluxes, inclusion of ocean surface waves in most state-of-the-art global climate models is lacking. Wind-wave processes (small-scale) have traditionally been excluded from ESMs due to high computational costs.

The Department of Energy (DOE) Next Generation Development (NGD) project for the ocean partly focuses on the inclusion of a wave model (WaveWatch III –WW3) into the Energy Exascale Earth System Model (E3SM). In order to incorporate WW3 to E3SM, we need to make it computationally less expensive. Taking advantage of the hybrid architectures at DOE leadership computing facilities, this work proposes to move the computationally intensive section (wave action source terms) in WW3 to GPGPU through the use of OpenACC pragmas. We discuss initial scalings of WW3, the strong potential for speed up with GPGPUs, and progress toward porting the wave action source terms to GPGPU.

Student Speaker: Carlos Mora Perez
Group: T-1, Physics and Chemistry of Materials
Mentor: Amanda Neukirch
Student Status: GRA
School Affiliation: University of Southern California

*Defect study on the electronic structure of a novel 2D-perovskite: n=1, $BA_2MA_{n-1}Pb_nI_{3n+1}$*

Abstract: Two-dimensional (2D) perovskites constitute a new realm of semiconducting materials suitable for solar cells and light emitting devices limited by nonradiative charge and energy losses facilitated by defects. In this work, 2D perovskite absorbers with the chemical formula $BA_2MA_{n-1}Pb_nI_{3n+1}$ (MA: methylammonium and BA: butylammonium) with n value of 1 are investigated. We are focusing on low formation energy and common point defects ($V_{BA}$, $V_{BAI}$, $V_{PbI2}$, $V_I$ (in-plane), $I_I$ (out-of-plane), $I_I$ (in-plane)). Halide defects that localize the hole or electron are the most detrimental to the electronic structure leading to lower performance. *Ab-initio* simulations are crucial for determining point defects with adverse effects on the development of high-efficiency devices.

Student Speaker: Akram Touil
Group: T-CNLS: Center for Nonlinear Studies
Mentor: Wojciech H. Zurek
Student Status: GRA
School Affiliation: University of Maryland, Baltimore County

*Eavesdropping on the Decohering Environment: Quantum Darwinism, Amplification, and the Origin of Objective Classical Reality*

Abstract: One of the major open problems in theoretical physics is understanding the emergence of classicality from underlying quantum principles. These seemingly peculiar principles are directly at odds with our classical intuition since they are absent in our familiar physical reality. However, within the framework of Quantum Darwinism, the well-studied features of quantum mechanics such as superposition and entanglement are the building blocks of nature that explain and account for our classical everyday observations, hence our perception of classicality. In this talk, I will give a brief overview of Quantum Darwinism, and some of the recent results we established within this framework regarding the capacity of the environment as a communication channel.

Los Alamos NATIONAL LABORATORY

# Exploring Electronic Structures of Dipicolinic Acid Derivatives with $Am^{3+}$ and $Nd^{3+}$

Emma Archer
Mentors: Ping Yang, Enrique Batista, and Daniel Burrill
Seaborg GRA Fellowship 2021

8/11/2021

# Spent Nuclear Fuel

- Waste highly radiotoxic
  - Long-lived minor actinides
    - Am(III) and Cm(III)
  - High volume
- Partitioning via solvent extraction
  - Reduce volume
  - Transmute the waste to shorter lived species
  - Prolong life of nuclear fuel

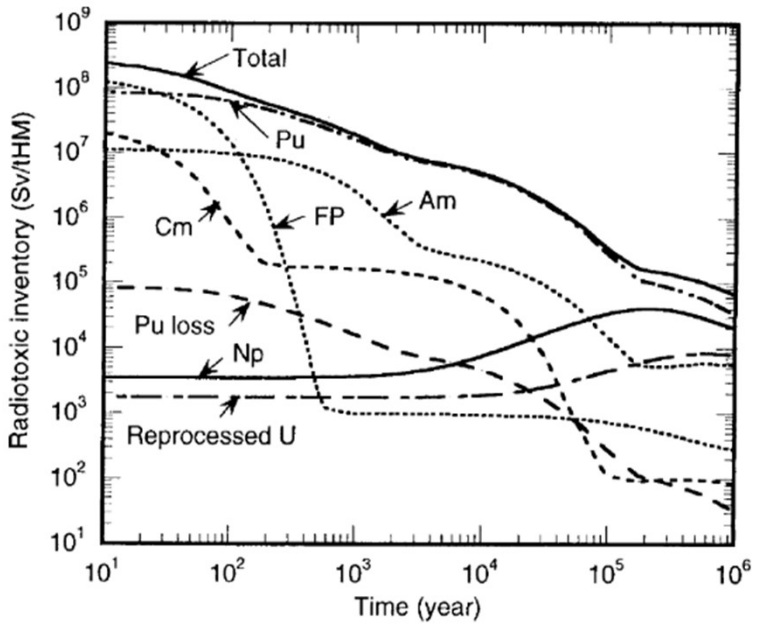


Salvatores, M. Nuclear Fuel Cycle Strategies Including Partitioning and Transmutation. *Nucl. Eng. Des.* **2005**, *235* (7), 805–816. https://doi.org/10.1016/J.NUCENGDES.2004.10.009.
Veliscek-Carolan, J. Separation of Actinides from Spent Nuclear Fuel: A Review | Elsevier Enhanced Reader. *J. Hazard. Mater.* **2016**, *318*, 266–281.

# Partitioning

- Ln(III) and An(III) are chemically similar
  - Same oxidation state
  - Similar ionic size
- Exploit electronic structure differences
  - 5f orbitals extend more
  - An(III) softer acids than Ln(III)
- Utilize ligands that will be selective for An(III) over the Ln(III)

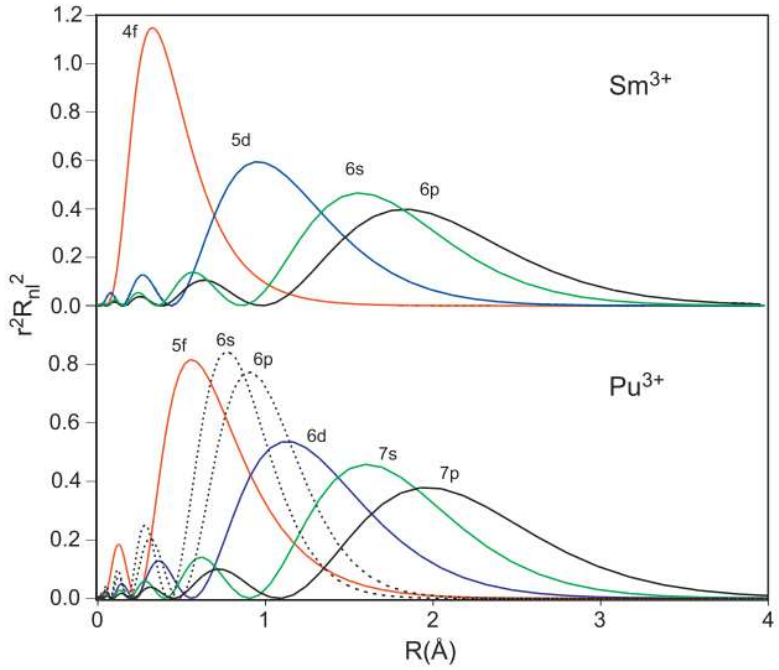


Neidig, M. L.; Clark, D. L.; Martin, R. L. Covalency in F-Element Complexes. *Coord. Chem. Rev.* **2013**, *257* (2), 394–406. https://doi.org/10.1016/j.ccr.2012.04.029.

# Ligands

- Many types
  - O, N, S
- N donors are reported to be the most selective for An(III)
  - Mixed N and O donors are even better
- Dipicolinic acid (DPA)
  - Highly symmetric
  - Tris-chelate
  - Makes 1:3 complexes
  - Radiolytically stable

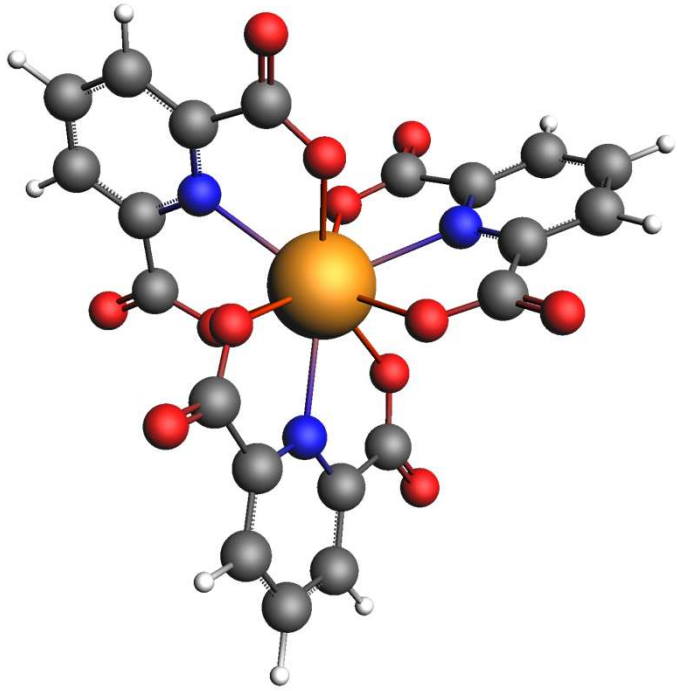

$Am(DPA)_3^{3+}$



Silver, M. A.; Cary, S. K.; Johnson, J. A.; Baumbach, R. E.; Arico, A. A.; Luckey, M.; Urban, M.; Wang, J. C.; Polinski, M. J.; Chemey, A.; Liu, G.; Chen, K.-W.; Van Cleve, S. M.; Marsh, M. L.; Eaton, T. M.; Van De Burgt, L. J.; Gray, A. L.; Hobart, D. E.; Hanson, K.; Maron, L.; Gendron, F.; Autschbach, J.; Speldrich, M.; Kögerler, P.; Yang, P.; Braley, J.; Albrecht-Schmitt, T. E. Characterization of Berkelium(III) Dipicolinate and Borate Compounds in Solution and the Solid State. *Science (80-. ).* **2016**, *353* (6302), 888. https://doi.org/10.1126/science.aaf3762.

# Dipicolinic Acid Derivative System

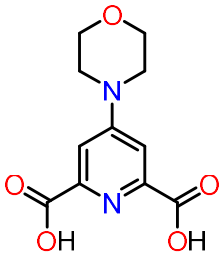

4-morphylinyl DPA

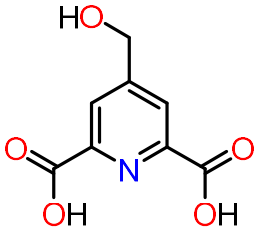

4-Hydroxymethyl DPA

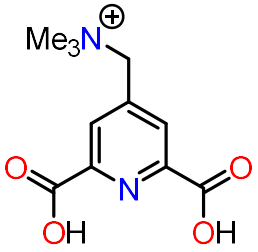

4-trimethylamine DPA

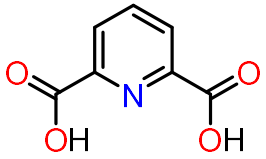

DPA

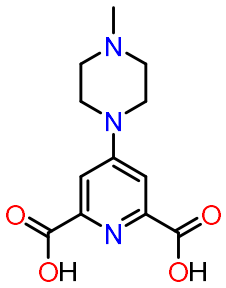

4-methylpiperizine DPA

- Functionalizing 4 position with various groups
  - Very few substituent effect studies with An(III) selectivity
- Model these ligands with $Am^{3+}$ and $Nd^{3+}$
  - Size analogs

# Calculation Process

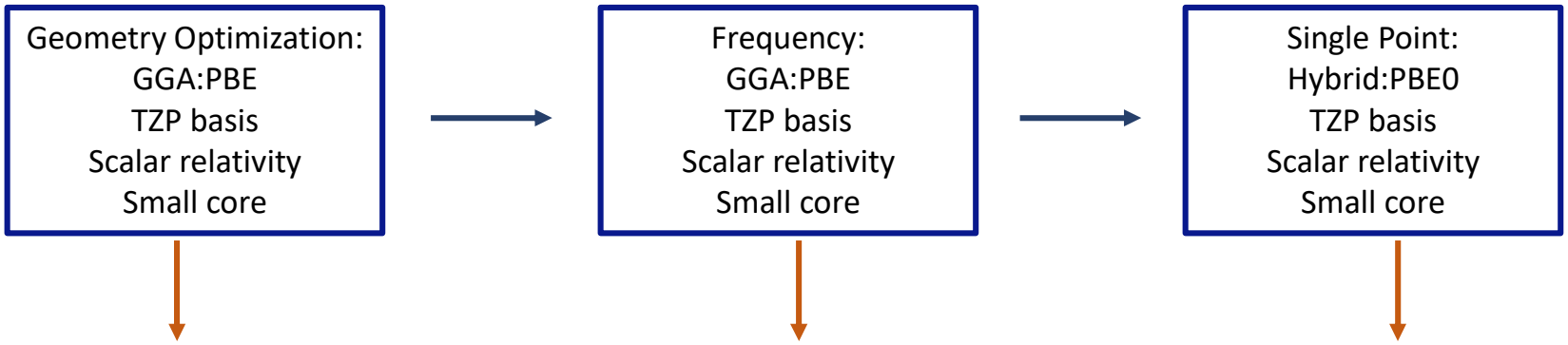


Optimized coordinates

Vibrational modes, thermodynamic data, etc.

Orbital population, contribution, energies, spin densities, Mulliken charges, bonding energies, etc.

Implicit solvation model: COSMO water

# Frontier Orbital Results

- The trend is the same for both metals
  - Ligand dictates the trend
  - QDPA is more $e^-$ withdrawing and stabilizes the HOMO/LUMO gap
- $Am^{3+}$ has a larger HOMO/LUMO gap
  - Increased metal-to-ligand interaction

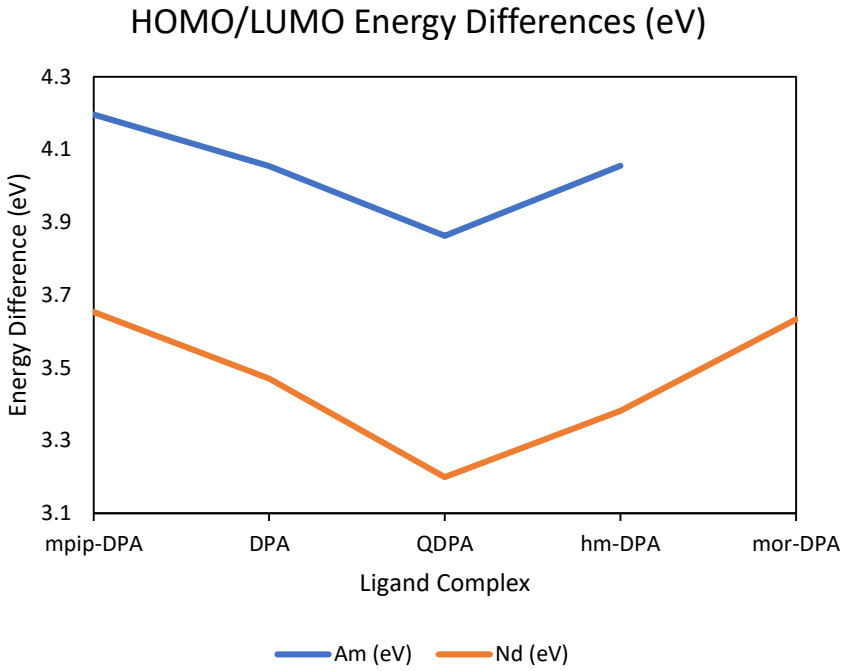

# Frontier Orbital Results

- $Nd^{3+}$ valence $e^-$ have larger contribution to frontier orbitals
  - $e^-$ more localized on the metal
  - more ionic bonding

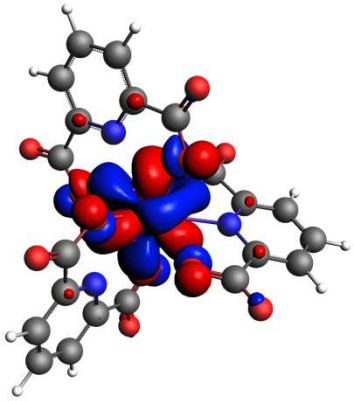

$Nd(DPA)_3^{3-}$

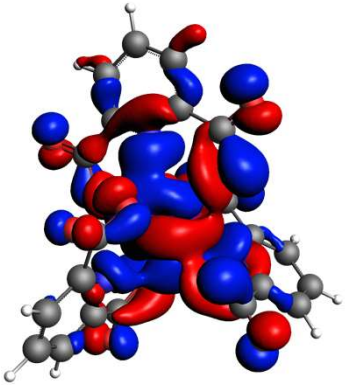

$Am(DPA)_3^{3-}$

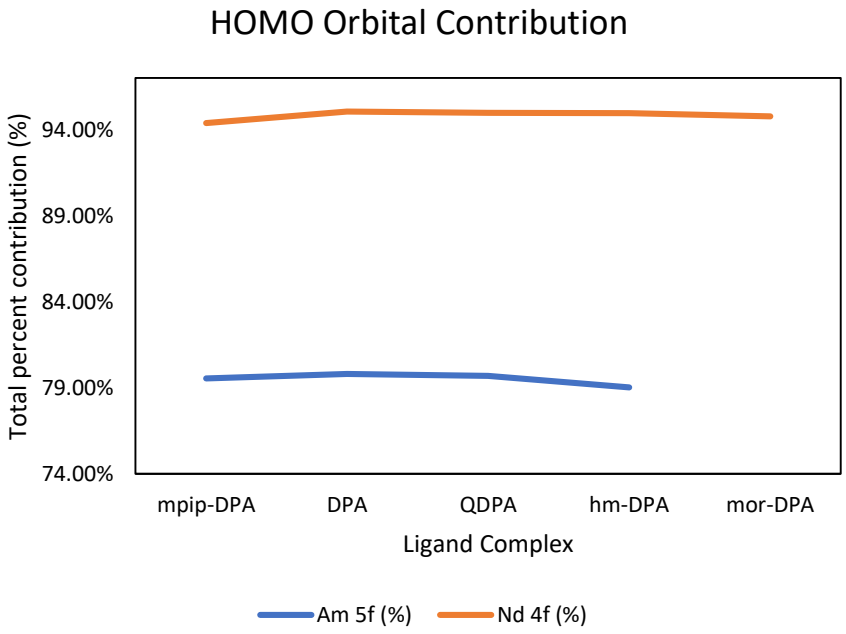

# Conclusions and Future Work

- Main takeaways
  - Modifying a ligand with various substituents allows us to probe and tune electronic properties of the An(III) and Ln(III)
  - The DPA derivatives interact more strongly with $Am^{3+}$ which means that modifying the ligand will change the interaction
- Moving forward
  - Look into the thermodynamic results of the water solvated calculations
  - Experimental work to compare these results

Los Alamos NATIONAL LABORATORY

# Acknowledgements

Glen T. Seaborg Institute at LANL
T-1

LANL:
Dr. Ping Yang
Dr. Enrique Batista
Dr. Daniel Burrill

Colorado School of Mines:
Shafer Research Group
Mines HPC

# Fast Fourier transform (FFT)-based modelling of microstructural effects in additively manufactured (AM) metals

Claire Adams

7/27/21

LA-UR-21-27312

# Fast Fourier Transform Based Model

Contents lists available at SciVerse ScienceDirect

International Journal of Plasticity

journal homepage: www.elsevier.com/locate/ijplas

An elasto-viscoplastic formulation based on fast Fourier transforms for the prediction of micromechanical fields in polycrystalline materials

Ricardo A. Lebensohn [a,*], Anand K. Kanjarla [a], Philip Eisenlohr [b]

[a] Materials Science and Technology Division, Los Alamos National Laboratory, MS G755, Los Alamos, NM 87845, USA
[b] Max-Planck-Institut für Eisenforschung, Max-Planck-Str. 1, 40237 Düsseldorf, Germany

ARTICLE INFO

*Article history:*
Received 26 August 2011
Received in final revised form 12 December 2011
Available online 28 December 2011

ABSTRACT

We present the infinitesimal-strain version of a formulation based on fast Fourier transforms (FFT) for the prediction of micromechanical fields in polycrystals deforming in the elasto-viscoplastic (EVP) regime. This EVP extension of the model originally proposed by Moulinec and Suquet to compute the local and effective mechanical behavior of a heterogeneous material directly from an image of its microstructure is based on an implicit time

Also: Texture development during deformation in alloys

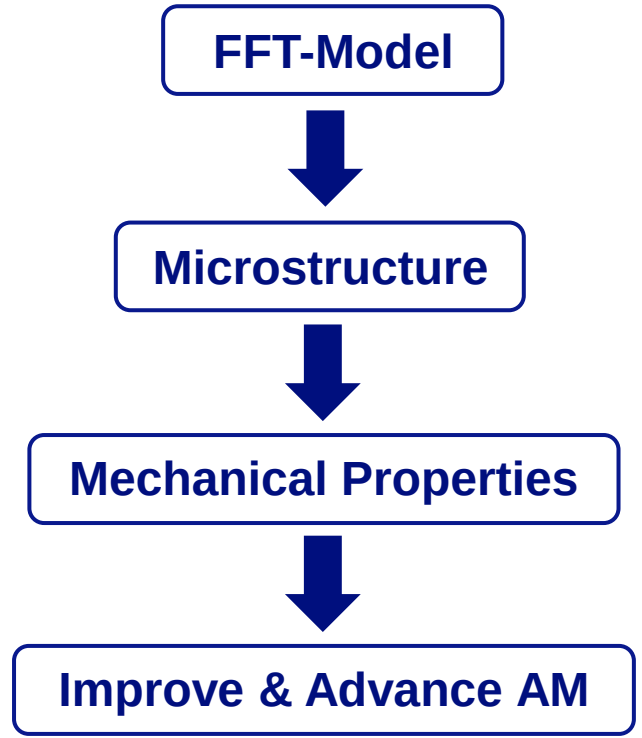




Lebensohn RA, K. A., Eisenlohr P. "An elasto-viscoplastic formulation based on fast Fourier transforms for the prediction of micromechanical fields in polycrystalline materials." International Journal of Plasticity. 2012;32-33: 59-69.

# Conceptualizing EVPFFT

Elasto-viscoplastic fast Fourier transform based model

- Direct Problem

  Initial Microstructure ➡ FFT-Model to Obtain Properties

- Inverse Problem

  Desired Properties ➡ FFT-Model to Adapt Microstructure

# Single Process

- No initial load
- Deformation (i.e. uniaxial tension)

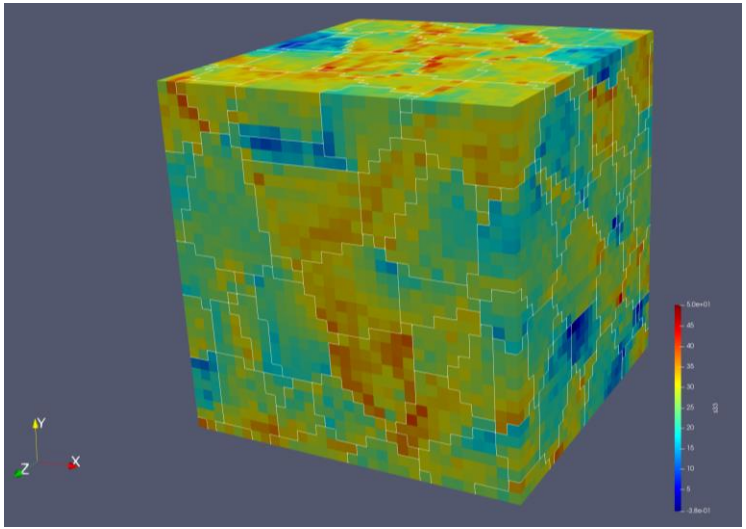

32x32x32 Copper Voronoi polycrystal
Showing stress field

# Multi-Process

- Initial thermal internal stresses
- Deformation (i.e. uniaxial tension)

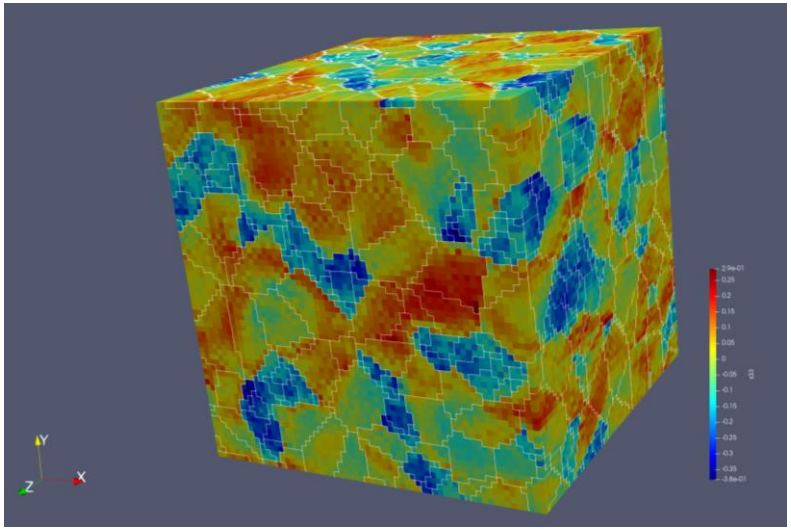

64x64x64, 90% Austenite, 10% Ferrite
Showing stress field

# 3D microstructure

**Modeled Microstates**
Stress Field (left)
Strain Field (right)
Elastic Strain
Strain Rate

**Code Type**
Single Process (Top)
Multi-Process (Bottom)

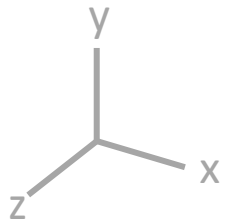


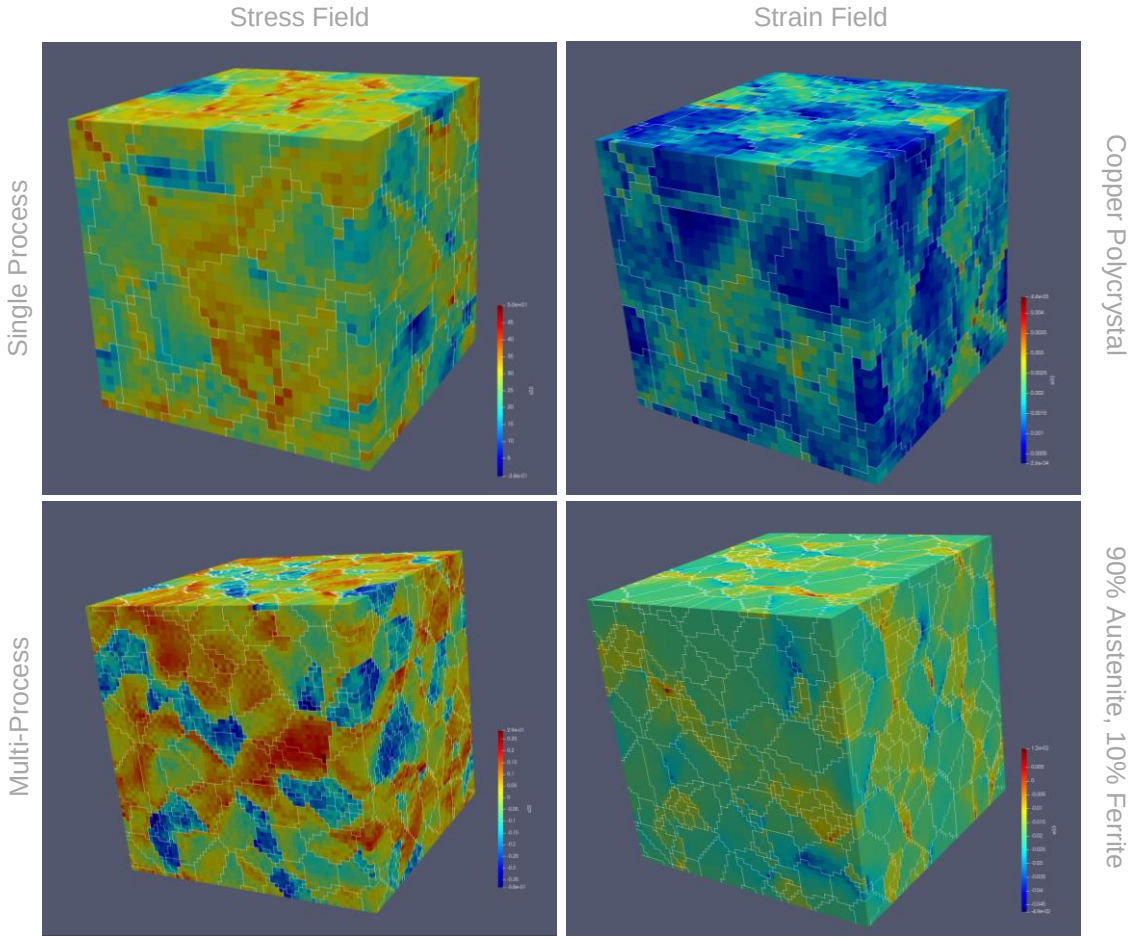

# Thermal Internal Stresses

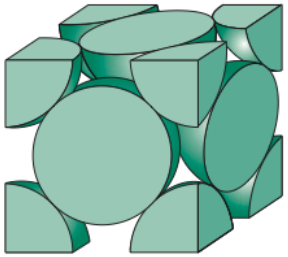

Austenite = FCC

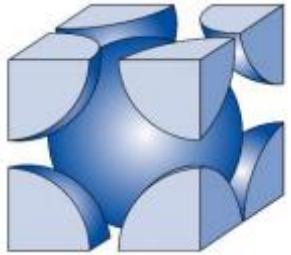

Ferrite = BCC

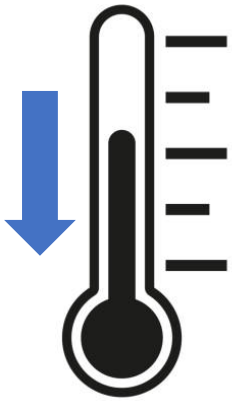

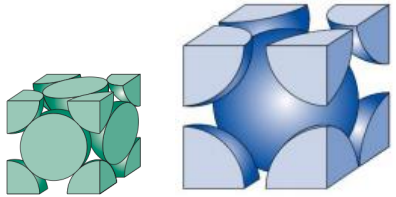

Spacing between atoms get smaller, not the atoms themselves


As T↓
bars want to…

Instead…

# Next Steps

- Real electron backscatter diffraction (EBSD) data of $Ti_6Al_4V$
  - Rather than synthetic data
- Thermal stresses from build temperature to room temperature

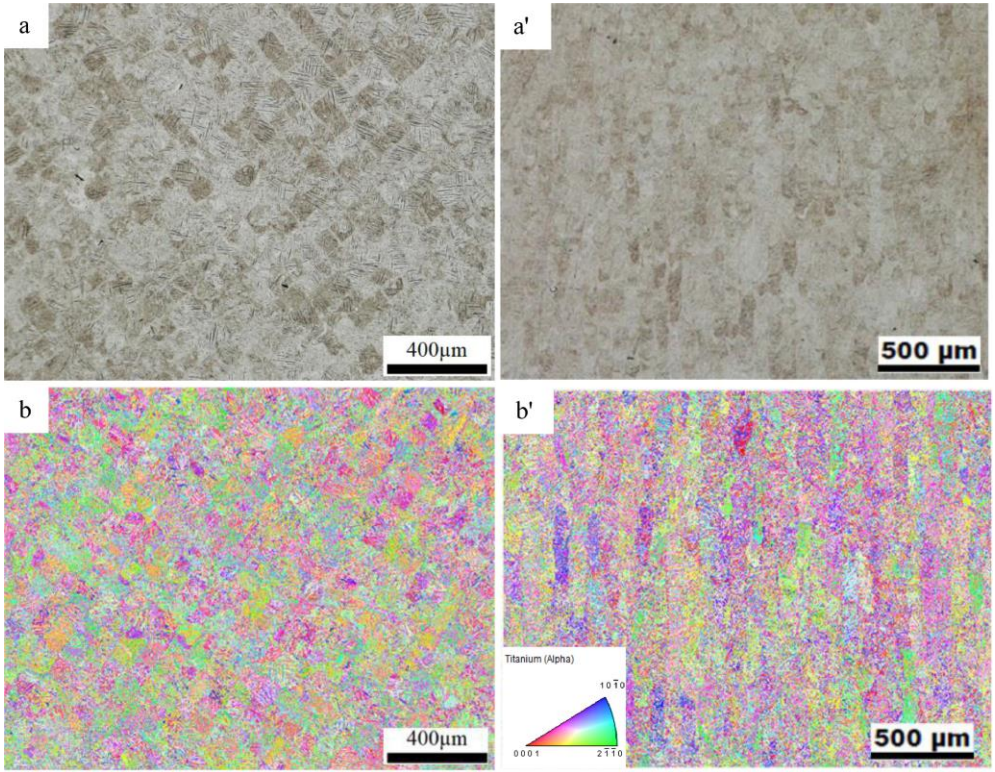


***Example*** of of $Ti_6Al_4V$ sample, (a)(a') Micrographs, (b)(b') Inverse pole figure maps from EBSD, with build direction perpendicular and vertical respectfully


Riyad IA, Feather WG, Vasilev E, Lebensohn RA, McWilliams BA, Pilchak AL, Knezevic M. "Modeling the role of crystallographic correlations in microstructures of Ti-6Al-4V using correlated structure visco-plastic self-consistent polycrystal plasticity formulation." Acta Materialia. 2021;203(116502)

# Questions?

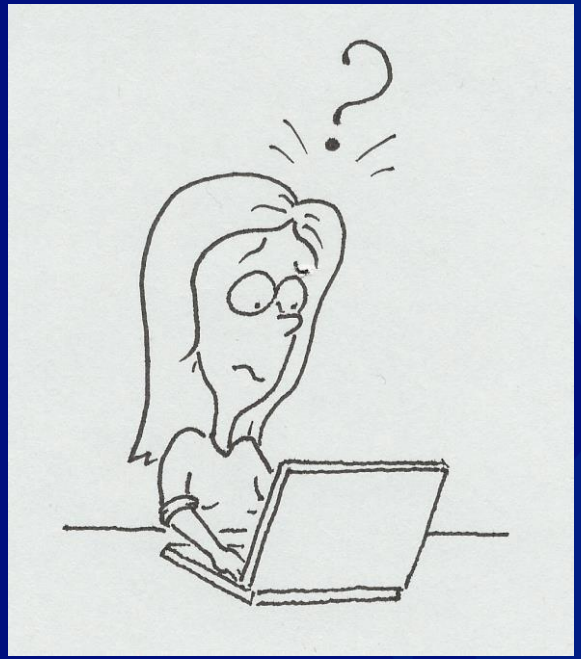

# What is microstructure?

- “The structural features of an alloy (e.g. grain and phase structure) subject to observation under a microscope”
- Grain shape and size

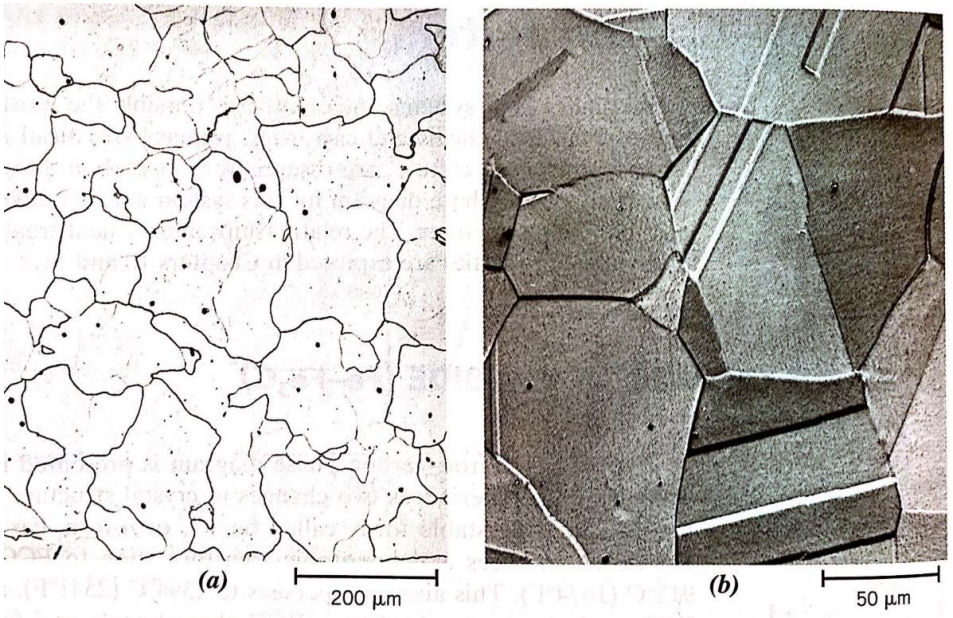


Photomicrographs of (a) α-ferrite (b) austenite

Callister WD, Rethwisch DG. Materials Science and Engineering: An Introduction. 9th ed. John Wiley & Sons; 2014.

# 2D slices of 3D microstructure

Copper Voronoi polycrystal
Single process, 100 “randomly” oriented grains, 32x32x32 points
X-cut at varying cut levels

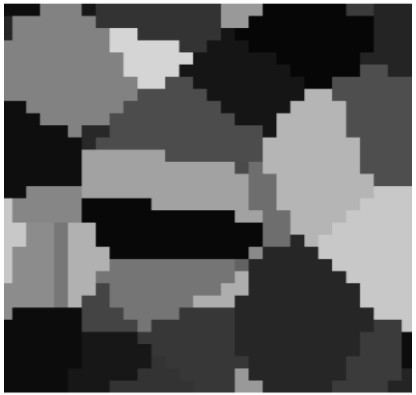

10

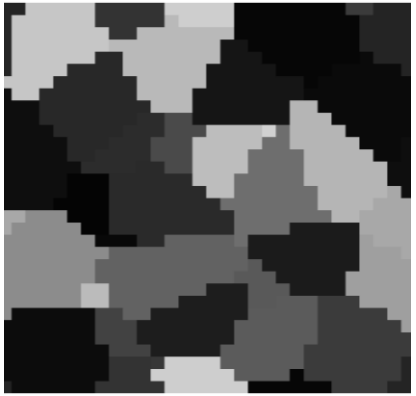

15

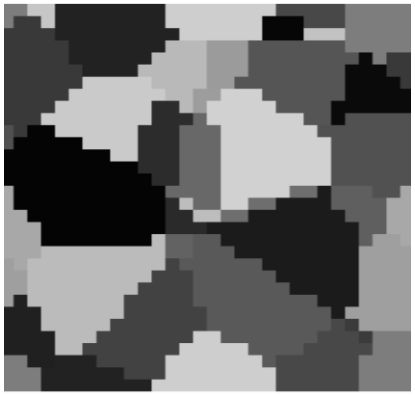

20

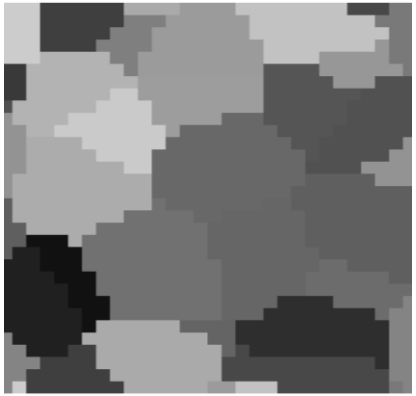

25

# “Randomness” in terms of computers

- Pseudo random number generator
  - Generates number sequence based on an initial integer or “seed”
  - **1** 2 3 4 5 6 8 7 9…
  - **2** 5 8 9 6 3 7 4 1…
  - **3** 4 5 7 8 9 1 6 2…
- Randomness corresponds to grain positions

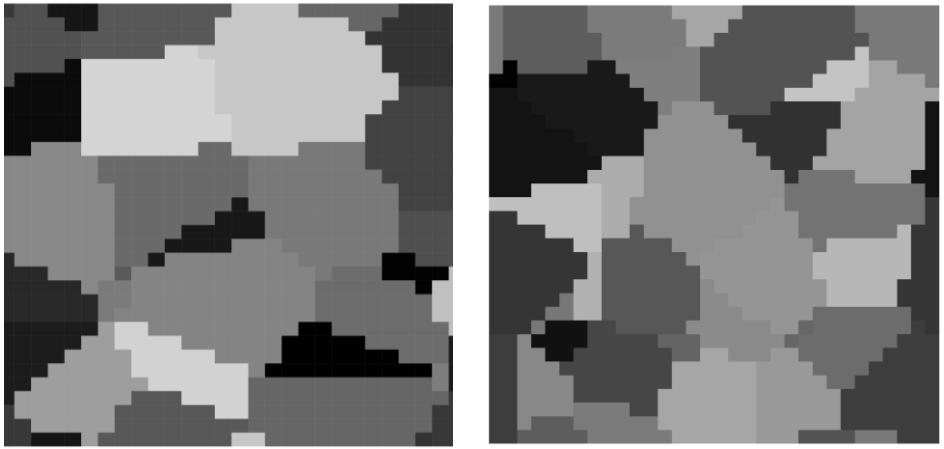

Both x-cut slices at point 1 of 32, but different random seeds were used

# Why do crystal structures contract or expand with temperature?

- Most solid materials will naturally expand upon heating and contract upon cooling
- Coefficient of Thermal Expansion (CTE)
  - Relates to how the size of something changes with temperature
  - From atomic perspective: average interatomic distance increases with temperature
  - Higher temperatures raise vibrational energy

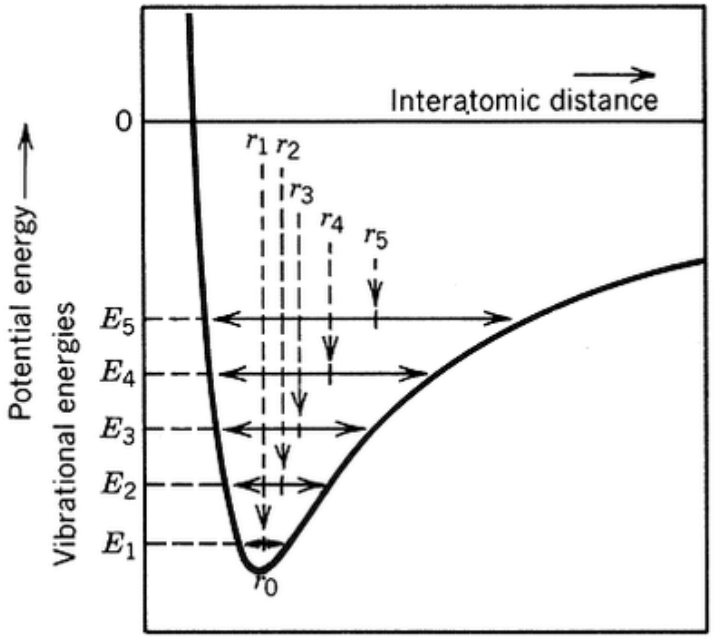


Demonstrates the increase in interatomic separation with rising temperature

Callister WD, Rethwisch DG. Materials Science and Engineering: An Introduction. 9th ed. John Wiley & Sons; 2014.

# Why does one phase contract more than the other?

- Austenite contracts more than ferrite in iron-carbon system
- Different materials, different phases, have different CTE's
- Contraction between phases may be affected by different equilibrium distance between atoms
  - Want equilibrium distances that minimize energy
  - Equilibrium positions of atoms in lattice as function of temperature are affected differently

Los Alamos NATIONAL LABORATORY

# Lightning Talks 2021: Theoretical Division

## Solving the quantum simulation problem via signal analysis

August 31, 2021

# Solving the quantum simulation problem via signal analysis

Armando Bellante
Politecnico di Milano

Gopikrishnan Muraleedharan
Theoretical Division, T4

Rolando D. Somma
Theoretical Division, T4

# Quantum simulation problem

Assume access to a system of $n$ qubits in the quantum state $\rho$ and to a Hamiltonian $H$.

We consider the quantum simulation problem whose goal is to compute

$$g_{\rho,H}(t) = Tr[e^{-itH}\rho]$$

within additive error $\epsilon$ and with success probability at least $c$.

# Computing $\overline{g}(t)$ with a quantum computer

This problem is in **BQP**.

Compute $\overline{g}(t) = \overline{\mathfrak{Re}\{g(t)\}} + \overline{\mathfrak{Im}\{g(t)\}}$

- $\overline{\mathfrak{Re}\{g(t)\}} = p_{a,0} - p_{a,1}$
- $\overline{\mathfrak{Im}\{g(t)\}} = p_{b,0} - p_{b,1}$

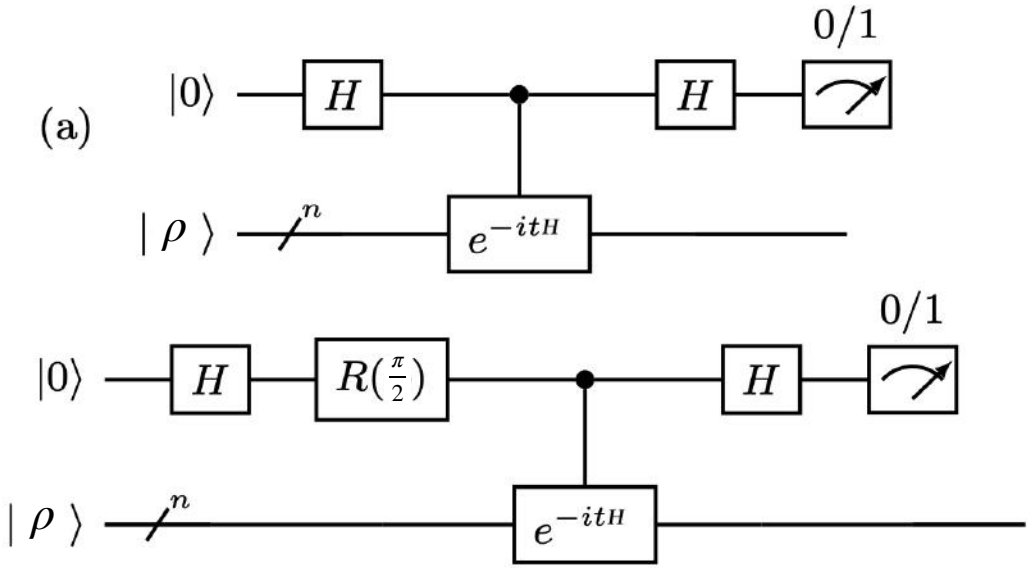


With current NISQ devices we can't run the simulation for too long.

The figure above is a modified version of Fig. 1 from arxiv:2104.08181.

# Quantum simulation with signal analysis

Let $\lambda_j$, $|\psi_j\rangle$ be the $j^{\text{th}}$ eigenvalue and eigenvector of $H$ respectively.

We can write the problem as:

$$g(t) = Tr[e^{-itH}\rho] = \sum_{j}^{M} p_j e^{-i\lambda_j t}$$

where $p_j = |\langle\psi_j|\rho|\psi_j\rangle|^2$ denotes the probability of finding $\rho$ in $|\psi_j\rangle$ and $\sum_{j}^{M} p_j = 1$.

# Quantum simulation with signal analysis

## Signal properties:

- Finite number of components
- Frequencies at $\lambda_j/(2\pi)$
- Complex periodic
- Stationary, mean zero
- $p_j \geq 0, \sum_j p_j = 1$

$$g(t) = Tr[e^{-itH}\rho] = \sum_j^M p_j e^{-i\lambda_j t}$$

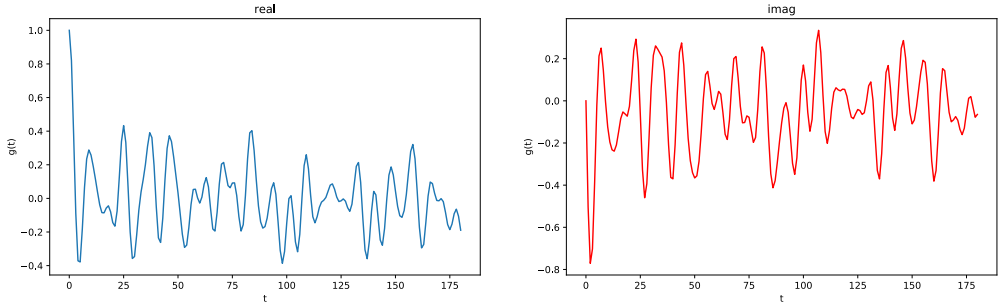

# Quantum simulation with signal analysis

## Signal properties:

- Finite number of components
- Frequencies at $\lambda_j/(2\pi)$
- Complex periodic
- Stationary, mean zero
- $p_j \geq 0, \sum_j p_j = 1$

$$g(t) = Tr[e^{-itH}\rho] = \sum_j^M p_j e^{-i\lambda_j t}$$

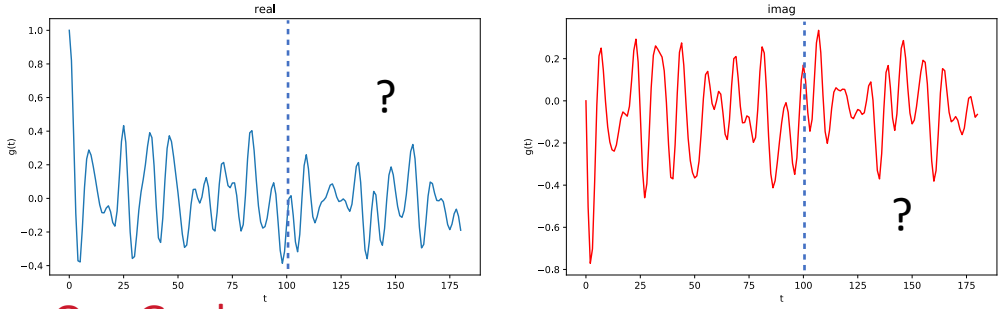


Our Goal:

Given $N$ samples of $g(t)$, to absolute precision $\xi$, at distance $\delta$ one another, we want to predict $g(t')$, with $t' > N\delta$, to absolute precision $\epsilon \sim O(f(t', N, \delta, \xi))$ for some function $f$.

# Why is this problem important?

- Physics simulations (e.g., scattering amplitudes)
- Promising application for current NISQ devices (it is a BQP problem)
- Might provide useful insights in complexity theory

# The approach

# The shift-matrix $\mathfrak{T}$

$$\mathfrak{T}\begin{bmatrix} 1 \\ e^{-i\lambda_j\delta} \\ \dots \\ e^{-i\lambda_j(M-1)\delta} \end{bmatrix} = e^{-i\lambda_j\delta}\begin{bmatrix} 1 \\ e^{-i\lambda_j\delta} \\ \dots \\ e^{-i\lambda_j(M-1)\delta} \end{bmatrix}, \forall j \in [M]$$

# The shift-matrix $\mathfrak{T}$

$$\mathfrak{T}\begin{bmatrix}1\\ e^{-i\lambda_j\delta}\\ \cdots\\ e^{-i\lambda_j(M-1)\delta}\end{bmatrix} = e^{-i\lambda_j\delta}\begin{bmatrix}1\\ e^{-i\lambda_j\delta}\\ \cdots\\ e^{-i\lambda_j(M-1)\delta}\end{bmatrix}, \forall j \in [M]$$

We define $g_k = g(\delta k) = \sum_j^M p_j e^{-i\lambda_j(k\delta)}, k \in \{0,\ldots,N-1\}.$

$$\mathfrak{T}\begin{bmatrix}g_0\\ \cdots\\ g_{M-1}\end{bmatrix} = \mathfrak{T}\sum_j^M p_j\begin{bmatrix}1\\ \cdots\\ e^{-i\lambda_j(M-1)\delta}\end{bmatrix} = \begin{bmatrix}g_1\\ \cdots\\ g_M\end{bmatrix}$$

# The shift-matrix $\mathfrak{T}$

We can compute the shift matrix as:

$$G_0 = \begin{bmatrix} g_0 & g_1 & \cdots & g_{L-1} \\ g_1 & g_2 & \cdots & g_L \\ \cdots & \cdots & \cdots & \cdots \\ g_{N-L-1} & g_{N-L} & \cdots & g_{N-2} \end{bmatrix} \quad G_1 = \begin{bmatrix} g_1 & g_2 & \cdots & g_L \\ g_2 & g_3 & \cdots & g_{L+1} \\ \cdots & \cdots & \cdots & \cdots \\ g_{N-L} & g_{N-L+1} & \cdots & g_{N-1} \end{bmatrix} \qquad \mathfrak{T} = \text{argmin}_{\mathfrak{T}} \|\mathfrak{T} G_0 - G_1\|$$

When $L \geq M$ and $N - L \geq M$, then $e^{-i\lambda_j \delta}$ are among the eigenvalues of $\mathfrak{T}$.

This formulation admits different solutions:

$$\mathfrak{T} = G_0^+ G_1$$

$M$ non-zero eigenvalues

$$\mathfrak{T} = \begin{bmatrix} 0 & 1 & \cdots & 0 \\ \cdots & \cdots & \cdots & \cdots \\ \cdots & \cdots & 0 & 1 \\ a_0 & a_1 & \cdots & a_{L-1} \end{bmatrix}$$

$M$ eigenvalues on the unit circle

# Two ways to go

1. Estimate the parameters $\{p_j, \lambda_j\}$ (*Matrix Pencil* approach):
   - Compute $\mathfrak{T} = G_0^+ G_1$
   - Find the eigenvalues $e^{-i\lambda_j \delta}$ of $\mathfrak{T}$
   - Compute $\begin{bmatrix} \overline{p_0} \\ \overline{p_1} \\ \cdots \\ \overline{p_{M-1}} \end{bmatrix} = \begin{bmatrix} g_0 \\ g_1 \\ \cdots \\ g_{N-1} \end{bmatrix} \begin{bmatrix} 1 & \cdots & 1 \\ e^{-i\lambda_0 \delta} & \cdots & e^{-i\lambda_{M-1}\delta} \\ \cdots & \cdots & \cdots \\ e^{-i\lambda_0 (N-1)\delta} & \cdots & e^{-i\lambda_{M-1}(N-1)\delta} \end{bmatrix}^{-1}$
   - Compute the $\overline{\lambda_j}$ as $ilog_{\mathbb{C}}(e^{-i\lambda_j \delta})$

$$\overline{g}(t) = \sum_j^M \overline{p_j} e^{-i\overline{\lambda_j} t}$$

2. Directly use the approximate shift matrix to predict the signal:

$$\overline{g}(t) = [1 \quad 0 \quad \cdots \quad 0]\, \mathfrak{T}^{t/\delta} \begin{bmatrix} g_0 \\ \cdots \\ g_{M-1} \end{bmatrix}$$

# Numerical Simulations

# Predicting g(t) at long times

- 20 frequencies - amplitudes uniformly at random in (0,1]
- 180 samples, $\delta$=1, 90x90 matrices

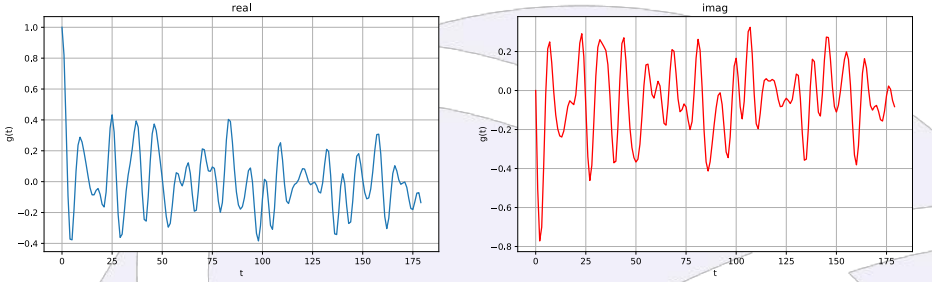


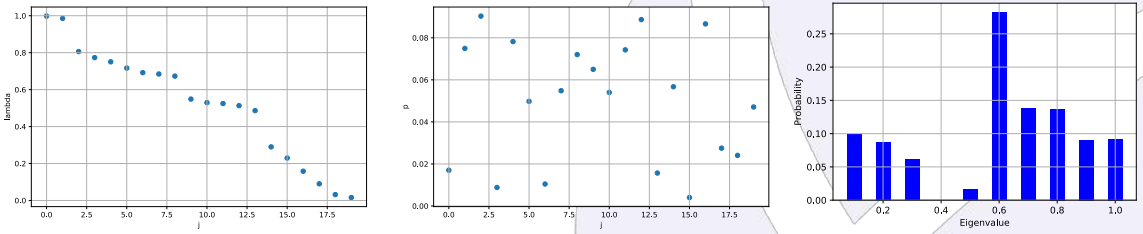

# Predicting g(t) at long times

- 20 frequencies - amplitudes uniformly at random in (0,1]
- 180 samples, $\delta$=1, 90x90 matrices

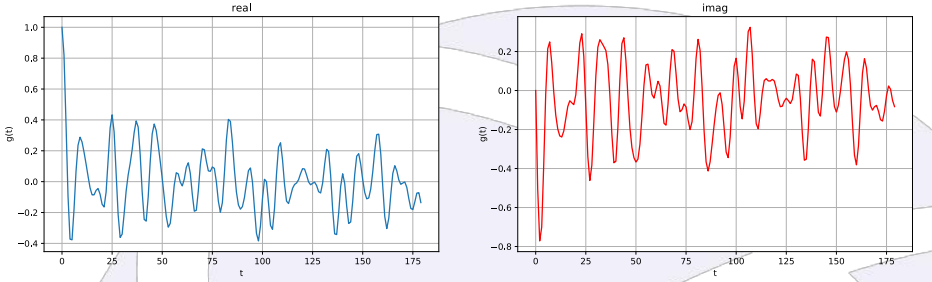


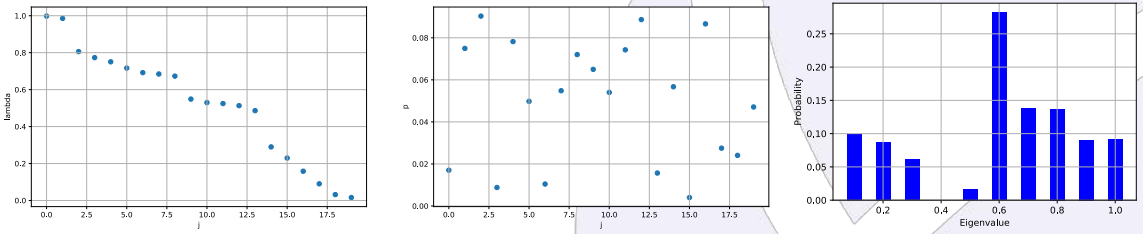


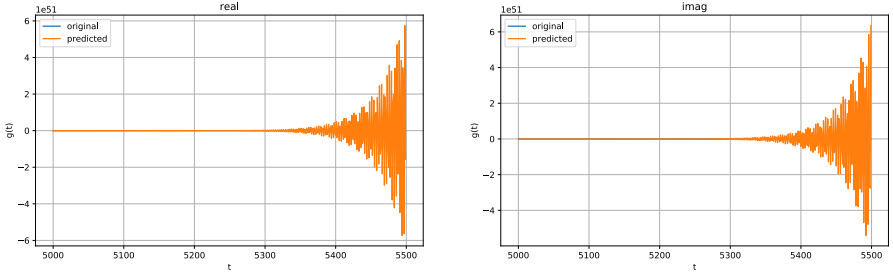


Direct estimation

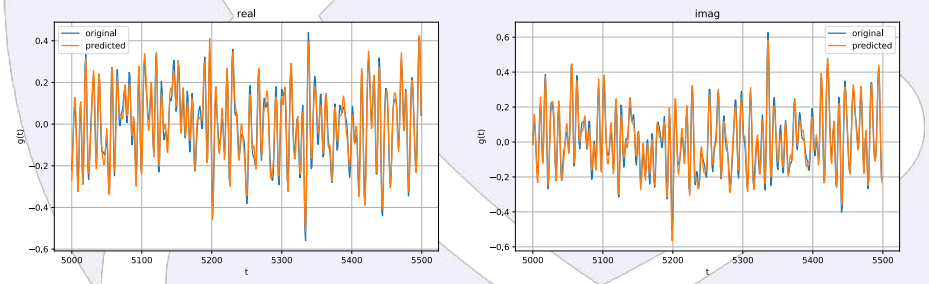


Parametric estimation

# Predicting g(t) at long times

- 1024 frequencies - amplitudes uniformly at random in (0,1] frequencies in 16 bins of 0.001
- 180 samples, $\delta$=1, 90x90 matrices

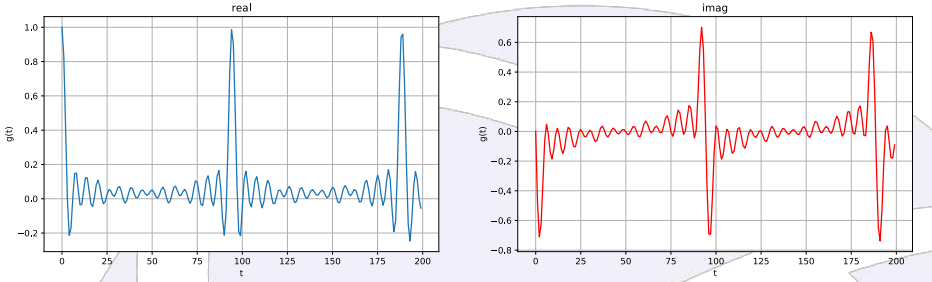


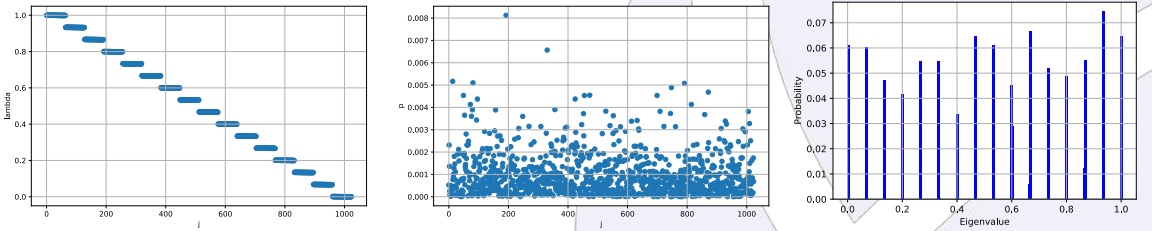


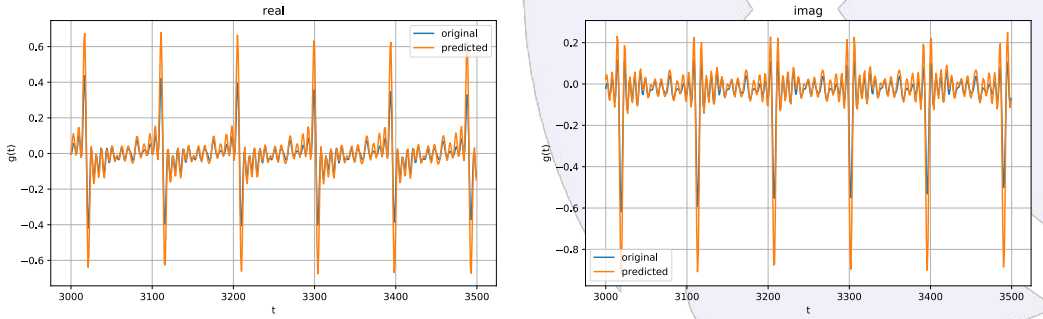


Parametric estimation

# Predicting g(t) at long times

- 1024 frequencies, amplitudes uniformly at random in (0,1]. Noise $\epsilon = 10^{-3}$.
- 180 samples, $\delta$=1, 90x90 matrices

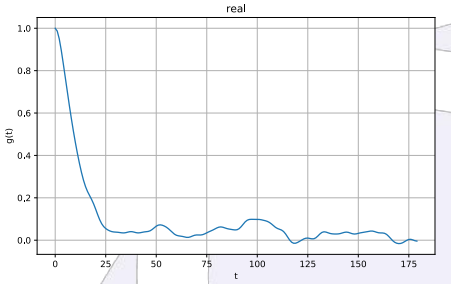


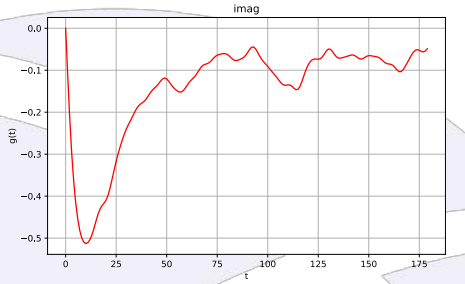


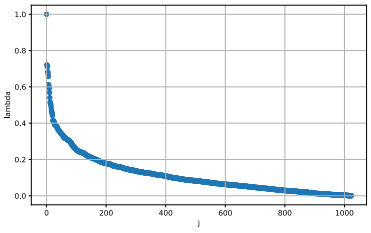


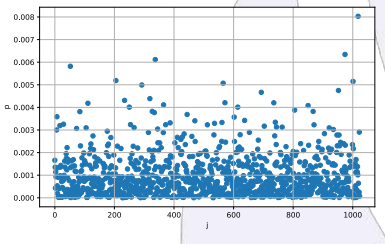


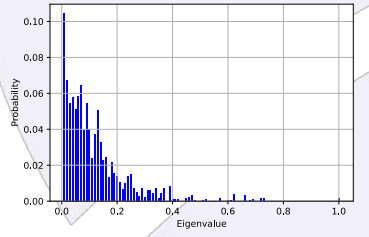


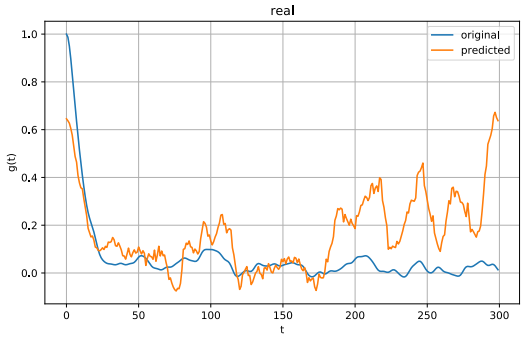


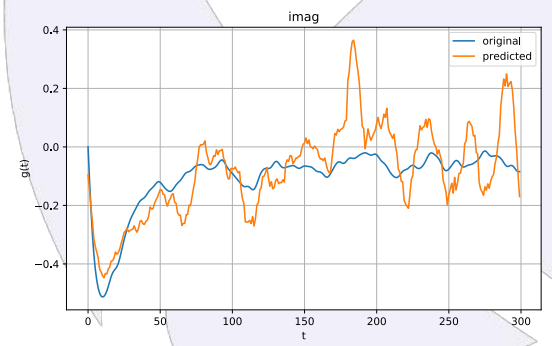


Parametric estimation

# Direct Est. + SVD denoising

- 1024 frequencies, amplitudes uniformly at random in (0,1]. Noise $\epsilon = 10^{-3}$.
- 180 samples, $\delta$=1, 90x90 matrices

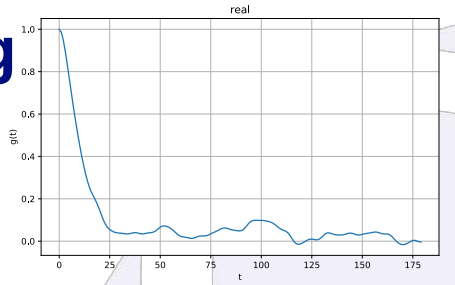


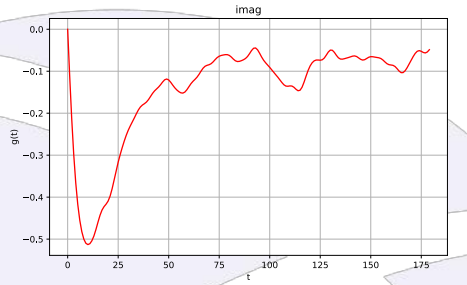


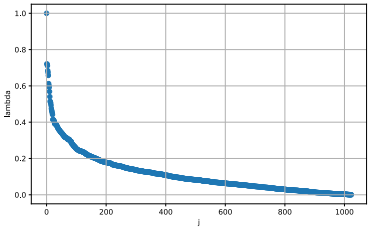


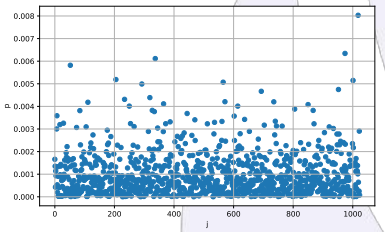


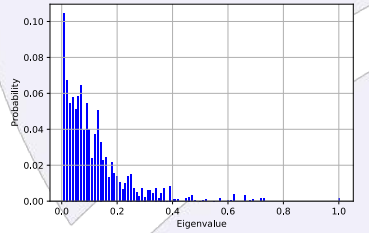


$$\overline{g}(t) = \begin{bmatrix} 1 \\ 0 \\ \cdots \\ 0 \end{bmatrix}^T \mathfrak{T}^{t/\delta} \begin{bmatrix} g_0 \\ \cdots \\ g_{M-1} \end{bmatrix}$$

$$G_0 = \begin{bmatrix} g_0 & g_1 & \cdots & g_{L-1} \\ g_1 & g_2 & \cdots & g_L \\ \cdots & \cdots & \cdots & \cdots \\ g_{N-L-1} & g_{N-L} & \cdots & g_{N-2} \end{bmatrix} \quad G_1 = \begin{bmatrix} g_1 & g_2 & \cdots & g_L \\ g_2 & g_3 & \cdots & g_{L+1} \\ \cdots & \cdots & \cdots & \cdots \\ g_{N-L} & g_{N-L+1} & \cdots & g_{N-1} \end{bmatrix}$$

$$G = \begin{bmatrix} g_0 & g_1 & \cdots & \cdots & g_L \\ g_1 & g_2 & \cdots & \cdots & g_{L+1} \\ \cdots & \cdots & \cdots & \cdots & \cdots \\ g_{N-L-1} & g_{N-L} & \cdots & \cdots & g_{N-1} \end{bmatrix}$$

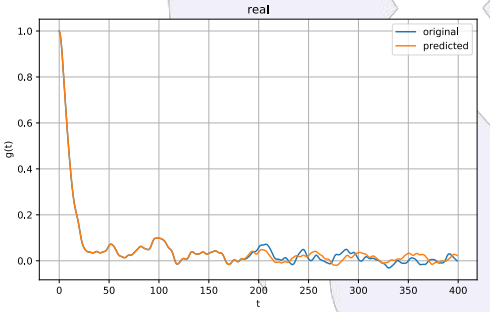


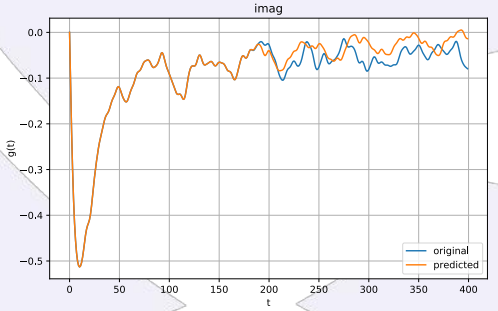


Direct estimation

# Analytical bounds - Sampling error + known freq.

- Perfect knowledge of $\lambda_j$s
- Error $\epsilon$ on the signal estimates $\|\mathbf{g} - \overline{\mathbf{g}}\|_1 \leq \epsilon$

$$\overline{g}(t) = \sum_j^M \overline{p}_j e^{-i\lambda_j t}$$

$$\begin{bmatrix} 1 & \cdots & 1 \\ e^{-i\lambda_0\delta} & \cdots & e^{-i\lambda_{M-1}\delta} \\ \cdots & \cdots & \cdots \\ e^{-i\lambda_0(N-1)\delta} & \cdots & e^{-i\lambda_{M-1}(N-1)\delta} \end{bmatrix} \begin{bmatrix} \overline{p}_0 \\ \overline{p}_1 \\ \cdots \\ \overline{p}_{M-1} \end{bmatrix} = \begin{bmatrix} \overline{g}_0 \\ \overline{g}_1 \\ \cdots \\ \overline{g}_{N-1} \end{bmatrix}$$

$$\left| g(t) - \overline{g}(t) \right| \leq \|p - \overline{p}\|_1$$

$$\|p - \overline{p}\|_1 \leq \|Q^{-1}\|\epsilon \quad \Longrightarrow \quad \left| g(t) - \overline{g}(t) \right| \leq \|Q^{-1}\|\epsilon$$

# Analytical bounds - Sampling error + known freq.

- Perfect knowledge of $\lambda_j$s
- Error $\epsilon$ on the signal estimates $\|\mathbf{g} - \overline{\mathbf{g}}\|_1 \leq \epsilon$

$$\overline{g}(t) = \sum_j^M \overline{p}_j e^{-i\lambda_j t}$$

$$\begin{bmatrix} 1 & \cdots & 1 \\ e^{-i\lambda_0\delta} & \cdots & e^{-i\lambda_{M-1}\delta} \\ \cdots & \cdots & \cdots \\ e^{-i\lambda_0(N-1)\delta} & \cdots & e^{-i\lambda_{M-1}(N-1)\delta} \end{bmatrix} \begin{bmatrix} \overline{p}_0 \\ \overline{p}_1 \\ \cdots \\ \overline{p}_{M-1} \end{bmatrix} = \begin{bmatrix} \overline{g}_0 \\ \overline{g}_1 \\ \cdots \\ \overline{g}_{N-1} \end{bmatrix}$$

$$\left| g(t) - \overline{g}(t) \right| \leq \|p - \overline{p}\|_1$$

$$\|p - \overline{p}\|_1 \leq \|Q^{-1}\|\epsilon \quad \Longrightarrow \quad \left| g(t) - \overline{g}(t) \right| \leq \|Q^{-1}\|\epsilon$$

However, $\|Q^{-1}\|$ can be very large, particularly if you have two frequencies that are close to each other

# Overcoming the bound

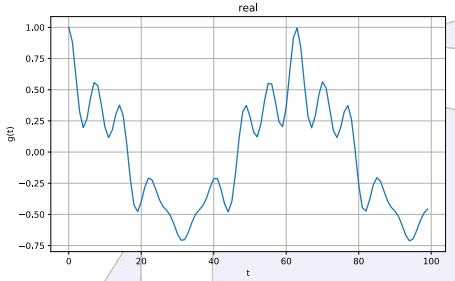


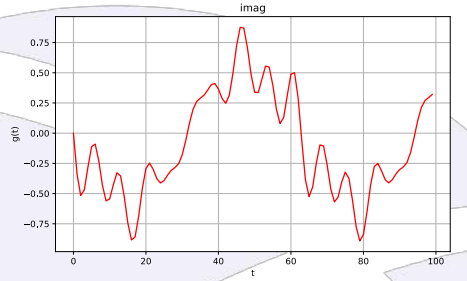


- 5 frequencies - amplitudes
  $\lambda_j$s = [0.1, 0.1001, 0.5, 0.8, 0.9]
  $p$ = [0.28571429, 0.28571429, 0.14285714, 0.14285714, 0.14285714]
- 5 samples, noise $\epsilon = 10^{-3}$

$$\bar{p} = \arg\min_{p} \|Qp - \bar{g}\|$$

$\|p - \bar{p}\|_1 = 361.14$ $\quad\quad$ $\|Q\bar{p} - \bar{g}\| = 3 \cdot 10^{-13}$

$\|Q^{-1}\|\|\mathbf{g} - \bar{\mathbf{g}}\|_1 = 449.82$

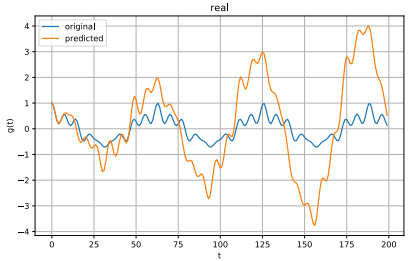


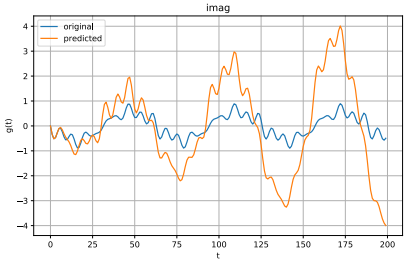

# Overcoming the bound

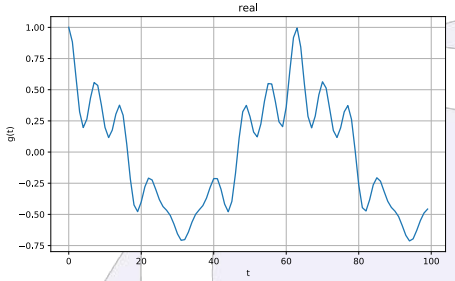


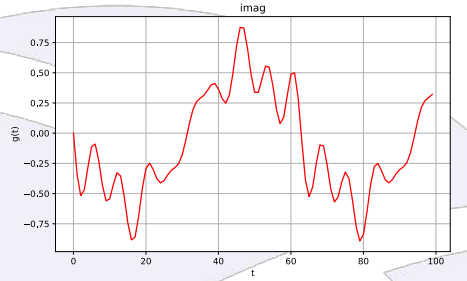


- 5 frequencies - amplitudes
  $\lambda_j$s = [0.1, 0.1001, 0.5, 0.8, 0.9]
  $p$ = [0.28571429, 0.28571429, 0.14285714, 0.14285714, 0.14285714]
- 5 samples, noise $\epsilon = 10^{-3}$

$$\bar{p} = \arg\min_{p} \|Qp - \bar{g}\|$$

$\|p - \bar{p}\|_1 = 361.14$
$\|Q^{-1}\|\|\mathbf{g} - \bar{\mathbf{g}}\|_1 = 449.82$

$\|Q\bar{p} - \bar{g}\| = 3 \cdot 10^{-13}$

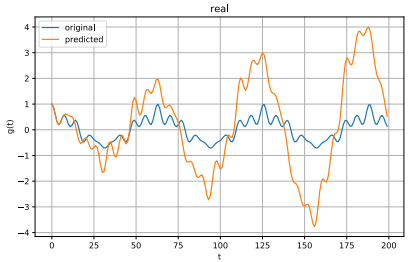


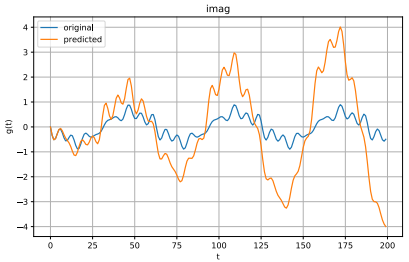


Non-Negative least square

$$\bar{p} = \arg\min_{p} \|Qp - \bar{g}\| \; s.t. \; p > 0$$

$\|p - \bar{p}\|_1 = 0.71$

$\|Q\bar{p} - \bar{g}\| = 0.018$

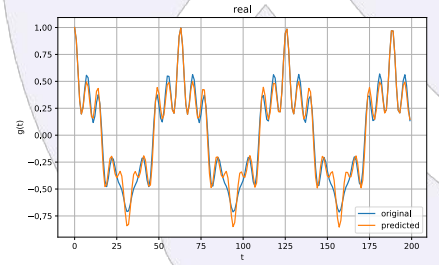


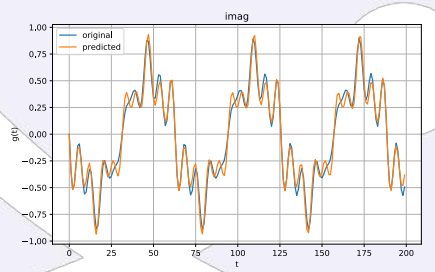

# An adversarial case

$$\rho_+ = |GHZ_+\rangle\langle GHZ_+| \qquad H = \frac{1}{n}\sum_j^n Y_j$$
$$\rho_- = |GHZ_-\rangle\langle GHZ_-|$$

where $|GHZ_\pm\rangle = \frac{1}{\sqrt{2}}(|00\cdots\rangle \pm |11\cdots\rangle)$ and $Y_j$ are the Pauli operators.

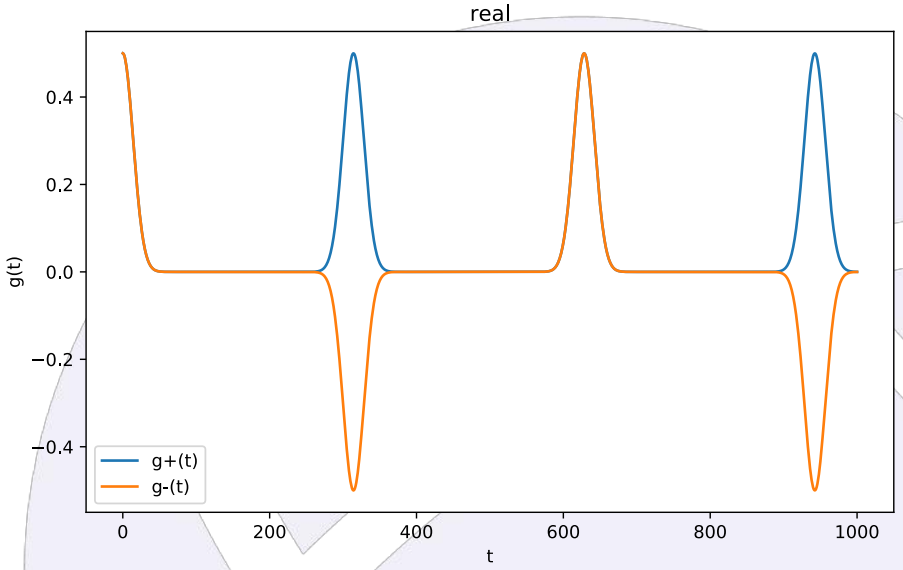


$$g_+(t) = \frac{1}{2}[cos(t/n)^n + sin(t/n)^n] \qquad g_-(t) = \frac{1}{2}[cos(t/n)^n - sin(t/n)^n]$$

These functions are exponentially close and they start differing significantly at $t \sim \Omega(n)$.

# Thanks!

Predict $g(t)$ at longer times from short time evolutions by modeling the quantum simulation problem as a signal problem.

Key takeaways:

- We can frame this quantum simulation problem as a signal analysis one.
- There is hope to predict $g(t)$ from short-time measurements, though some signals are harder than others.
- Non-negative least square and SVD denoising can help in case of sampling error.

Future works:

- Study how the distribution of frequencies/amplitudes affects the prediction.
- Refine the bounds in case of sampling error with non-negative least square.
- Study to what extent we can use the same shift matrix when we use the same $H$ on two different states $\rho_1, \rho_2$.

# Theory and modeling of quantum mechanical transport for electron and negative-ion sources

Group: T-CNLS, T-5
Mentor(s): Chengkun Huang, Andrei Piryatinski, Anna Marie Alexander
Student Status: GRA
School Affiliation: Michigan State University
PhD Advisor: Prof. Peng Zhang

# Acknowledgement


- Diamond emitter modeling project:
  - H. L. Andrews, R. C. Baker, R. L. Fleming, C.-K. Huang, D. Kim, T. J. T. Kwan, A. Piryatinski, V. Pavlenko, E. I. Simakov ; LANL
- Negative ion source project:
  - Anna Alexander, Heather Andrews, Chengkun Huang, En-chuan Huang, and Dongsung Kim, Rod McCrady, Anju Poudel ; LANL
  - Peng Zhang ; MSU

# Motivation

- Electron and negative-ion sources are critical for fusion, high-energy particle accelerators, neutron generation, and mass spectroscopy.
- Both electron and negative-ion sources rely on field emission.
- Electron field emission → quantum mechanical tunneling of electrons from surfaces under a strong bias electric field
- Nanotip based electron emission sources produce high current electron beams.
- Electron transport and emission properties of a diamond nanotip have been investigated by Ref [1], including the effects of quantum confinement.
- A comprehensive study of beam's transverse properties is required.
- The state-of-art models [2][3] to characterize negative ion sources use assumptions to simplify the charge transfer process from surface-to-atom.

[1] Piryatinski et al., J. Appl. Phys. 125, 214301 (2019)
[2] M.E. Kishinevskii, Zh. Tekh. Fiz. 48, 1281 (1978)
[3] Vadim Dudnikov, "Development and Applications of Negative-Ion Sources", Springer (2019)

# Introduction

## Electron transport and emission from a semiconductor nanotip modeling

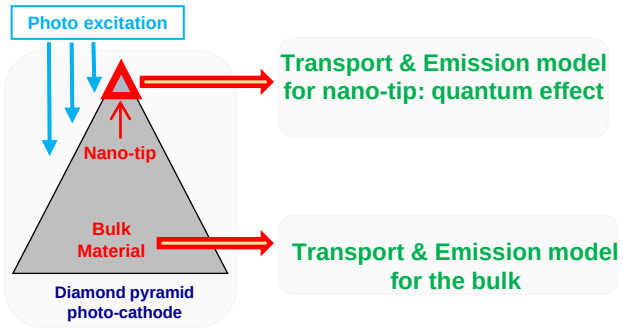


Piryatinski et al., J. Appl. Phys. 125, 214301 (2019)

### Goals

- To investigate the transverse properties of the emitted electron beam.
- To improve the divergence ratio.

## Negative-Ion Source Modeling

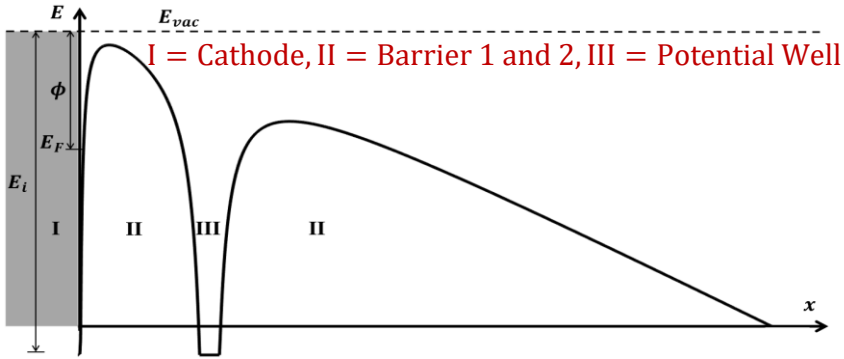


Potential near the cathode surface in the presence of an ion/atom

### Goals

- To model the resonant electron transfer process from cathode to nearby atoms.
- To improve the negative ion yield.

# Electron Emission from Diamond Nanotip

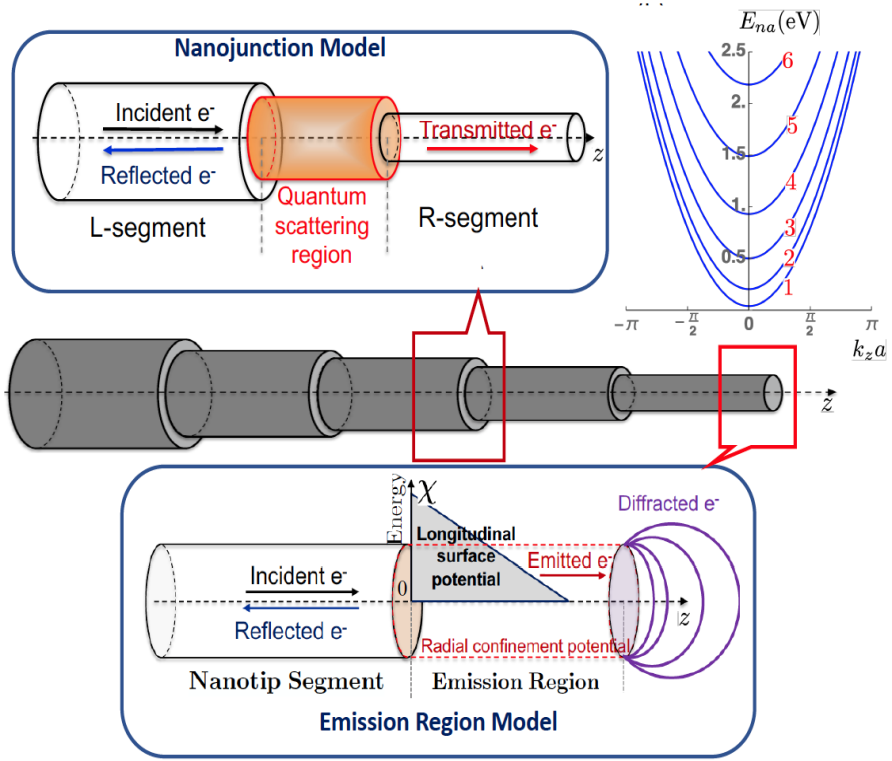


Priyatinski et al., J. Appl. Phys. 125, 214301 (2019)

- Methods : Monte Carlo approach combined with scattering and emission models. Includes the effects of conduction band quantization and electron-phonon scattering.
- Radial momentum $\kappa_\alpha$
- Longitudinal momentum

$$k_z = \sqrt{\frac{2m}{\hbar^2}(E - V) - \kappa_\alpha^2}.$$

- $Divergence\ ratio = \frac{\kappa_\alpha}{k_z}$

# Divergence Ratio of the Emitted Beam

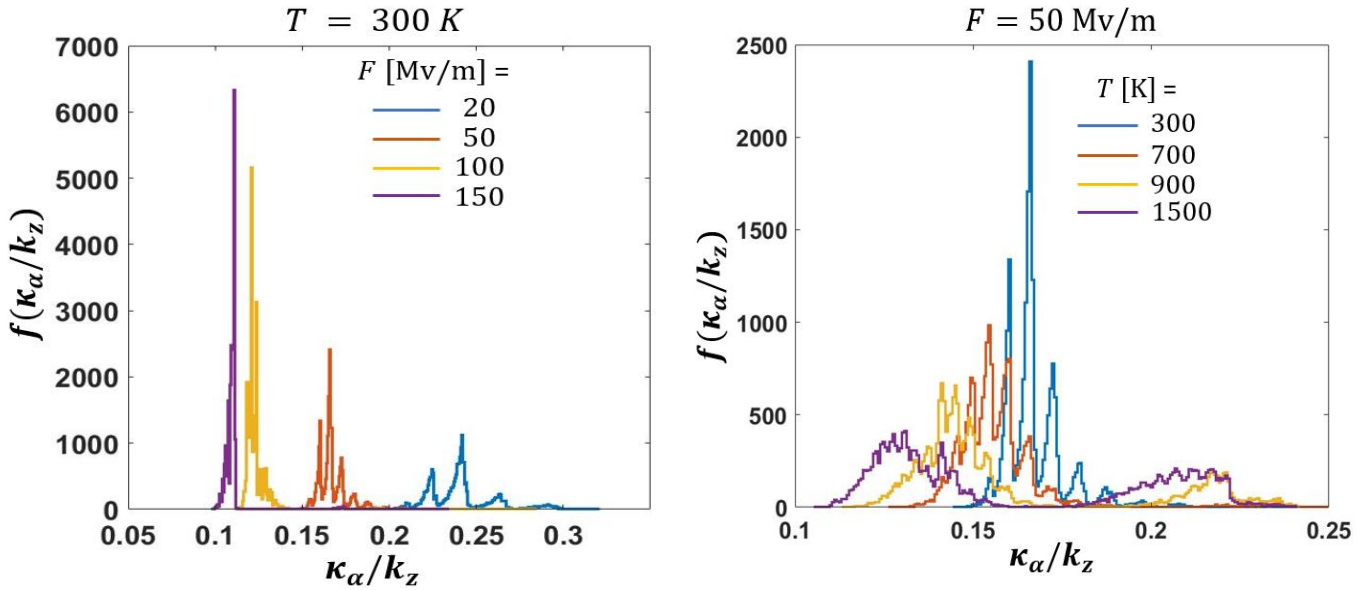


- $\frac{\kappa_\alpha}{k_z}$ decreases when external field F increases. The spread of the histograms also decreases.
- $\frac{\kappa_\alpha}{k_z}$ decreases when temperature T increases. However, the spread increases because more electrons move to higher quantum state n.

# Negative Ion Source Modeling

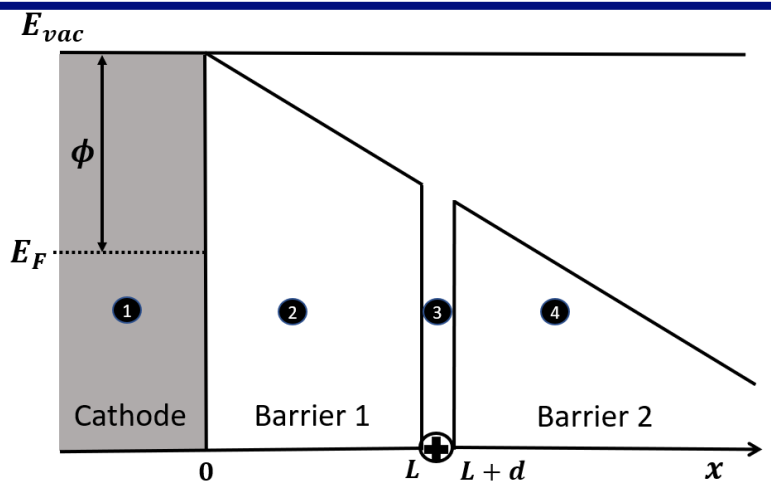


**Objective:**
To calculate the probability of trapping or yield $\beta$ and investigate its parametric dependence.

- Analytically solved $-\frac{\hbar^2}{2m}\frac{d^2\psi}{dx^2} - [V(x) - E]\psi = 0$ in region 1, 2, 3, 4.

In (1) : $\psi_1(x) = a_1 \exp(ik_1 x)$, In (2) : $\psi_2(x) = a_2 Ai(-\eta) + b_2 Bi(-\eta)$

In (3) : $\psi_3(x) = a_3 \exp(ik_3 x) + b_3 \exp(-ik_3 x)$, In (4) : $\psi_4(x) = a_4\big(Ai(-\eta) - iBi(-\eta)\big)$

- Total outgoing flux is calculated from $\psi_1(x)$ and $\psi_4(x)$
- $\beta$ is calculated from [1]



[1] R K Janev 1974 J. Phys. B: Atom. Mol. Phys. 7 1506

# Yield of The Negative Ion Source

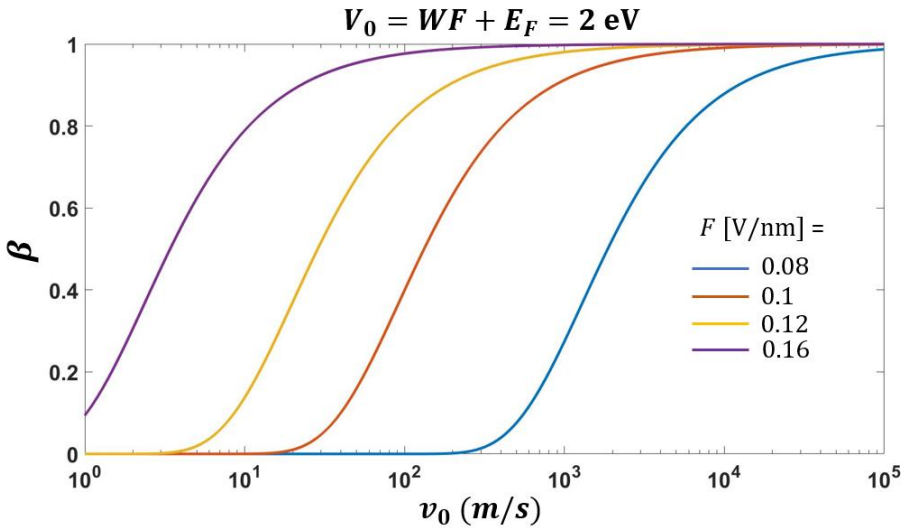


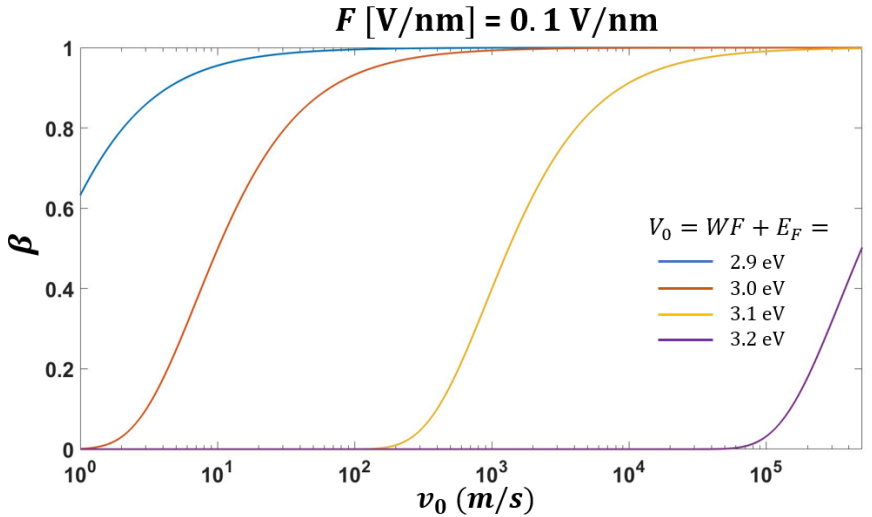


- Trapping probability $\beta$ increases with the velocity of the atom $v_0$.
- $\beta$ increases with applied field $F$ and decreases with work function of the cathode.

# Summary and Future Work

- We investigated the divergence ratio of an electron beam emitted from a diamond nanotip, and found it depends on applied field, temperature, and initial quantum states.
- In future, the Monte Carlo transport and scattering model can be extended to include bulk transport and arbitrary number of nanowire segments.

- We have developed an analytical framework to model a negative ion source. We found that the trapping probability depends on atom velocity, applied field and work function of the cathode.
- In future, negative ion yield can be investigated for
  - i) different electron excitation, ii) electron affinity levels of the cathode surface, iii) properties of the approaching atoms.

# Thank you!

# Learning to Accelerate Globally Optimal Solutions to the AC Optimal Power Flow Problem

Presenter: Fatih Cengil
Mentors: Harsha Nagarajan (T-5), Russell Bent (T-5)

09.02.2021

# Table of Contents

1. AC Optimal Power Flow Problem

2. Overview of the Optimality–based Bound Tightening (OBBT) Algorithm

3. Deep Neural Network for the ACOPF Problem

4. Preliminary Results

# Learning to Accelerate Globally Optimal Solutions to the AC Optimal Power Flow Problem

## Power Flow Network

- Bus
- Branch
- Generator
- Admittance on branch
- Voltage
- Phase angle difference
- Apparent power
- Reactive power
- Power demand

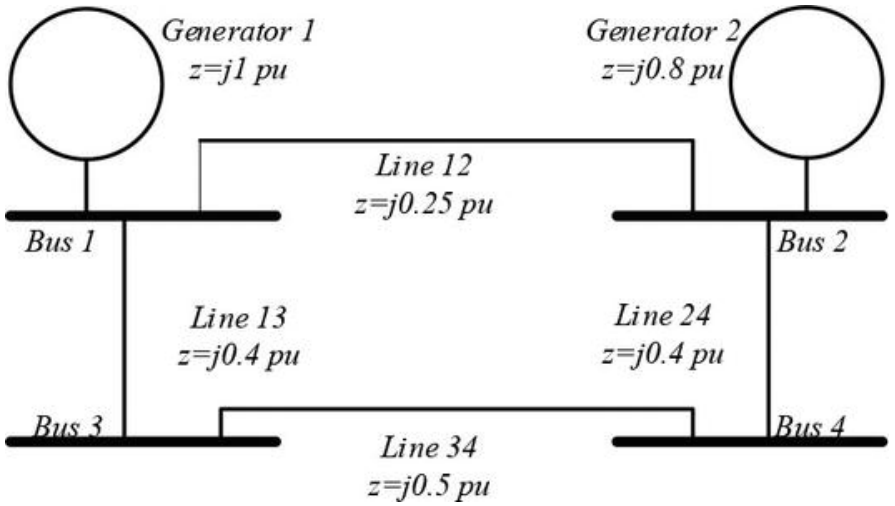

# Learning to Accelerate Globally Optimal Solutions to the AC Optimal Power Flow Problem

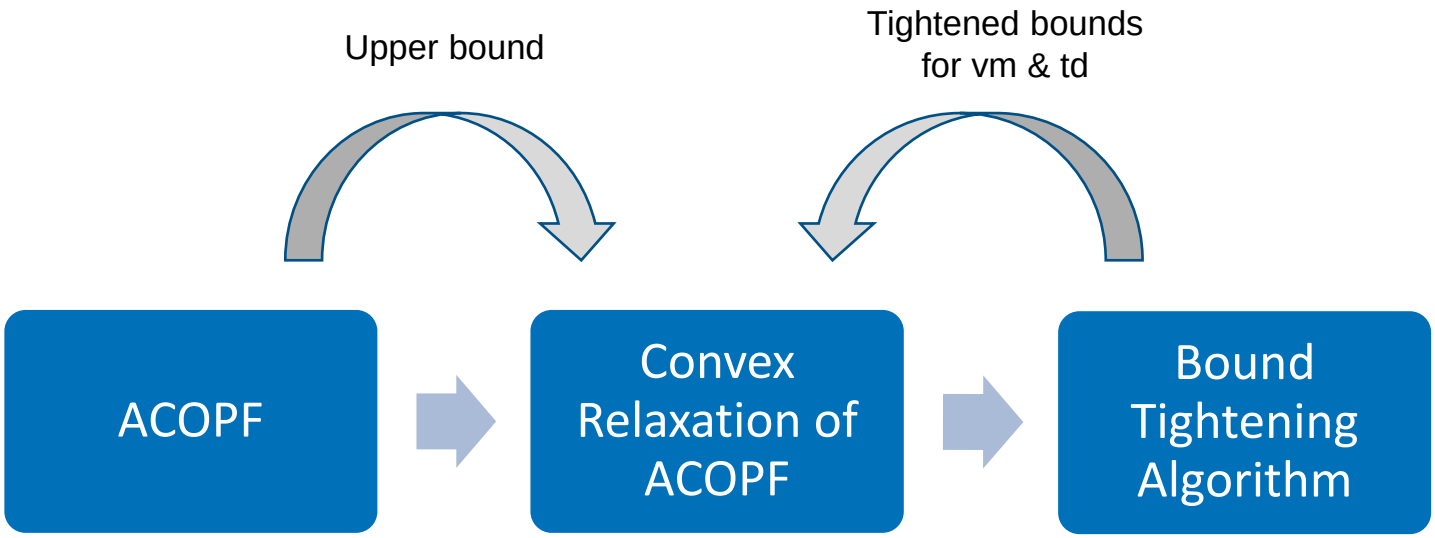


vm: Voltage magnitude

td: Phase angle difference

- Optimization-Based Bound Tightening using a Strengthened QC-Relaxation of the Optimal Power Flow Problem
- K. Sundar, H. Nagarajan, S. Misra, M. Lu, C. Coffrin, R. Bent
- arXiv:1809.04565

# Learning to Accelerate Globally Optimal Solutions to the AC Optimal Power Flow Problem

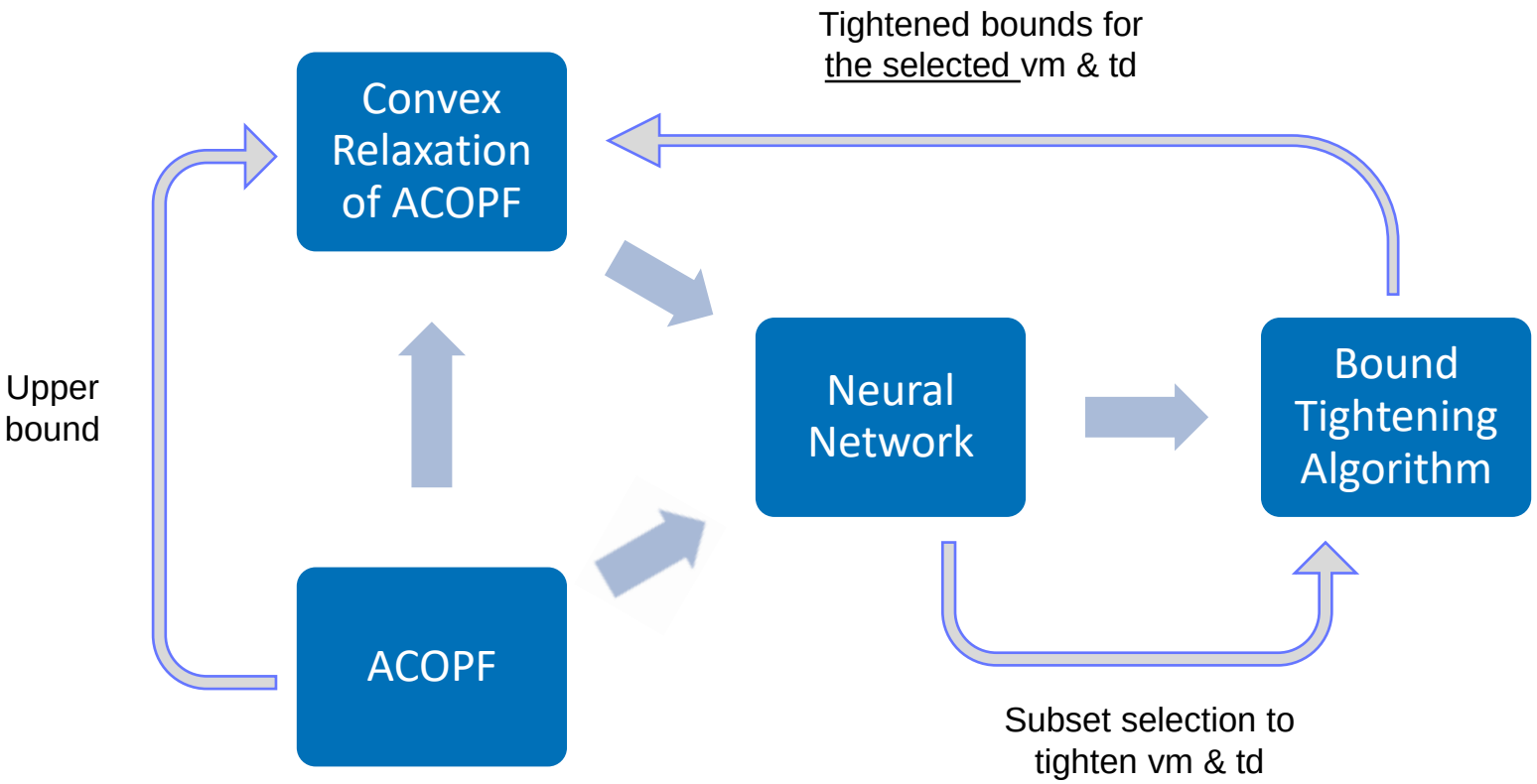

# Learning to Accelerate Globally Optimal Solutions to the AC Optimal Power Flow Problem

**Model 1** AC Optimal Power Flow (AC-OPF) problem

$$\textbf{minimize:} \quad \sum_{i \in \mathcal{G}} c_{2i}(\Re(S_i^g)^2) + c_{1i}\Re(S_i^g) + c_{0i} \tag{1a}$$

**subject to:**

$$\sum_{k \in \mathcal{G}_i} S_k^g - \boldsymbol{S_i^d} = \sum_{(i,j) \in \mathcal{E} \cup \mathcal{E}^{\mathcal{R}}} S_{ij} \quad \forall i \in \mathcal{N} \tag{1b}$$

$$S_{ij} = \boldsymbol{Y_{ij}^*} W_{ii} - \boldsymbol{Y_{ij}^*} W_{ij} \quad \forall (i,j) \in \mathcal{E} \tag{1c}$$

$$S_{ji} = \boldsymbol{Y_{ij}^*} W_{jj} - \boldsymbol{Y_{ij}^*} W_{ij}^* \quad \forall (i,j) \in \mathcal{E} \tag{1d}$$

$$W_{ii} = |V_i|^2 \quad \forall i \in \mathcal{N} \tag{1e}$$

$$W_{ij} = V_i V_j^* \quad \forall (i,j) \in \mathcal{E} \tag{1f}$$

$$\boldsymbol{\theta_{ij}^l} \leqslant \theta_{ij} \leqslant \boldsymbol{\theta_{ij}^u} \quad \forall (i,j) \in \mathcal{E} \tag{1g}$$

$$(\boldsymbol{v_i^l})^2 \leqslant W_{ii} \leqslant (\boldsymbol{v_i^u})^2 \quad \forall i \in \mathcal{N} \tag{1h}$$

$$\boldsymbol{S_i^{gl}} \leqslant S_i^g \leqslant \boldsymbol{S_i^{gu}} \quad \forall i \in \mathcal{G} \tag{1i}$$

$$|S_{ij}| \leqslant \boldsymbol{s_{ij}^u} \quad \forall (i,j) \in \mathcal{E} \cup \mathcal{E}^{\mathcal{R}} \tag{1j}$$

- Optimization-Based Bound Tightening using a Strengthened QC-Relaxation of the Optimal Power Flow Problem
- K. Sundar, H. Nagarajan, S. Misra, M. Lu, C. Coffrin, R. Bent
- arXiv:1809.04565

# Learning to Accelerate Globally Optimal Solutions to the AC Optimal Power Flow Problem

## Relaxation of Non-linear, Non-convex Terms

$$W_{ii} = v_i^2 \quad \forall i \in \mathcal{N} \qquad \langle x^2 \rangle^T \equiv \begin{cases} \breve{x} \geqslant x^2 \\ \breve{x} \leqslant (\boldsymbol{x^u} + \boldsymbol{x^l})x - \boldsymbol{x^u}\boldsymbol{x^l} \end{cases}$$

$$W_{ij} = V_i V_j^* \quad \forall (i,j) \in \mathcal{E} \qquad \langle xy \rangle^M \equiv \begin{cases} \breve{xy} \geqslant \boldsymbol{x^l}y + \boldsymbol{y^l}x - \boldsymbol{x^l}\boldsymbol{y^l} \\ \breve{xy} \geqslant \boldsymbol{x^u}y + \boldsymbol{y^u}x - \boldsymbol{x^u}\boldsymbol{y^u} \\ \breve{xy} \leqslant \boldsymbol{x^l}y + \boldsymbol{y^u}x - \boldsymbol{x^l}\boldsymbol{y^u} \\ \breve{xy} \leqslant \boldsymbol{x^u}y + \boldsymbol{y^l}x - \boldsymbol{x^u}\boldsymbol{y^l} \end{cases}$$

$$\Re(W_{ij}) = v_i v_j \cos(\theta_{ij}) \quad \forall (i,j) \in \mathcal{E}$$
$$\Im(W_{ij}) = v_i v_j \sin(\theta_{ij}) \quad \forall (i,j) \in \mathcal{E}$$

$$\langle \cos(x) \rangle^C \equiv \begin{cases} \breve{cs} \leqslant 1 - \frac{1-\cos(\boldsymbol{x^m})}{(\boldsymbol{x^m})^2}x^2 \\ \breve{cs} \geqslant \frac{\cos(\boldsymbol{x^l})-\cos(\boldsymbol{x^u})}{(\boldsymbol{x^l}-\boldsymbol{x^u})}(x - \boldsymbol{x^l}) + \cos(\boldsymbol{x^l}) \end{cases}$$

$$\langle \sin(x) \rangle^S \equiv \begin{cases} \breve{sn} \leqslant \cos\left(\frac{\boldsymbol{x^m}}{2}\right)\left(x - \frac{\boldsymbol{x^m}}{2}\right) + \sin\left(\frac{\boldsymbol{x^m}}{2}\right) \\ \breve{sn} \geqslant \cos\left(\frac{\boldsymbol{x^m}}{2}\right)\left(x + \frac{\boldsymbol{x^m}}{2}\right) - \sin\left(\frac{\boldsymbol{x^m}}{2}\right) \\ \breve{sn} \geqslant \frac{\sin(\boldsymbol{x^l})-\sin(\boldsymbol{x^u})}{(\boldsymbol{x^l}-\boldsymbol{x^u})}(x-\boldsymbol{x^l})+\sin(\boldsymbol{x^l}) \text{ if } \boldsymbol{x^l} \geqslant 0 \\ \breve{sn} \leqslant \frac{\sin(\boldsymbol{x^l})-\sin(\boldsymbol{x^u})}{(\boldsymbol{x^l}-\boldsymbol{x^u})}(x-\boldsymbol{x^l})+\sin(\boldsymbol{x^l}) \text{ if } \boldsymbol{x^u} \leqslant 0 \end{cases}$$

$$\Re(W_{ij}) = \langle v_i v_j \breve{cs}_{ij} \rangle \quad \forall (i,j) \in \mathcal{E}$$
$$\Im(W_{ij}) = \langle v_i v_j \breve{sn}_{ij} \rangle \quad \forall (i,j) \in \mathcal{E}$$

$$\langle x_1 x_2 x_3 \rangle^\lambda \equiv \begin{cases} \breve{x} = \sum_{k=1}^8 \lambda_i \, \varphi(\boldsymbol{\xi_k^1}, \boldsymbol{\xi_k^2}, \boldsymbol{\xi_k^3}) \\ x_i = \sum_{k=1}^8 \lambda_k \, \boldsymbol{\xi_k^i} \quad \forall i = 1,2,3 \\ \sum_{k=1}^8 \lambda_k = 1, \quad \lambda_k \geqslant 0 \quad \forall k = 1,\ldots,8 \end{cases}$$

# Learning to Accelerate Globally Optimal Solutions to the AC Optimal Power Flow Problem

**Algorithm 1** The OBBT Algorithm

**Input:** A QC Relaxation (Model 2/3/4) to construct $\Omega$
**Output:** $v^{l}$, $v^{u}$, $\theta^{l}$, $\theta^{u}$

1: **repeat**
2: $\quad v^{l0}, v^{u0}, \theta^{l0}, \theta^{u0} \leftarrow v^{l}, v^{u}, \theta^{l}, \theta^{u}$
3: $\quad \Omega \leftarrow$ QC relaxation given $v^{l0}, v^{u0}, \theta^{l0}, \theta^{u0}$
4: $\quad$ **for all** $i \in \mathcal{N}$ **do**
5: $\quad\quad v_i^{l} \leftarrow \min\{v_i : \Omega\}$
6: $\quad\quad v_i^{u} \leftarrow \max\{v_i : \Omega\}$
7: $\quad$ **for all** $(i,j) \in \mathcal{E}$ **do**
8: $\quad\quad \theta_{ij}^{l} \leftarrow \min\{\theta_{ij} : \Omega\}$
9: $\quad\quad \theta_{ij}^{u} \leftarrow \max\{\theta_{ij} : \Omega\}$
10: **until** $v^{l0}, v^{u0}, \theta^{l0}, \theta^{u0} = v^{l}, v^{u}, \theta^{l}, \theta^{u}$

- Optimization-Based Bound Tightening using a Strengthened QC-Relaxation of the Optimal Power Flow Problem
- K. Sundar, H. Nagarajan, S. Misra, M. Lu, C. Coffrin, R. Bent
- arXiv:1809.04565

# Learning to Accelerate Globally Optimal Solutions to the AC Optimal Power Flow Problem

- Relaxed terms
  - Sin
  - Cos
  - Trilinear terms
  - Voltage magnitude
  - Phase angle difference
- Power flows
  - Real power
  - Reactive power
- Power generation

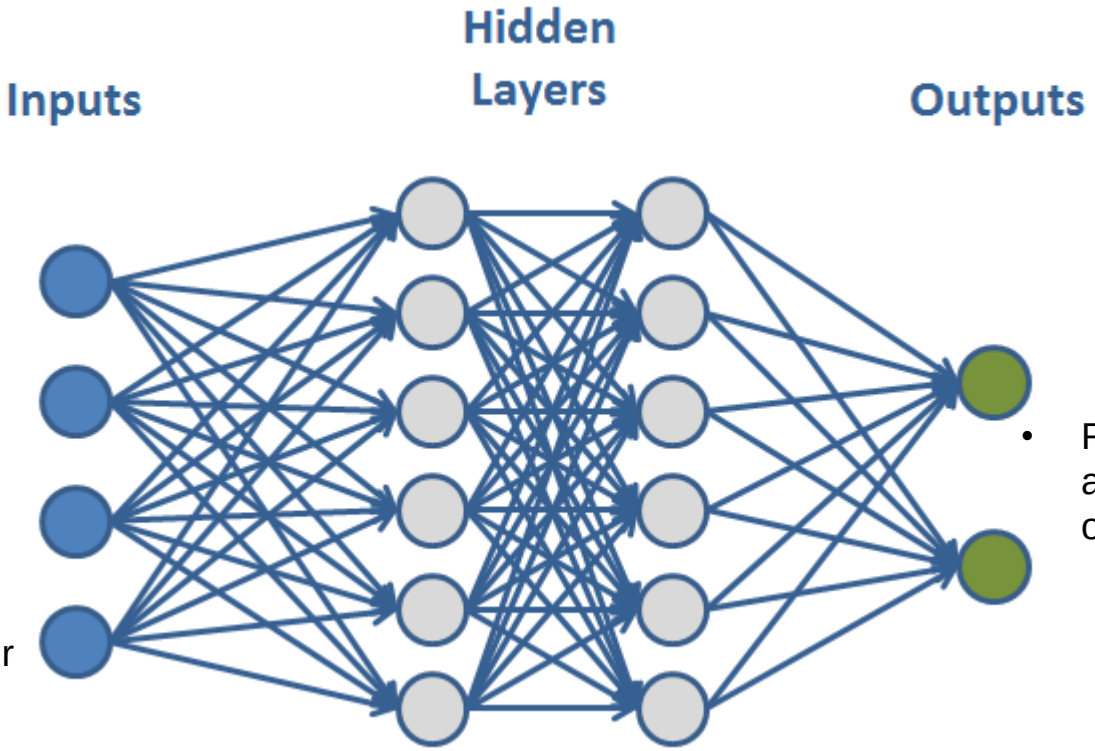


- Ranking of the buses and branches in terms of subset selection

- Activation function: ReLU, Sigmoid
- Optimizer: Adam
- Loss Function: Mean Squared Error (MSE)

# Learning to Accelerate Globally Optimal Solutions to the AC Optimal Power Flow Problem

## Preliminary Results

| | | | | Optimality Gap (%) | | | Average running time (sec.) | | |
|---|---|---|---|---|---|---|---|---|---|
| **Instances** | **\|N\|** | **\|E\|** | **R-Squared** | **TLM w/out OBBT** | **GO-OBBT w/out NN** | **GO-OBBT with NN** | **GO-OBBT w/out NN** | **GO-OBBT with NN** | **Time reduction (%)** |
| case14_ieee__api | 14 | 20 | 0.94 | 5.13% | 0.08% | 0.71% | 25.7 | 9.3 | 63.8% |
| case14_ieee__sad | 14 | 20 | 0.85 | 19.16% | 0.18% | 0.44% | 30.1 | 15.4 | 48.9% |
| case30_ieee | 30 | 41 | 0.62 | 5.45% | 0.16% | 0.23% | 64.9 | 49.6 | 23.6% |
| case30_ieee__api | 30 | 41 | 0.66 | 18.67% | 0.09% | 0.75% | 209.0 | 52.2 | 75.0% |
| case30_ieee__sad | 30 | 41 | 0.71 | 5.66% | 0.04% | 0.14% | 65.2 | 44.0 | 32.6% |
| case73_ieee_rts__sad | 73 | 120 | 0.52 | 2.37% | 0.03% | 0.46% | 571.2 | 437.0 | 23.5% |

# Thank you!

# Spin dynamics in the Kagome lattice

Abigail A. Coker, GRA
Academic Institution: University of Utah
Mentor: Jian-Xin Zhu, T-4/CNLS

August 3rd, 2021

LA-UR-21-27684

# Magnetism for technological advancement

R. Morganstein. 2006. https://www.morgenstein.com/

A bottleneck in technological advancement:

- Limitations on the size, speed, and reliability of electronic computing devices
- Look to quantum mechanics
- Solutions in magnetism

Quantum ‘spin’:

- Magnons for information transport
- Spin liquid state for topological quantum computers

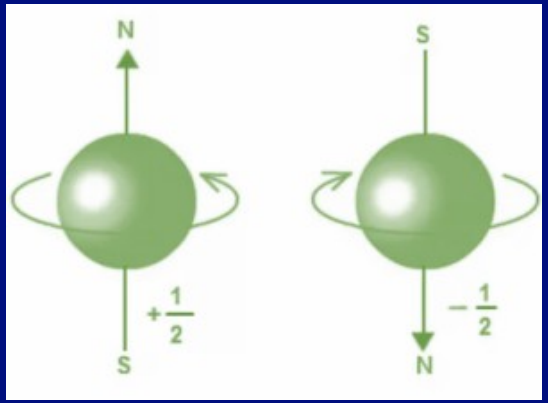


Kok-Wei Bong et al. 2021

Los Alamos NATIONAL LABORATORY

# Spin waves for quantum computation

- Spin waves: propagation of a disturbance in the quantum mechanical property ‘spin’ throughout the atoms in a lattice
- Spintronics: the development of devices which utilize spin waves as a means to transport information

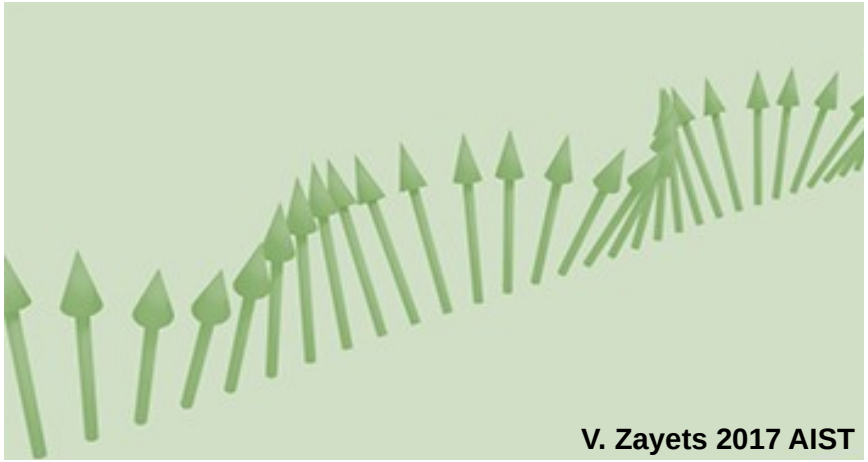


Electronic excitations -> eV

Spin waves -> meV

- Smaller environmental footprint
- Orders of magnitude faster
- Greater computing power for scientific research
- More reliable systems
- A compelling answer to our computing needs!

# An ideal host for spintronics

Spins interact via:

- magnetic dipole-dipole coupling
- “exchange” interaction

Lattice structure is very important

Want to identify ideal lattice structures for hosting unique spin dynamics

Wikimedia commons. Retrieved 2021

Los Alamos NATIONAL LABORATORY

# The Kagome Lattice

- Tri-hexagonal lattice
- Exhibits unique spin behaviors
  - spin liquid candidacy
    T.-H. Han et. al. Nature. 2012
  - topologically protected bands
    R. Chisnell et al. PRL. 2015
  - dirac material
    M. Kang et al. Nature Materials. 2019
  - magnon transport
    J. Mukherjee et al. PRB. 2021

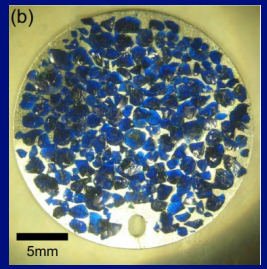

R. Chisnell et. al. PRB. 2016

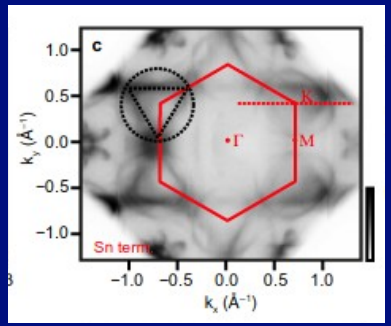

M. Kang et al. Nature Materials. 2019

J -X. Yin et al. Nature. 2018

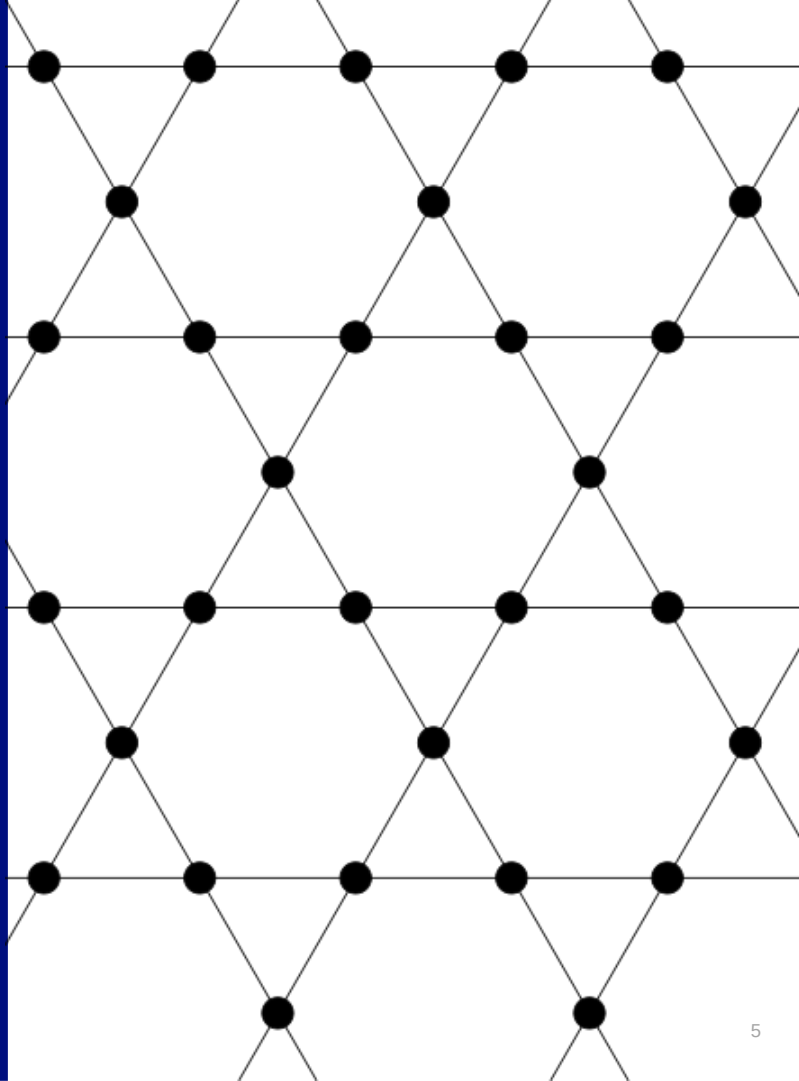

# The Kagome Lattice

- Tri-hexagonal lattice
- Exhibits unique spin behaviors
- Geometric magnetic frustration

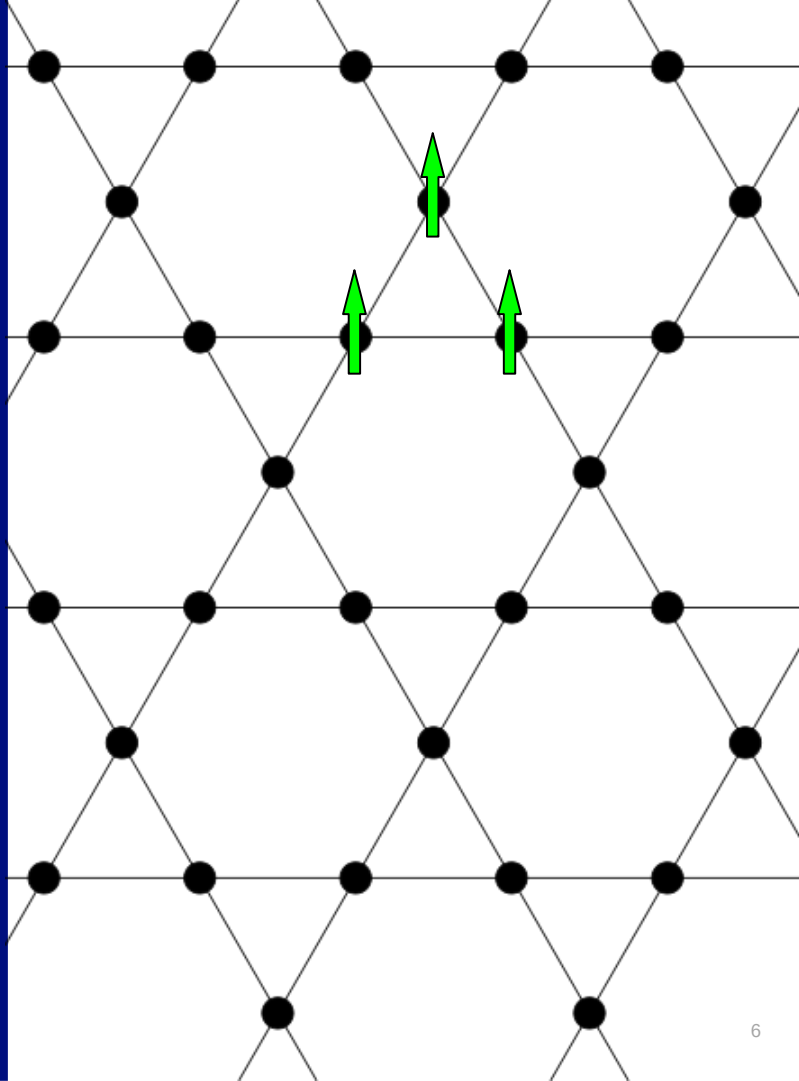

From Wikimedia Commons

# The Kagome Lattice

- Tri-hexagonal lattice
- Exhibits unique spin behaviors
- Geometric magnetic frustration

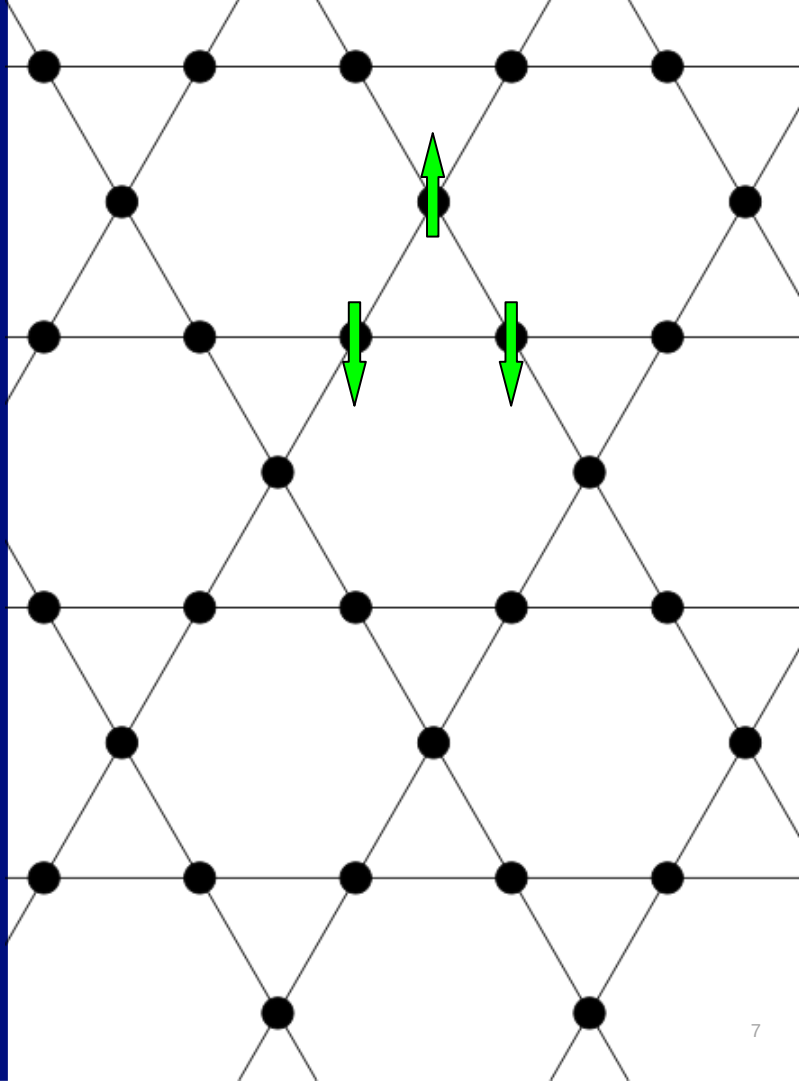

From Wikimedia Commons

# The Kagome Lattice

- Tri-hexagonal lattice
- Exhibits unique spin behaviors
- Geometric magnetic frustration
- Hosts unique static spin configurations

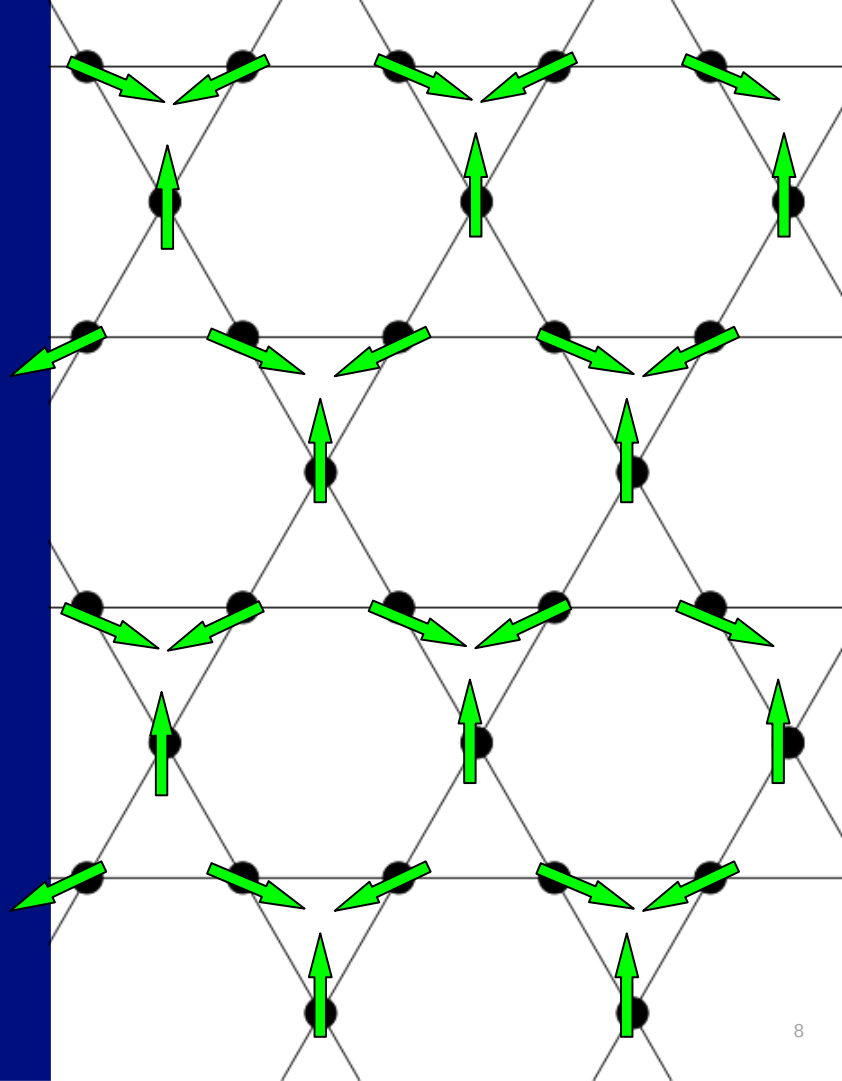

From Wikimedia Commons

# The Kagome Lattice

- Tri-hexagonal lattice
- Exhibits unique spin behaviors
- Geometric magnetic frustration
- Hosts unique static spin configurations
- Promising candidate for spintronics

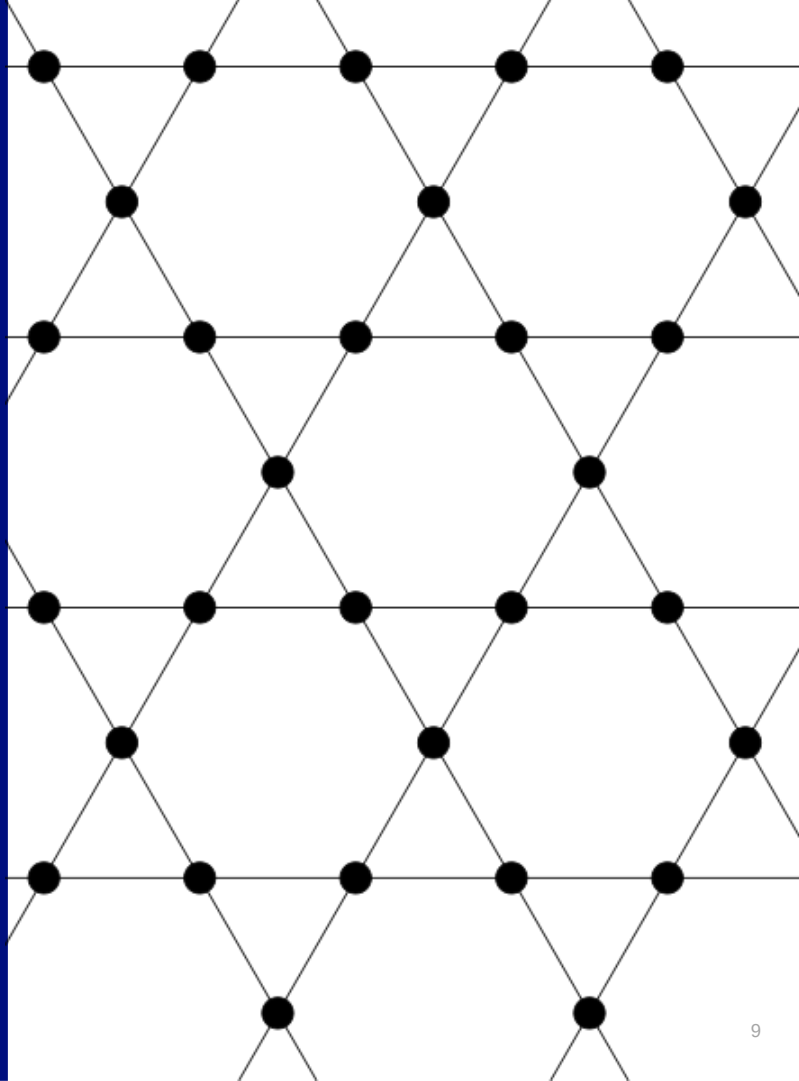

From Wikimedia Commons

# Moving forward with the Kagome Lattice

- Robustly characterize the spin dynamics in the Kagome lattice
- Identify the behavior of various interactions' contribution to the spin waves

$$H = \underbrace{-\frac{1}{2}\sum_{i\neq j} J_{ij}\mathbf{S}_i \cdot \mathbf{S}_j}_{\text{Exchange}} \underbrace{-\sum_i D_i(\mathbf{S}_i)_z^2}_{\text{Anisotropy}} \underbrace{-B\sum_i \mathbf{S}_{iz}}_{\text{Magnetic field}} \underbrace{-\sum_{i\neq j} \mathbf{DM}_{ij} \cdot \mathbf{S}_i \times \mathbf{S}}_{\text{Antisymmetric exchange}}$$

# Demystifying the energy components

$$= -\frac{1}{2}\sum_{i\neq j} J_{ij}\bar{\mathbf{S}}_i \cdot \underline{U}_i\underline{U}_j^{-1}\bar{\mathbf{S}}_j - D\sum_i (\underline{U}_i^{-1}\bar{\mathbf{S}}_i)_z^2 - B\sum_i (\underline{U}_i^{-1}\bar{\mathbf{S}}_i)_z - \sum_{i\neq j} DM_{ij}\cdot \underline{U}_i^{-1}\mathbf{S}_i \times \underline{U}_j^{-1}\mathbf{S}_j$$

$$S_{ix} = \sqrt{\frac{S_i}{2}}(a_i^\dagger + a_i)$$

$$S_{iy} = i\sqrt{\frac{S_i}{2}}(a_i^\dagger - a_i)$$

$$S_{iz} = S_i - a_i^\dagger a_i$$

Classical energy

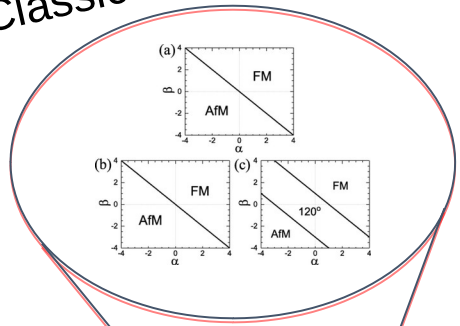


Spin waves

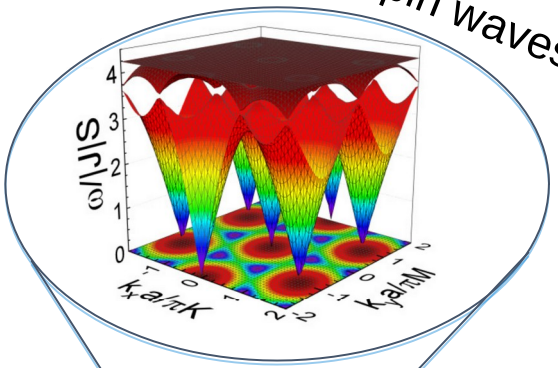


$$H = E_0 + H_1 + H_2 + \cdots$$

A. A. Coker. et al. 2021. PRB

# Qualifying the spin waves

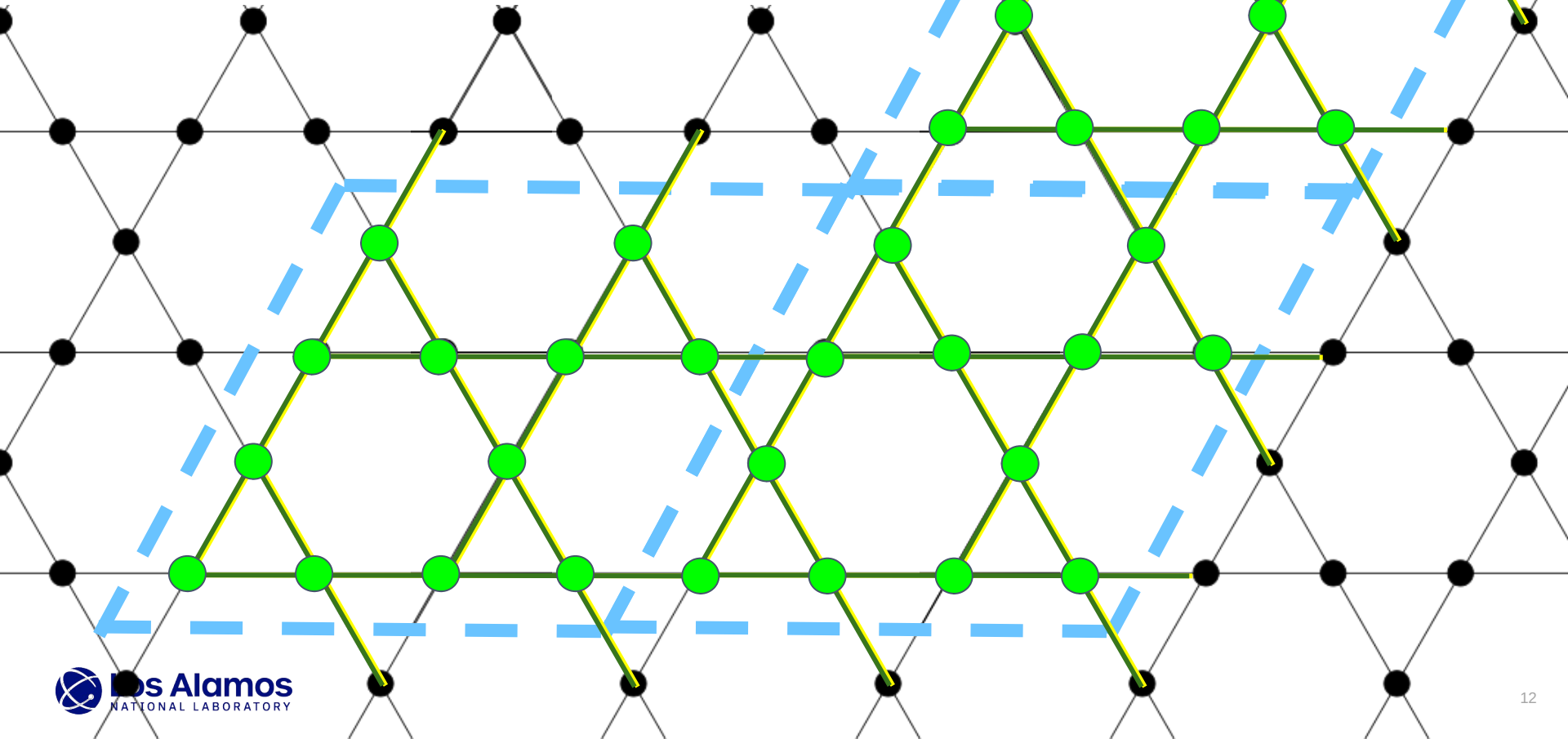

# Characterizing the Kagome Lattice

- Determine the ground state
- General formula for the spin waves
- Use the ground state to explore effects of competing energy components on the spin-waves

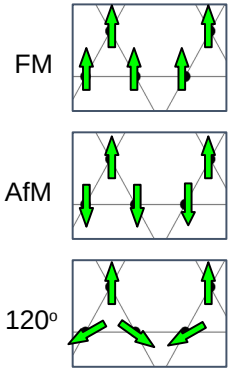


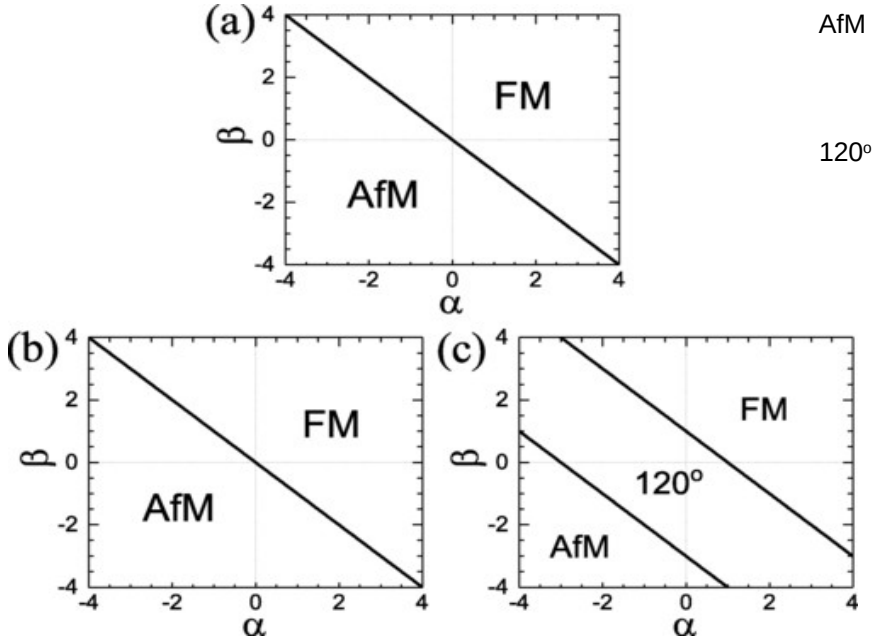


A. A. Coker. et al. 2021. PRB

# Exploring the spin waves

- Use python libraries to numerically calculate spin waves
- Various distorting and amplifying parameters:
  - Different static spin configurations
  - Effect of imbalance of exchange interaction between atoms
  - Weight of exchange (J) vs antisymmetric exchange (DM)
  - Effect of Anisotropy
  - Applied magnetic field results

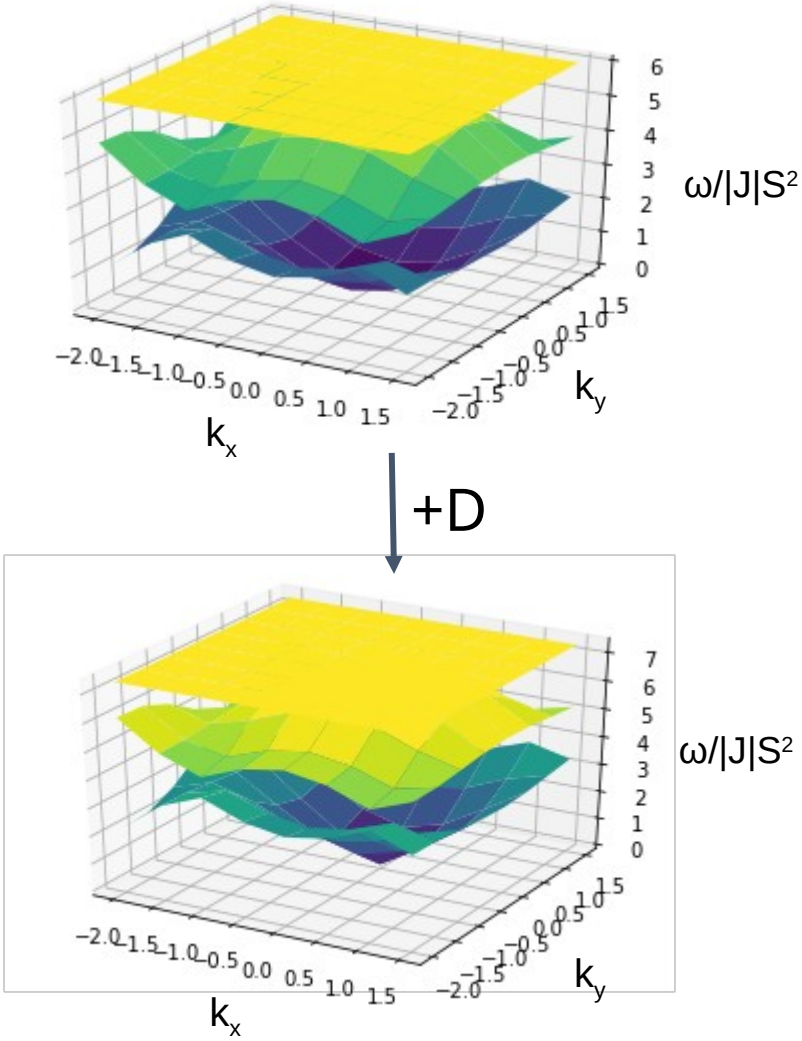

# Conclusion

What we are accomplishing

- Determine the ground state
- Introduce a previously un-quantified interaction
- Build spin dynamics profile for neutron scattering experimentalists
- Uncover details on efficacy of kagome materials in spintronics
- In-depth characterization of key physical behaviors in lattice

Theoretical spin wave analyses

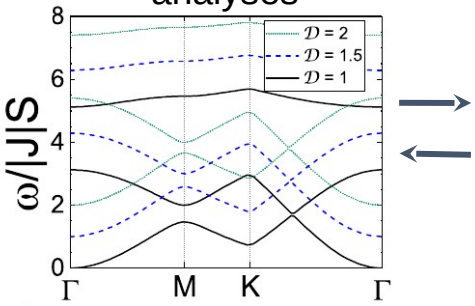


A. A. Coker. et al. 2021. PRB

Experimental results

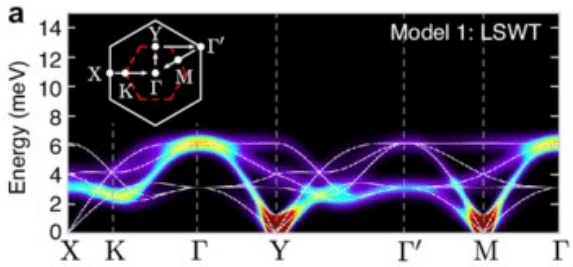


S. M. Winter. et al. 2017. Nature Communications

# Acknowledgements

A. A. Coker, J. T. Haraldsen, and J. -X. Zhu would like to acknowledge the support of the Center for Non-Linear Studies at Los Alamos National Laboratory for the completion of this research.

Los Alamos NATIONAL LABORATORY

Center for Nonlinear Studies

SymPy NumPy

# Thank you for your time!

Questions?

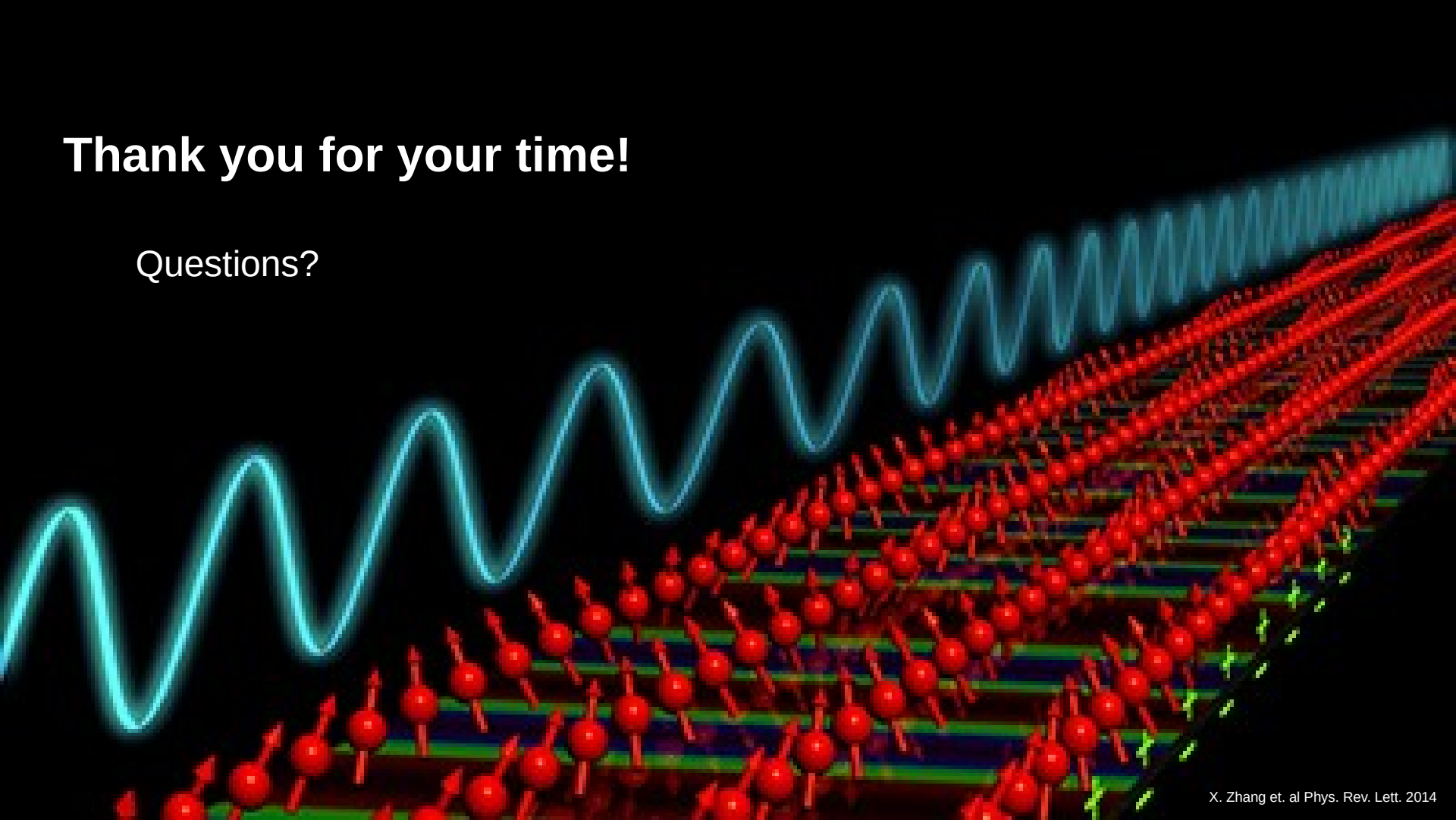

X. Zhang et. al Phys. Rev. Lett. 2014

Los Alamos
NATIONAL LABORATORY

# Exploring Nuclear Magnetic Resonance Spectroscopy, specifically J - coupling, for Identifying Chemical Warfare Agents.

Tayra Eidenbenz
Group: T-1
Mentors: Tammie Nelson and Derrick Kaseman
Status: Undergraduate
School: University of California, Davis

# Motivation:

- Chemical Warfare Agents (CWAs): extremely toxic, artificial materials that can be dispersed as a gas, liquid, or an aerosol that can be lethal or incapacitate humans
- Types:
  - Blood, Blister, Nerve, Nettle, Pulmonary, Vomiting
- History: mainly used in the world wars
  - WW I: mustard and chlorine
  - WW II: sarin and soman
- Biggest use today: terrorism and war situations
- Why do we want to detect them so quickly?
  - Prevent a loss of life to those exposed
  - Determine quantity and type released to create a subsequent treatment plan

This gif is a scene from the movie *Wonder Woman,* but mustard gas isn't able to crack glass

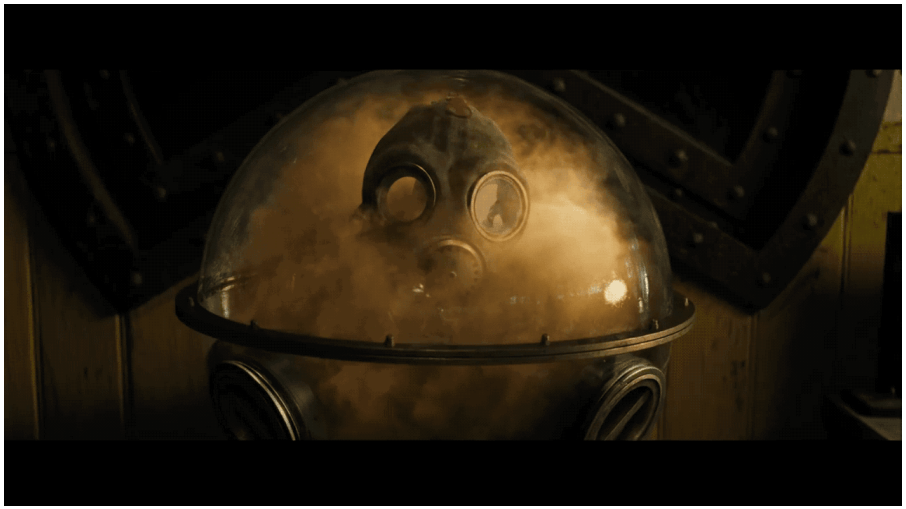

# Motivation:

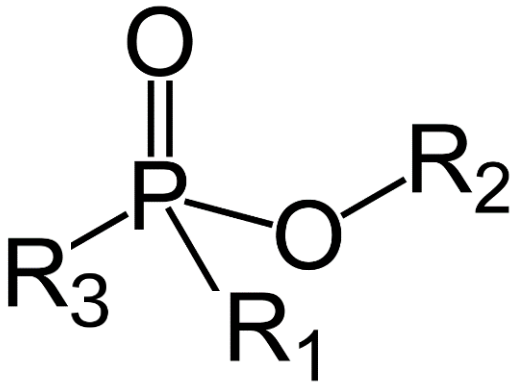


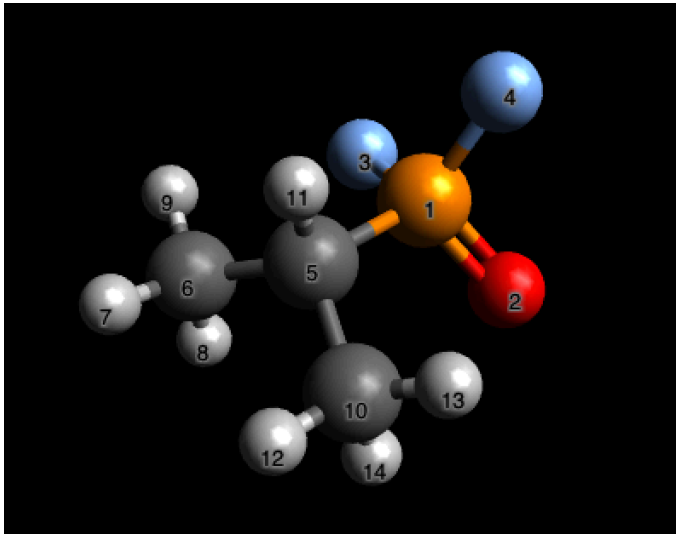


# Nuclear Magnetic Resonance (NMR)

- Definition: a method of observing local magnetic fields are atomic nuclei using spectroscopy. (Like a medical MRI)
- It has become the most prominent technique for analyzing organic structures
  - Good results can be obtained with samples of less than a milligram (with good instruments)
  - NMR is non destructive

High Field 16.0 T NMR


Earth's Field 50 microtesla NMR

# J-Coupling

- Through bond interaction between nuclei containing spin, like the hydrogen, phosphorus, and fluorine found in CWAs
- J couplings split the NMR Signals into distinct patterns
- Pascal's Triangle pattern: ratio of heights of each peak in a split pattern
- J couplings are the primary information source in LANL's Earth's field NMR spectrometers
- Ratio and height of peaks can allow us to determine the composition of a molecule if it is unknown

| | | | | | | | |
|---|---|---|---|---|---|---|---|
| | | | 1 | | | | H=0 |
| | | 1 | | 1 | | | H=1 |
| | 1 | | 2 | | 1 | | H=2 |
| 1 | | 3 | | 3 | | 1 | H=3 |
| | 1 | | 4 | | 6 | | 1 |
| 1 | | 5 | | 10 | | 10 | 5 1 |
| | 1 | | 6 | | 15 | | 20 15 6 1 |
| 1 | | 7 | | 21 | | 35 | 35 21 7 1 |

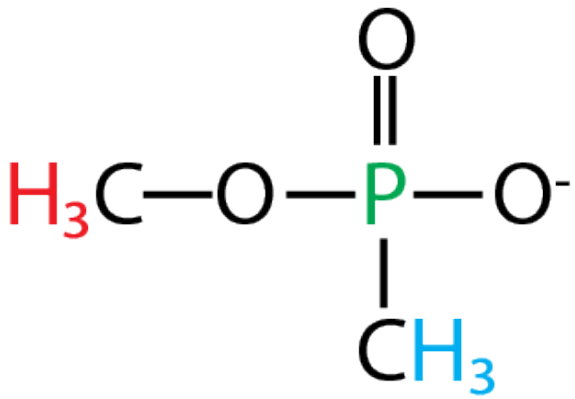


Earth's field spectrum of this molecule

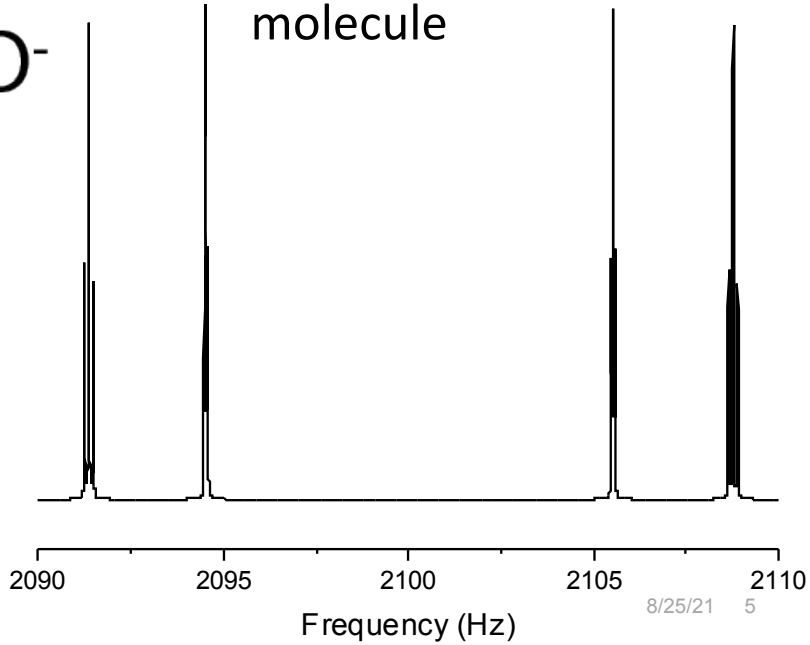

# Project At LANL

Goal:

- Better way to identify CWAs in the field
  - Earth's field NMR = affordable and portable
- Find a correction factor between our simulated J couplings and our experimental J couplings
  - Use this to simulate unmeasured molecules
- Create a database of J coupling values
- Use this data to quickly identify chemical warfare agents

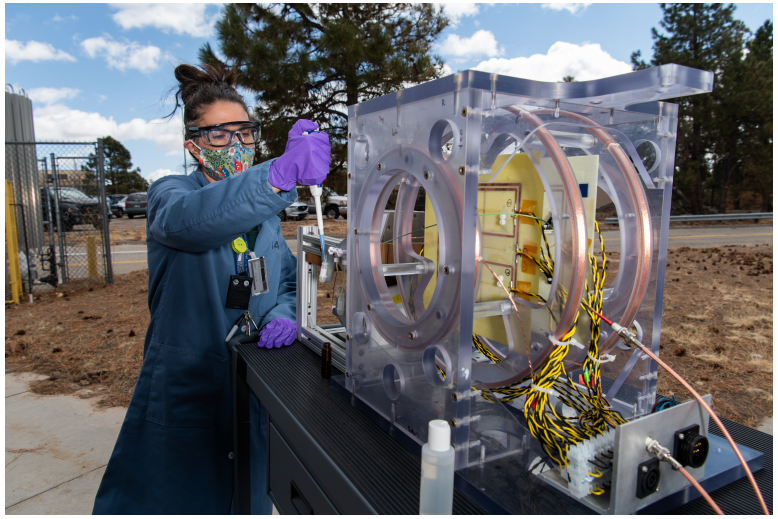

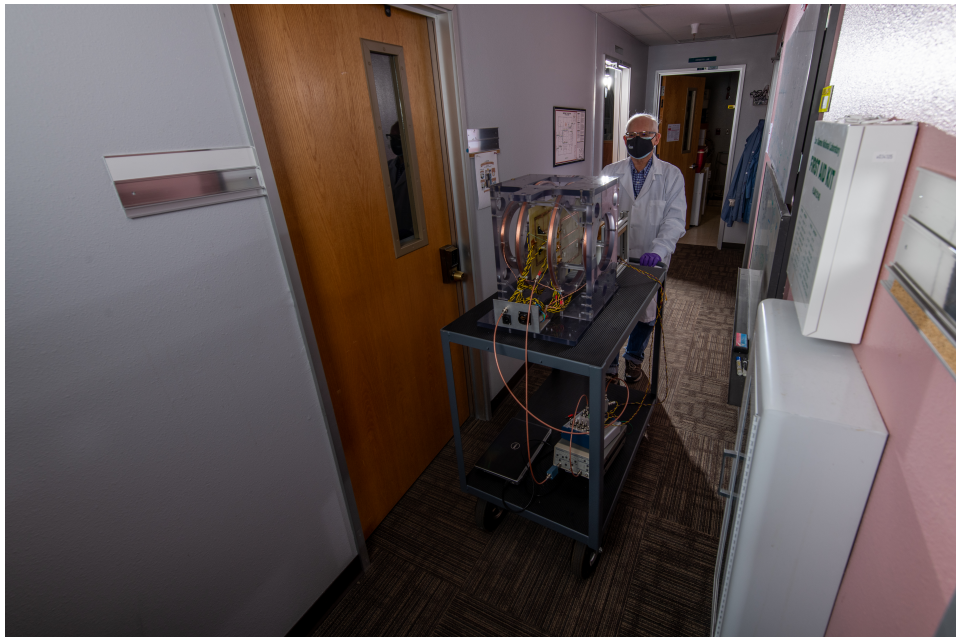

# Project At LANL

Steps:

1. Build all the molecules in Avogadro

2. On the high performance computers (HPCs) run a job to optimize the geometry of each molecule and carry out the NMR simulations

3. Extracting all the J coupling data for the preferred nuclei and filling out the excel sheet

4. Find correlation between simulated value and experimental standard by graphing a linear regression

# Project At LANL

- After creating an excel database:
  - Create a correlation between the simulated value and the experimental value to correct future data
- Things to fix:
  - Which electronic contribution is most important
  - Making a graph for each contribution to see which data set gives us the most ideal $R^2$ value

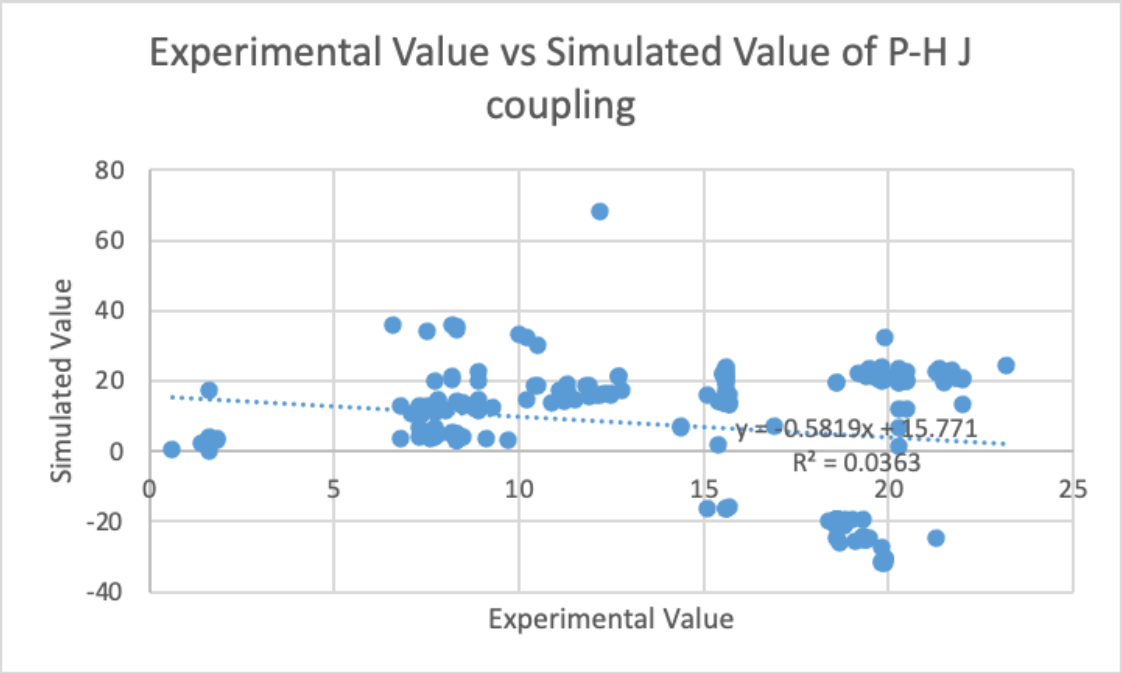


Slope = .5819

Intercept = 15.771

$R^2$ = .036320

# All About Gaussian

- Gaussian is a quantum chemistry program
- Based on Density Functional Theory (DFT): predicts and calculates the behavior of materials based on quantum mechanics
  - Primarily investigates the ground state
  - Electrons and their behavior
- Why Gaussian?
  - Experiment live would be too dangerous
  - Already has a precedent for extracting valuable J-coupling data
- Using badger HPC cluster
- What I am doing on the HPCs?
  - Geometry optimization
  - NMR calculations
- Functional: cM06
- Basis set: a set of functions that describe the electron density:
  - 6-311g**

# Data Set/Example

methylphosphonic acid difluoride

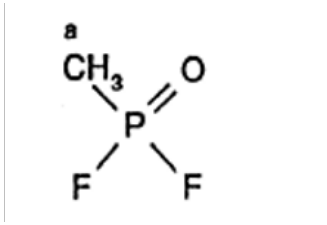


J Couplings between P and ‘A’

Average = 21.176433Hz

Experimental Value = 19.4Hz

methyl ethylphosphonofluoridate

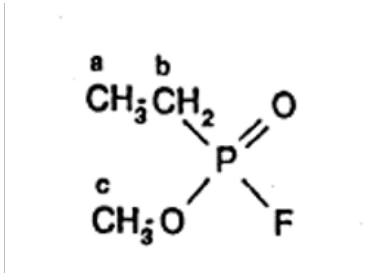


J Couplings between P and ‘A’

Average = 22.30331Hz

Experimental Value = 21.4Hz

J Couplings between P and ‘B’

Average = 24.5241Hz

Experimental Value = 19.3Hz

# Expected Results and Next Steps

- We hope that:
  - The expected value is equal to or similar to the value from the simulation
  - Often, the number is within 2 Hz, but not exact.
- Next Steps:
  - Examining the correlation between the expected value and the simulated number
    - Linear regression -> correction factor
    - Then apply the correction factor to other molecules to determine accuracy
  - Finding J couplings from other atoms, not just hydrogens and phosphorus
    - Hydrogen-hydrogen
    - Phosphorus-Fluorine
    - Hydrogen-Fluorine
  - **Simulating** Earth's Field spectra for CWAs

# Final Conclusions and Big Picture

- CWA's are a threat to national security and human life
  - By using NMR, specifically J-coupling, we hope to quickly identify CWAs based on their chemical composition
  - Gaussian provides us with a safe option to measure NMR parameters
- My work this summer: finding the J couplings of 127 molecules using Gaussian simulations and comparing our simulated data to experimental constants to find a correction factor
  - This correction factor tests the accuracy of the general procedure

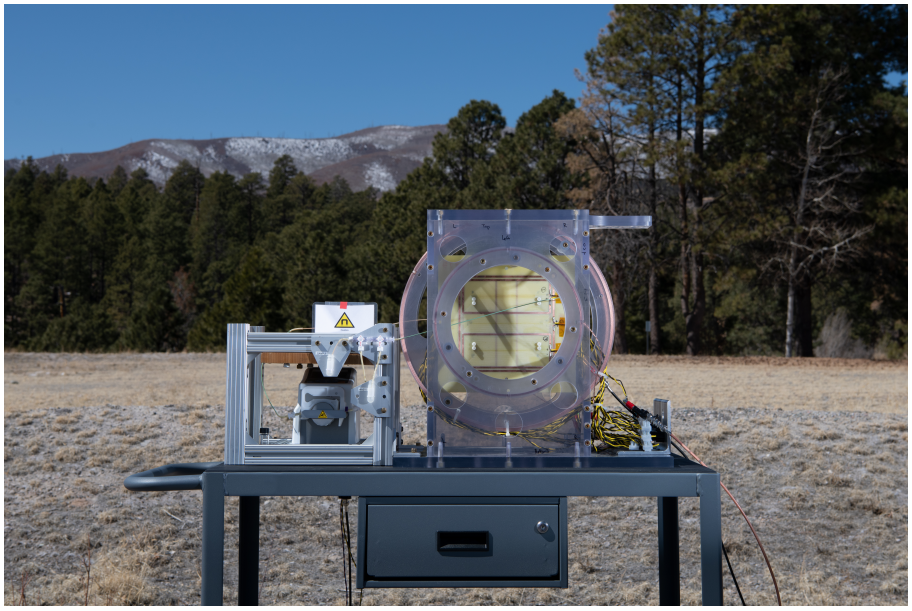

Los Alamos
NATIONAL LABORATORY

# Exploring Nuclear Magnetic Resonance Spectroscopy, specifically J - coupling, for Identifying Chemical Warfare Agents.

Tayra Eidenbenz
Group: T-1
Mentors: Tammie Nelson and Derrick Kaseman
Status: Undergraduate
School: University of California, Davis

Los Alamos NATIONAL LABORATORY

# Inferring Causality in Human Medicine: a survey of challenges

Rebecca L. Hehl

August 24, 2021

# Agenda

- 3 Prevalent Defeaters to Inference to Causality
- Example Hard Case
  - Epistemic/ Behavioral Variable influences
  - Dependent variable (suicidal ideation) is itself inferred… from patient testimony
- Bolstering/ defeating (both in degrees) the available inference toward causality using directed acyclic graphs
- Formal log likelihood
- Structuring with decision trees
  - Example: Mental Health dx and MI dx can proceed from precisely the same data set
  - Aim: identify variables that bolster/ defeat inference regarding branch progression

# Inferring Causality: 3 defeaters

Direct Causal Effect


Reverse Causality

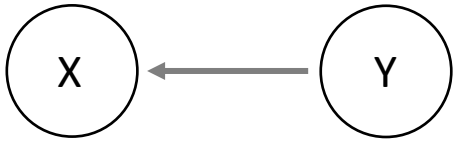


Confounding
(Omitted Variable)

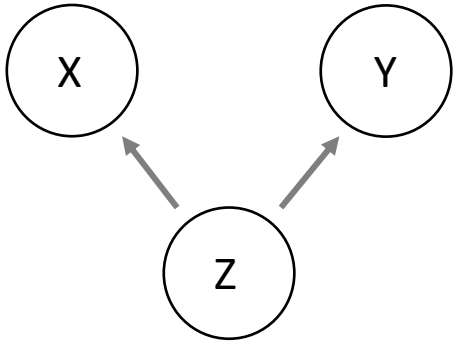


Conditioning on a
Collider

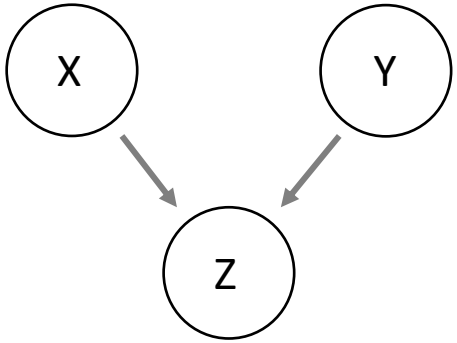


Davis, A. (2018). *Applied Data Analysis.*

Pearl, J., & Mackenzie, D. (2018). *The Book of Why: the new science of cause and effect.* Basic Books.

Sprites, P., Glymour, C. N., Scheines, R., & Heckerman, D. (2000). *Causation, prediction, and search.* MIT press.

# Confounding Variable

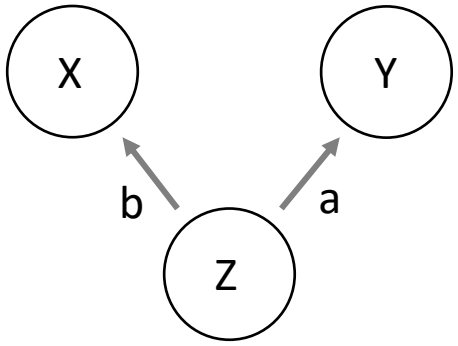


$Y = a * Z + e1$
$X = b * Z + e2$
$L = e3$

$X - e2/b = Z$
$Y = a * (X - e2/b) + e1$
$Y = (a/b) * X - (a/b) * e2 + e1$

# Collider

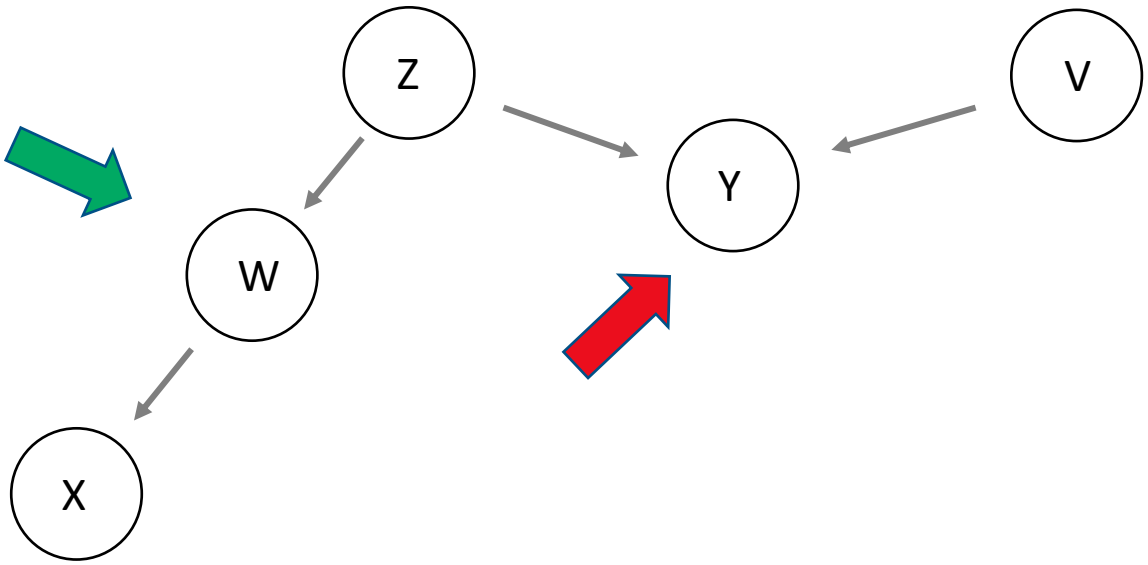


Davis, A. (2018). *Applied Data Analysis.*

Sprites, P., Glymour, C. N., Scheines, R., & Heckerman, D. (2000). *Causation, prediction, and search.* MIT press.

# Reverse Causality

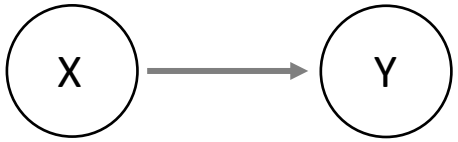


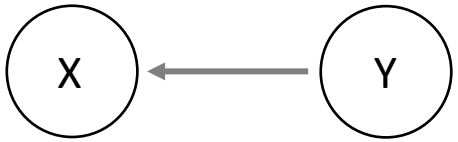


No statistical way to distinguish them

*a posteriori knowledge* such as
X preceding Y in time

# Agenda

- 3 Prevalent Defeaters to Inference to Causality
- Example Hard Case
  - Epistemic/ Behavioral Variable influences
  - Dependent variable (suicidal ideation) is itself inferred… from patient testimony
- Bolstering/ defeating (both in degrees) the available inference toward causality using directed acyclic graphs
- Formal log likelihood
- Structuring with decision trees
  - Example: Mental Health and MI dx can proceed from precisely the same data set
  - Aim: identify variables that bolster/ defeat inference regarding branch progression

# Example Hard Case: Suicidal Ideation

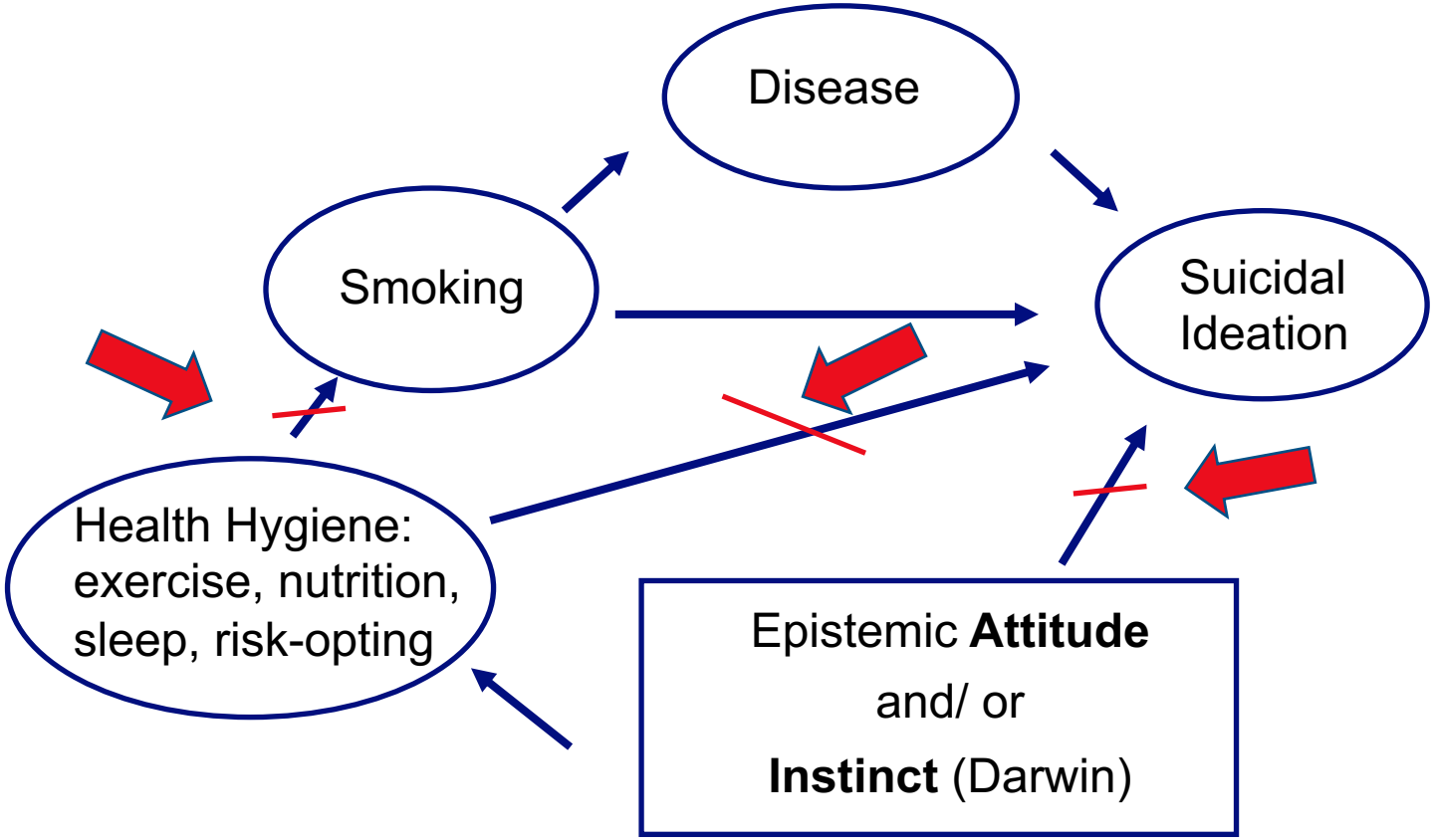

# Agenda

- 3 Prevalent Defeaters to Inference to Causality
- Example Hard Case
  - Epistemic/ Behavioral Variable influences
  - Dependent variable (suicidal ideation) is itself inferred… from patient testimony
- Bolstering/ defeating (both in degrees) the available inference toward causality using directed acyclic graphs
- Formal log likelihood
- Structuring with decision trees
  - Example: Mental Health and MI dx can proceed from precisely the same data set
  - Aim: identify variables that bolster/ defeat inference regarding branch progression

# Bolster/ defeat the inference in favor of causality

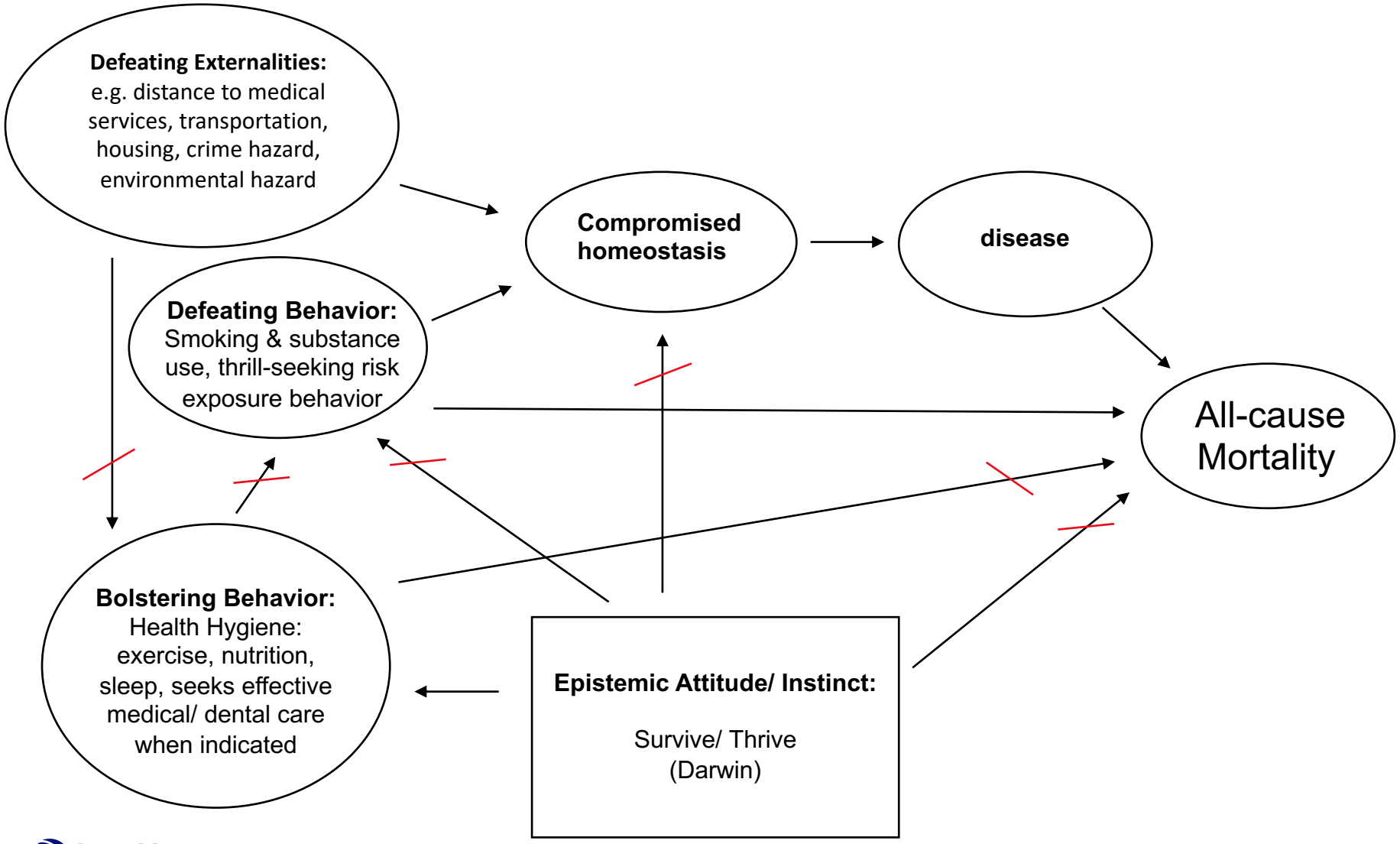

# Agenda

- 3 Prevalent Defeaters to Inference to Causality
- Example Hard Case
  - Epistemic/ Behavioral Variable influences
  - Dependent variable (suicidal ideation) is itself inferred… from patient testimony
- Bolstering/ defeating (both in degrees) the available inference toward causality using directed acyclic graphs
- Formal log likelihood
- Structuring with decision trees
  - Example: Mental Health and MI dx can proceed from precisely the same data set
  - Aim: identify variables that bolster/ defeat inference regarding branch progression

# HbA1c example: Predictive/ Protective

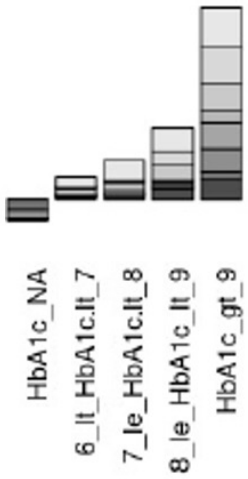


Logistic regression provides 0.75 AUROC
Random forest provides 0.80 AUROC
TabNet (Nnet) provides 0.82 AUROC

# Agenda

- 3 Prevalent Defeaters to Inference to Causality
- Example Hard Case
  - Epistemic/ Behavioral Variable influences
  - Dependent variable (suicidal ideation) is itself inferred… from patient testimony
- Bolstering/ defeating (both in degrees) the available inference toward causality using directed acyclic graphs
- Formal log likelihood
- Structuring with decision trees
  - Example: Mental Health and MI dx can proceed from precisely the same data set
  - Aim: identify variables that bolster/ defeat inference regarding branch progression

# A Tale of 2 Trajectories

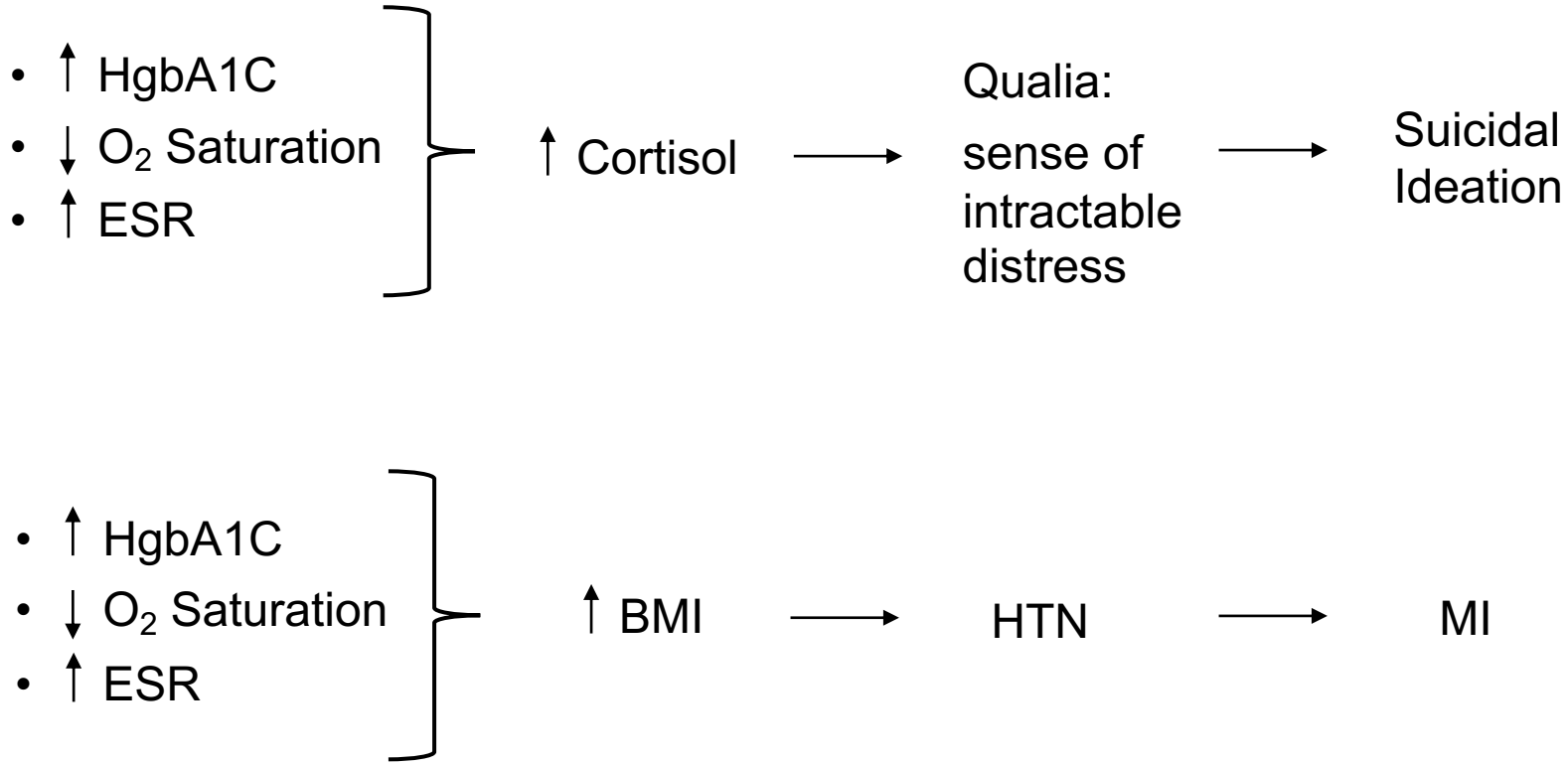


Imbens, G. W. (2020). Potential outcome and directed acyclic graph approaches to causality: Relevance for empirical practice in economics. *Journal of Economic Literature,* 58(4), 1129-79.

# Cardiac and Mental Health ICD Codes dominate

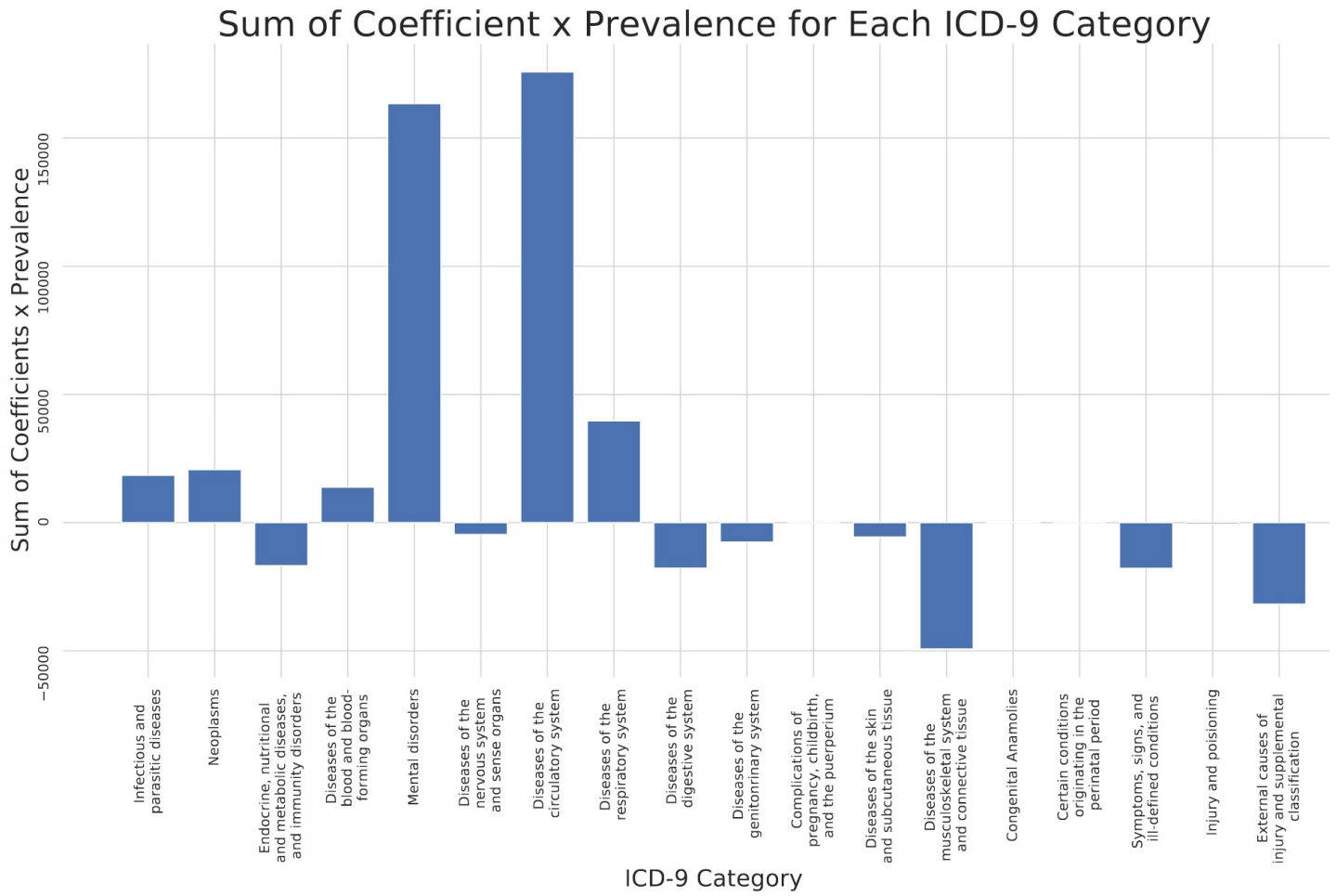

# Thank You

- Los Alamos National Laboratory/ T-6
  - Ben McMahon
  - Nick Hengartner
  - Sayera Dhaubhadel
- Carnegie Mellon University, Engineering & Public Policy (Pittsburgh, PA)
- The GEM Consortium

Los Alamos
NATIONAL LABORATORY

# Machine Learning to Guide Design of Novel Antibiotics

Liam Herndon

19 August 2021

# Outer Membrane and Efflux Pumps Create Barriers to Drug Entry

- Need for novel antibiotics
- Gram-negative bacteria are particularly hard to develop antibiotics for
- Outer membrane hard to permeate
- Multi-drug efflux pumps expel drugs

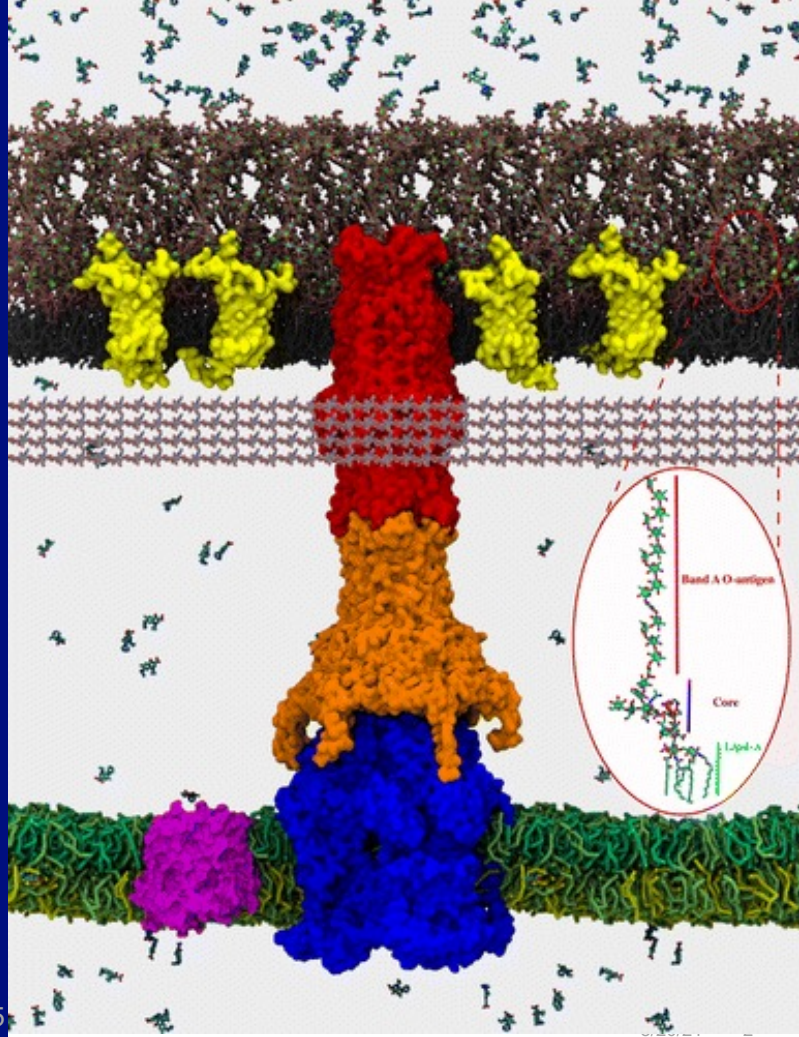


Zgurskaya et al. 2015

# Computational Models Have Identified Relevant Physico-Chemical Properties

- Previous research on top permeators and efflux avoiders
- Focused on physico-chemical properties
- Assigned coefficients describing effects of properties

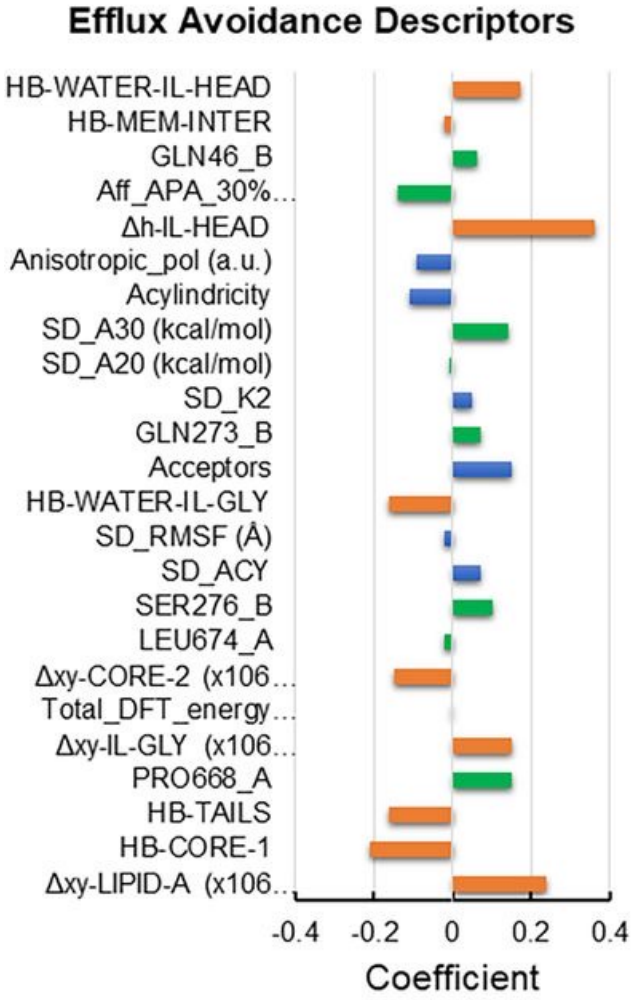


Mehla et al. 2021

# Many Ways to Achieve Target Properties

- Some potential antibiotics are poor permeators
- Want to add groups to improve permeation
- Past research suggests broad properties
- Hundreds of ways to achieve properties

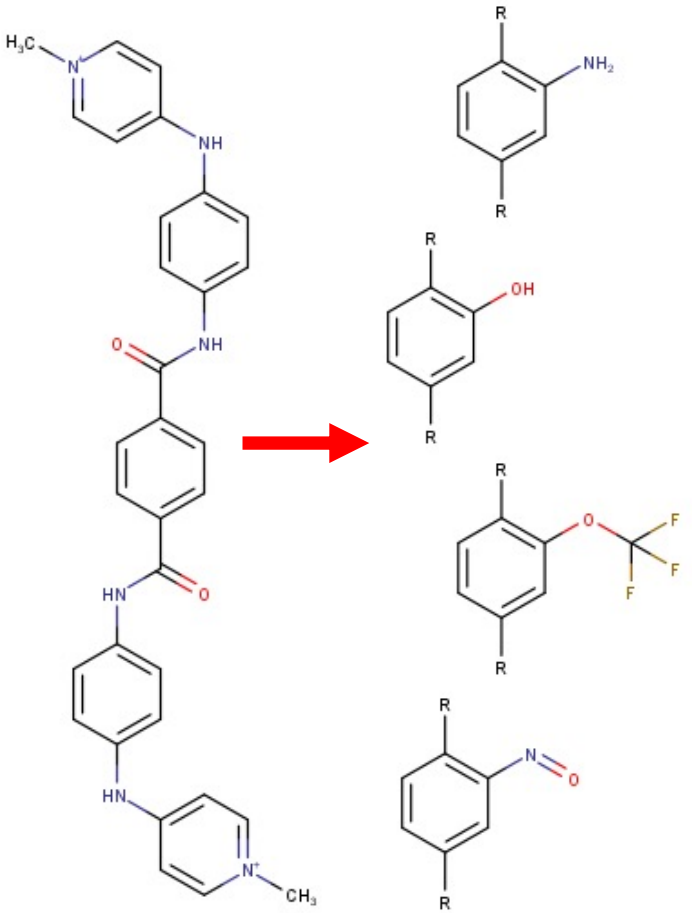


OU-31526

# Assessment of Modifications

- Expensive to empirically test all modifications
- Want to predict affects of modification before designing compound
- Need algorithm to predict effects of proposed modifications

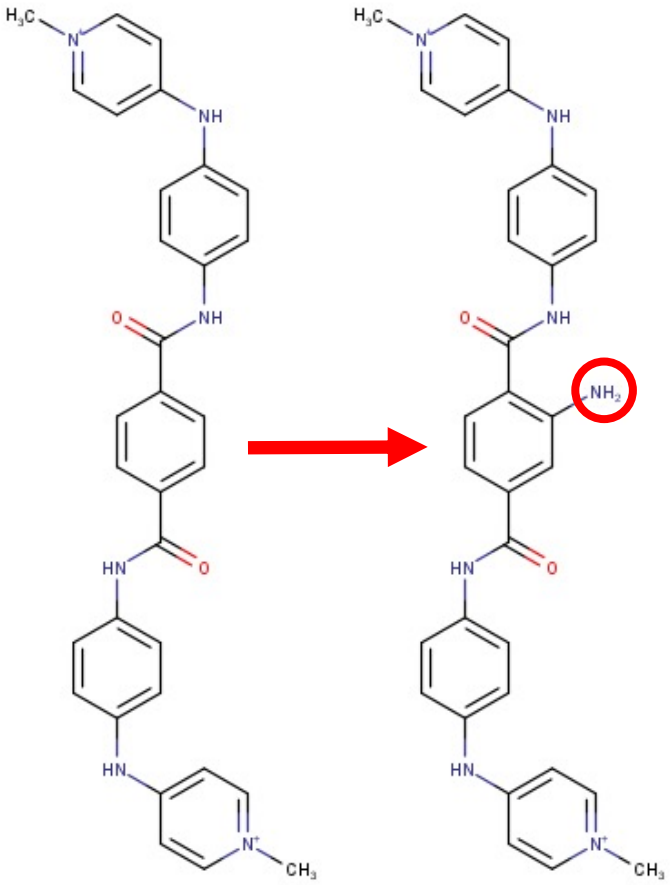

# Fragments Provide More Detailed Information About Compounds

- Describe atoms within 1 or 2 bond lengths of central atom
- >2,000 unique fragments generated from library of compounds
- Can compute descriptors for fragments

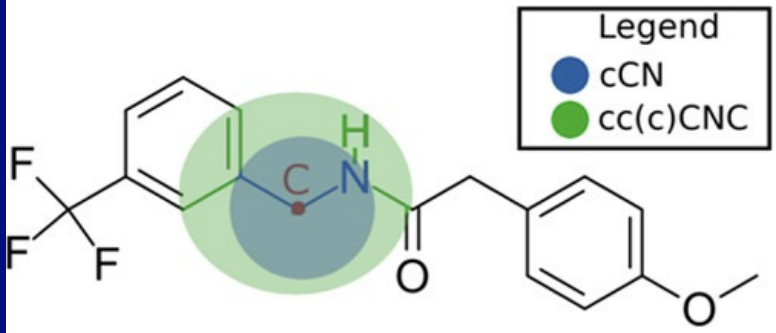


Mansbach et al. 2020

# Vector-space of Fragment Descriptors Can Describe Modification

**Modification Site**

ccc(C(N)=O)c(c)N
cccc(c)N
cc(c)N
cc(C)cc(c)N
ccc(N)cc

**Other Regions**

cccnc
ccc(cc)NC
ccc[n+](c)C
cc(c)NC(c)=O
ccc(cc)C(N)=O

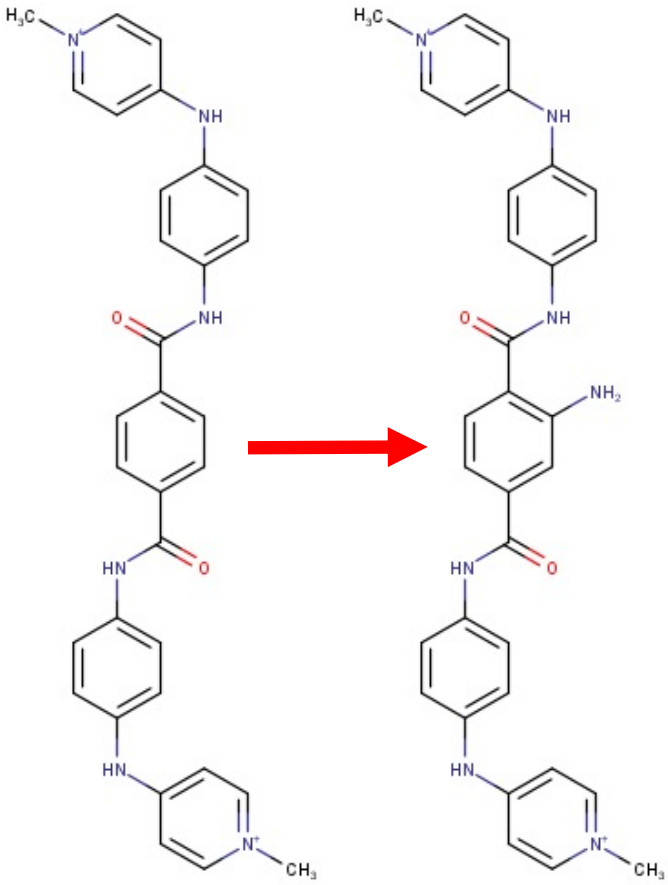

# Machine Learning to Score Modification

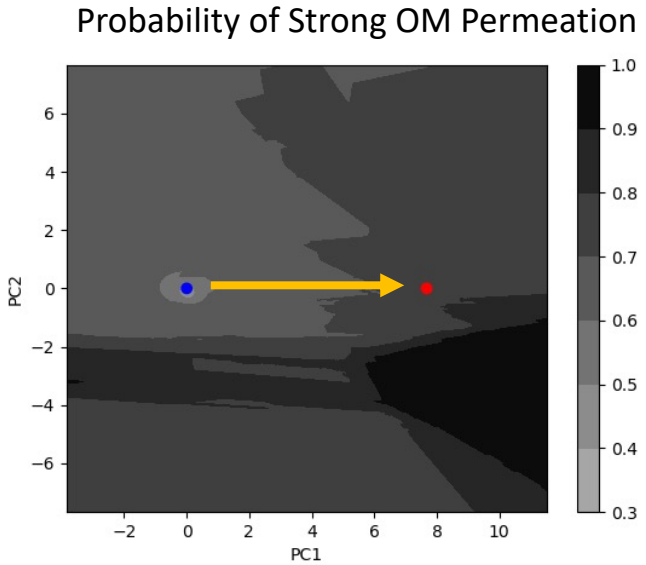


- Calculate probabilities with ML model
- Assess how modification affects probabilities

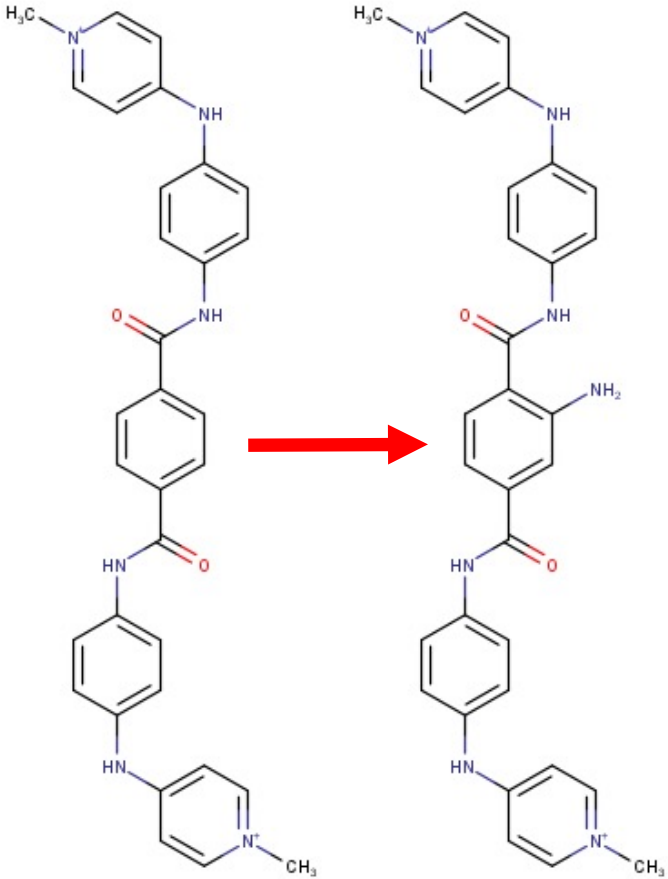

# Validation of Model

- Validated on existing modified compounds
- Reliable accuracy
  - 67.9% for permeation
  - 62.5% for efflux avoidance
- Can effectively narrow down modifications to synthesize

# Recommended Compounds

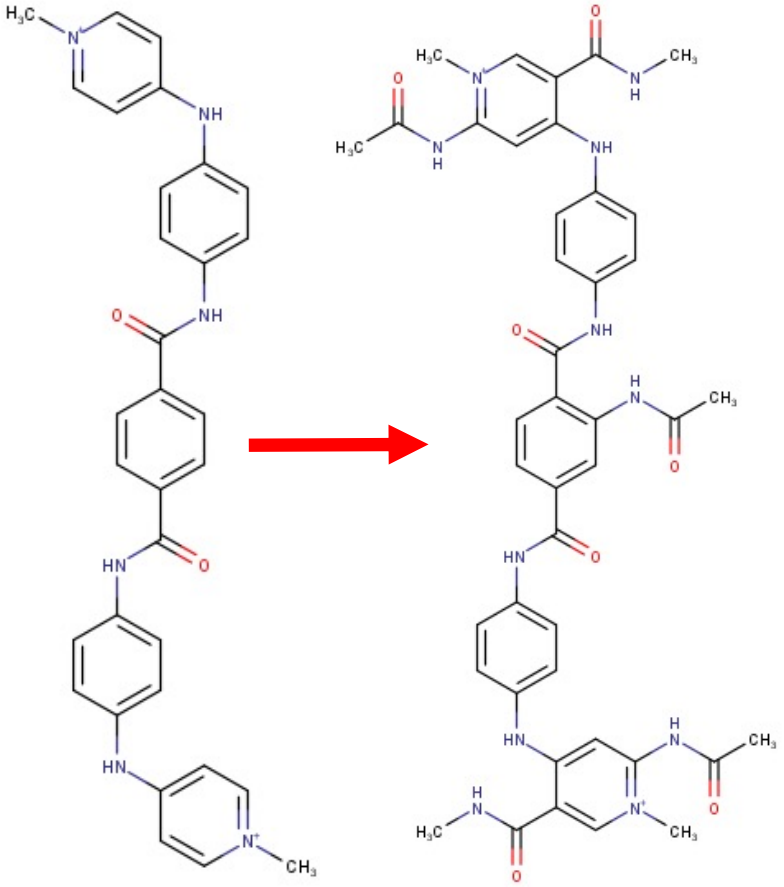

Probability of Strong OM Permeation

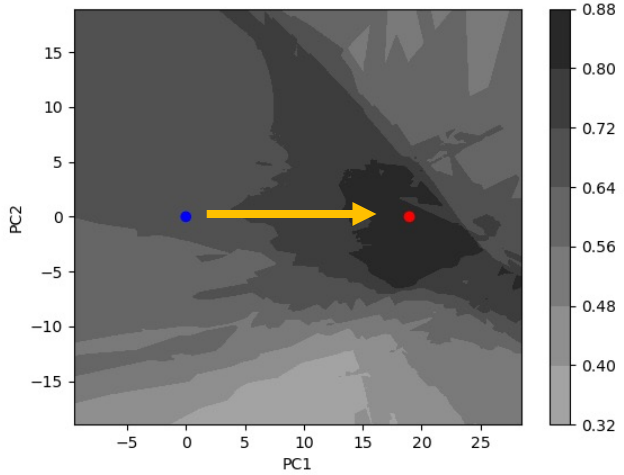


Probability of Strong Efflux Avoidance

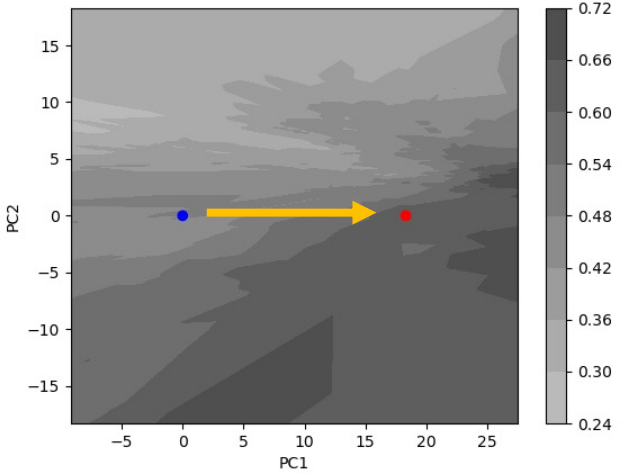


Los Alamos NATIONAL LABORATORY

# Conclusions

- Fragment analysis can accurately predict the effects of specific groups on OM permeation and efflux avoidance
- This focus on the effects of individual groups is ideal for predicting how specific modifications will affect drug activity
- These predictions can potentially guide drug modification to design antibiotic analogs with improved permeation and efflux avoidance

# Works Cited


- Mansbach et al. **2020**. “Machine learning algorithm identifies anantibiotic vocabulary for permeating gram-negative bacteria.” *J.Chem. Inf. Model.* 60(6).
- Mehla et al. **2021**. “Predictive rules of efflux inhibition and avoidance in *Pseudomonas aeruginosa*.” *mBio*. 12(1).
- O’Neill. **2014**. “Antimicrobial resistance: Tackling a crisis for the health and wealth of nations.”
- Zgurskaya et al. **2015**. “Permeability Barrier of Gram-Negative Cell Envelopes and Approaches To Bypass It.” *ACS Infect. Dis.* 1(11).

# Acknowledgments

**LANL**
S. Gnanakaran
Pedro Manrique
Cesar López
Nicolas Hentgartner

**University of Oklahoma**
Helen Zgurskaya
Valentine Rybenkov

**St Louis University**
John Walker

# Antibiotic Resistance Poses a Critical Threat to Public Health

- Antibiotic resistance outpaces drug discovery
- Emergence of multi-drug resistant strains
- Post-antibiotics era

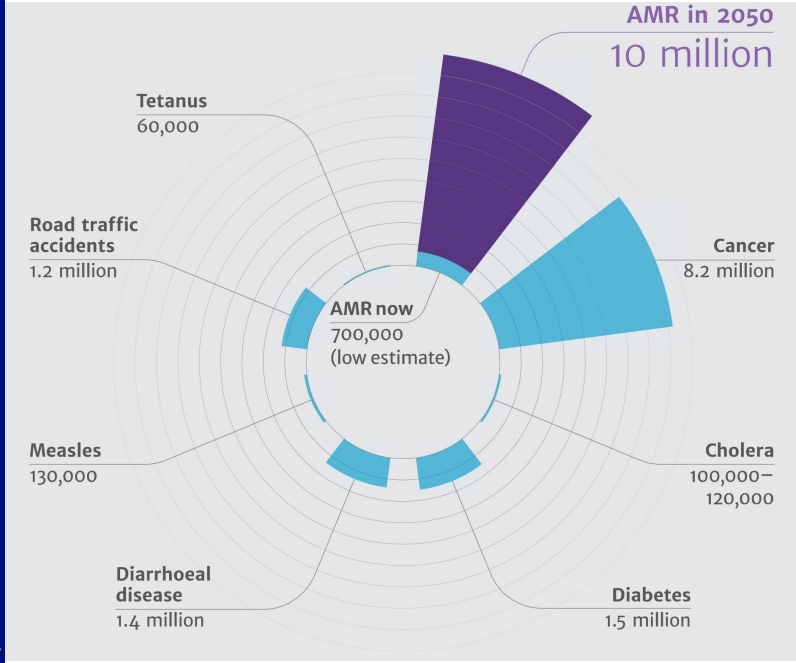


O'Neill 2014

# PORTING WAVE ACTION SOURCE TERMS TO GPU ON WAVEWATCH III

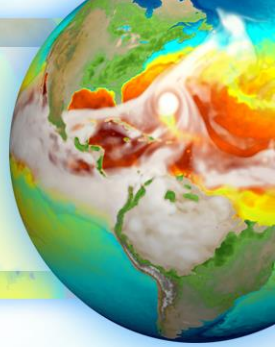

Los Alamos NATIONAL LABORATORY

## Parallel Computing Summer Research Internship 2021


Olawale James Ikuyajolu

**(Georgia Tech)**

**PhD Candidate in Ocean Science and Engineering**


Mentor

Dr. Luke van Roekel & Dr. Steven Brus (ANL)


**LA-UR-21-27720**


E3SM Energy Exascale Earth System Model

September 2, 2021

U.S. DEPARTMENT OF ENERGY

# Motivation

- WAVEWATCHIII is a 3rd generation wind wave spectral model developed at the Marine Modelling and Analysis Branch (MMAB) of the Center of Environmental Prediction (NOAA/NCEP).

- Wind generated waves play an important role in modifying physical processes at the atmosphere-ocean interface

- Such processes include:
  - Momentum, heat and moisture fluxes
  - Ocean vertical mixing
  - Albedo white-capping
  - Fracturing of sea-ice

- Wind wave are also crucial for simulation of coastal flooding

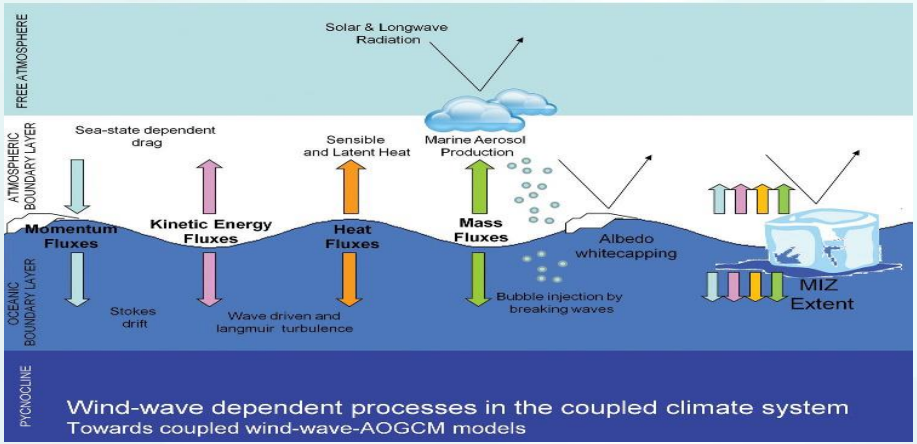


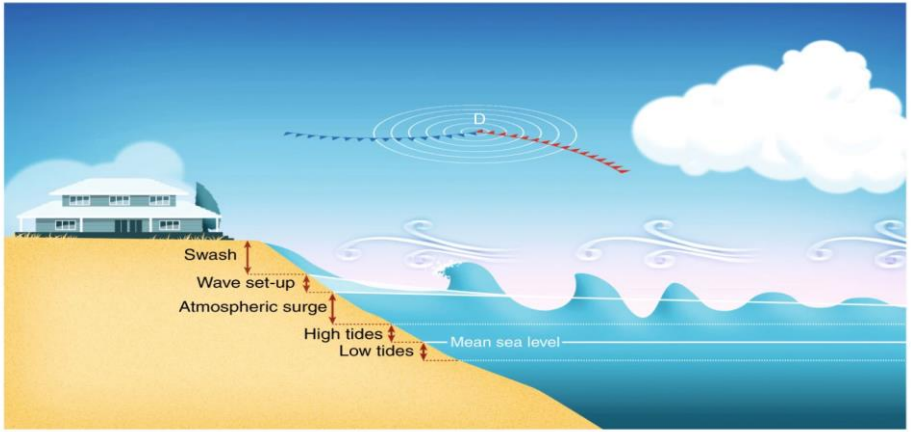


**Sources:** Calveri et al 2012; Melet et al 2018; Tolman 2008

# Motivation

- Wind-wave processes (small-scale) have generally been excluded from coupled Earth system models due to its high computational cost.

- The Next Generation Development (NGD) goal focuses on the inclusion of a wave model (WaveWatch III – WW3) into E3SM

- **Can we utilize GPU capabilities to reduce the computational cost of WW3?**

**Existing E3SM Components**

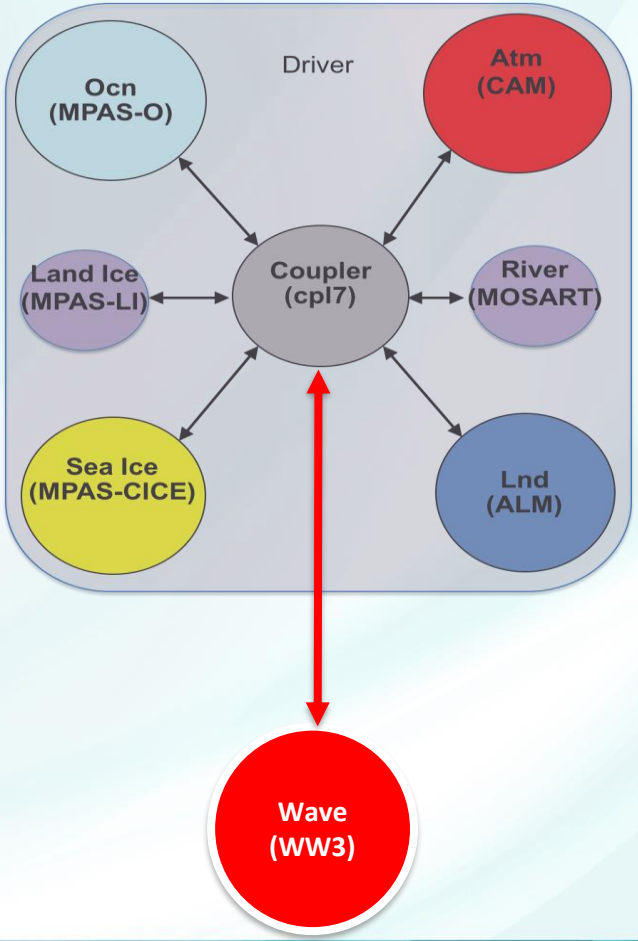


Sources: https://e3sm.org/about/organization/ngd-sub-projects/ngd-coastal-waves/

# WaveWatch III (WW3)

Solves the random phase spectral action density.

$$N(\emptyset, \lambda, \sigma, \theta, t) = \frac{F}{\sigma}$$

$F$ – Energy density

$\emptyset$:lon; $\boldsymbol{\lambda}$ - lat; $\boldsymbol{\sigma}$-relative frequency; $\boldsymbol{\theta}$-direction ; $\boldsymbol{t}$-time

$$\frac{\partial N}{\partial t} + \underbrace{\frac{\partial (C_\phi N)}{\partial \phi} + \frac{\partial (C_\lambda N)}{\partial \lambda}}_{\text{Advection by group velocity and currents}} \underbrace{\frac{\partial (\sigma N)}{\partial \sigma}}_{\text{Frequency Dispersion (Stretching)}} + \underbrace{\frac{\partial (C_\theta N)}{\partial \theta}}_{\text{Refraction (bending)}} = \underbrace{\sum_i S_i}_{\text{Sources and Sinks of energy/action}}$$

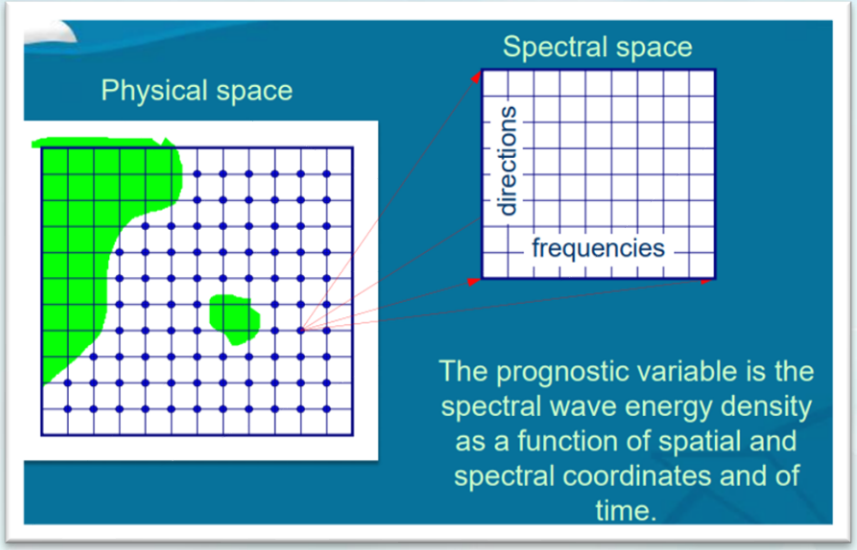


- ✓ $S_{in}$ – *Wind input*
- ✓ $S_{ds}$ – *Dissipation*
- ✓ $S_{nl}$ – *Nonlinear wave interactions*
- ✓ $S_{bot}$ – *wave-bottom interactions*
- ✓ $S_{tr}$ – *Triad wave-wave interactions*
- ✓ $S_{sc}$ – *scattering*
- ✓ $S_{ref}$ – *reflection*
- ✓ $S_{db}$ – *depth limited breaking*
- ✓ $S_{ice}$ – *wave-ice interactions*

$$S_{ds,l}(k, \theta) = -2u_* hk^2 \phi N(k, \theta)$$

Sources: https://e3sm.org/wp-content/uploads/2020/06/AllHandsPresentation_06-25-2020_opt.pdf; https://polar.ncep.noaa.gov/waves/workshop/pdfs/

# Porting Methodology & RoadMap

**WW3 Setup**

- Unstructured global domain with 16,160 nodes and 30,559 elements
- 50 x 36 spectral grid resolution on a global domain
- 1 day simulation period

Hardware: Kodiak

- CPU: Intel(R) Xeon(R) CPU E5-2695 v4 @ 2.10GHz
- GPU: Tesla P100-PCIE-16GB

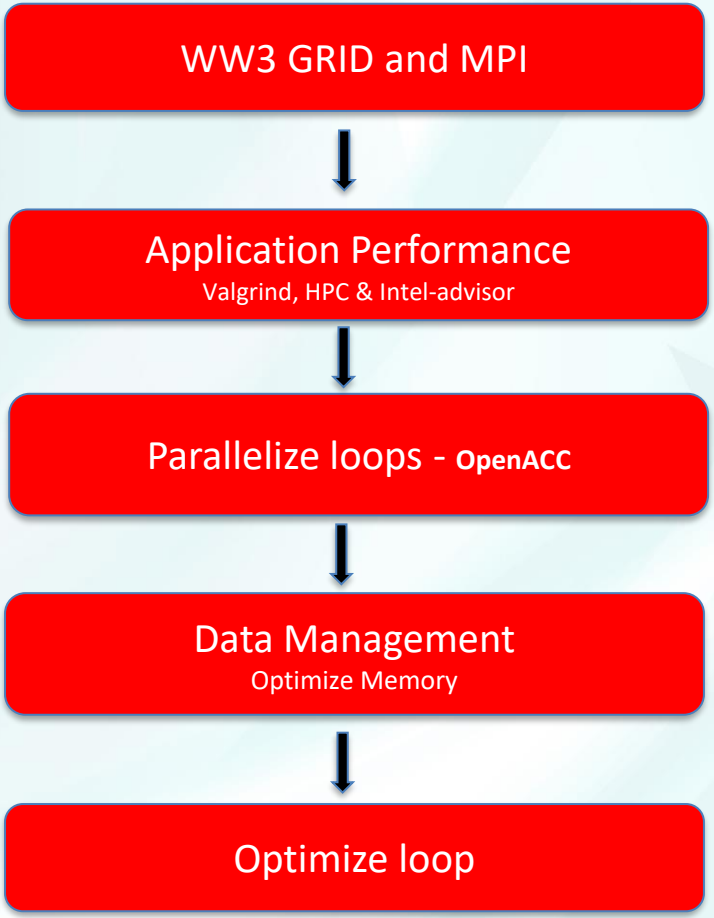

# WW3 GRID & MPI

GRID CELLS + MPI Process

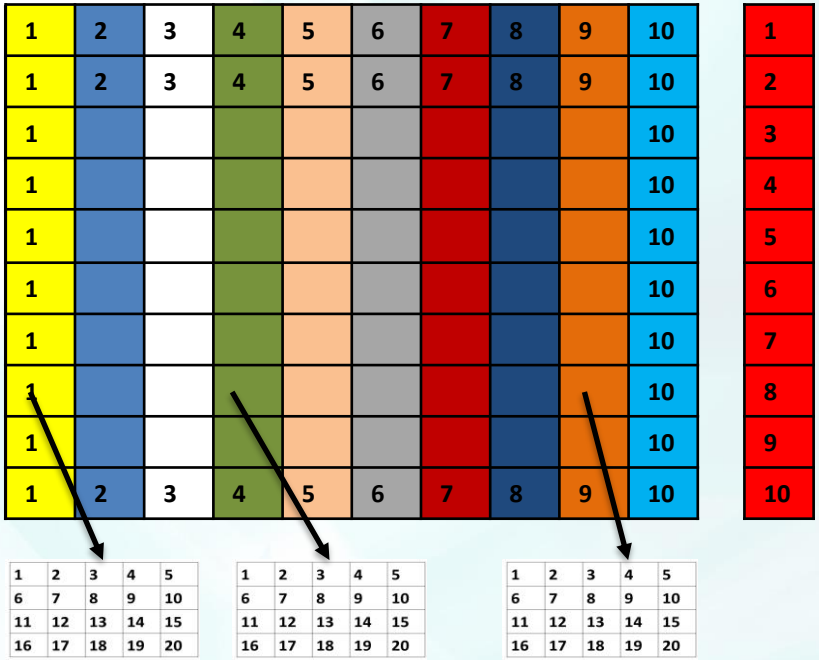


Local grid Counter







Spectral Grids

**Source Term Integration**

$DO\ I = 1, LocGRIDS$

$\quad \text{CALL WSCRE}(XY_i)$

$END\ DO$

$\text{WSCRE}(XY_i)$ SUBROUTINE CALL

$DO\ J = 1, NTH$

$\quad \text{CALL } W3SNL_{XY_i}(j)$

$END\ DO$

NTH = Freq x NDIR

# Application Performance

## Valgrind/Callgrind: 6 Nodes and 1 day

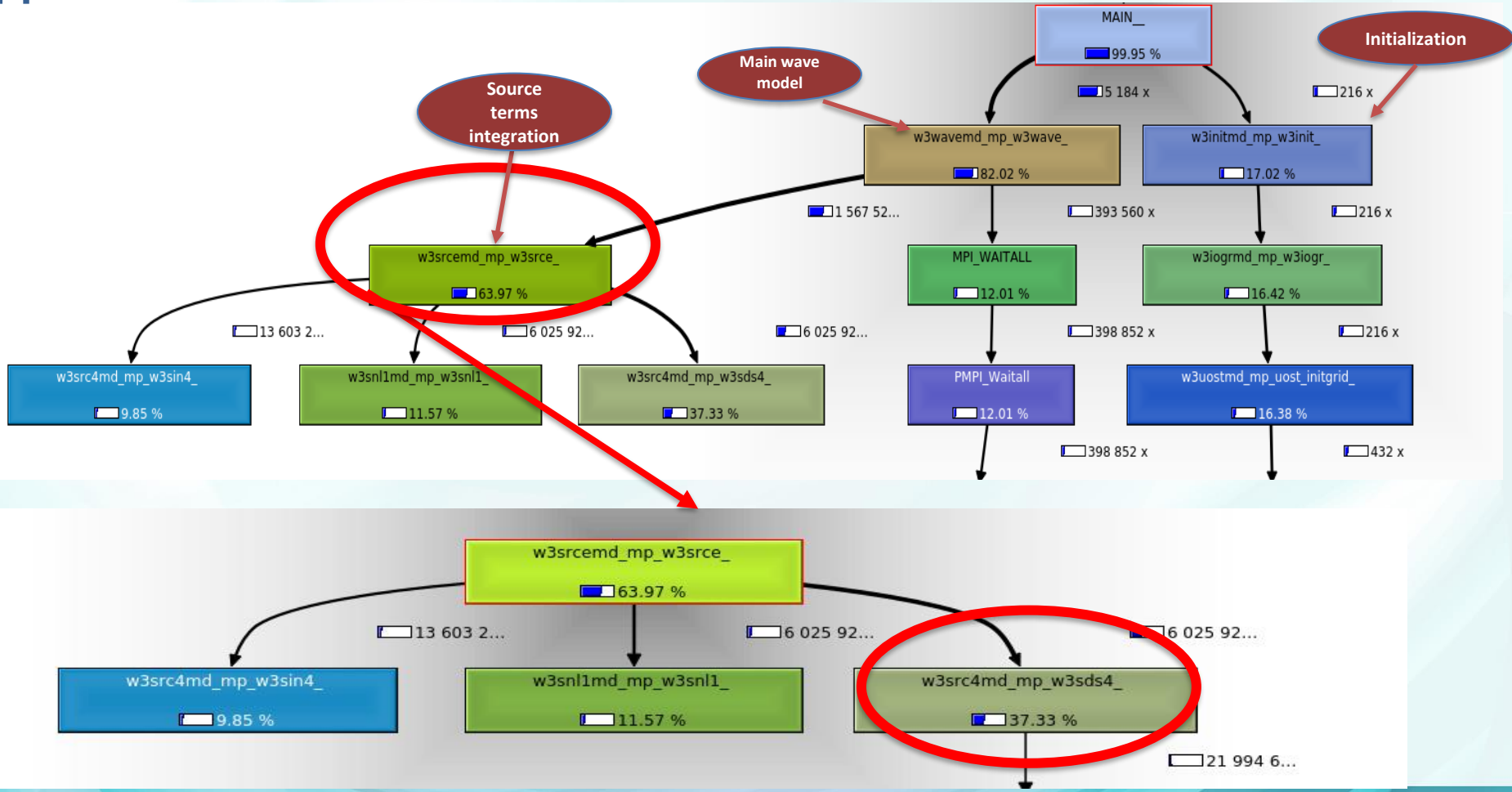

# Application Performance

## Intel Advisor: 6 Nodes

Summary | Survey & Roofline | Refinement Reports — INTEL ADVISOR

### Top time-consuming loops

| Loop | Self Time | Total Time |
|---|---|---|
| loop in w3snl1 at w3snl1md.F90:302 | 68.132s | 68.132s |
| loop in w3sds4 at w3src4md.F90:2082 | 65.604s | 65.604s |
| loop in w3snl1 at w3snl1md.F90:341 | 50.477s | 50.477s |
| loop in w3sds4 at w3src4md.F90:1751 | 38.606s | 38.606s |
| loop in w3sin4 at w3src4md.F90:442 | 37.824s | 47.324s |

### Refinement analysis data

*No data available. Collect MAP or Dependency to see the results.*

### Recommendations

- Vectorize math function calls inside loops loop in w3sds4 at w3src4md.F90:1664
- Vectorize math function calls inside loops loop in w3sds4 at w3src4md.F90:1839
- Vectorize math function calls inside loops loop in w3outg at w3iogomd.F90:1355
- Add data padding loop in w3sds4 at w3src4md.F90:1681
- Vectorize math function calls inside loops loop in w3spr4 at w3src4md.F90:233

# Parallelize Loops: OpenACC

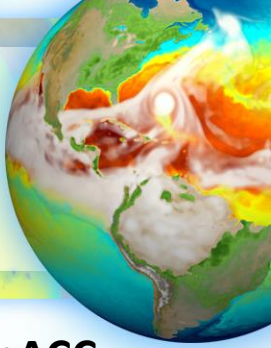

OpenACC is a directive-based API for parallel computing on accelerators (mostly on NIVDIA GPU).

It is designed to simplify GPU programming

**Source Code**

```
      DO IFR=1, NFR
        CONX = TPIINV / SIG(IFR) * CG(IFR)
        DO ITH=1, NTH
          ISP       = ITH + (IFR-1)*NTH
          UE (ISP) = A(ISP) / CONX
          CON(ISP) = CONX
          END DO
        END DO

      DO IFR=NFR+1, NFRHGH
        DO ITH=1, NTH
          ISP       = ITH + (IFR-1)*NTH
          UE(ISP) = UE(ISP-NTH) * FACHFE
          END DO
        END DO


      DO ISP=1-NTH, 0
        UE   (ISP) = 0.
        SA1 (ISP) = 0.
        SA2 (ISP) = 0.
        DA1C(ISP) = 0.
        DA1P(ISP) = 0.
        DA1M(ISP) = 0.
        DA2C(ISP) = 0.
        DA2P(ISP) = 0.
        DA2M(ISP) = 0.
        END DO
```

**With OpenACC**

```
!$acc loop independent
      DO IFR=1, NFR
        CONX = TPIINV / SIG(IFR) * CG(IFR)
!$acc loop independent
        DO ITH=1, NTH
          ISP       = ITH + (IFR-1)*NTH
          UE (ISP) = A(ISP) / CONX
          CON(ISP) = CONX
          END DO
       END DO

!$acc loop independent collapse(2)
      DO IFR=NFR+1, NFRHGH
        DO ITH=1, NTH
          ISP       = ITH + (IFR-1)*NTH
          UE(ISP) = UE(ISP-NTH) * FACHFE
          END DO
        END DO


!$acc loop
      DO ISP=1-NTH, 0
        UE   (ISP) = 0.
        SA1 (ISP) = 0.
        SA2 (ISP) = 0.
        DA1C(ISP) = 0.
        DA1P(ISP) = 0.
        DA1M(ISP) = 0.
        DA2C(ISP) = 0.
        DA2P(ISP) = 0.
        DA2M(ISP) = 0.
        END DO
```

# Parallelize Loops: OpenACC

- Parallelize the top two computational WSRCE subroutines
- GPU code is x4 the serial code
- Too many data transfers between host and device due to WW3 code structure

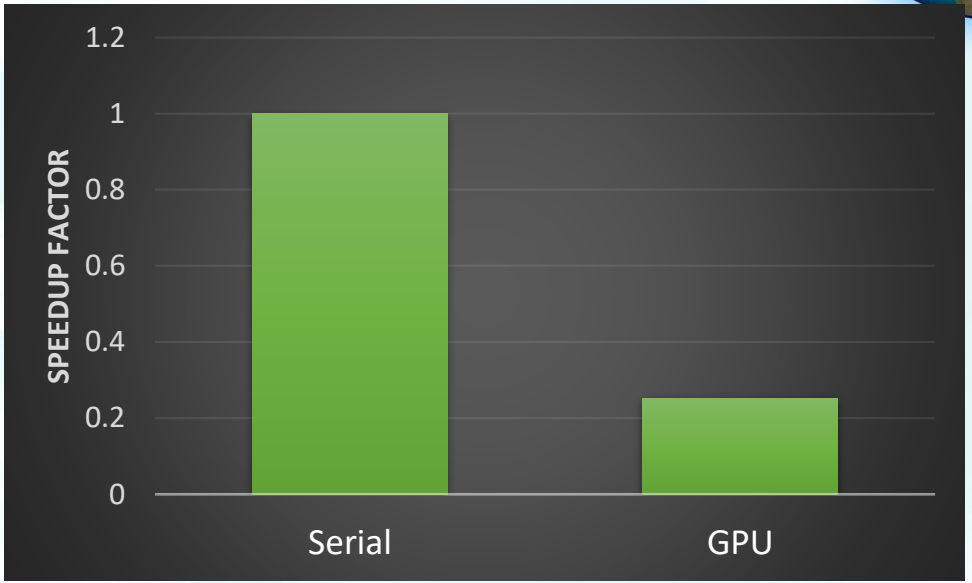


$$\text{Speedup factor} = \frac{1\ CPU\ runtime}{1\ CPU + 1\ GPU\ \ runtime}$$

# Current Challenges

- WW3 code structure
- Repeated launch of OpenACC kernels

**Source Term Integration**

*DO I = 1, LocGRIDS*
CALL WSCRE($XY_i$)
*END DO*

*DO J= 1, NTH*
CALL $W3SNL_{XY_i}(j)$
*END DO*

CALL WSCRE
*DO I = 1, LocGRIDS*
*DO J= 1, NTH*
CALL $W3SNL_{XY_i}(j)$
*END DO*
*END DO*

```
 OpenACC (excl):   79.25%  363.487s    acc_enqueue_launch@w3snl1md.F90
:276 (w3snl1_276_gpu)
                   17.14%  78.6162s    acc_exit_data@w3snl1md.F90:276
                    1.79%  8.22424s    acc_enter_data@w3snl1md.F90:276
                    0.63%  2.87860s    acc_enter_data@w3snl1md.F90:272
                    0.42%  1.90924s    acc_exit_data@w3snl1md.F90:272
                    0.41%  1.89994s    acc_compute_construct@w3snl1md.
F90:276
                    0.35%  1.58382s    acc_wait@w3snl1md.F90:276
                    0.01%  45.536ms    acc_device_init
                    0.00%  462.56us    acc_update@w3wavemd.F90:460
                    0.00%  144.22us    acc_enqueue_upload
        API calls:  98.14%  337.065s    cuEventSynchronize
                    0.79%  2.71918s    cuLaunchKernel
                    0.49%  1.66745s    cuEventRecord
                    0.23%  788.10ms    cuStreamSynchronize
                    0.16%  546.93ms    cuDevicePrimaryCtxRetain
                    0.14%  480.26ms    cuEventElapsedTime
                    0.03%  97.490ms    cuDevicePrimaryCtxRelease
```

# Moving Forward

1. Move the source term subroutine to GPU
2. Parallelize the other source term integration subroutine
3. Optimize loops
4. Optimize number of GPUs

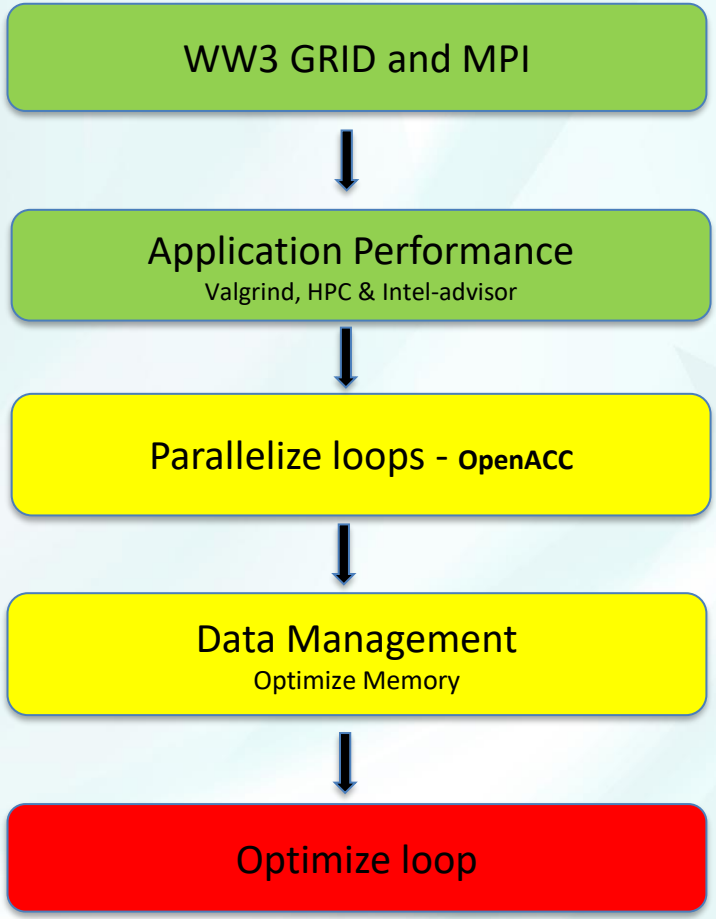

# THANK YOU

# Efficient Bayesian Inference with MCMC Samplers

Chris Kang

Washington State University

Visitng LANL T-6 Group

CNLS

August 18, 2021

## Problems in Bayesian inference of model parameters:

- The performance of most common Markov chain Monte Carlo (MCMC) methods is not scalable as the parameter dimensions grow.
- However, there are a few methods that *may be* scalable: Hamiltonian Monte Carlo (HMC).

We want to answer the following...

- Given that the gradient (sensitivity in respect to the parameters) evaluation of the Likelihood function is expensive... is HMC *practical*?

## More on HMC and other MCMC samplers

- Metropolis-Hastings algorithm randomly explores the parameter space. Not scalable!
- In contrary, HMC uses the gradient information to deterministically explore the parameter space.
- When dealing with ODE model-constrained likelihood functions, the gradient information depends on simulation outputs. This computation is expensive!

## Case study: Susceptible-Infected-Recovered (SIR) model

We aim to infer parameters (infection rate, $k_1$ and recovery rate, $k_2$) of the SIR model with HMC with different gradient computation methods.

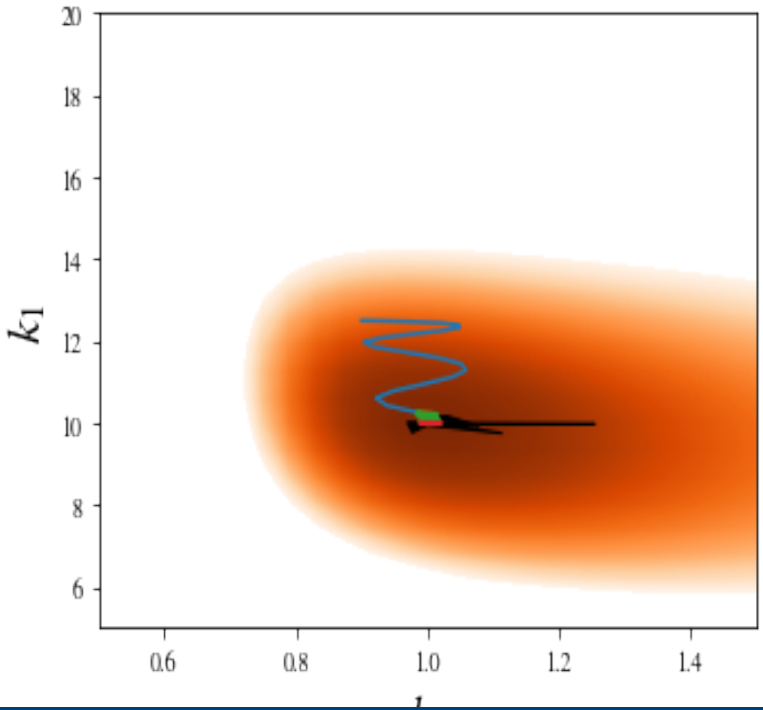


$$\dot{S} = -\frac{k_1}{N} SI$$

$$\dot{I} = \frac{k_1}{N} SI - k_2 I$$

$$\dot{R} = k_2 I$$

## Tasks Accomplished So Far:

- Applied gradient computation for linear/non-linear system of ODEs with analytical solutions.
  - Finite Difference
  - Forward Sensitivity
  - Adjoint Sensitivity
- Implemented a small Python module of gradient computation methods for HMC in the SIR model.
- Began utilizing different MCMC samplers with the gradient methods for other ODE-constrained models.

## Future Directions

- Qualitatively measure the practicality of HMC with increasing number of parameters.
- If HMC is indeed impractical, it will require the development of a new algorithm.
- Implementation of an efficient sampler in PyBioNetFit.
- Use-case in my own thesis.

## Acknowledgment:

I would like to thank Zachary Fox, Yen Ting Lin, William Hlavacek for the mentorship.

This work was supported by:

- NIH/NIGMS Grant R01GM111510
- Support from CNLS

*Thank You!*

Los Alamos NATIONAL LABORATORY

# Characterization of Graphene Quantum Dots in Terms of Their Electronic and Optical Properties

Noor Md Shahriar Khan
Graduate Intern (Summer)
T-1, Theoretical division

August 10, 2021

# Motivation

### *Graphene*

Two-dimensional honeycomb lattice made of $sp^2$-hybridized carbon atoms

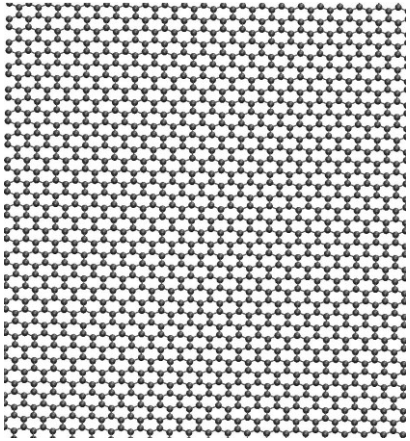

Lack of band-gap

### *Graphene Quantum Dots*

- Finite size (< 100 nm)
- Quantum confinement and edge effect

*Application*

- Tunable optical and photoelectronic properties
- Bioimaging
- LEDs
- Photodetectors
- OPV solar cells
- Photoluminescent material

# Motivation

### *Graphene*

Two-dimensional honeycomb lattice made of $sp^2$-hybridized carbon atoms

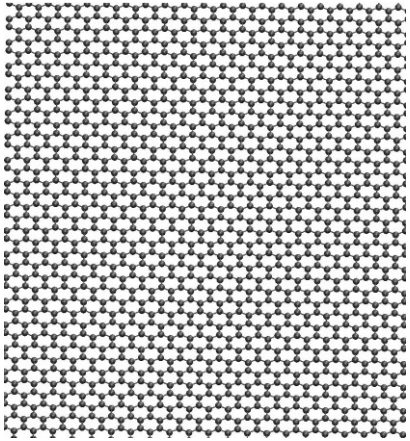

Lack of band-gap

### *Graphene Quantum Dots*

- Finite size (< 100 nm)
- Quantum confinement and edge effect

*Application*

- Tunable optical and photoelectronic properties
- Bioimaging
- LEDs
- Photodetectors
- OPV solar cells
- Photoluminescent material

### *Tunable Optical Features of Graphene Quantum Dots from Edge Functionalization*

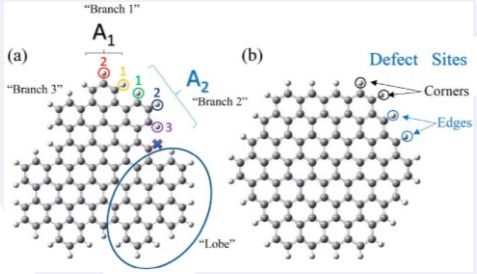


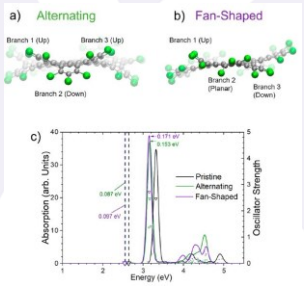


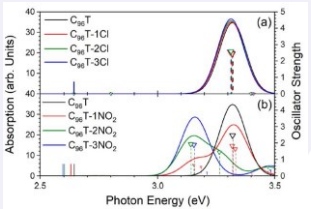


*J. Phys. Chem. C 2021, 125, 9244−9252*

# Presentation Outline

Theoretical Investigation of Graphene Quantum Dots (GQDs) in terms of their optical and electronic properties

***Part I***

Different Shapes of $C_{96}$ graphene flakes

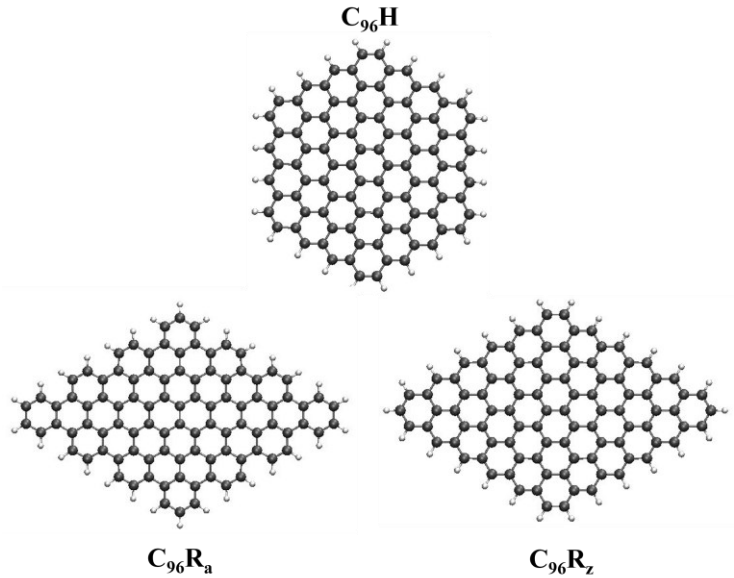


***Part II***

Different isomers of $C_{118}S$ graphene flakes

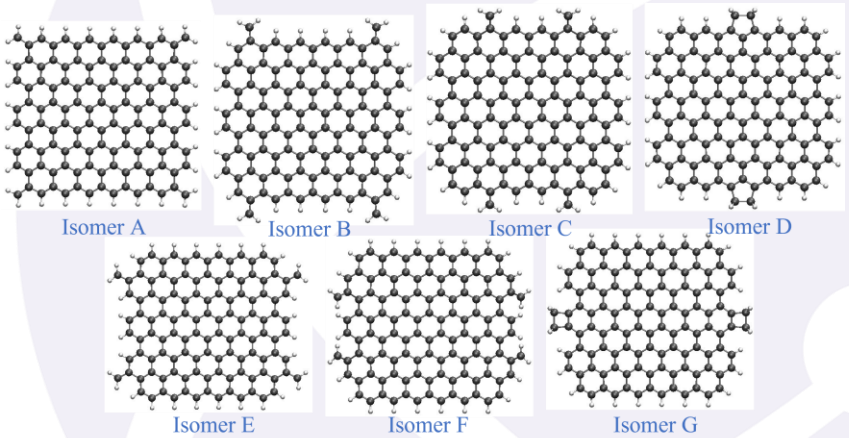


*Methodology: Electronic Structure Theory (CAM-B3LYP/6-31G)*

# Change of Optical Properties based of different Shapes of $C_{96}$ Graphene Flakes

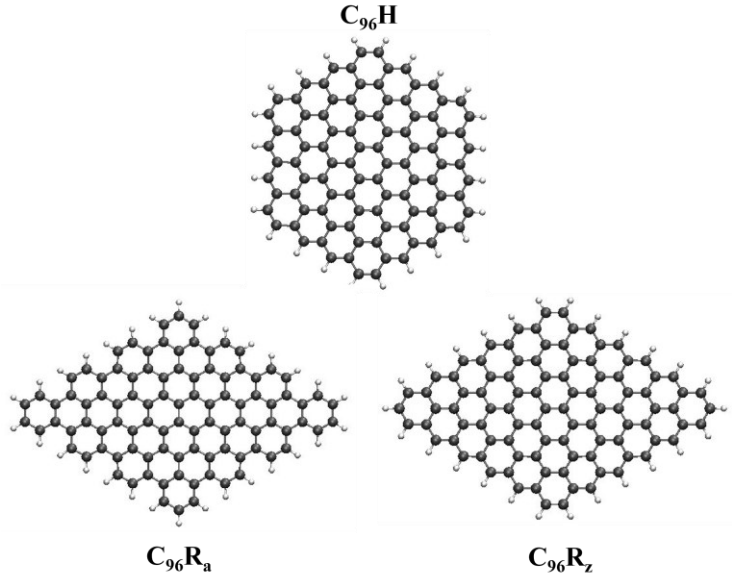

# Change of Optical Properties based of different Shapes of $C_{96}$ Graphene Flakes

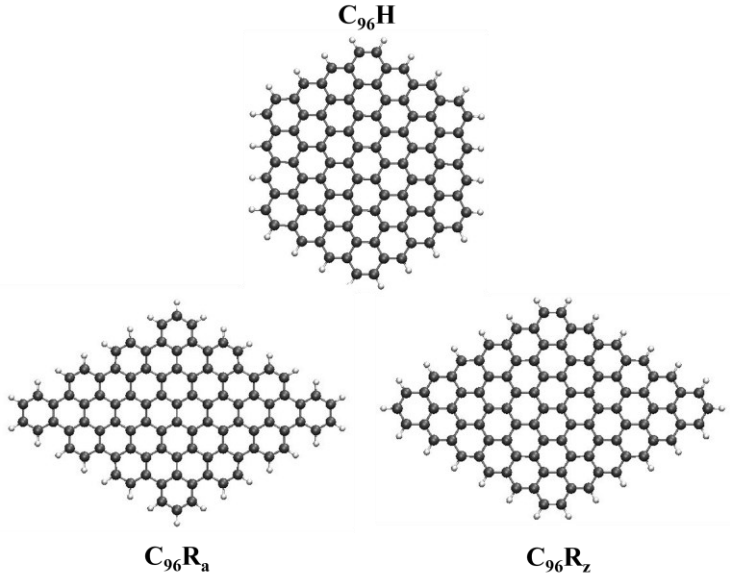


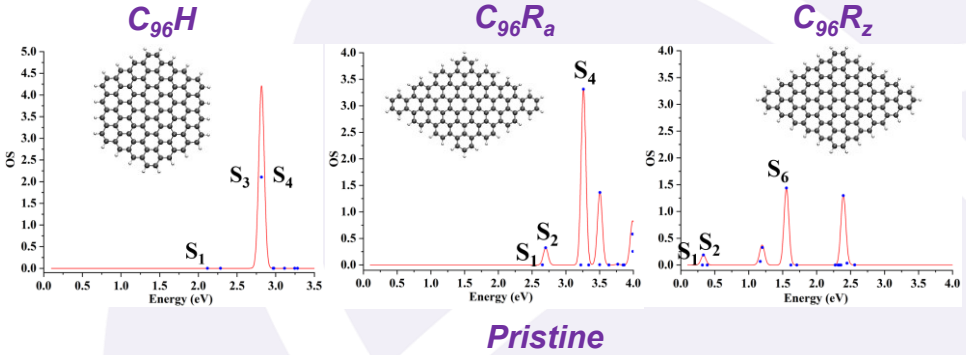


*Pristine*

# Change of Optical Properties based of different Shapes of $C_{96}$ Graphene Flakes

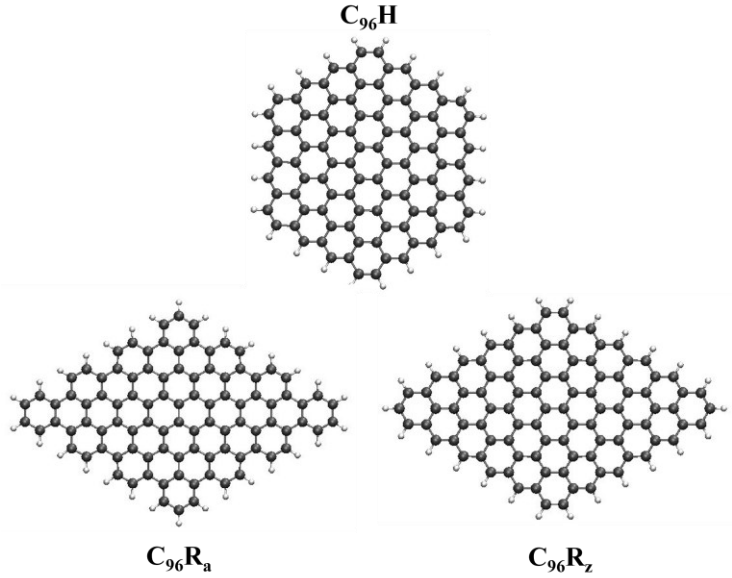


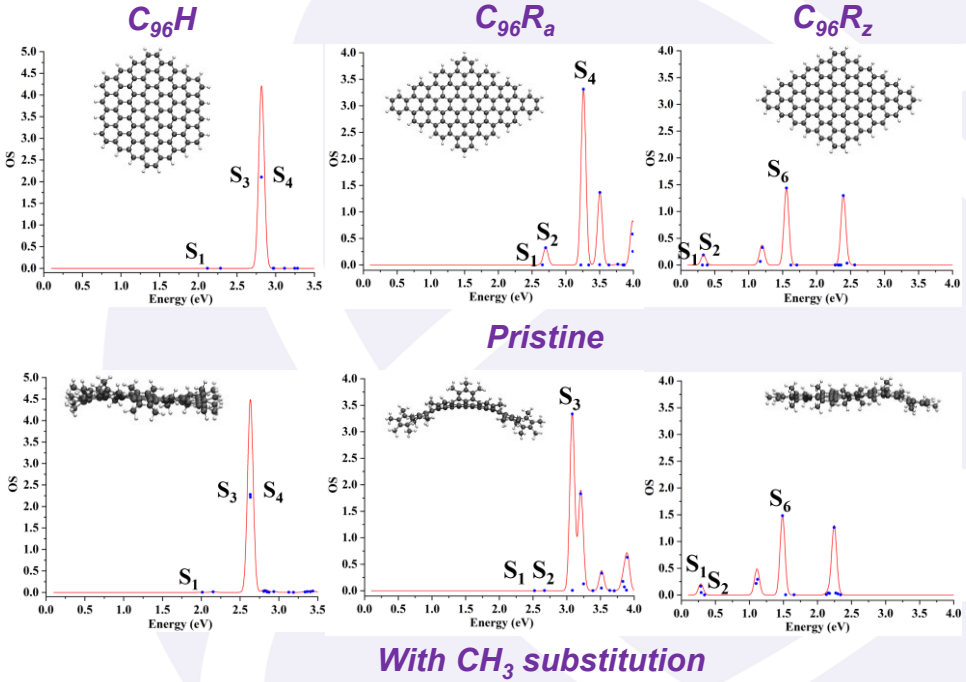

# Change of Optical Properties based of different Shapes of $C_{96}$ Graphene Flakes

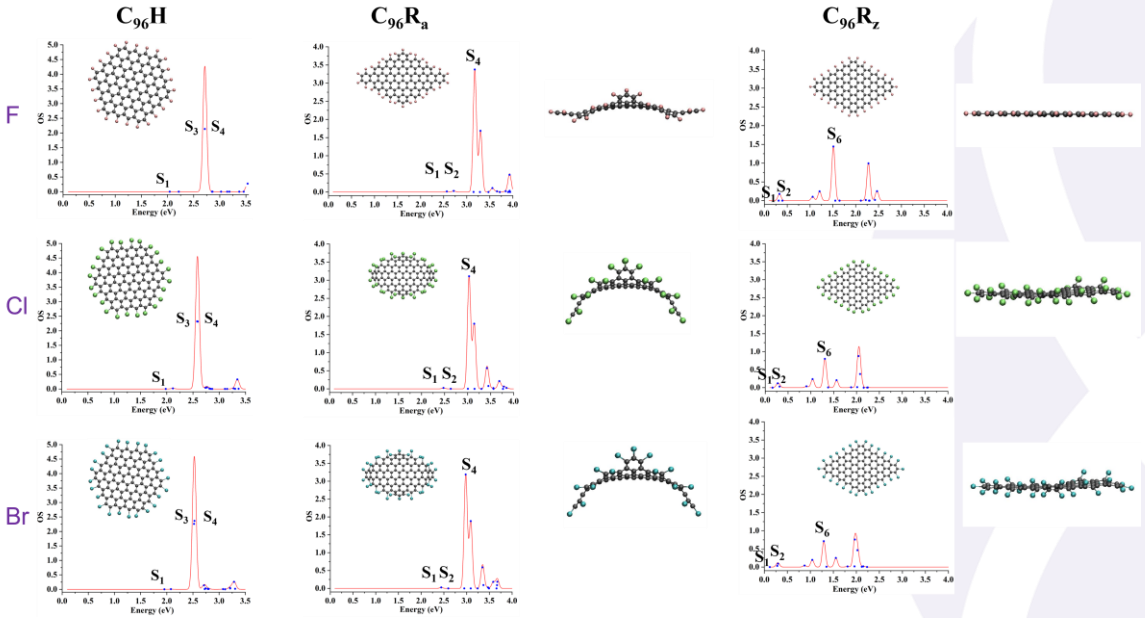


*With F/Cl/Br substitution*

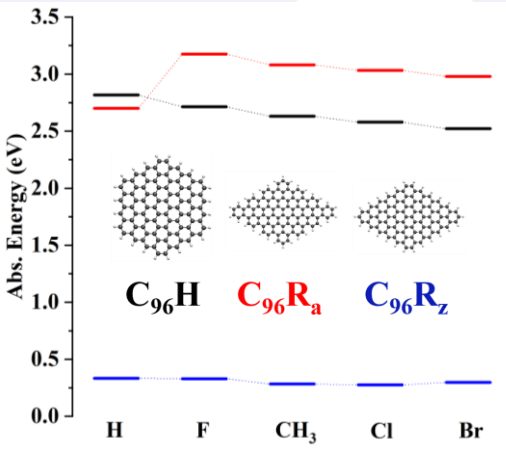

# Change of Optical Properties for Different Isomers of $C_{118}$ Square Graphene Flakes

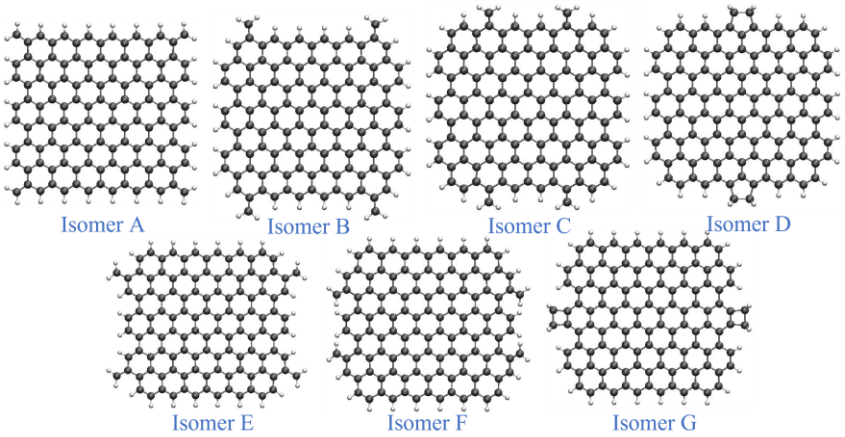


*Seven isomers based on the position of $CH_2$ substitution*

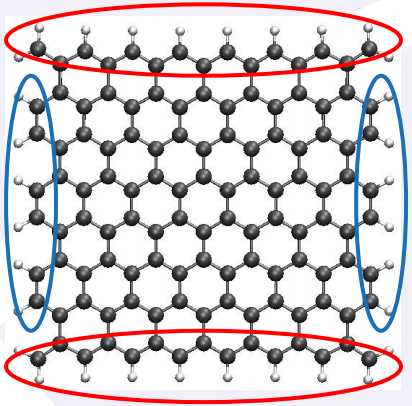

Zigzag Edge
Armchair Edge

# Change of Optical Properties for Different Isomers of $C_{118}$ Square Graphene Flakes

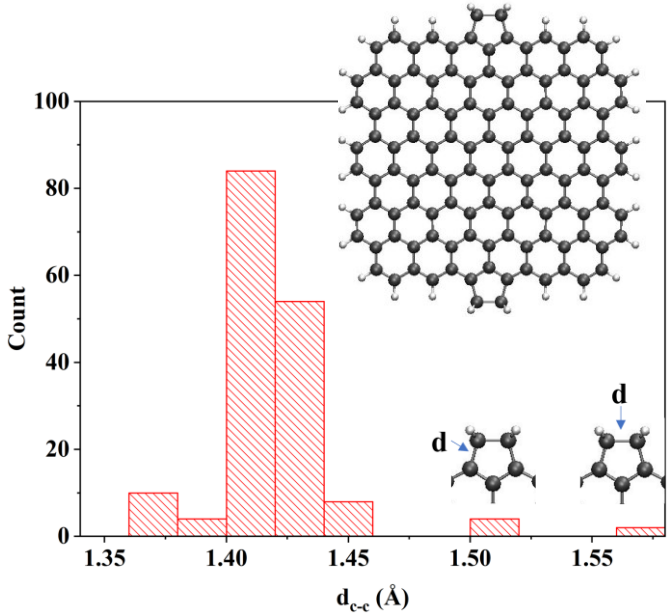


*C-C bond distances for isomer D*

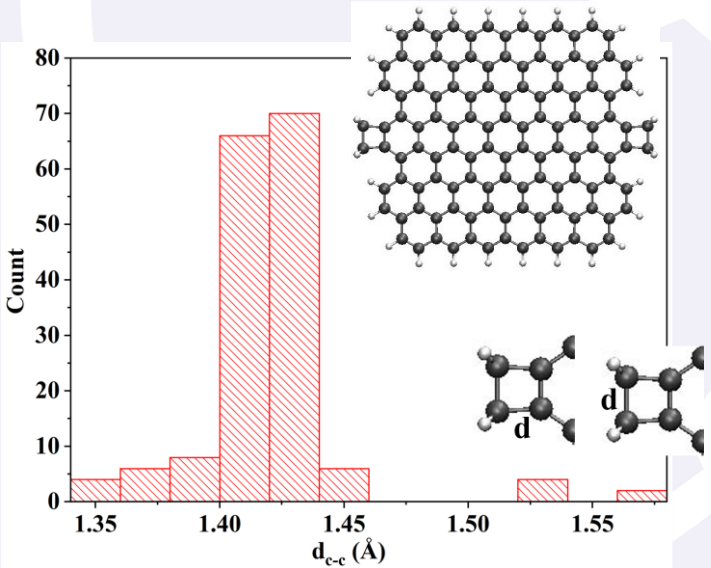


*C-C bond distances for isomer G*

# Change of Optical Properties for Different Isomers of $C_{118}$ Square Graphene Flakes

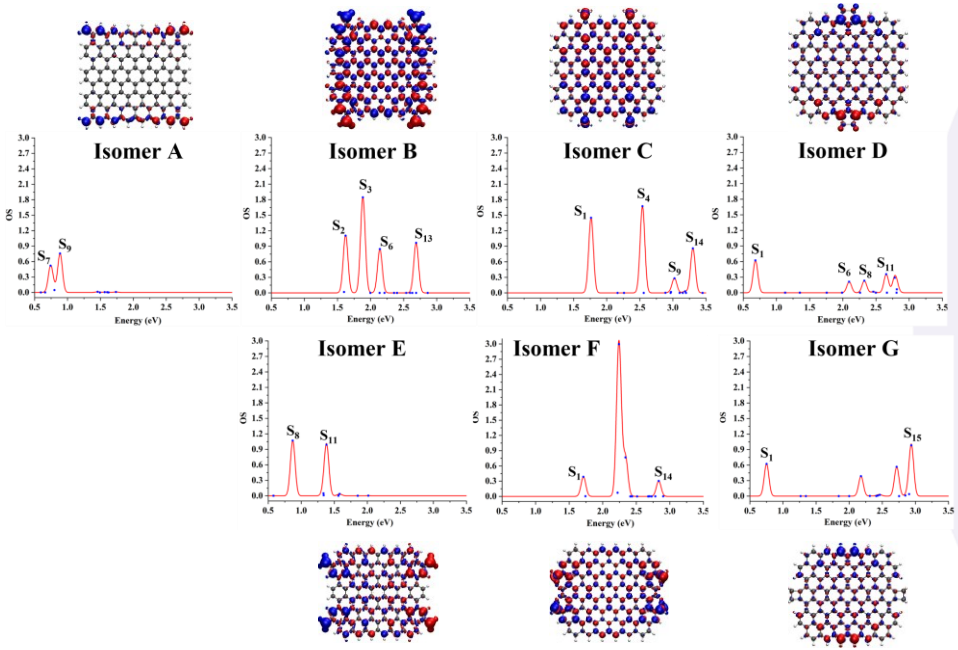


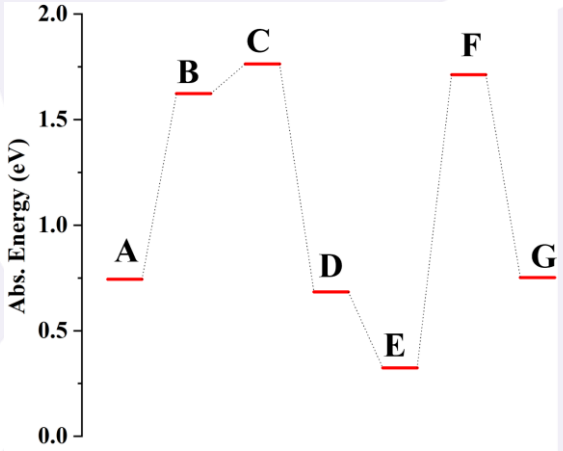


***Absorption energy depends on the position of $CH_2$ substitution***

# In Summary

- We have studied hexagonal, rhombic and square shape of two-dimensional $sp^2$ hybridized graphene flakes and their edge functionalized species
- A comparison of optical properties between $C_{96}$ hexagon and $C_{96}$ rhombus graphene flake is reported. $C_{96}$ rhombus with all-armchair edge has higher absorption energy than all-zigzag edge
- For the $C_{96}$ rhombus shape, the armchair edge has additional flexibility for edge functionalization
- For $C_{118}$ square graphene flakes, four methylene substitution at the edge is probed
- The position of methylene substitution determines the electronic and optical properties of the corresponding graphene flakes

# Acknowledgement

T-1, Theoretical Division, LANL
Dr. Sergei Tretiak
Dr. Alan Bishop
Dr. Brendan Gifford
Braden Weight

Laboratory Directed Research and Development Program (LDRD)

***Thank You***

# Predicting Cardiovascular disease (CVD) risk using VA patients data

Beauty Kolade
T-CNLS / T-6
08/25/2021


Mentors: Benjamin Mcmahon (T-6), Kumkum Ganguly (B-10)

# Cardiovascular Diseases

- Diseases that affect the circulatory system
- Heart Attack (AMI), Stroke and Atherosclerotic CVD (ASCVD) death
- According to the CDC, about 655,000 Americans die from heart disease each year—that's 1 in every 4 deaths

# Pooled Cohort equation (PCE)

- risk prediction equations from Framingham Heart Study served as the basis for developing PCE
- provide sex and race specific estimates of 10-year ASCVD risk for patients between ages 40 - 79
- Current clinical practice uses eight variables and a score to estimate CVD risk

We want to use 200 time-dependent variables, including Labs, Vitals, Comorbidities and Treatments

| | Age, *y* | Sex | Systolic BP, *mm Hg* | BP Treatment | Total Cholesterol Level | | HDL Cholesterol Level | | Smokes Tobacco | Diabetes |
|---|---|---|---|---|---|---|---|---|---|---|
| | | | | | *mmol/L* | *mg/dL* | *mmol/L* | *mg/dL* | | |
| **Black-white estimated risk ratios <0.7 per 2013 PCEs** | | | | | | | | | | |
| 1 | 46 | Male | 108 | No | 6.79 | 262 | 0.85 | 33 | Yes | No |
| 2 | 68 | Male | 115 | No | 5.08 | 196 | 1.04 | 40 | No | No |
| 3 | 43 | Female | 111 | No | 7.28 | 281 | 2.07 | 80 | Yes | No |
| 4 | 76 | Female | 132 | Yes | 3.63 | 140 | 1.73 | 67 | No | No |
| 5 | 70 | Male | 138 | No | 3.96 | 153 | 0.96 | 37 | No | No |

# Approach

1. Collect predictor variables (labs, diagnoses, treatments) on 1 million patients with CVD outcome and 1 million controls
2. use predictive modeling to predict outcome
   - Logistic Regression: 0.75 AUC
   - Random forest (decision tree): 0.80 AUC
   - Deep learning (neural network): 0.82 AUC
3. compare accuracy measures and understand determinants of outcome

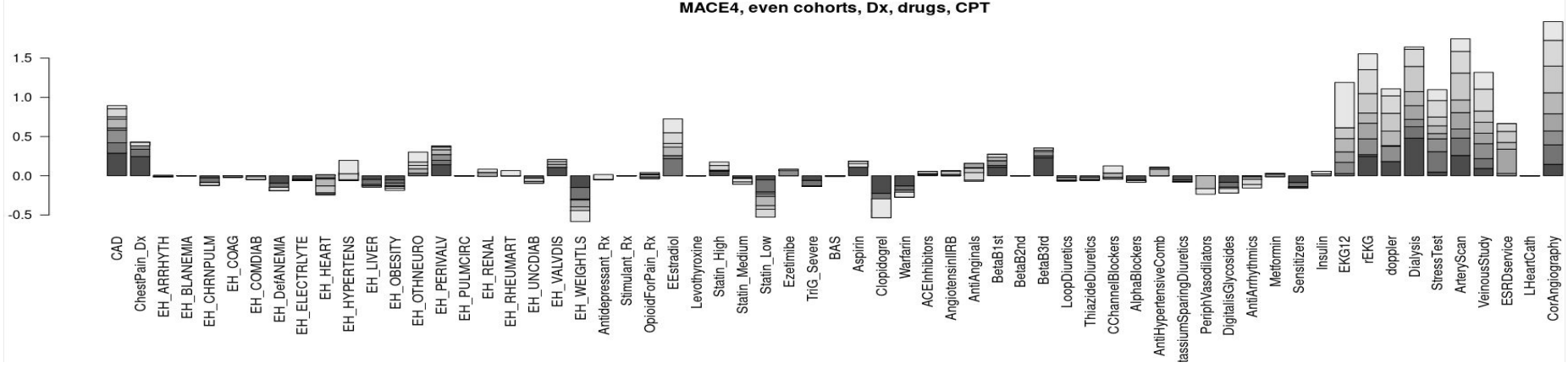

# Longitudinal Case-control Study Design is efficient


Figure 1: Case-Control Study Design

Cases and Controls- 1 million each, using measurements of 200 variables.

# Example Results

## Vital Sign

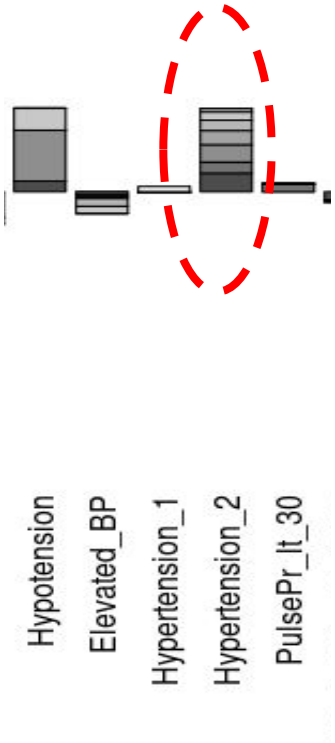


## Lab test

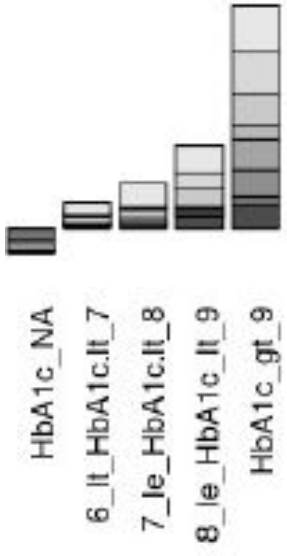


## Procedure

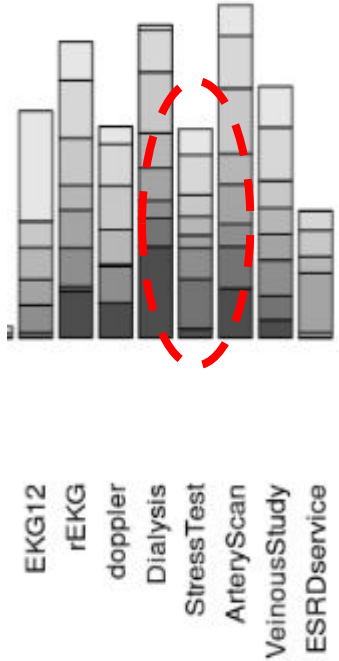

# Results are more interpretable if standard of care used

**Table 1. High-, Moderate-, and Low-Intensity Statin Therapy (Used in the RCTs Reviewed by the Expert Panel)***

| *High intensity* | *Moderate intensity* | *Low intensity* |
|---|---|---|
| Daily dosage lowers LDL-C by approximately ≥ 50% on average | Daily dosage lowers LDL-C by approximately 30% to 50% on average | Daily dosage lowers LDL-C by < 30% average |
| **Atorvastatin (Lipitor), 40† to 80 mg** | **Atorvastatin, 10** *(20)* **mg** | *Simvastatin, 10 mg* |
| **Rosuvastatin (Crestor), 20** *(40)* **mg** | **Rosuvastatin,** *(5)* **10 mg** | **Pravastatin, 10 to 20 mg** |
| | **Simvastatin (Zocor), 20 to 40 mg‡** | **Lovastatin, 20 mg** |
| | **Pravastatin (Pravachol), 40** *(80)* **mg** | *Fluvastatin, 20 to 40 mg* |
| | **Lovastatin (Mevacor), 40 mg** | *Pitavastatin, 1 mg* |
| | *Fluvastatin XL (Lescol XL), 80 mg* | |
| | **Fluvastatin, 40 mg twice daily** | |
| | *Pitavastatin (Livalo), 2 to 4 mg* | |


**Mapping the drugs and dosages to the standard of care leads to a clear, interpretable result**

# Next steps

- Work through the rest of the variables.
- Optimize variables/ model and compare risk predicting abilities with that of PCE
- Expand on the impact of Genetics on variable and how it can increase or decrease risk

# Acknowledgement

CNLS:Angel Garcia


Mentors: Benjamin Mcmahon, Kumkum Ganguly

Group Members: Sayera Dhaubhadel, Ruy Ribeiro, Rebecca Hehl, Haedi Deangelis

# Thank you!

# Diversification of ML Datasets Using Bias Potentials as Functions of "Uncertainty"

Maksim Kulichenko

3rd year PhD, Utah State University

T-1 Division

Mentor: Justin Smith

Co-mentor: Sergei Tretiak

Collaborator: Kipton Barros

# Make Dataset Better

Purpose: the ideal ratio between *Time, Size, Diversity*

- Capture as much conformational and configurational space as possible
- Dataset diversity increase
- Dataset preparation time decrease

# The ANI neural network potential

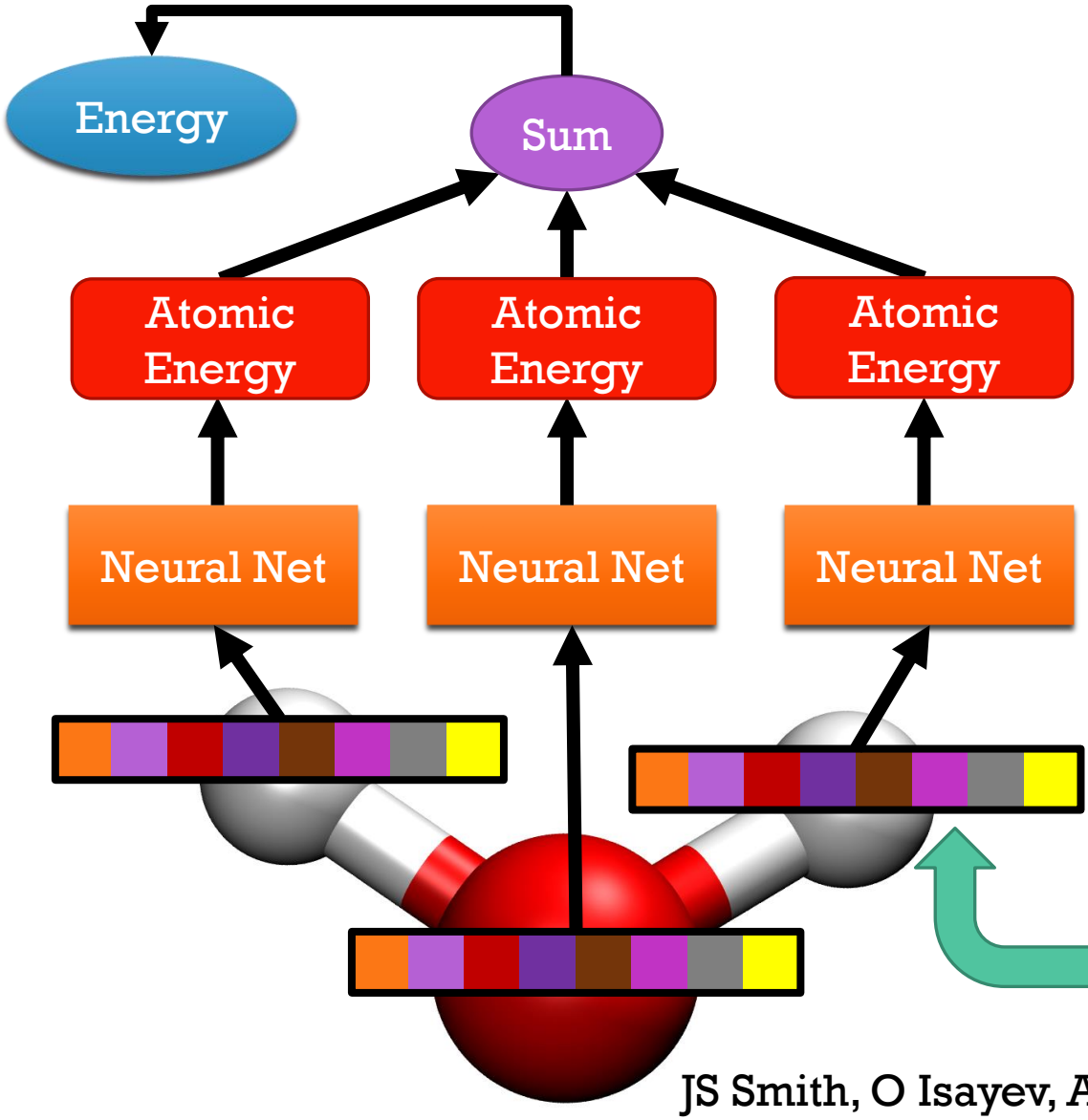


**Angular environment**

Angle over *j*,*k* neighbors centered on atom *i*

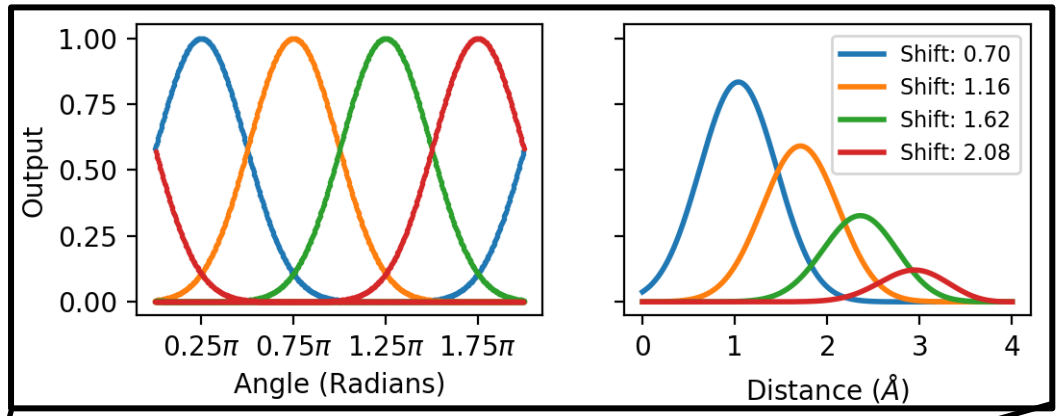


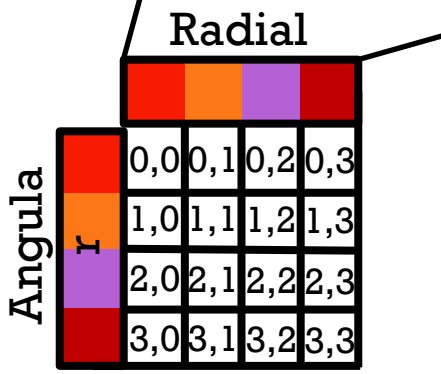


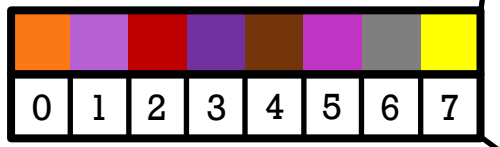


**Radial environment**

Distance over *j* neighbors centered on atom *i*

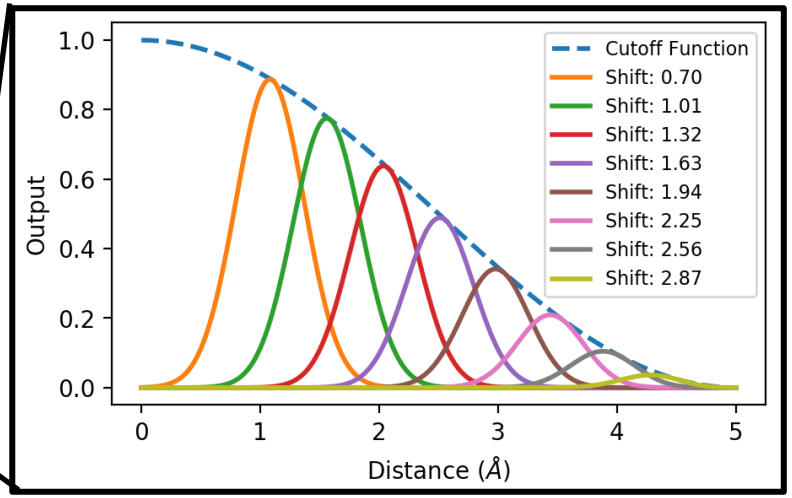


JS Smith, O Isayev, AE Roitberg, *Chem. Sci.*, 2017, **8**, 3192-

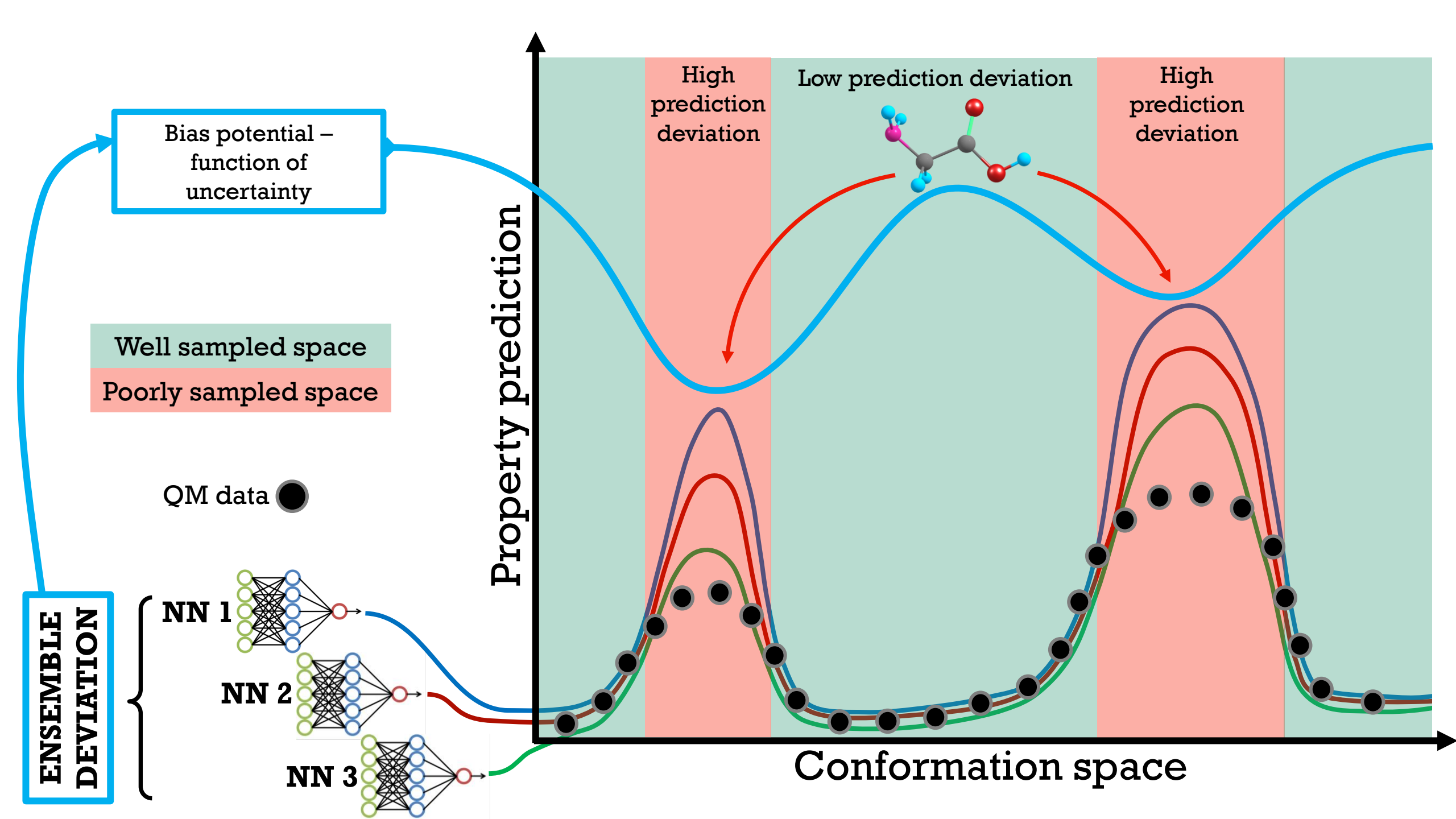
Bias potential – function of uncertainty
Well sampled space
Poorly sampled space
QM data
ENSEMBLE DEVIATION
NN 1
NN 2
NN 3
High prediction deviation
Low prediction deviation
High prediction deviation
Property prediction
Conformation space

- Math of Energy uncertainty

# Moving towards Low Sampled Region

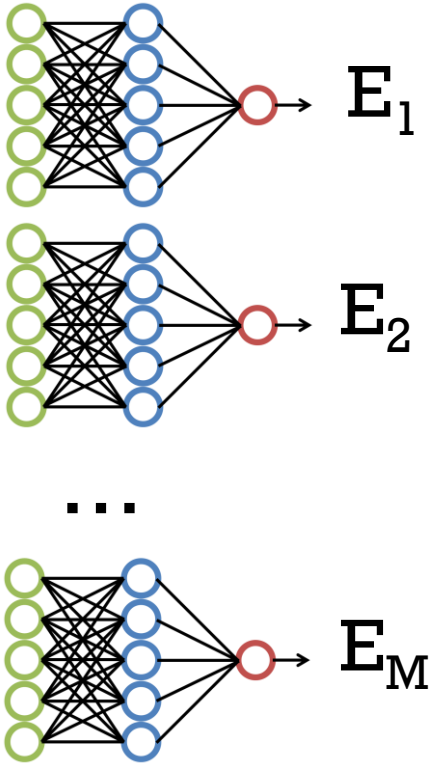


$$\bar{E} = \frac{1}{M}\sum_{m=1}^{M}\hat{E}_m$$

$$\sigma_E^2 = \frac{1}{M(M-1)}\sum_{m=1}^{M}\delta E_m{}^2,$$

$$\delta E_m = \hat{E}_m - \bar{E},$$

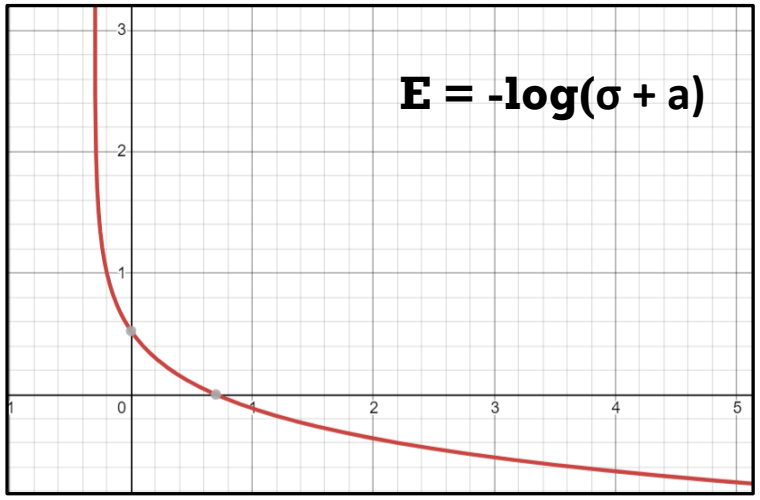

# UQ Test

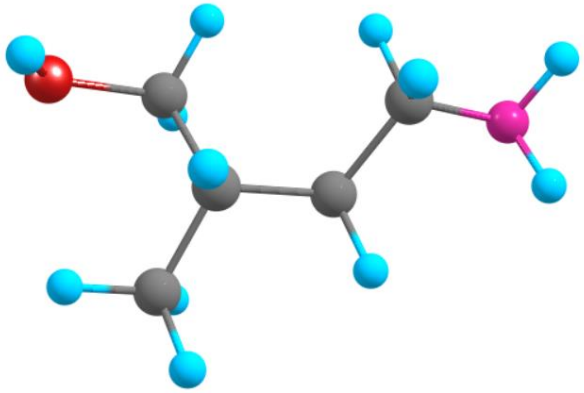

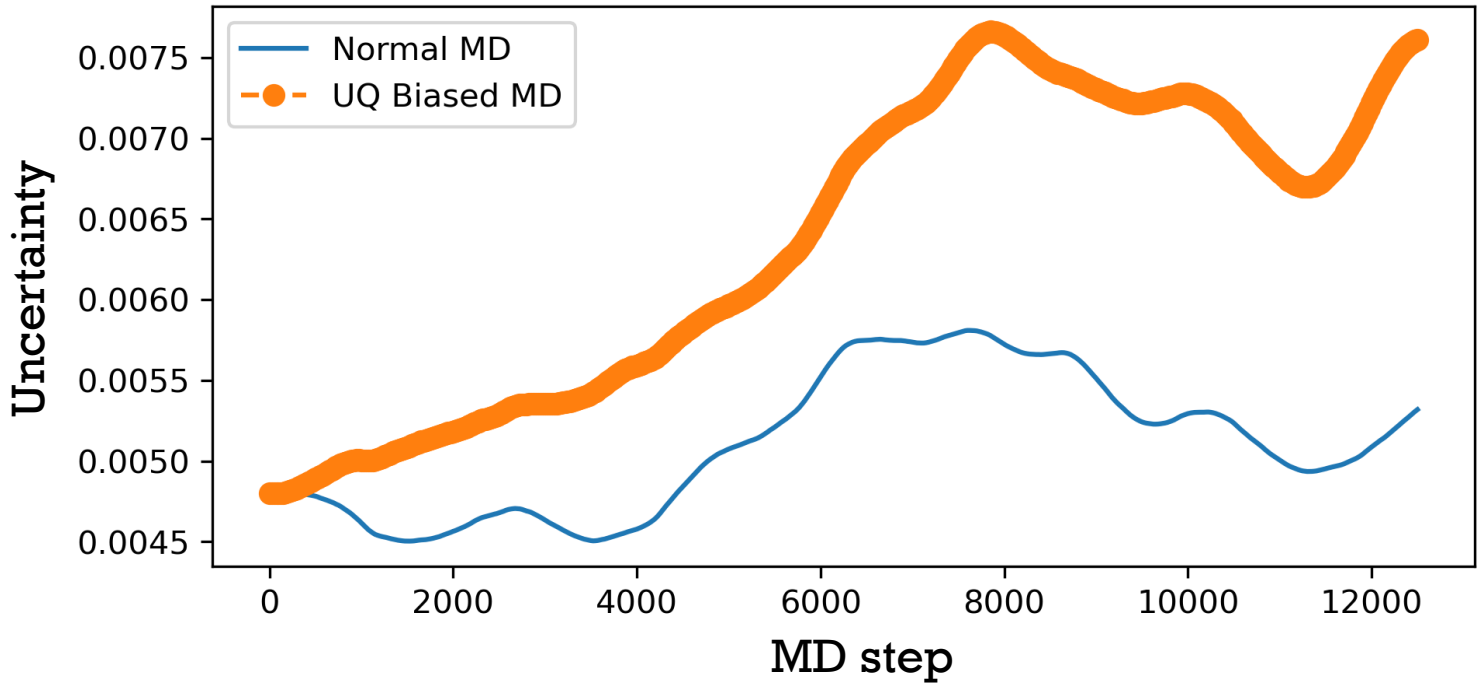
Normal MD
UQ Biased MD
Uncertainty
0.0075
0.0070
0.0065
0.0060
0.0055
0.0050
0.0045
0
2000
4000
6000
8000
10000
12000
MD step

# t-SNE Latent Space

Plot biased and non-biased Active learning over lond scale MD (25 ns)

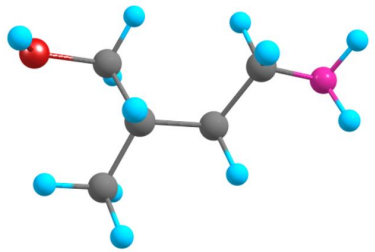

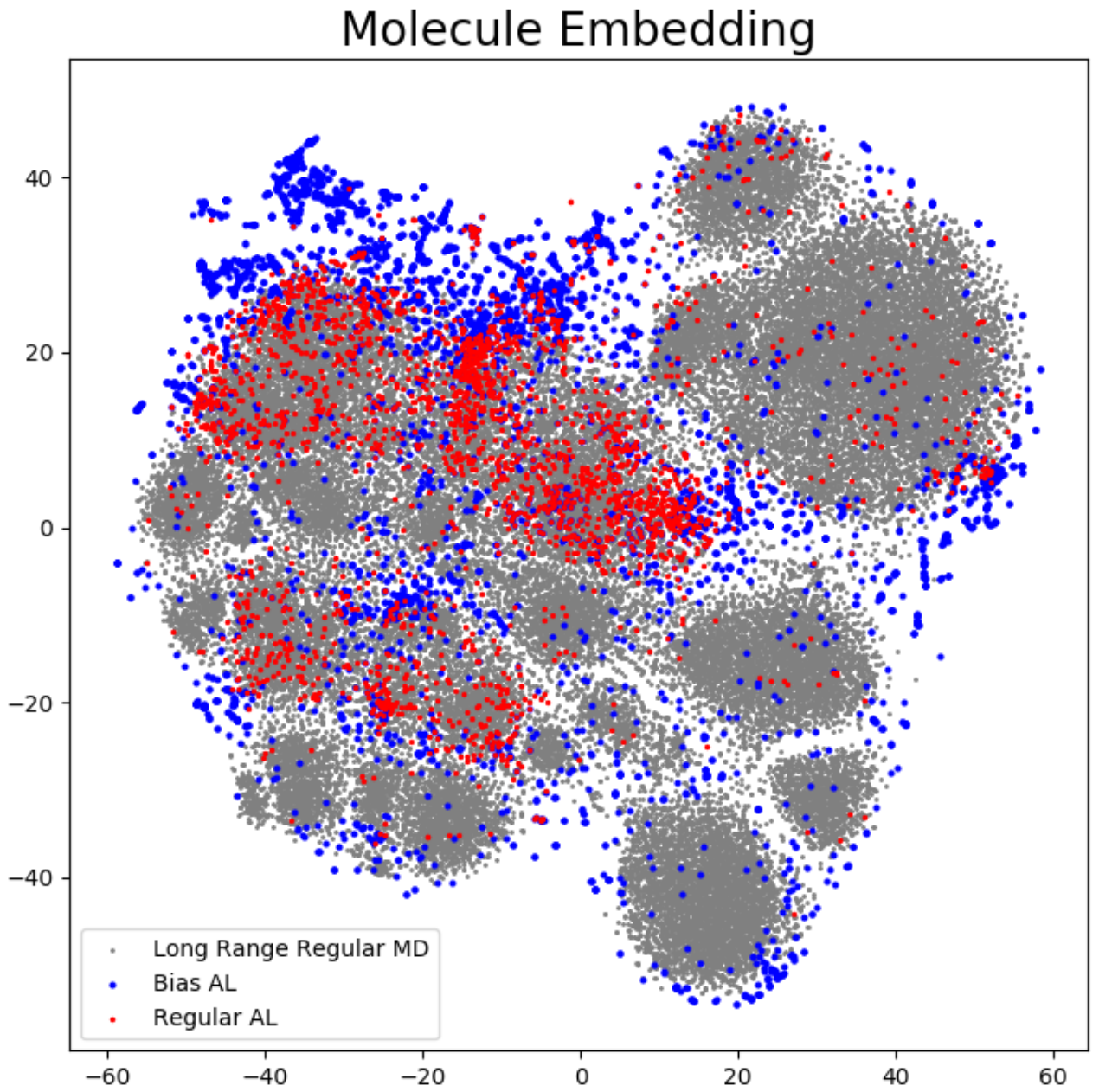

# Feeding Long Range MD data to…

## Model trained on non-biased AL data

## Model trained on biased AL data

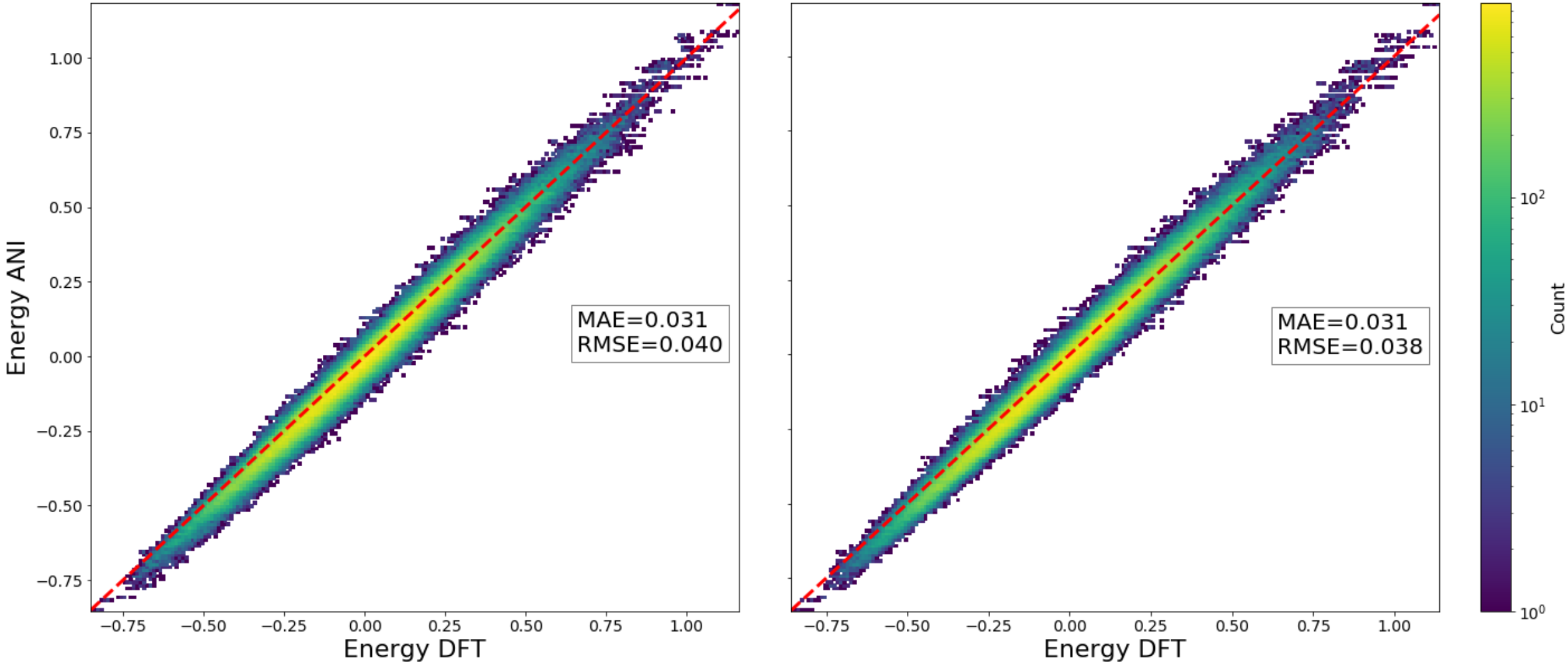


x1.5-2 faster

# ANI-1ccx NN-potential

## Acetylacetone

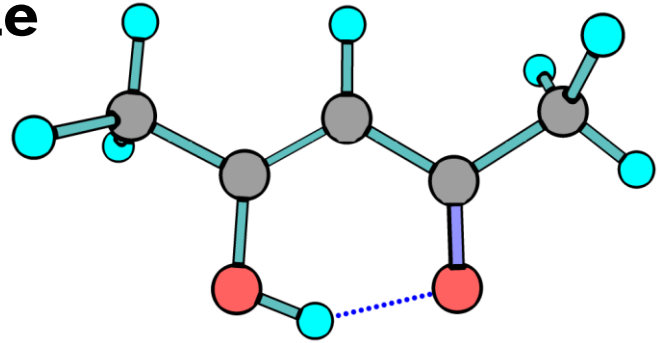

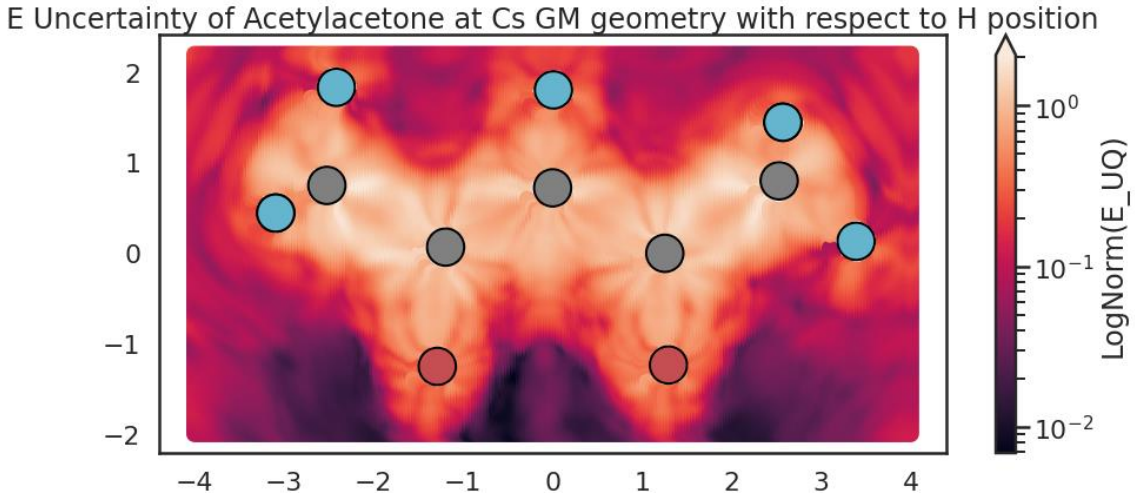


## Bias OFF

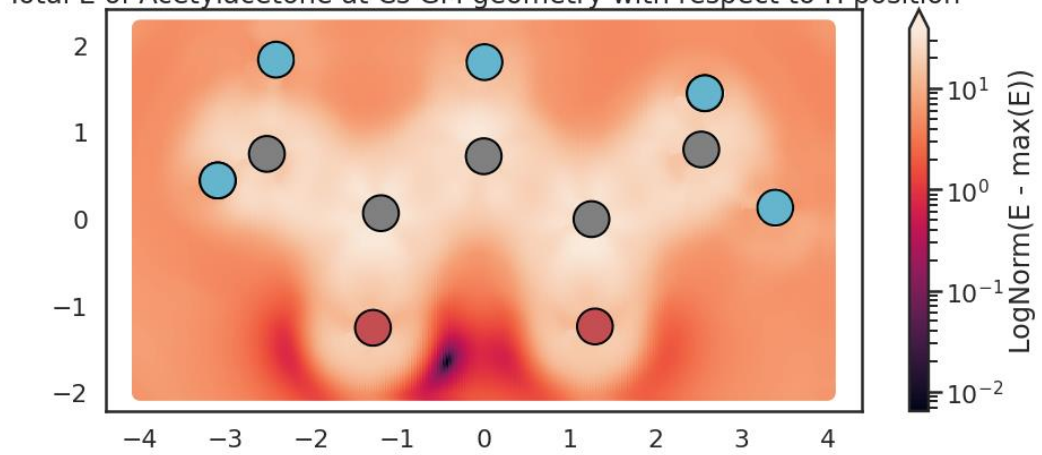


## Bias ON

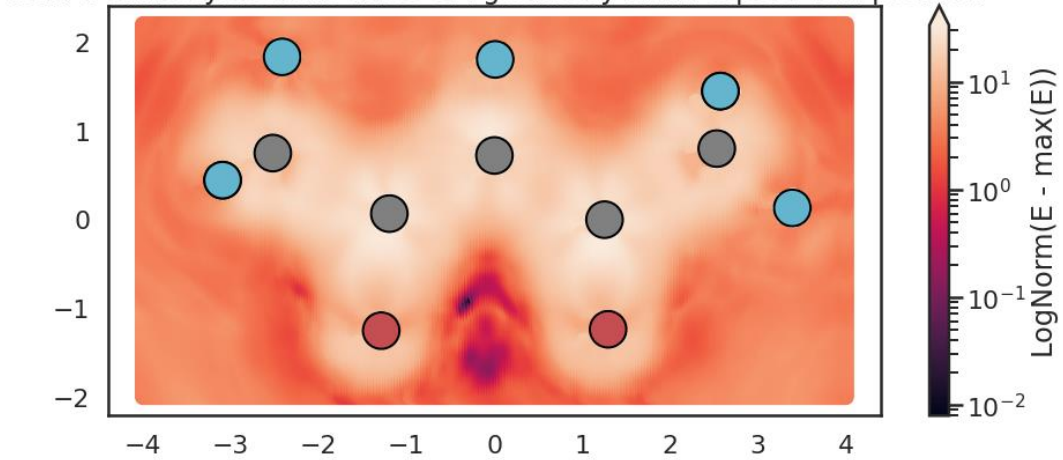


## O-H distances in MD, 0.04 ns

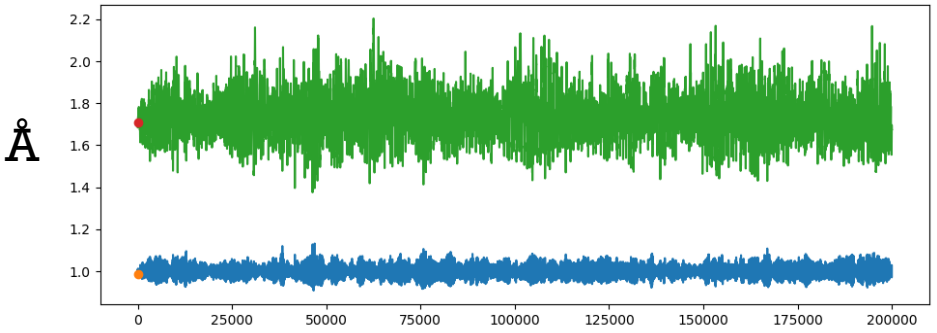


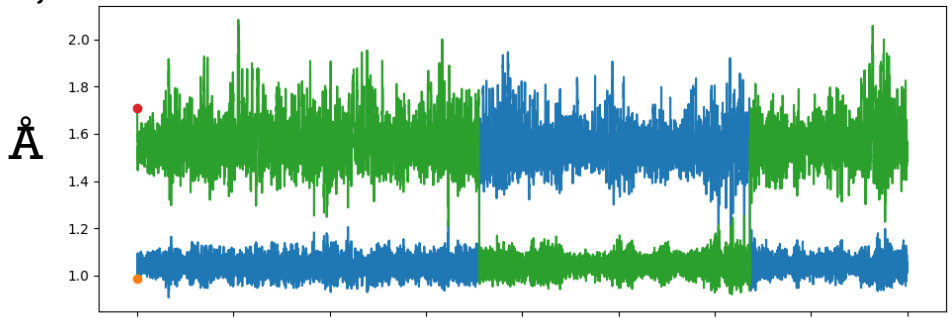

**Los Alamos National Laboratory**

**Utah State University**

# Thank you for your attention!

**Many thanks to**

- Mentor: Justin Smith
- Co-mentor: Sergei Tretiak
- Kipton Barros
- Advisor: Alex Boldyrev

Los Alamos NATIONAL LABORATORY

THEORETICAL DIVISION Since 1943 Lightning Talks

# 2021 Virtual Theoretical Division Lightning Talk Series

LA-UR-21-24973

27/07/21

Martin Larocca[1,2] @ **Theoretical Division, Los Alamos National Lab.**

**1. PhD @ Universidad de Buenos Aires, Argentina.**
**2. GRA @ T4, Los Alamos National Laboratory, USA.**

**Mentor:** Diego Wisniacki
**Mentors:** Patrick J. Coles, Marco Cerezo

# Diagnosing Barren Plateaus with tools from Quantum Optimal Control.

**ArXiv 2105.14377**

ML, Piotr Czarnik, Kunal Sharma, Gopikrishnan Muraleedharan, Patrick J. Coles, and M. Cerezo

Los Alamos NATIONAL LABORATORY

UNIVERSIDAD·DE·BUENOS·AIRES

# Introduction

# Introduction to Variational Quantum Algorithms (VQAs) and Barren Plateaus

Quantum Computers promise speed-ups.

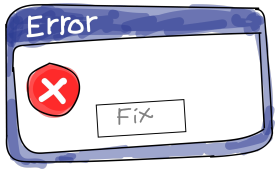


Present Day devices are noisy and error prone.

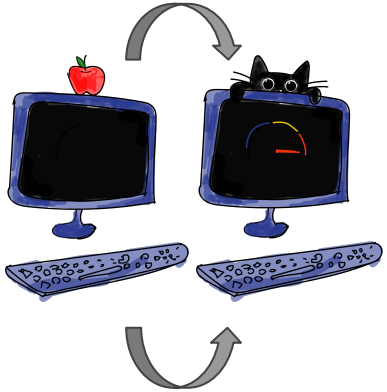

Hybrid Quantum-Classical Algorithms are believed to constitute a way around this problem.

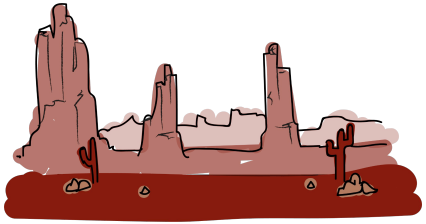

However, Barren Plateaus may arise and compromise their trainability (and thus speed-ups).

**Do these forecast a winter for variational algorithms?**

# Common Framework for VQAs and QOC

# Introduction to Quantum Optimal Control

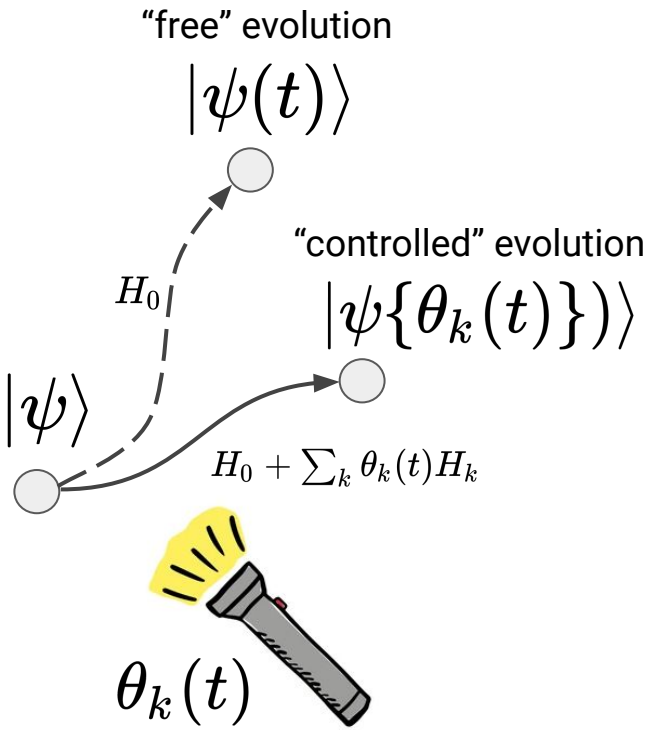


Parametrize the control fields

$$\{\theta_k(t)\} \longrightarrow \vec{\theta}$$

Define cost function

$$C(\theta) = \mathrm{Tr}[\rho(\theta)\mathrm{O}]$$

Find optimal parameters

$$\vec{\theta}_{opt} = \mathrm{argmin}_\theta \mathrm{C}(\theta)$$

# Generalized Framework for QOC and VQA

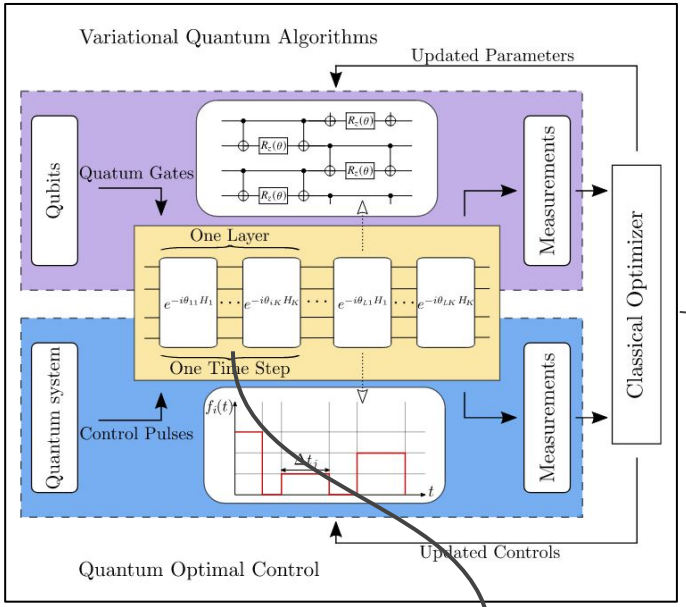


Goal: minimize Cost

$$\min_{\boldsymbol{\theta}} C(\boldsymbol{\theta})$$

$$C(\boldsymbol{\theta}) = \mathrm{Tr}[OU(\boldsymbol{\theta})\rho U^{\dagger}(\boldsymbol{\theta})]$$

**Message:** the circuit is fundamentally determined by the set of generators

Set of Generators

$$\mathcal{G} = \{H_k\}_{k=0}^{K}$$

Single Layer Propagator

$$U_l^{\mathrm{VQA}} = \prod_{k=0}^{K} e^{-iH_k\theta_{lk}}$$

$$U_l^{\mathrm{QOC}} = e^{-i(H_0+\sum_{k=1}^{K}\theta_{lk}H_k)\Delta t_l}$$

# Barren Plateaus[1,2]

No Barren Plateau, trainable

Barren Plateau, untrainable (random walk)

It is crucial to determine which conditions allow **barren plateaus** to arise… can we **predict** their presence?

1. McClean et al., “Barren plateaus in quantum neural network training landscapes,” Nature communications 9, 1–6 (2018).
2. Cerezo et al., “Cost function dependent barren plateaus in shallow parametrized quantum circuits,” Nature communications 12, 1–12 (2021).

# Results

# Controllability and the Dynamical Lie Algebra (DLA)

What's the set of all possible reachable states?

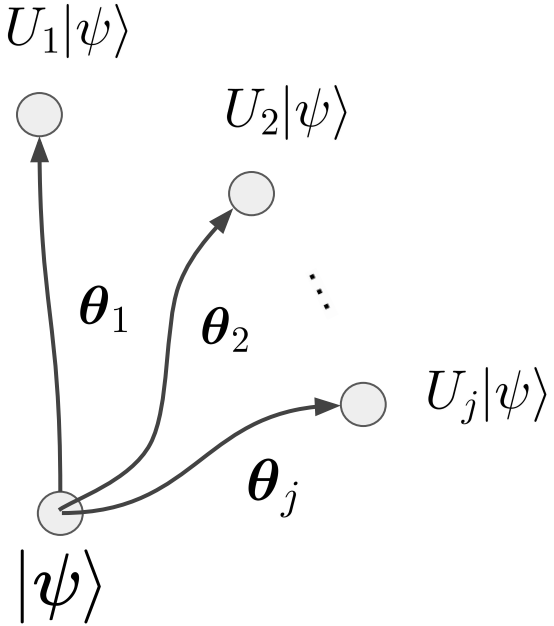


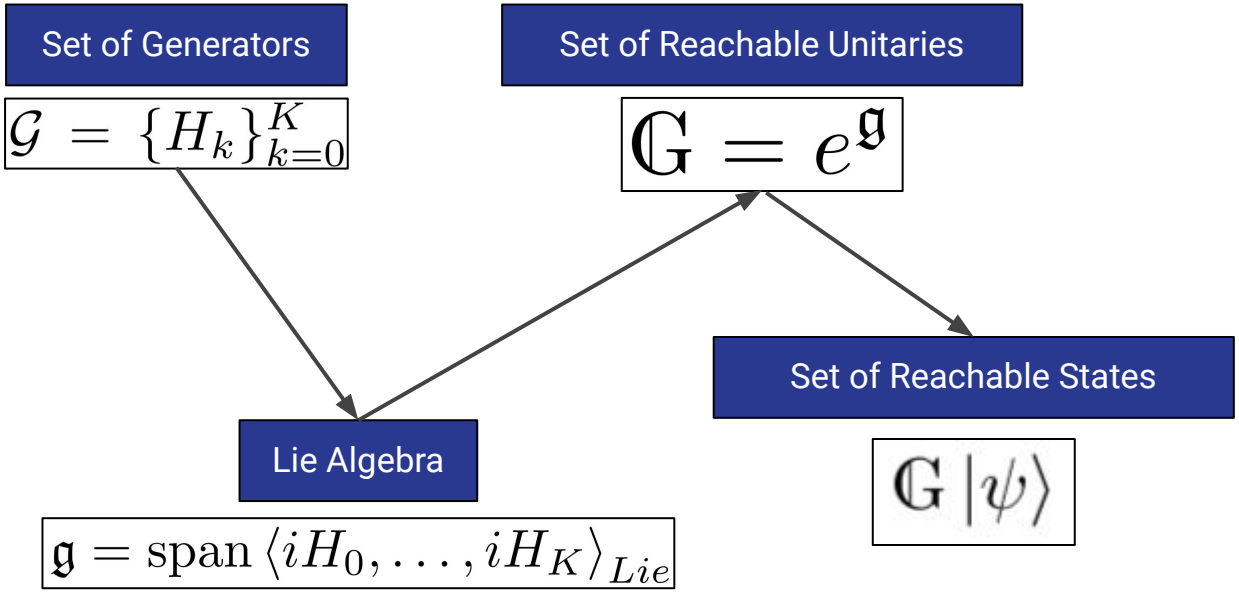


The **bigger** G, the more "**expressible**" the control system.

# Algebra, Expressibility and Gradient Scaling

Consider two sets of unitaries, one solving **problem A** and another solving **problem B**

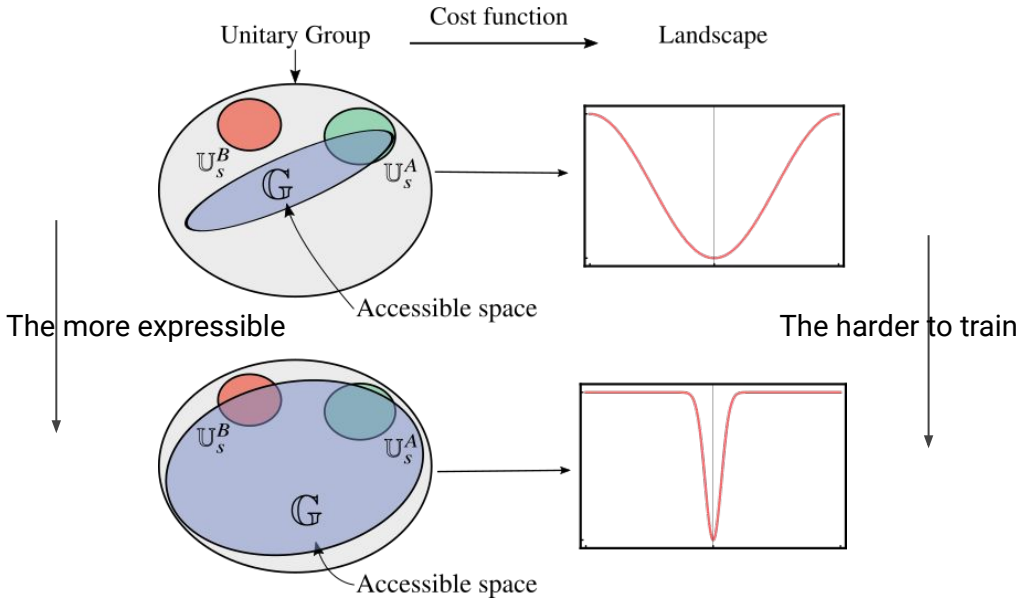


**Observation 1.** *Let the state $\rho$ belong to a subspace $\mathcal{H}_k$ associated with a DLA $\mathfrak{g}_k$. Then, the scaling of the variance of the cost function partial derivative is inversely proportional to the scaling of the dimension of the DLA as*

$$\mathrm{Var}_{\boldsymbol{\theta}}[\partial_\mu C(\boldsymbol{\theta})] \in \mathcal{O}\left(\frac{1}{\mathrm{poly}(\dim(\mathfrak{g}_k))}\right). \qquad (24)$$

**Expressibility** is directly connected to the (size of) **algebra!**

**polynomially growing algebras** can exhibit **polynomially vanishing gradients**

**exponentially growing algebras** will exhibit **exponentially vanishing gradients**.

* Holmes et al., "Connecting ansatz expressibility to gradient magnitudes and barren plateaus," arXiv:2101.02138 (2021).

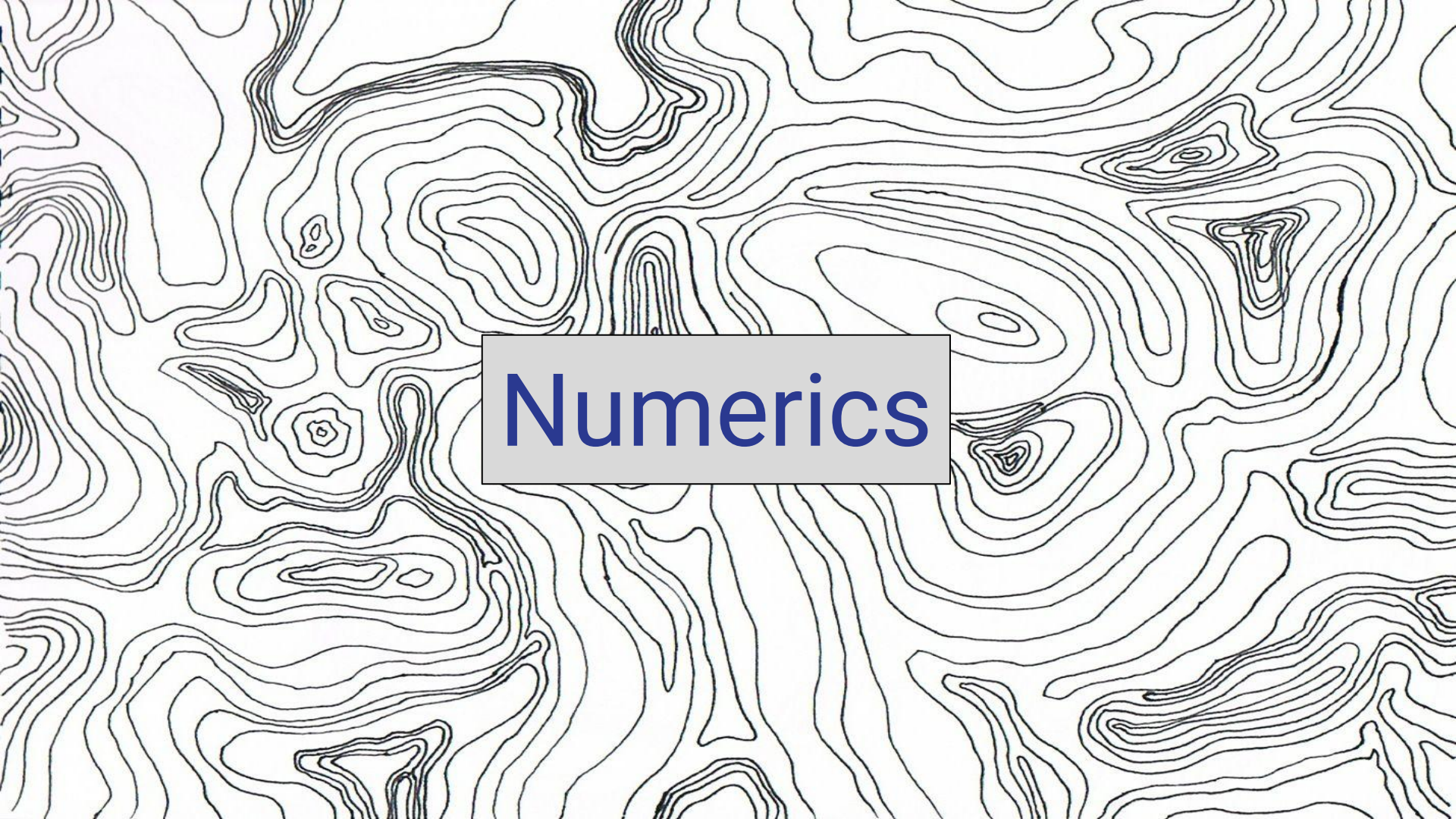
Numerics

# Example: Transverse Field Ising Model

Single layer of the circuit

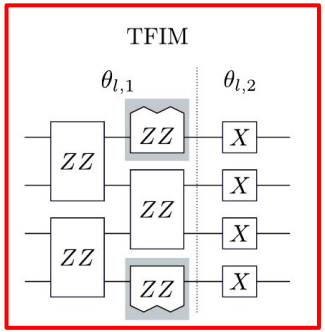


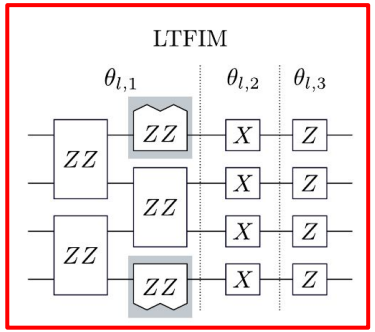


Expressibility? Look at the **algebras**!

**TFIM has a Polynomial algebra**

**LTFIM has an Exponential algebra**

Numerics

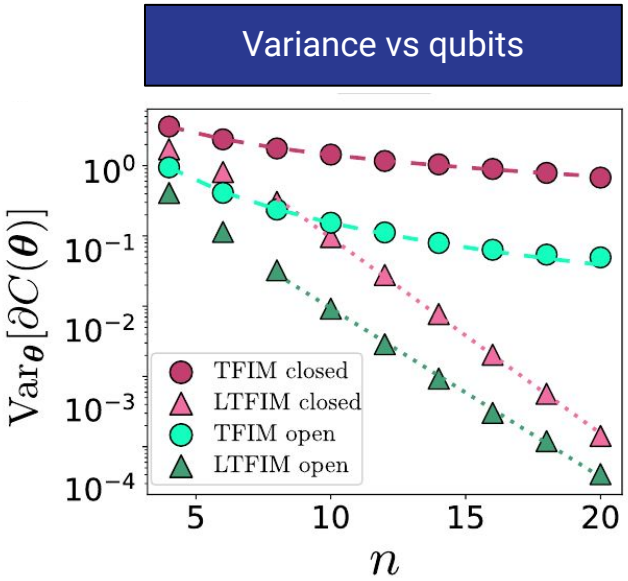


Conclusions

# Summary

- Our work provides rigorously proven **theorems** connecting the dimension of **algebra** to the existence or absence of **barren plateaus.**

**Corollary 1.** *Let the single layer expressibility of a controllable system be* $\|\mathcal{A}^{(2)}_{U_1(\boldsymbol{\theta})}\|_\infty = 1 - \delta(n)$, *with* $\delta(n)$ *being at most polynomially vanishing with* $n$, *i.e., with* $\delta(n) \in \Omega(1/\operatorname{poly}(n))$. *Then, if* $L(n) \in \Omega(n/\delta(n))$, $U(\boldsymbol{\theta})$ *will be no worse than an* $\varepsilon(n)$*-approximate 2-design (i.e.,* $\|\mathcal{A}^{(2)}_{U(\boldsymbol{\theta})}\|_\infty \leqslant \varepsilon(n)$*) with* $\varepsilon(n) \in \mathcal{O}(1/2^n)$, *where we have added the* $n$*-dependence in* $L$ *and* $\varepsilon$ *for clarity.*

**Theorem 2** (Subspace controllable)**.** *Consider a system that is reducible (so that the Hilbert space is* $\mathcal{H} = \bigoplus_j \mathcal{H}_j$ *with each* $\mathcal{H}_j$ *invariant under* $\mathbb{G}$*), and controllable on some* $\mathcal{H}_k$ *of dimension* $d_k$. *Then, if the initial state is such that* $\rho \in \mathcal{H}_k$, *the variance of the cost function partial derivative is given by*

$$\operatorname{Var}_{\boldsymbol{\theta}}[\partial_\mu C(\boldsymbol{\theta})] = \frac{2d_k}{(d_k^2-1)^2}\Delta(H_\mu^{(k)})\Delta(O^{(k)})\Delta(\rho^{(k)}). \quad (16)$$

**Proposition 1** (Controllable)**.** *There exists a scaling of the depth for which controllable systems form* $\varepsilon$*-approximate 2-designs with* $\varepsilon \in \mathcal{O}(1/2^n)$, *and hence the system exhibits a barren plateau according to Definition 1.*

**Corollary 2.** *Consider a PSA of the form in (2) giving rise to a reducible DLA, and let* $\rho \in \mathcal{H}_k$, *with* $\mathcal{H}_k$ *some invariant subspace that is controllable (i.e. the DLA reduced to such subspace is full rank). If,* $\operatorname{Tr}[(H_\mu)^4], \operatorname{Tr}[O^4] \in \mathcal{O}(2^n)$, *the cost function will exhibit a barren plateau for any subspace such that* $d_k \in \mathcal{O}(2^n)$.

**Proposition 2.** *The following two sets of generators generate full rank DLAs, and concomitantly lead to controllable systems:*

- $\mathcal{G}_{\text{HEA}} = \left\{X_i, Y_i\right\}_{i=1}^n \bigcup \left\{\sum_{i=1}^{n-1} Z_i Z_{i+1}\right\}$,
- $\mathcal{G}_{\text{SG}} = \left\{\sum_{i=1}^n X_i, \sum_{i<j}(h_i Z_i + J_{ij} Z_i Z_j)\right\}$, *with* $h_i, J_{ij} \in \mathbb{R}$ *sampled from a Gaussian distribution.*

**Theorem 1.** *Consider a controllable system. Then, the PSA* $U(\boldsymbol{\theta})$ *will form an* $\varepsilon$*-approximate 2-design, i.e.* $\|\mathcal{A}^{(2)}_{U(\boldsymbol{\theta})}\|_\infty = \varepsilon$ *with* $\epsilon > 0$, *when the number of layers* $L$ *in the circuit is*

$$L = \frac{\log(1/\varepsilon)}{\log\left(1/\|\mathcal{A}^{(2)}_{U_1(\boldsymbol{\theta})}\|_\infty\right)}. \quad (14)$$

**Theorem 3.** *Consider a system that is reducible and let* $\rho \in \mathcal{H}_k$ *with* $\mathcal{H}_k$ *an invariant subspace of dimension* $d_k$. *Then, the variance of the cost function partial derivative is upper bounded by*

$$\operatorname{Var}_\theta[\partial_\mu C(\boldsymbol{\theta})] \leqslant \min\{G_A(\rho^{(k)}), G_B(O^{(k)})\}, \quad (21)$$

*with*

$$G_B(\rho^{(k)}) = \left(\left\|\mathcal{A}_{U_B^{(k)}}\left((\rho^{(k)})^{\otimes 2}\right)\right\|_2 - \frac{\Delta(\rho^{(k)})}{d_k^2-1}\right)\operatorname{Tr}\left[\langle X^2\rangle_{U_A^{(k)}}\right]$$

$$G_A(O^{(k)}) = \left(\left\|\mathcal{A}_{U_A^{(k)}}\left((O^{(k)})^{\otimes 2}\right)\right\|_2 - \frac{\Delta(O^{(k)})}{d_k^2-1}\right)\operatorname{Tr}\left[\langle Y^2\rangle_{U_B^{(k)}}\right].$$

# Implications of our results

- Novel insights into circuit design for quantum machine learning tasks, e.g. **predict** if a given ansatz, or a modification of one, will be **trainable**.
- Some ansatz **proposals** in the literature need to be **revised**.
- Pave the way towards **trainability-aware** circuit design.

# Thank you! questions?

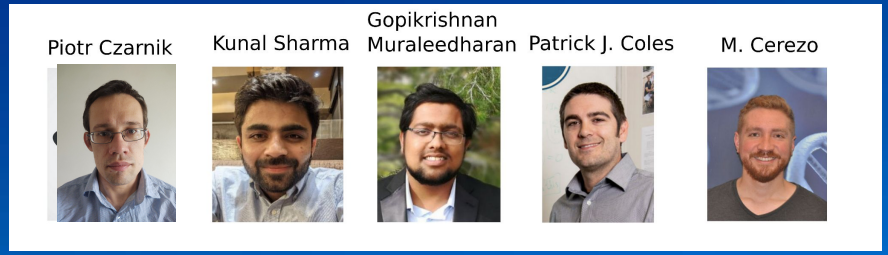


**ArXiv 2105.14377**

# Investigating electronic excitations in non-stoichiometric quantum dots


Presenter: Manav Bhati, T-1 GRA, Rice University

Mentors: Dr. Sergei Tretiak

Dr. Sergei Ivanov

Dr. Dibyajyoti Ghosh


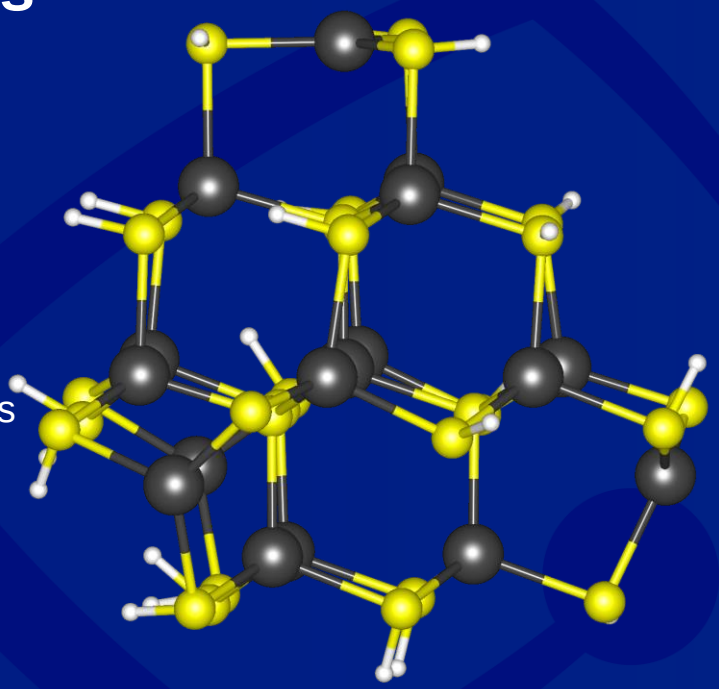


- LDRD: Quantum Photonics with Semiconductor Nanocrystals (Project #20200213DR, 2020-2022)
- Center for Nonlinear Studies (CNLS)


*2021 Virtual Ligthning Talk Series: Theoretical Division*

*2021, July 27th*

Bhati M., Ivanov S. A., Tretiak S., Ghosh D., *Nature of Electronic Excitations in Non-stoichiometric Quantum Dots,* **2021** *(under preparation)*

# What are colloidal Quantum dots (QDs)?

- Semiconductor nanocrystals (artificial atoms) in a solution

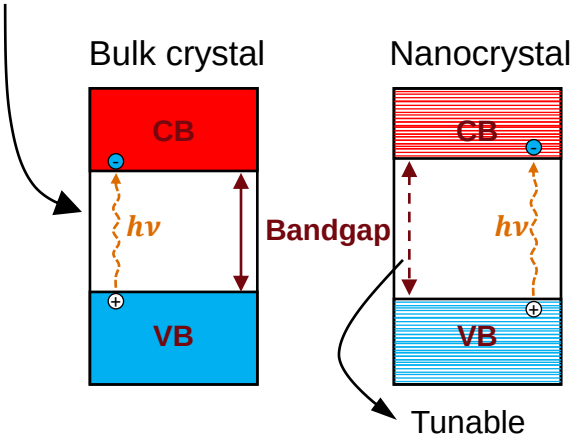


- 0D crystals
- Quantum confinement effects
- Size dependent properties
- Facile and cheap synthesis

**$Cd_{33}Se_{33}$**

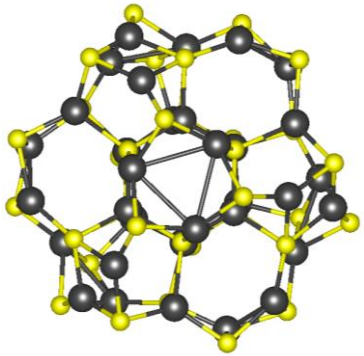

# Why they are important?

- LEDs, displays, solar cells
- Bio-imaging, labeling
- Photocatalysis
- Quantum computing: need QDs that emit single wavelength photons


*Image: Samsung*

Rhyner et al., *Nanomedicine* **2006**, *1* (2), 209–217.

# Our work

- Stoichiometry breaks in most experimentally synthesized QDs
- Electronic excitations in non-stoichiometric QDs

**$Cd_{17}Se_{28}$** (Se-rich)

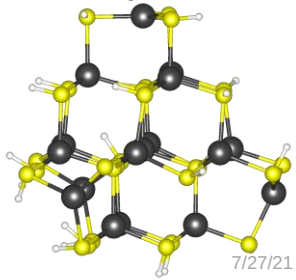

# Stoichiometric vs Non-stoichiometric QDs: Absorption spectra

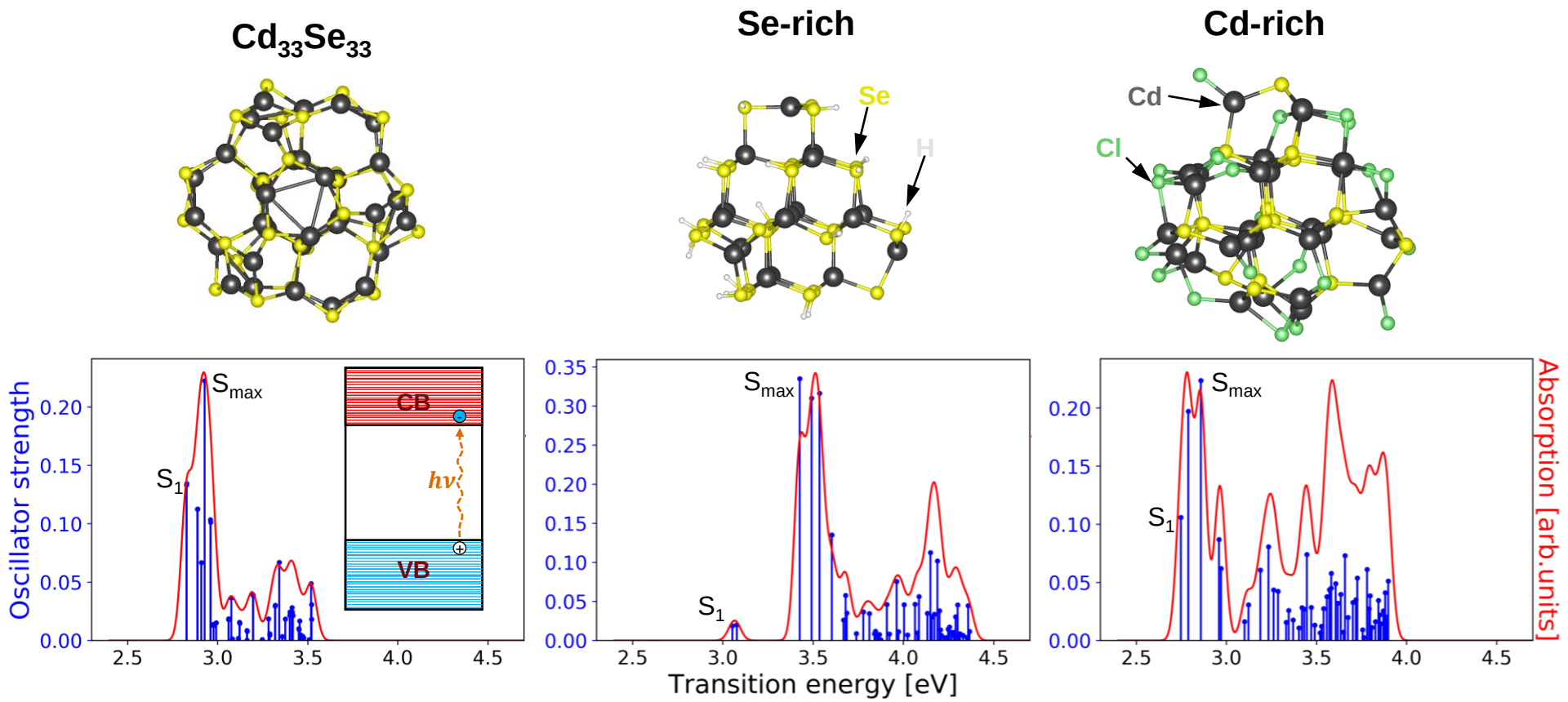


- $S_1$: Lowest energy transitions → represent emission
- $S_{max}$: Maximum oscillator strength → represent absorption
- Non-stoichiometric QDs: poor emission, good absorption (especially in Se-rich QD)

# Stoichiometric vs Non-stoichiometric QDs: Electronic excitations

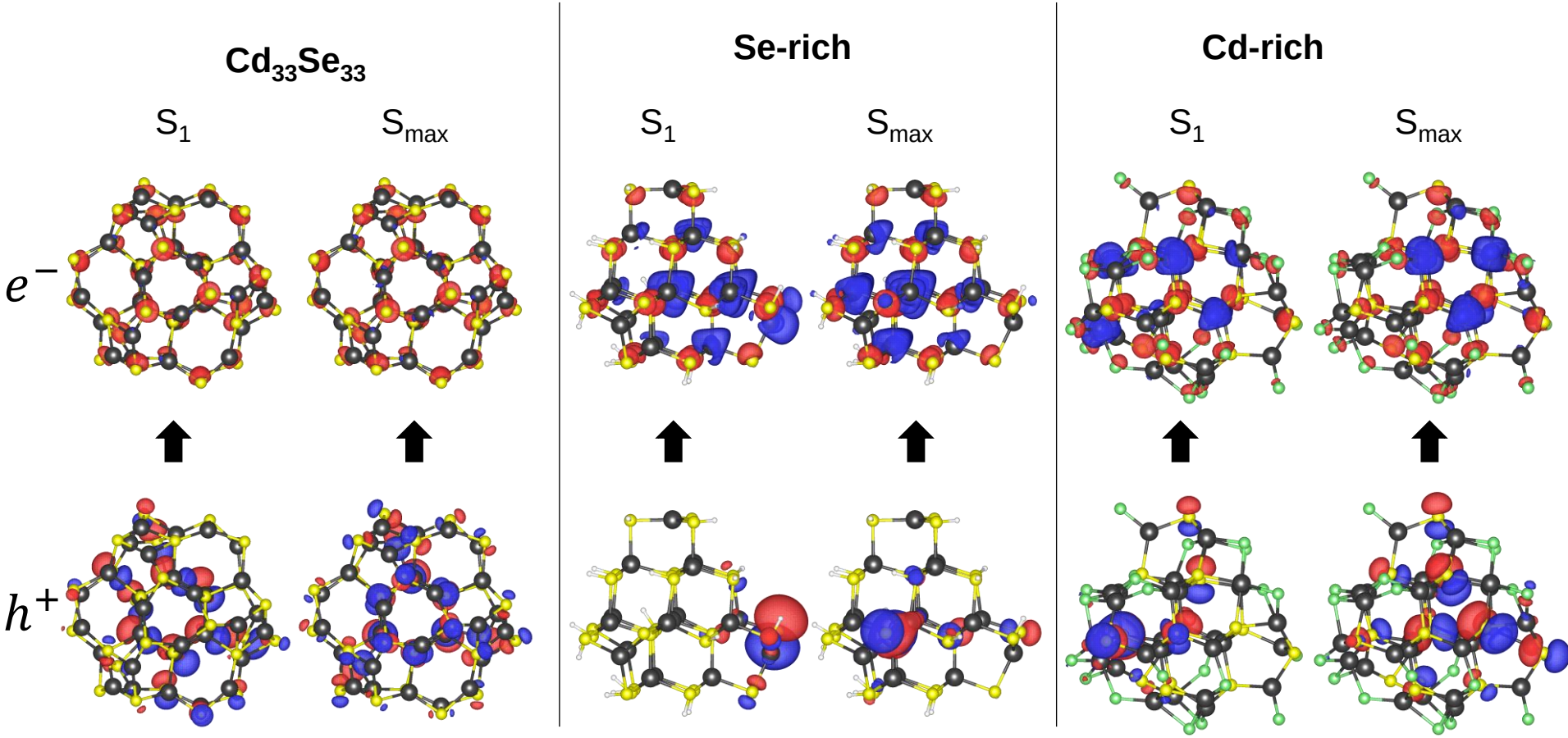


- $S_1$ in non-stoichiometric QDs: higher charge localization → poor emission
- $S_{max}$ in non-stoichiometric QDs: lower charge localization → good absorption (similar to stoichiometric QD)

# Stoichiometric vs Non-stoichiometric QDs: Nature of electronic excitations

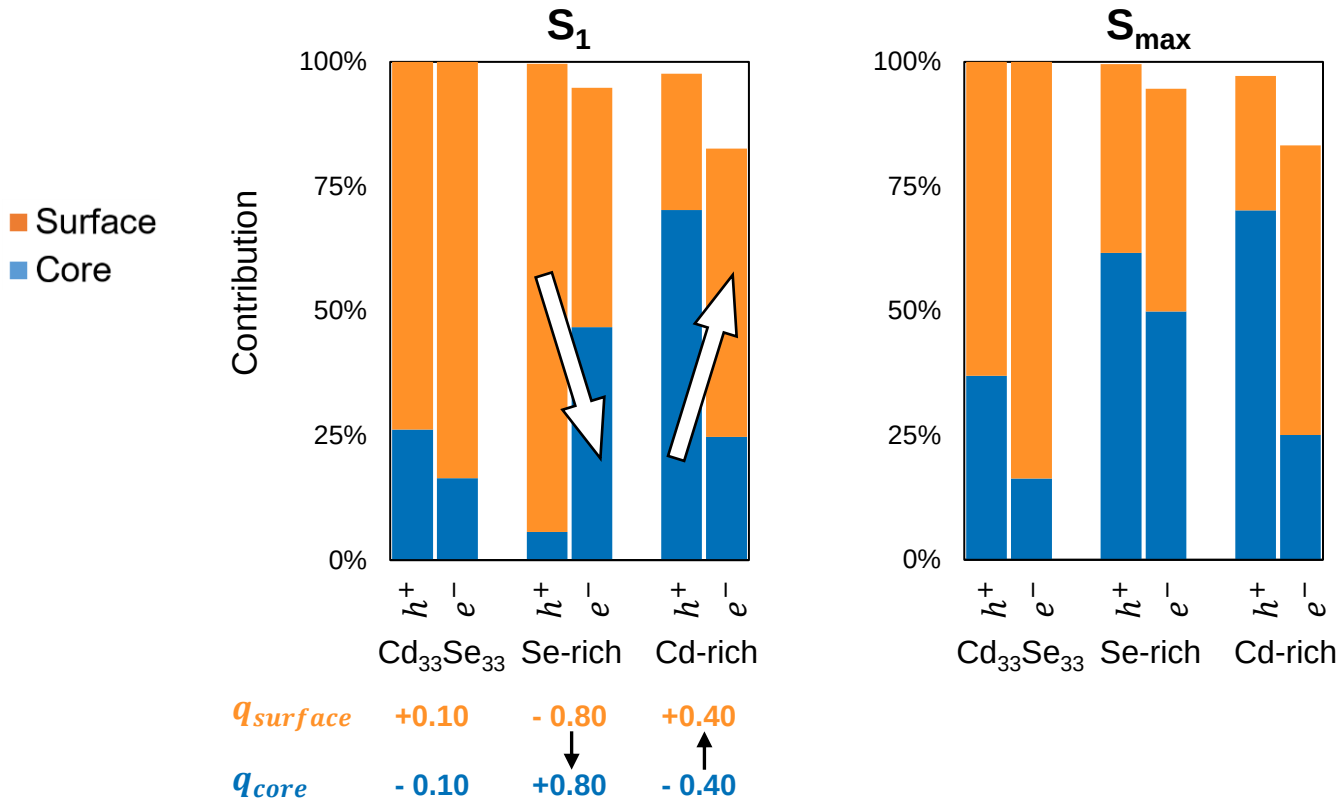


- Se-rich: surface to core → $h^+$ on surface
- Cd-rich: core to surface → $e^-$ on surface

} *good for photocatalysis*

- $S_1$ in non-stoichiometric QDs: Charge transfer (CT) because of charge imbalance →poor emission
- $S_{max}$ in non-stoichiometric QDs: No CT (similar to stoichiometric QD) →good absorption

# Conclusion

- Investigated electronic excitations in less explored non-stoichiometric QDs
- Non-stoichiometric QDs have **charge localization** and **CT** type excitations at low energy transitions → **poor emission and good absorption**
- Non-stoichiometric QDs → **photocatalysis**
- Stoichiometric QDs → **quantum computing**
- Working on **strategies to improve emission in non-stoichiometric QDs**

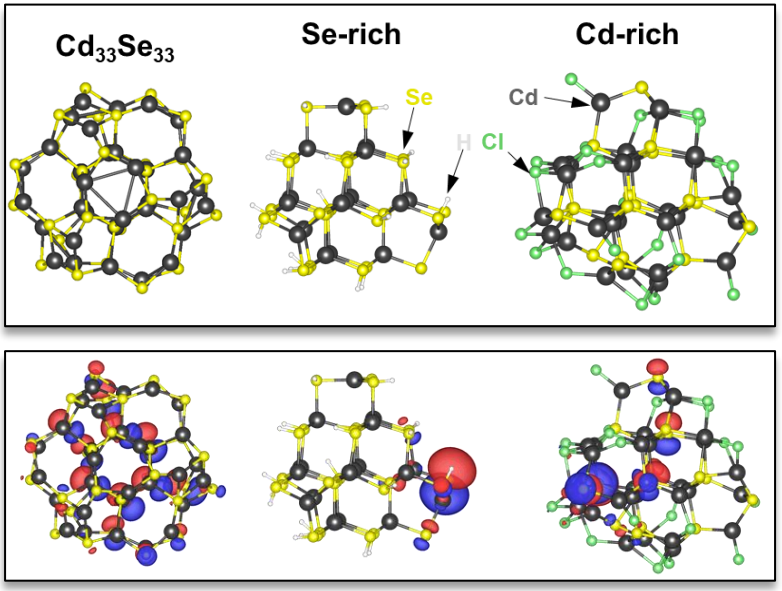


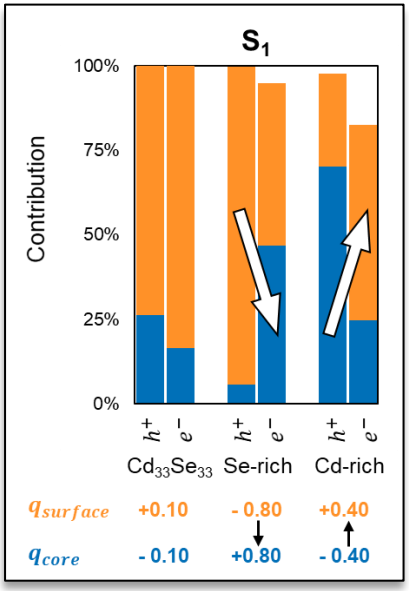


***Thank you!***



Bhati M., Ivanov S. A., Tretiak S., Ghosh D., **2021** *(in preparation)*

Los Alamos NATIONAL LABORATORY

# A Three-Dimensional Graph-Based Model for Porous Media Fluid Flow

Brendan Miller

Mentors: Christian Negre, Joaquin Jimenez-Martinez, Joshua Finkelstein

Affiliation: Northern Illinois University

4 August 2021

# Eigenvector Centrality

- Ranks nodes based on their influence

$$\lambda c_i = \sum_{t \in N(i)} c_t$$

$$\Longleftrightarrow$$

$$\lambda c_i = \sum_{j \in V(G)} A_{ij} c_j$$

$$\Longleftrightarrow$$

$$\lambda \boldsymbol{c} = \boldsymbol{A}\boldsymbol{c}$$

- $A =$ adjacency matrix
- $c_i =$ centrality score of node i

- For sparse matrices, a small $\delta$ term is added to each entry

# Graph Theory and Porous Media

- Extract a “pore network” from a porous medium
  - 2-D image or 3-D volumetric image
- Use eigenvector centrality to find influential nodes
- Compute a Spatially Projected Eigenvector Centrality

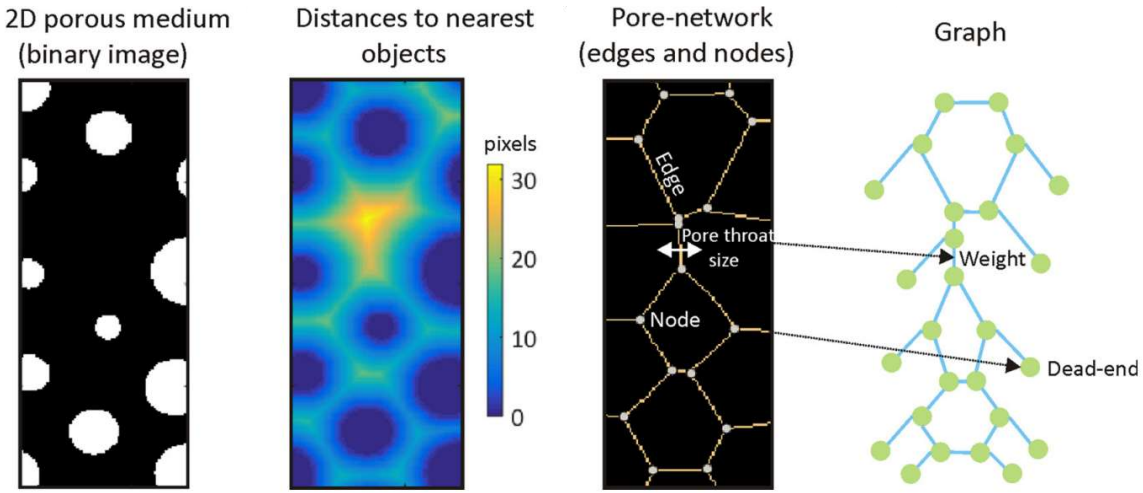


Jimenez-Martinez & Negre (2017)

# Network Extraction

- Old method found edges first
  - Nodes defined as intersections of edges
  - Lines of local maxima become edges
- Does not generalize well to 3-D
  - Local maxima form planes or curved surfaces
- New methods propose nodes first
  - We present the methods for 2-D first

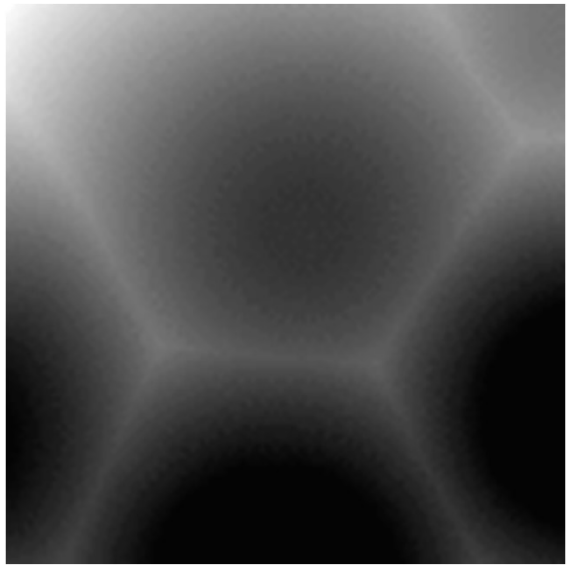

GIF of 3-D DNO transform

# Network Extraction: Skeletonizing

- Convert grayscale DNO transform back to BW
  - Use adaptive threshold
  - Goldilocks situation

- Skeletonize new image

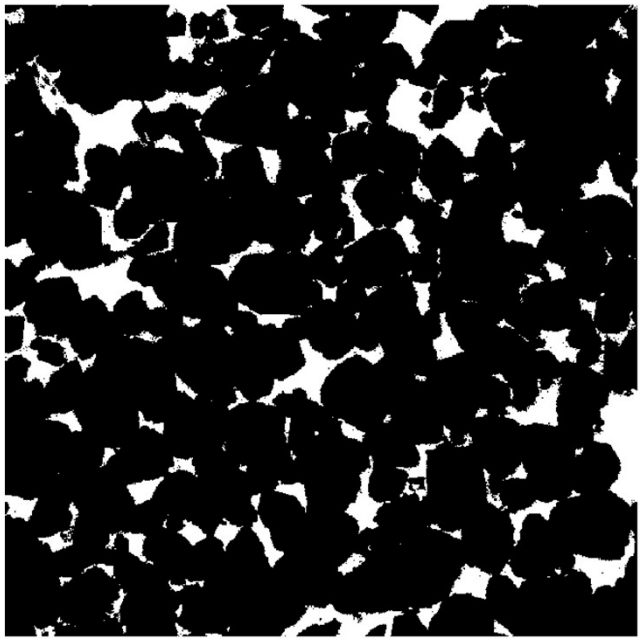

2-D Porous Medium

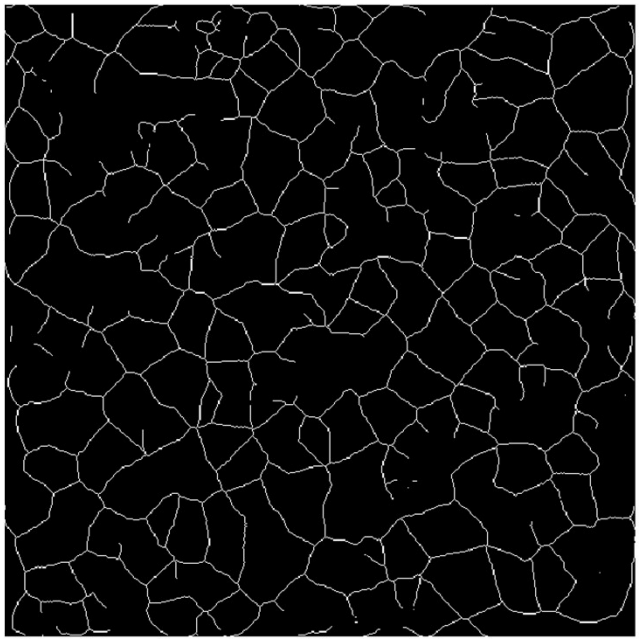

2-D Pore Network

2-D porous medium

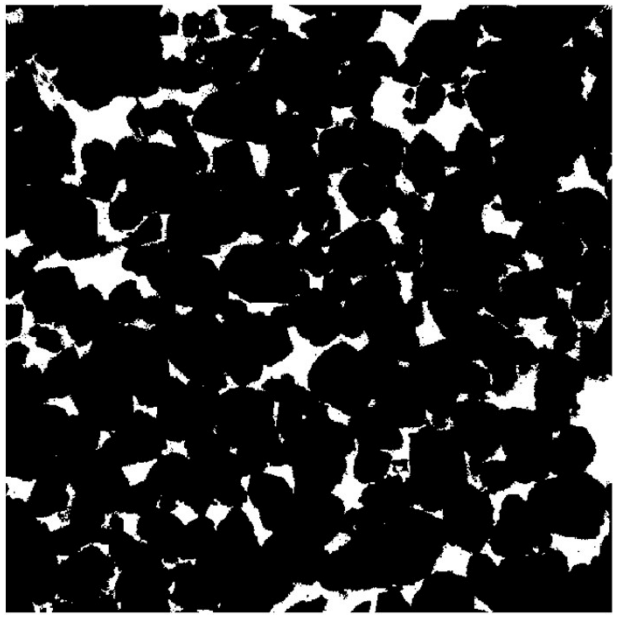

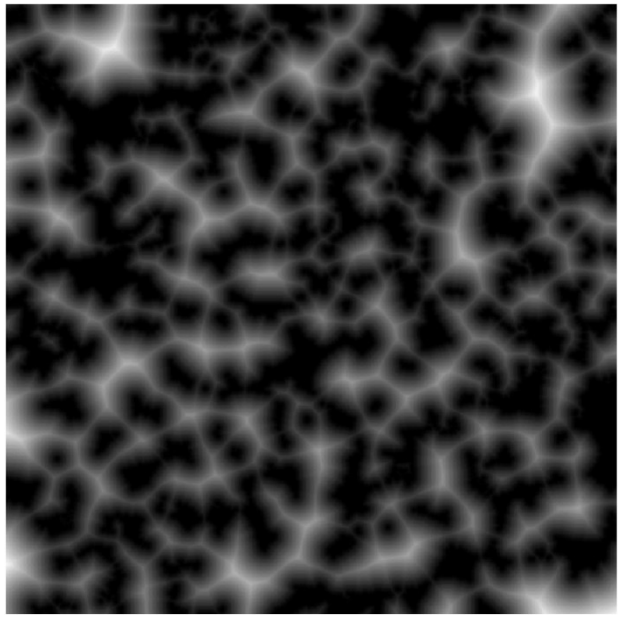

DNO transform

DNO transform converted to BW

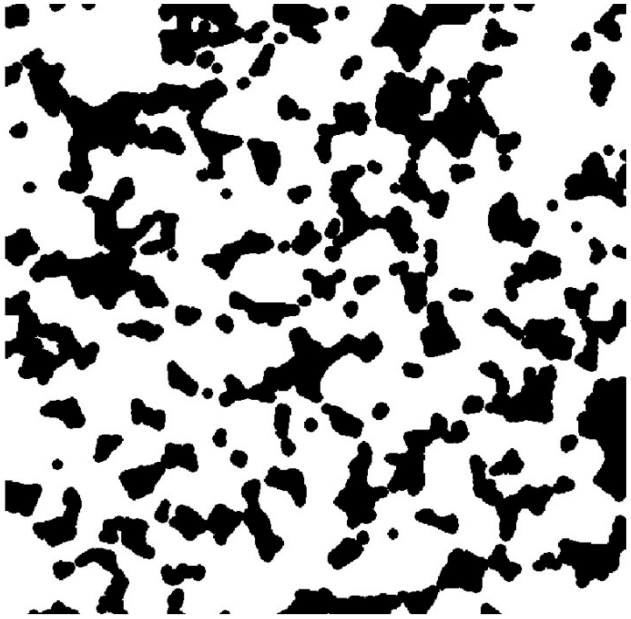

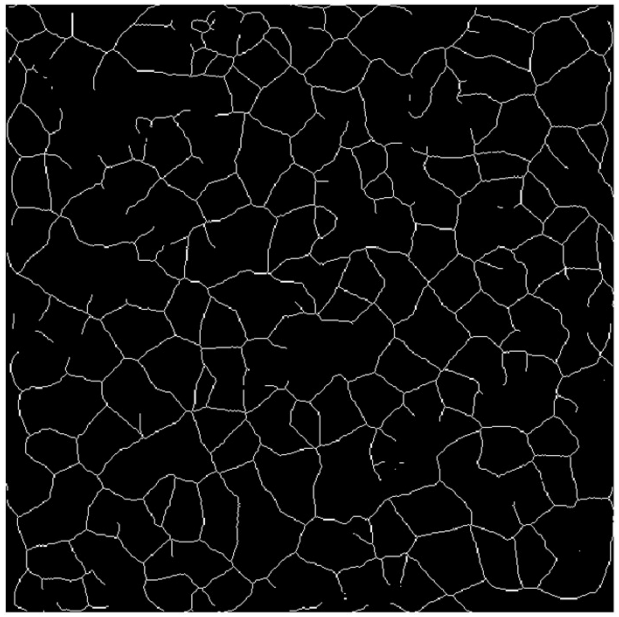

Skeletonized image

# Generalization to 3-D

- All methods stay the same!

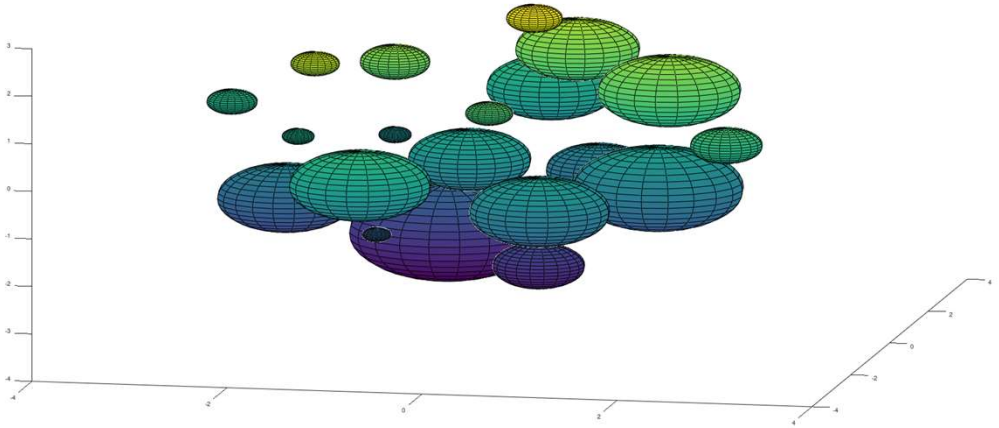

3-D Porous Medium

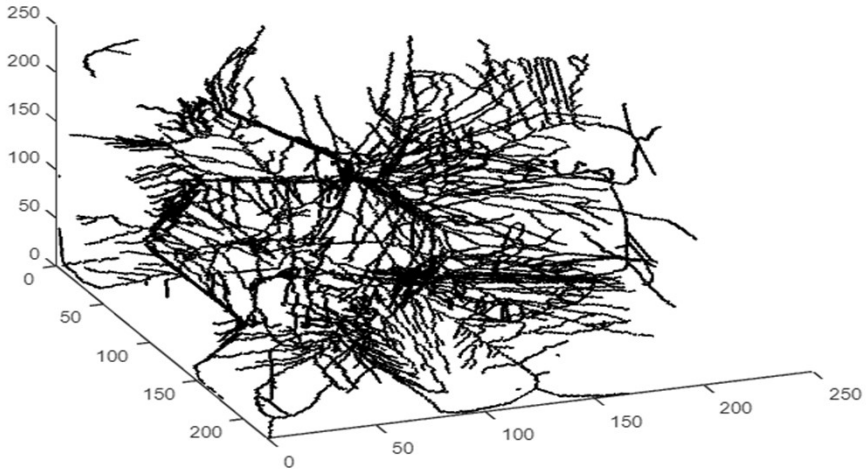


3-D Pore Network

# Skeleton and DNO Transform

3-D Pore Network

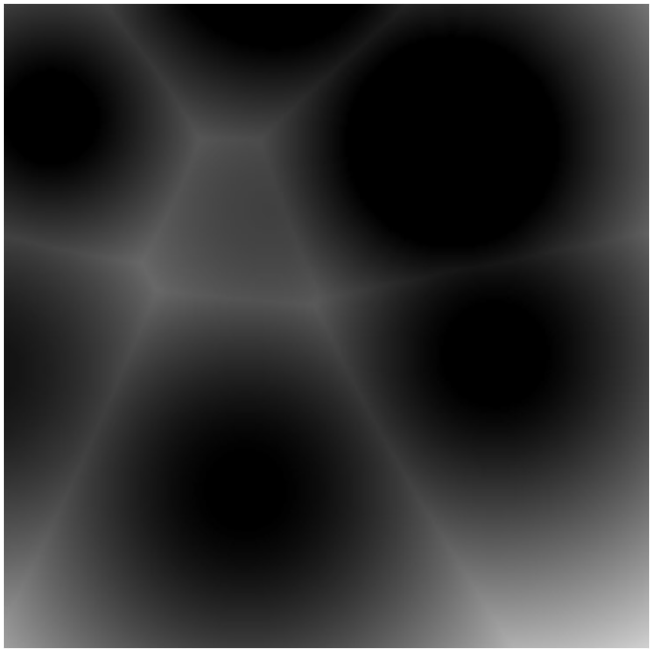

3-D DNO Transform

# Centrality Changes (Tentative)

- Old adjacency matrix:

$$A_{ij} = \begin{cases} e^{-1/s_{ij}} & i \text{ adjacent to } j \\ 0 & \text{otherwise} \end{cases}$$

- $s_{ij} = \text{size of pore throat}$
- Add small $\delta$ term to each entry

- New adjacency matrix:

$$A_{ij} = \begin{cases} e^{-1/s_{ij}} * e^{-d_{ij}/d_0} & \text{no object between } i \text{ and } j \\ 0 & \text{otherwise} \end{cases}$$

- $d_{ij} = \text{distance between nodes } i \text{ and } j$
- $d_0 = \text{average distance to nearest neighbor}$

# Normalized Centrality

- New adjacency matrix yields a well-connected network
  - No need to add small $\delta$ term

- Using normalized centrality prevents localization

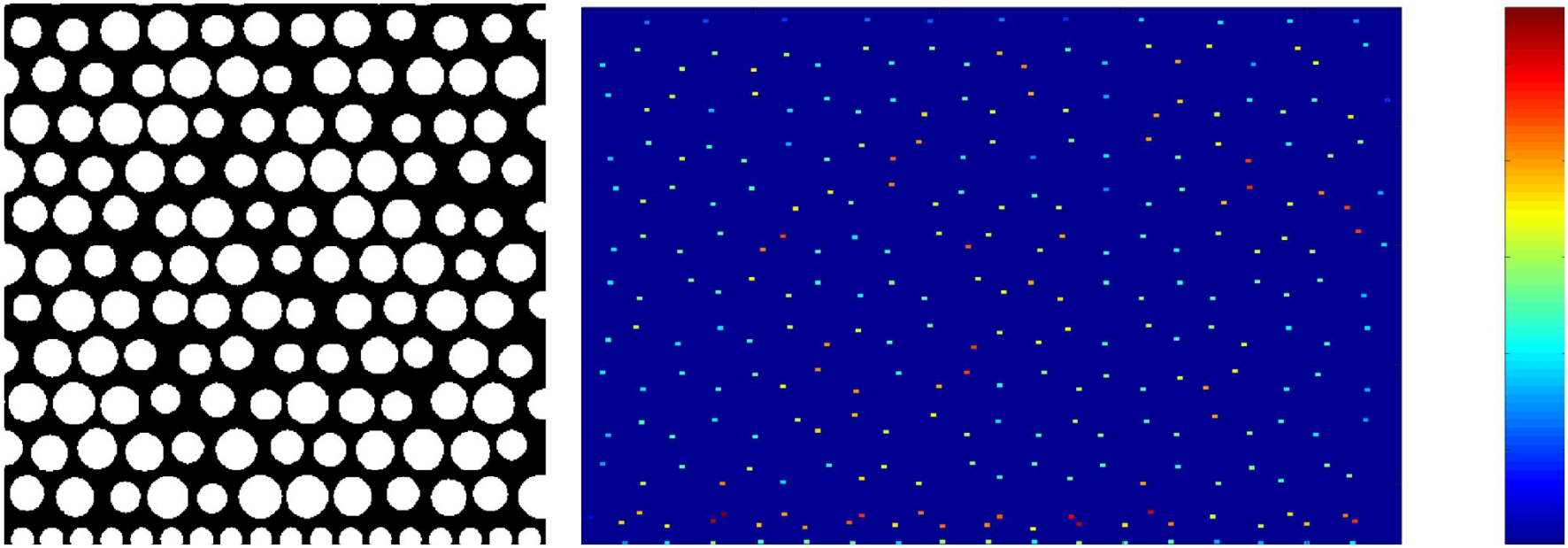

Porous medium (left) and node locations with centrality score (right)

# Acknowledgement

This research and internship is funded by the National Science Foundation and Los Alamos National Laboratory. I would like to thank my mentors Christian Negre, Joshua Finkelstein, and Joaquin Jimenez-Martinez for their guidance and feedback throughout this project.

Los Alamos NATIONAL LABORATORY

# Post-Optimality Sensitivity Analysis of Routing Problems Solved Using Branch-and-Price

Presenter: Christopher Montez

Mentor: Kaarthik Sundar

8/11/2021

# What are Vehicle Routing Problems (VRPs)

Brief Notation Introduction

**Graph:** $G = (V, E)$

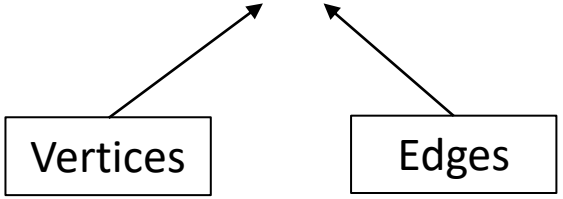


**Start:** $s \in V$

**End:** $d \in V$

**Number of Vehicles:** $m$

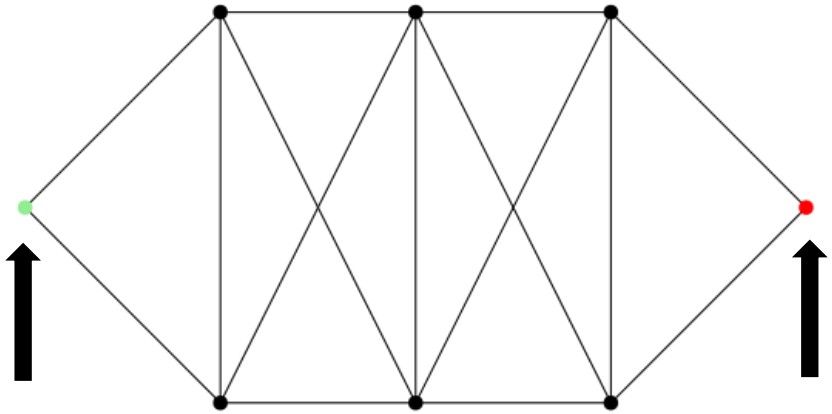

**VRP**

$m$ vehicles go from $s$ to $d$ while satisfying certain constraints

# Why Do We Care?

**Many Real-World Applications**

- Crew scheduling for airlines
- Task scheduling for factories
- Robot path planning
- Drilling holes for boards

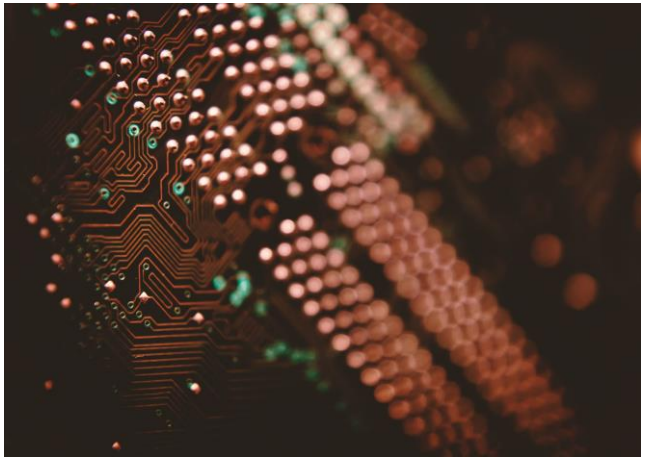

# Modeling (Mathematical Programming)

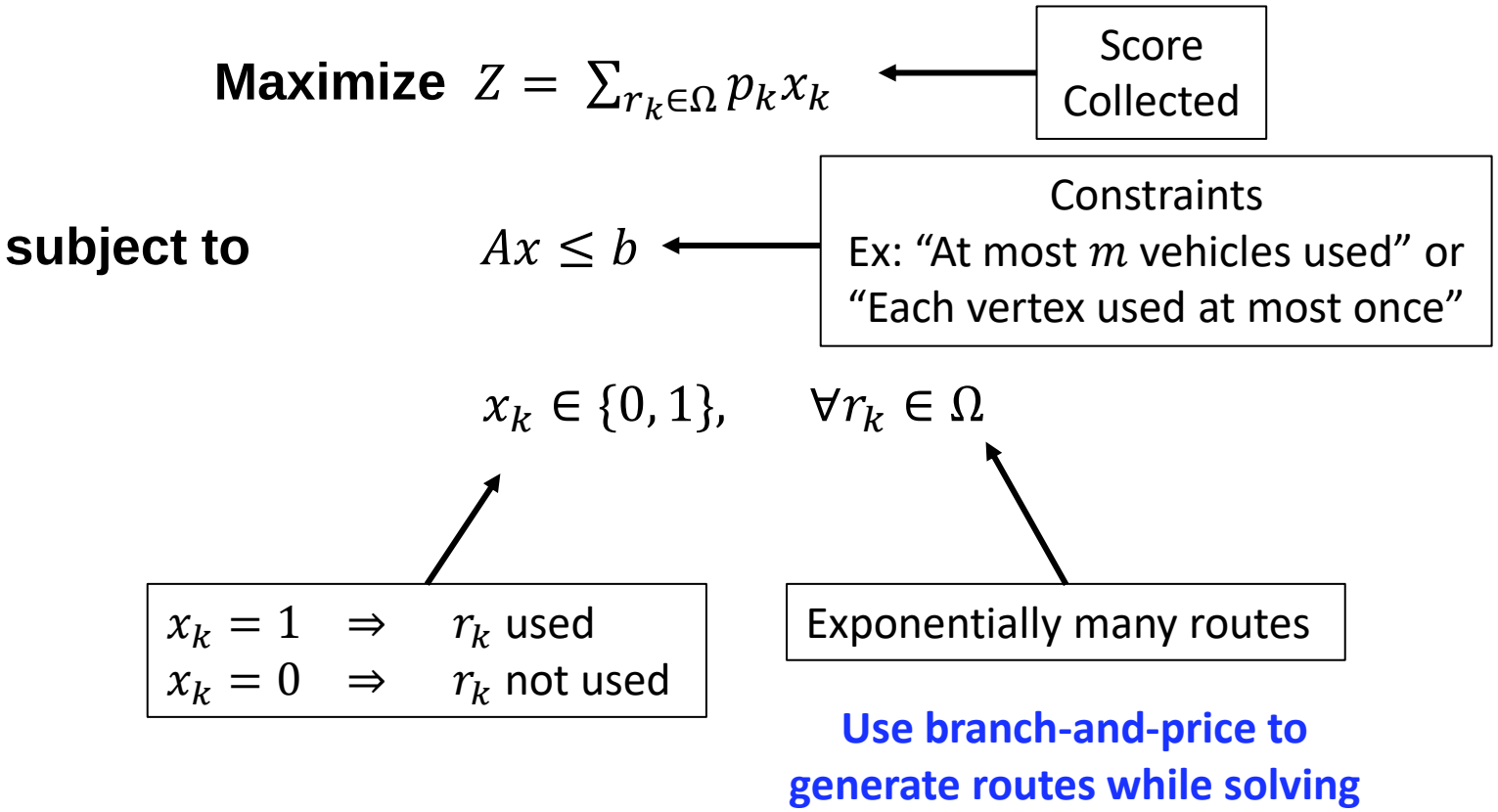

# What is Sensitivity Analysis?

**Study effects of slightly perturbing a problem**

- One more/less vehicle used
- One more/less place to visit
- Multiple visits allowed
- Different costs

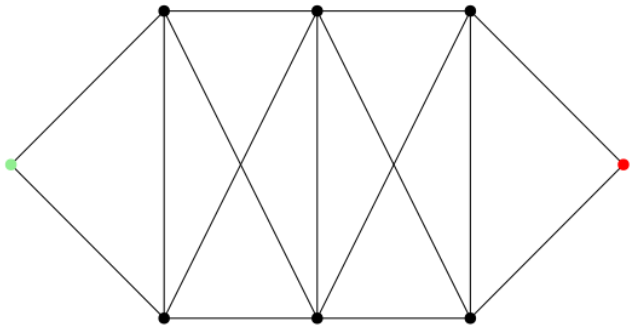

vs

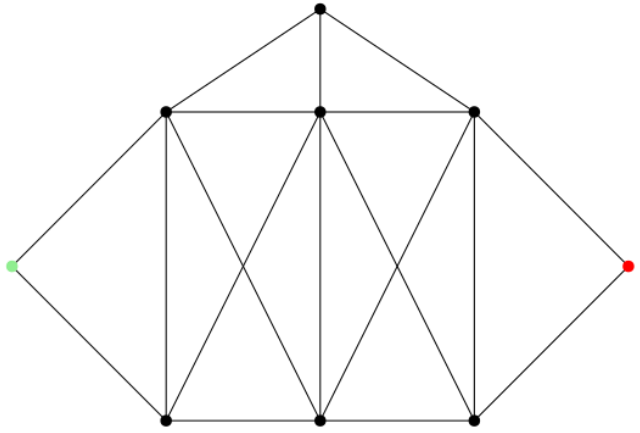

# Issues with Sensitivity Analysis

- **Computationally expensive**
  - Original and perturbed problems are hard
  - Typically solve perturbed problem from scratch

- **Sophisticated methods may be difficult to implement**

**Resolution:** **Use information from original solution**

# Post-Optimality Sensitivity Analysis

- Use information from given/found solution to make conclusions about a perturbed problem

- Type of perturbation affects what conclusions can be made
  - Change constraint or change objective

- Method of solving affects what conclusions can be made
  - Some methods contain more information than others
  - Brute force has a large amount of information, but is too costly
  - Trade information for speed to solve problems typically

# Work Done

- Upper bound for change in number of vehicles and addition/removal of vertices

$$Ax \leq b \quad \rightarrow \quad Ax \leq d$$

- Could **NOT** find upper bound for change in objective

$$\sum_{r_k \in \Omega} p_k x_k \quad \nrightarrow \quad \sum_{r_k \in \Omega} p'_k x_k$$

# Work Done

**Upper bounds <u>without solving the perturbed problem</u>**

- Takes advantage of the structure of branch-and-price
- Requires slightly more memory, but typically not an issue
- Increase in computational time is practically negligible
- Can easily be generalized for multiple scenarios using a single solution
- Can be easily implemented

# Thank you

Los Alamos
NATIONAL LABORATORY

# Defect study on the electronic structure of a novel 2D-perovskite

$n = 1;\ BA_2MA_{n-1}Pb_nI_{3n+1}$

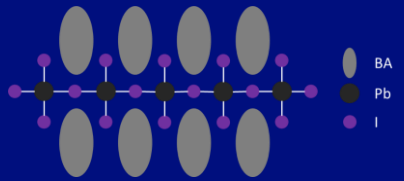


**Carlos Mora**, Dibyajyoti Ghosh, Amanda Neukirch
T-1, Physics and Chemistry of Materials
University of Southern California

# Metal Halide Perovskites

## Motivation

- Perovskites most abundant mineral on earth!!
- Advantages
  - Direct gap semiconductor
    - Easily tunable & cover wide light range
    - High PL quantum yield & power conversion efficiency
    - Favorable properties for solar cell & LED devices
  - Low-cost raw materials and equipment
  - Facile Synthesis
    - Solution-based methods at low temperature

## Challenge

- Perovskite Dimensionality?
  - 3D (Bulk) → 0D (Quantum Dots)
- How to increase efficiency?
  - Reduce unavoidable defects
    - Which defects are most detrimental to performance?



**Szuromi, P.; Grocholski, B. Natural and engineered perovskites. *Science* 2017, *358*, 732-733.**

# 2D-perovskite: $BA_2MA_{n-1}Pb_nI_{3n+1}$

- BA: Butylammonium

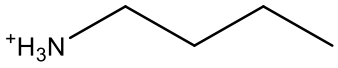


- Single layer: n=1
  - $BA_2PbI_4$
- Primitive Cell (1×1×1)
  - a = 8.69250 Å  α = 90.0000°
  - b = 27.60140 Å  β = 90.0000°
  - c = 8.87640 Å  γ = 90.0000°
  - V = 2129.6718 Å$^3$
  - Formula: $H_{96}C_{32}N_8Pb_4I_{16}$ (156 atoms)
  - 432 number of electrons

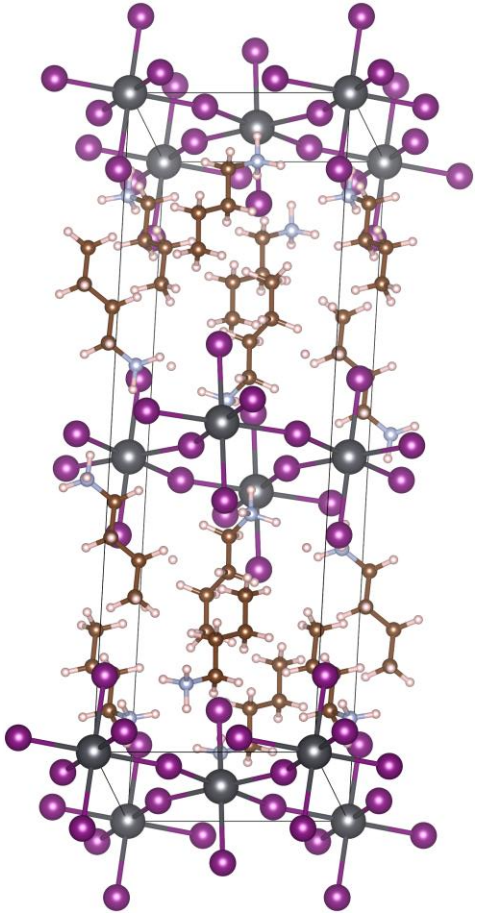

# Low Formation Energy Defects

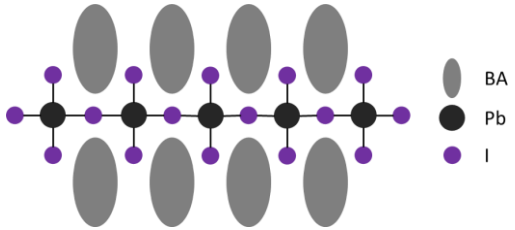


$V_{BA}$

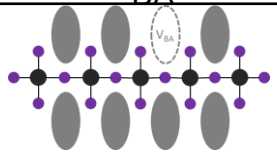

$V_{BAI}$

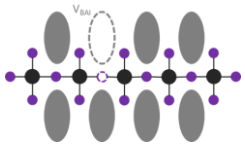

$V_{PbI2}$

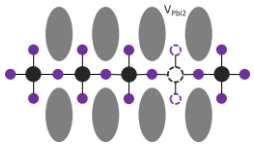

$V_I$ (in-plane)

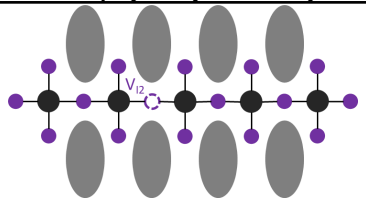

$V_I$ (out-of-plane)

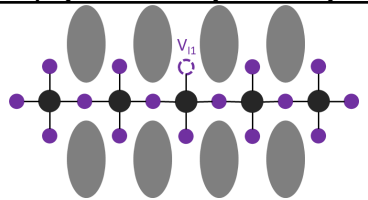

$I_I$ (in-plane)

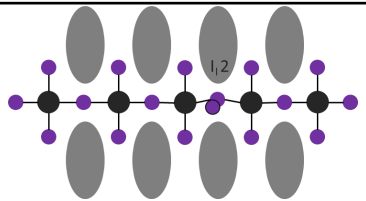

$I_I$ (out-of-plane)

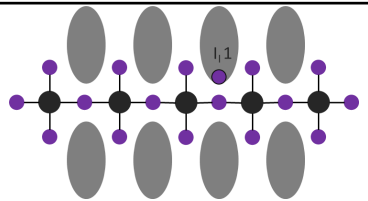

# Understanding Pristine System (2×1×2)

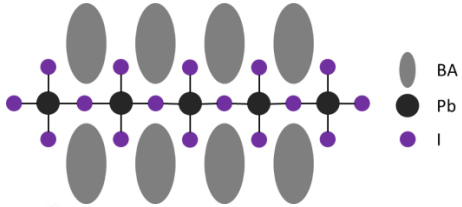


- Direct Bandgap (Γ→ Γ)
  - 2.12 eV
- Band edge states are delocalized across the Pb-I (in-plane) layer

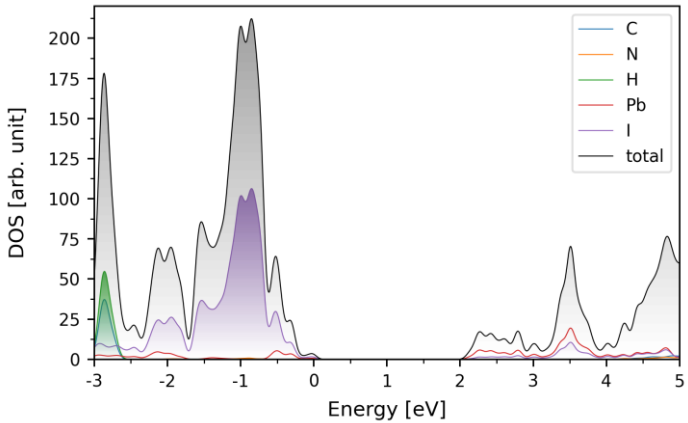


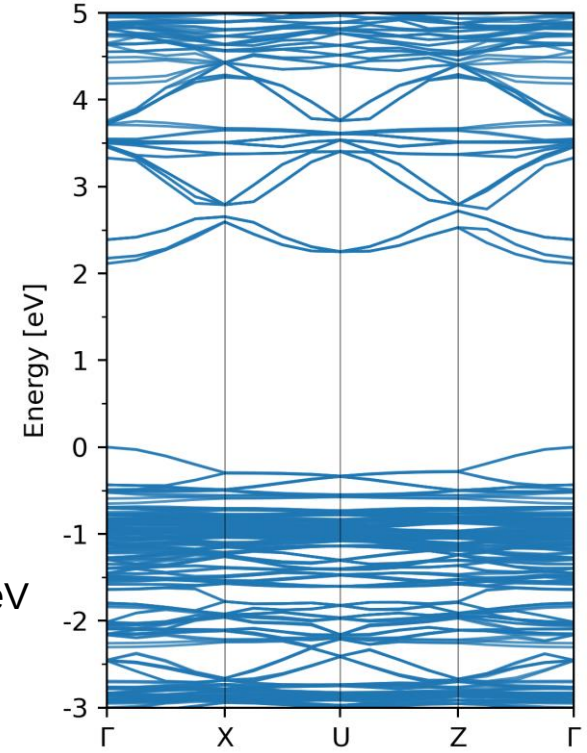


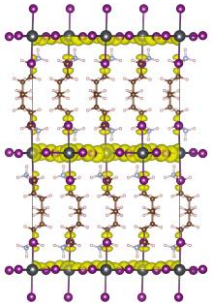

VBM
Energy: 0.2406 eV

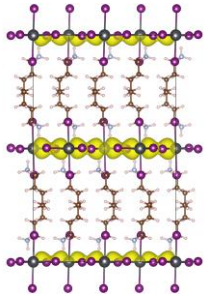

CBM
Energy: 2.3521 eV

# Halide defects are the most detrimental!

$V_I$ (in-plane)

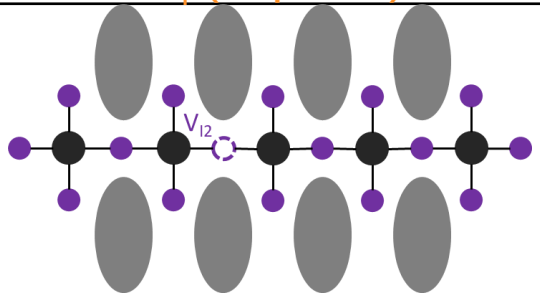


$V_I$ (out-of-plane)

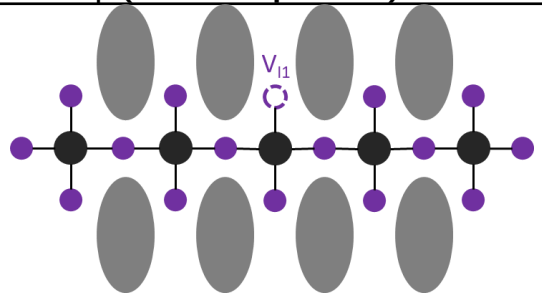


$I_I$ (in-plane)

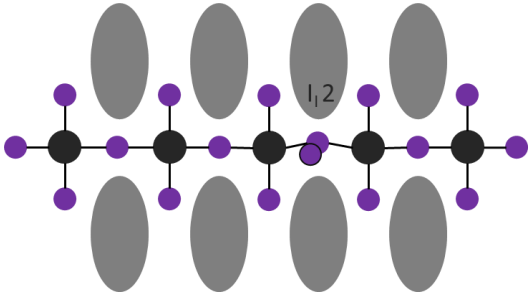


$I_I$ (out-of-plane)

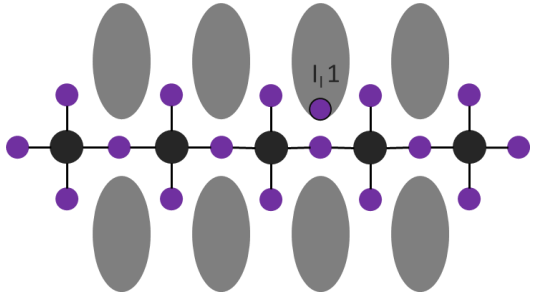

# $V_I$ (in-plane) (2×1×2)

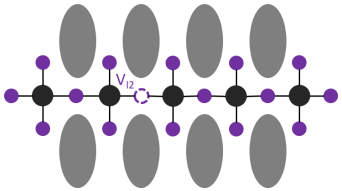


- Direct Bandgap (Γ→ Γ)
  - 0.29 eV (spin states of same orbital)
- Band edge states are localized near vacancy
- Introduce N-Type defect

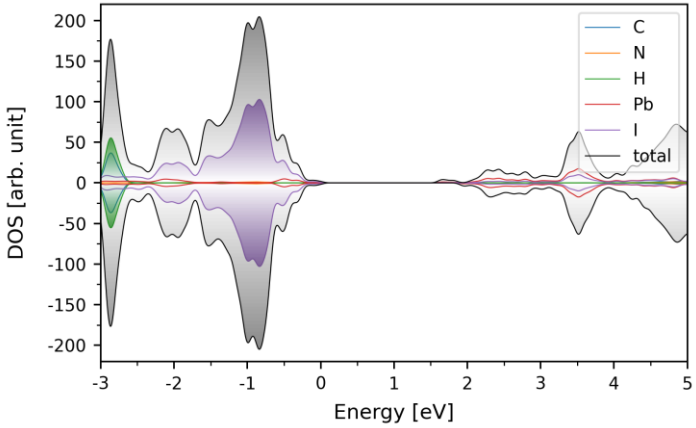


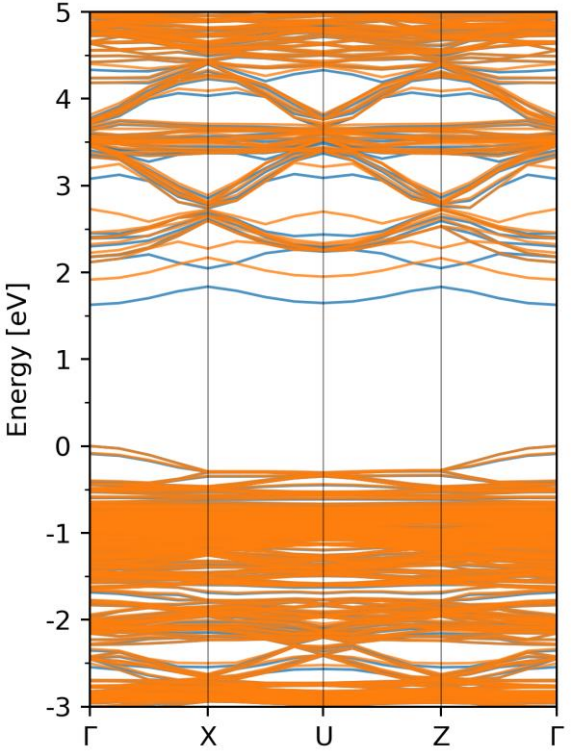


VBM

↑Energy: 1.8237 eV

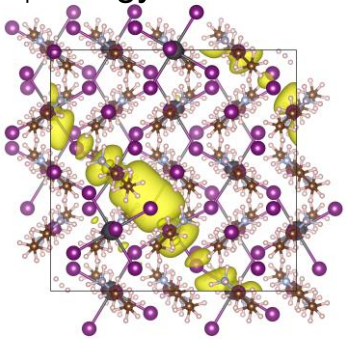

CBM

↓Energy: 2.1137 eV

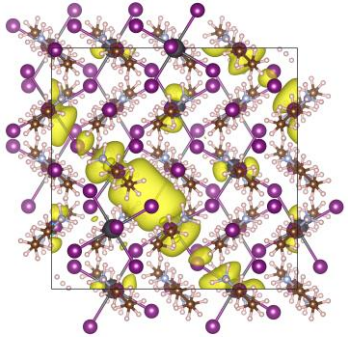

Los Alamos NATIONAL LABORATORY

# $I_I$ (out-of-plane) (2×1×2)

- Direct Bandgap (Γ→ Γ)
  - 0.565 eV (spin states of same orbital)
- Band edge states are highly localized
- Introduce P-Type defect

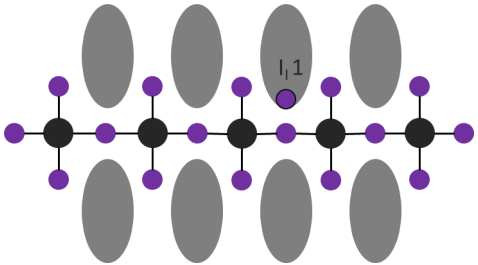


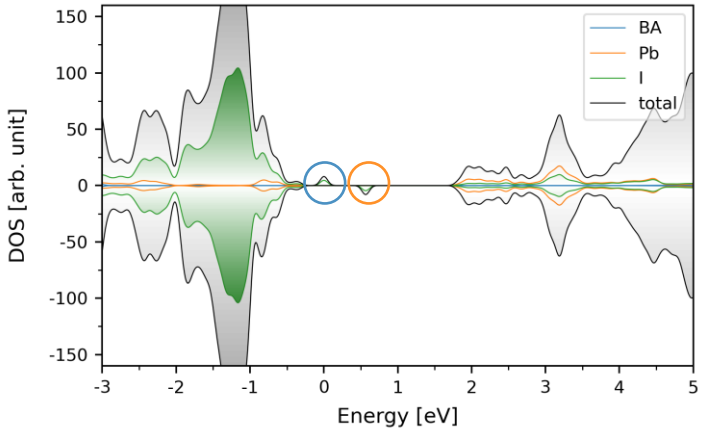


CBM
↓Energy: 1.156 eV

VBM
↑Energy: 0.591 eV

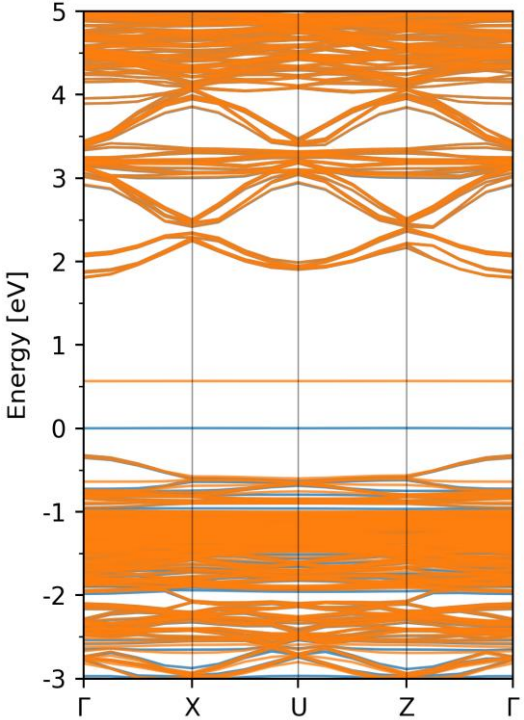

# $V_I$ (in-plane) layer dependence

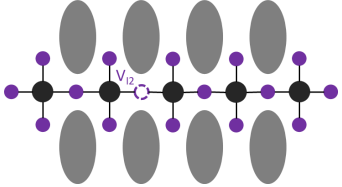


- Defect state remain regardless of layer depth

1×1×1

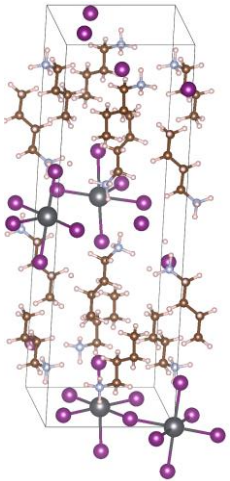

1×3×1

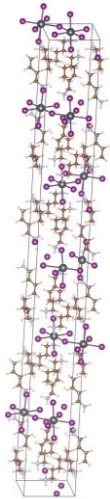

1×1×1 1×2×1 1×3×1

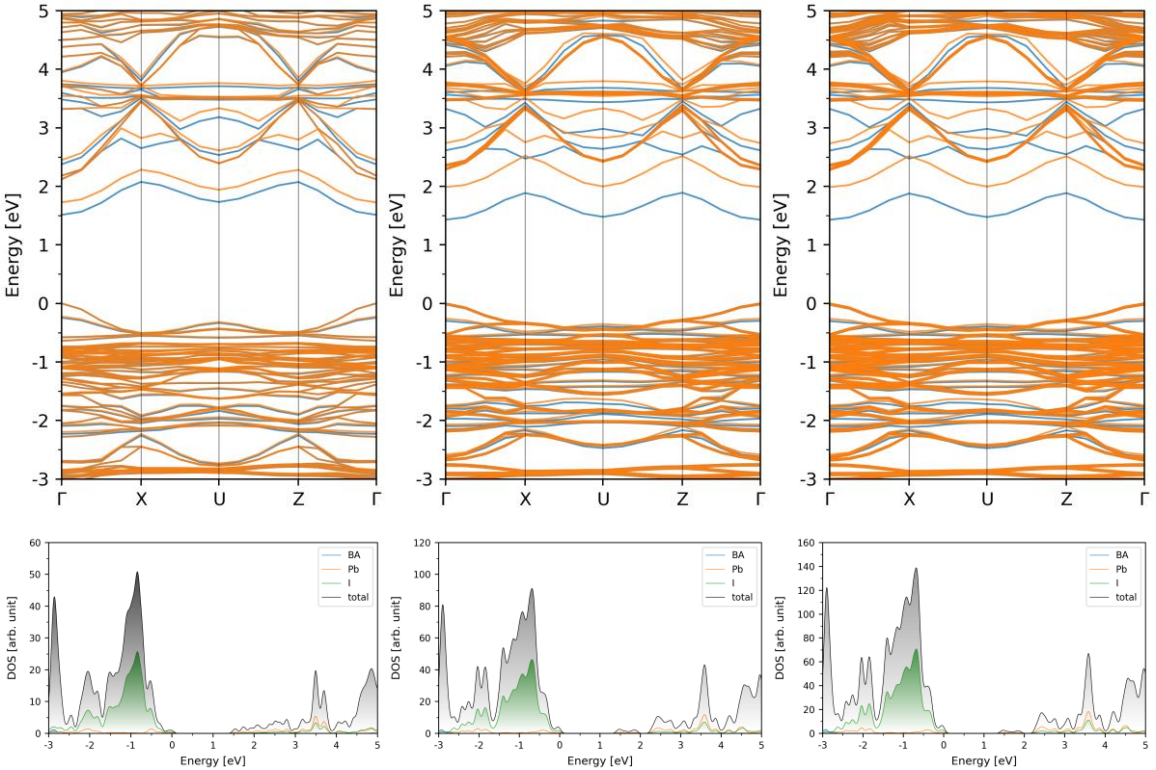

# Future of the project

## Lessons learned

- Defects which break electron pair introduce trap states.
  - $V_{BA}$, $V_{BAI}$, $V_{PbI2}$ are do not significantly perturb the electronic structure.

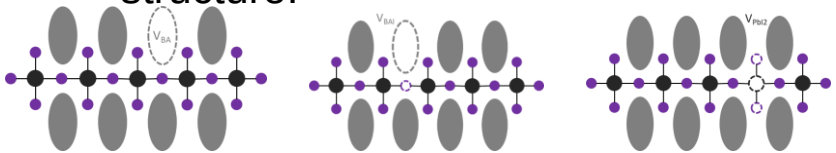

- Halide defects are the most detrimental to performance!
- Trap states remain regardless of cell thickness.

## Continued work

- Non-adiabatic molecular dynamics (NAMD)
  - Charge carrier lifetimes/dynamics
    - Pristine
    - $V_I$ (in-plane)
    - $I_I$ (in-plane)

# LOW-TEMPERATURE PLASMA TRANSPORT COEFFICIENTS DERIVED FROM SCATTERING ANGULAR DISTRIBUTION FUNCTIONS

Ryan M. Park[1,2] (T-1)

Mark C. Zammit[1] (T-1)

Willem Kupets,[1] James Colgan,[1] Christopher J. Fontes,[3] Xian-Zhu Tang,[1]

Liam H. Scarlett,[4] Dmitry V. Fursa,[4] Igor Bray,[4] Nathan A. Garland[1,5,6]

1) Theoretical Division, Los Alamos National Laboratory, Los Alamos, NM 87545, USA
2) Tulane Department of Chemical and Biomolecular Engineering, Tulane University, New Orleans, LA 70118, USA
3) Computational Physics Division, Los Alamos National Laboratory, Los Alamos NM 87545, USA
4) Curtin Institute for Computation and department of Physics, Astronomy and Medical Radiation Sciences, Curtin University, Perth, Western Australia 6102, Australia
5) School of Environment, Science & Engineering, Southern Cross University, Lismore, NSW 2480, Australia
6) School of Environment & Science, Griffith University, Brisbane, QLD4111, Australia



LA-UR-21-27525

# PLAN

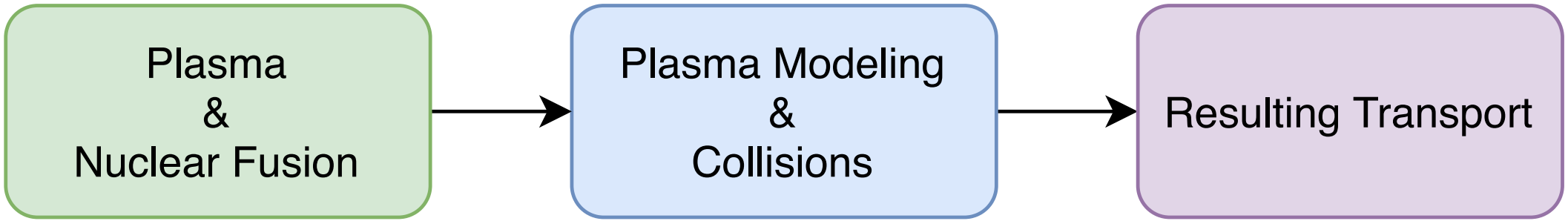
Plasma
&
Nuclear Fusion
Plasma Modeling
&
Collisions
Resulting Transport

# NUCLEAR FUSION

- Nuclear fusion reactions require extreme temperatures (~10 keV), where hydrogen exists as plasma

D-T Fusion: $${}^{2}_{1}H + {}^{3}_{1}H \rightarrow {}^{4}_{2}He + n + 17.5MeV$$

- Magnetic Confinement of Plasma
  - High temperature ionized gas
  - Large magnets suspend plasma away from reactor walls
- Detachment is essential for an efficient and lasting reactor

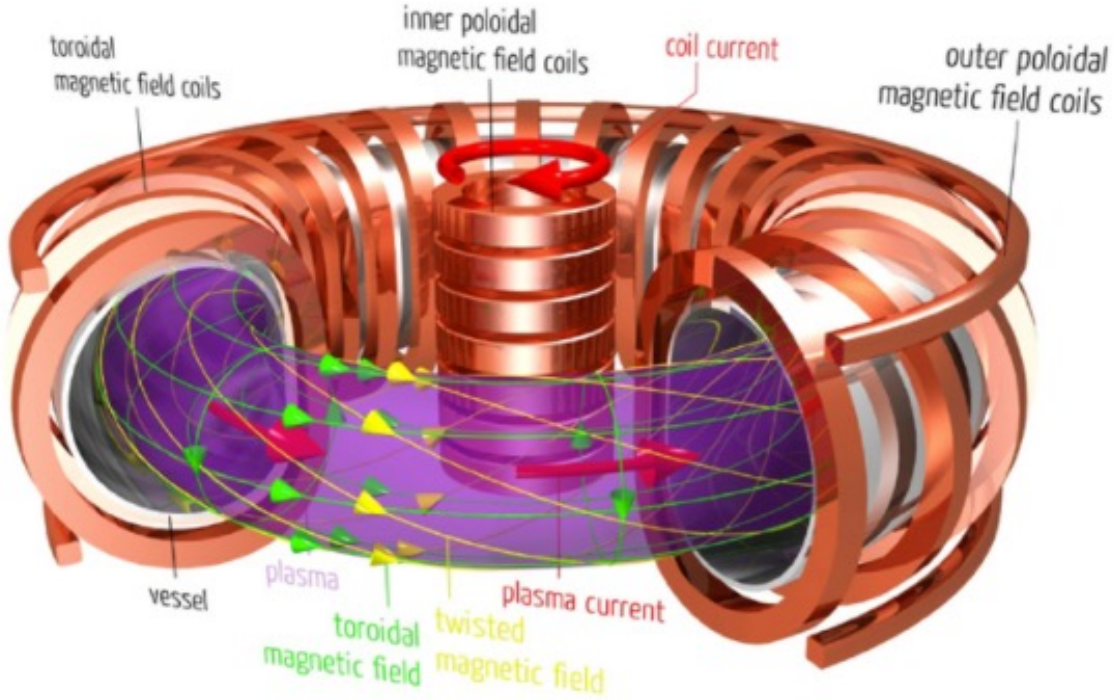

# ITER AND THE WALL PROBLEM

- International Thermonuclear Experimental Reactor (ITER)
  - Has been in the works since 1985
  - A research experiment with a lowest projected cost over $20 billion
- The wall problem
  - Plasma-surface interactions are critical to steady-state operation
  - High energy (MeV) electrons can destroy the walls of the reactor
  - Disruption can cause quenching and generate these runaway electrons
- Desire for accurate low-temperature plasma modeling near the wall

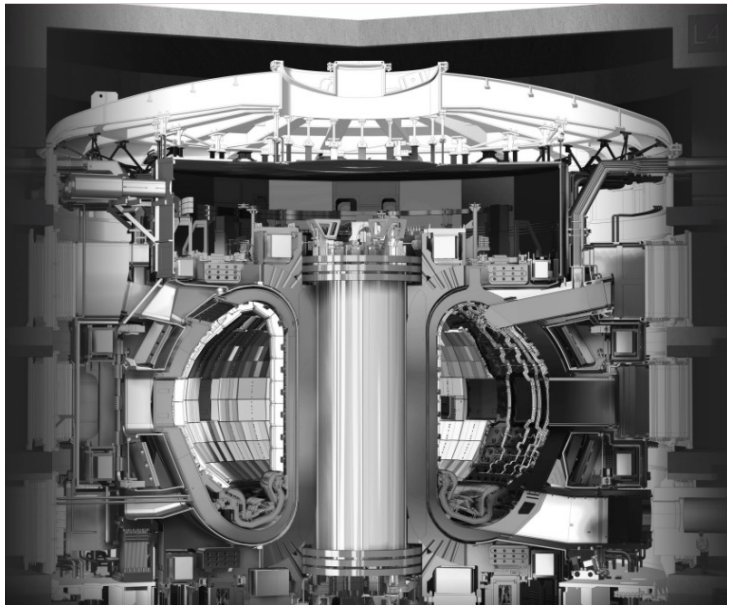

www.iter.org/mach

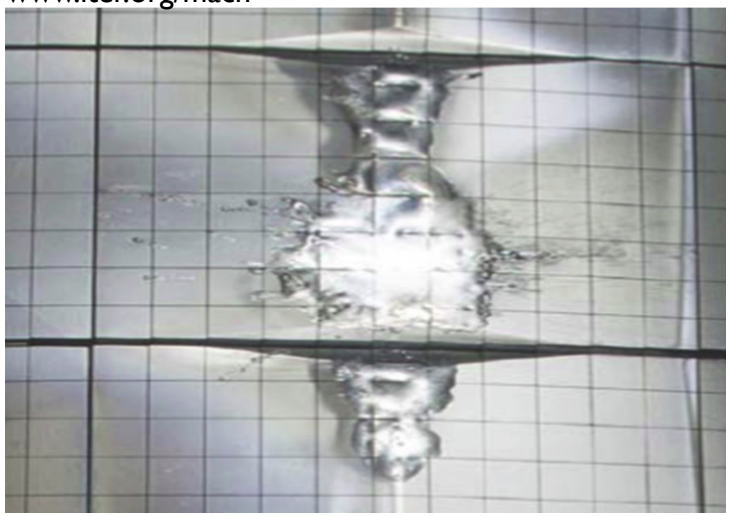

A damaged Beryllium wall.

# METHODS FOR MODELING PLASMA

- Particle in Cell (PIC) technique
  - Numerical method to integrate equations of motion
  - Challenging to deal with the singularity of collisions
- Monte-Carlo techniques can be used to account for collisions (PIC-MC)
  - Scattering cross sections and the angular distribution
- Boltzmann Solvers
  - Numerical solution to the Boltzmann Equation
  - Boltzmann and PIC calculators solve the same problem

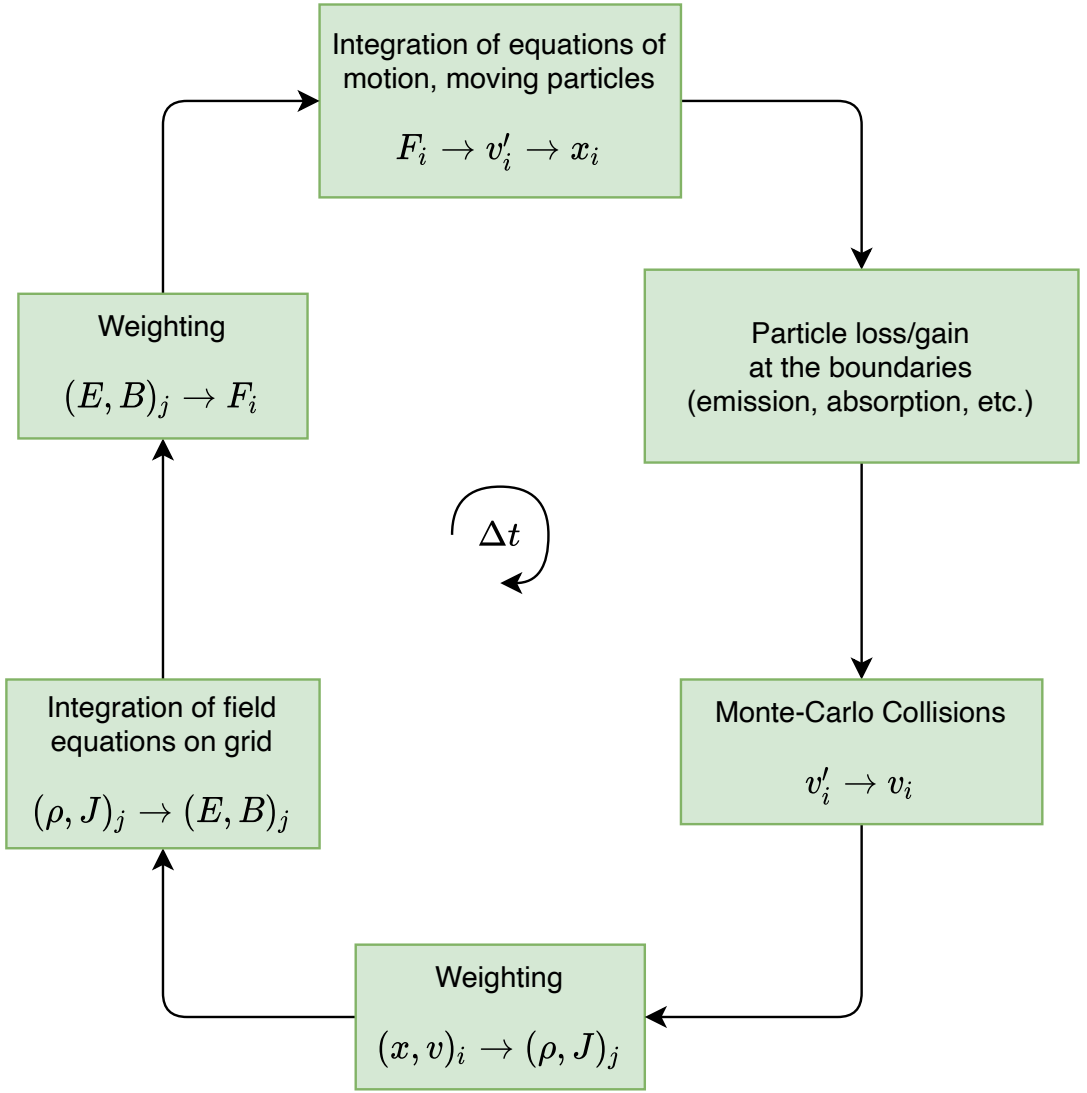

# SCATTERING CONCEPTS FOR MONTE-CARLO

- Types of scattering
  - Elastic $e^-(\epsilon) + He \rightarrow e^-(\epsilon, \chi) + He$
  - Excitation $e^-(\epsilon) + He \rightarrow e^-(\epsilon_a, \chi) + He^*$
  - Ionization $e^-(\epsilon) + He \rightarrow e^-(\epsilon_a, \chi_a) + e^-(\epsilon_b, \chi_b) + He^+$
- There is an angular distribution associated with each type of scattering

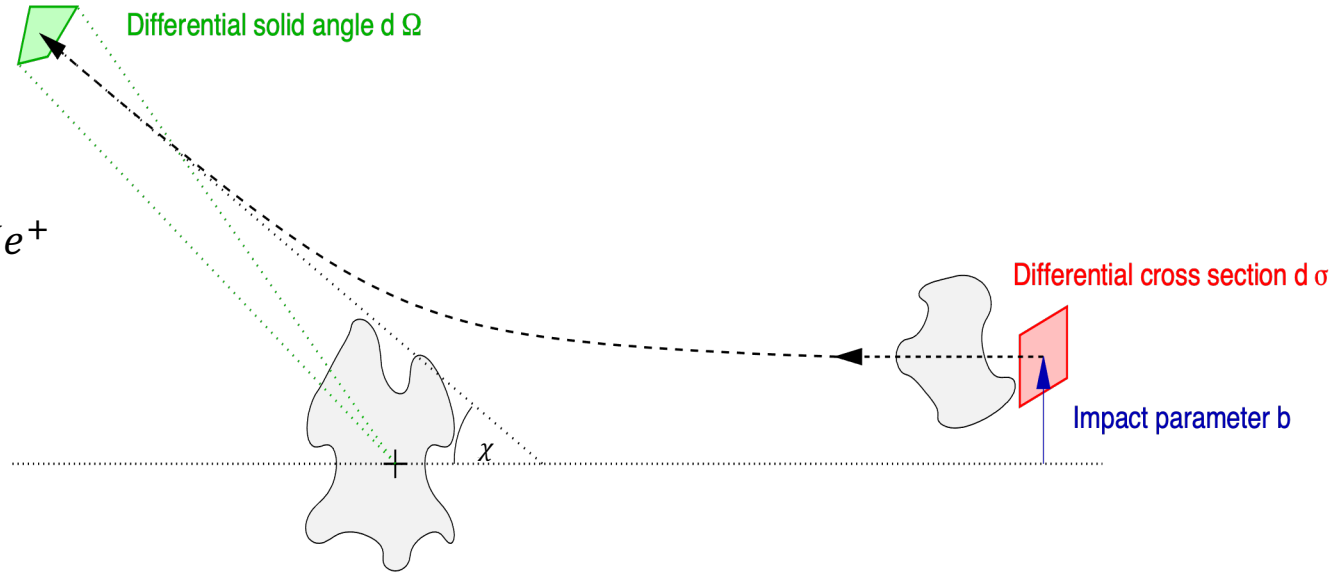


$$\chi(\epsilon) \rightarrow \frac{\partial\sigma(\epsilon,\chi)}{\partial\Omega} \rightarrow \mathrm{I}(\epsilon,\chi)$$

$Scattering\ Angle \rightarrow Differential\ Cross\ Section \rightarrow Angular\ Distribution$

# THE LANL ANGULAR DISTRIBUTION

- The LANL Angular Distribution
  - Elastic: $e^-(\epsilon) + He \rightarrow e^-(\epsilon, \chi) + He$
  - Applies to neutral species, (H, D, T, $H_2$, $D_2$, $T_2$, He) at low-temperatures
  - Characterized by greater backscattering at lower energies
- Monte-Carlo requires an invertible angular distribution to run efficiently
  - It is too complicated to predict when, where, and how every single collision will occur.
  - Instead, estimate a collision frequency for each type of collision
  - For each collision and each particle, sample from the angular distribution.

Comparison of Angular Distributions compared to benchmark CCC data for He elastic collisions.

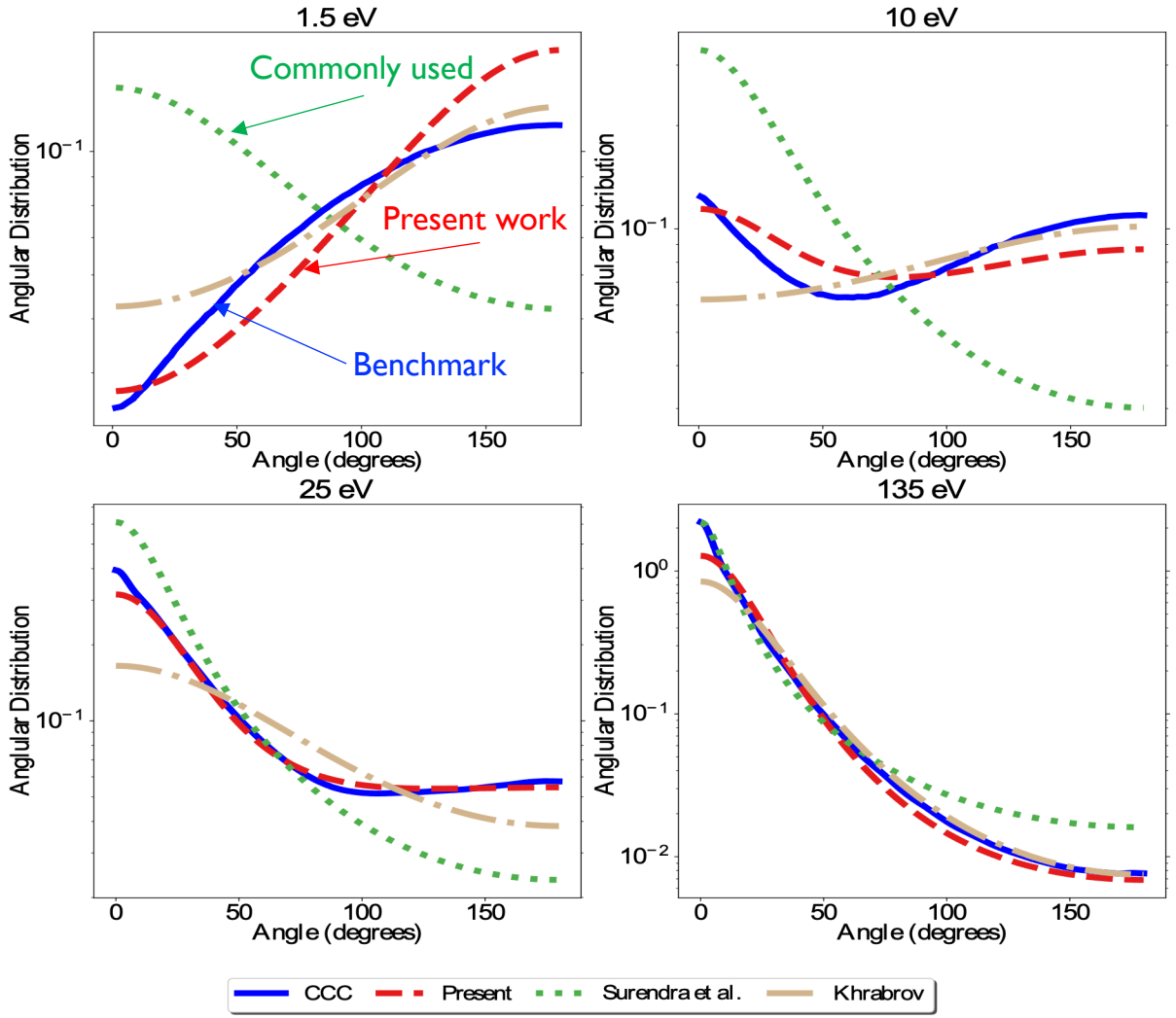


W. Kupets et al. in preparation (2021); M. Surendra, D. B. Graves, and G. M. Jellum, Phys. Rev. A 41, 1112 (1990); A.V. Khrabrov and I. D. Kaganovich, Physics of Plasmas 19, 093511 (2012); I. Bray, D.V. Fursa, A. S. Kheifets, and A.T. Stelbovics, J. Phys. B 35, R117 (2002).

# CROSS SECTION MODELS FOR HELIUM

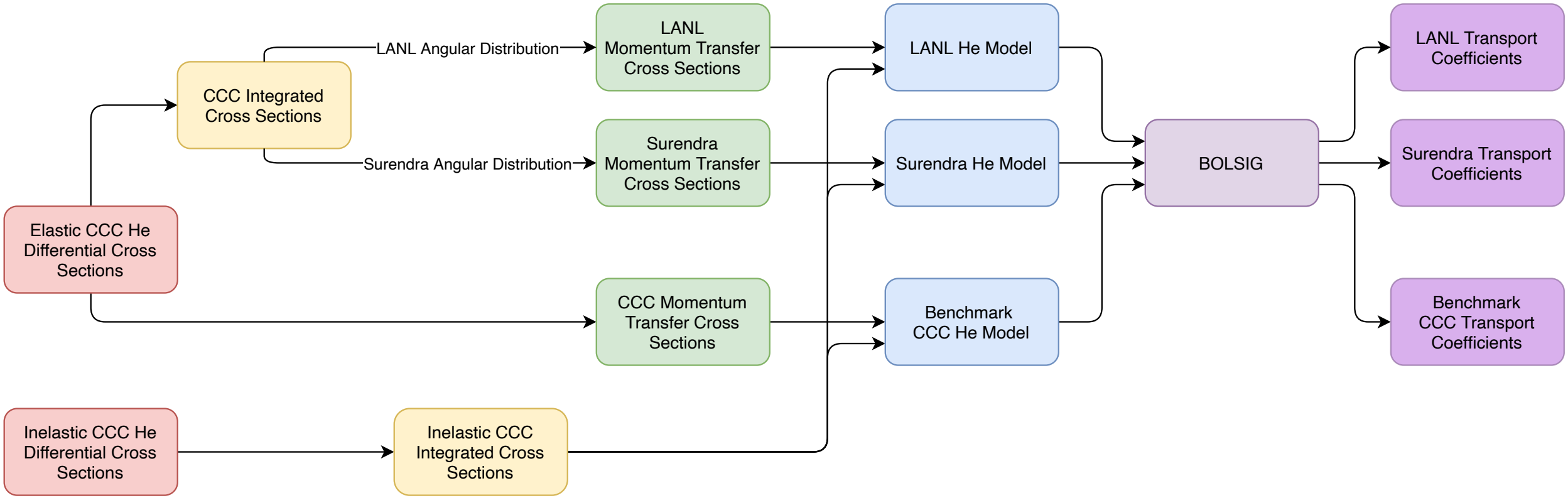


$$\sigma_M(\epsilon) = 2\pi\sigma(\epsilon)\int_0^{\pi} I(\epsilon,\chi)(1-cos\chi)sin\chi d\chi$$

# RESULTS

- Benchmark CCC curves based on cross sections obtained from QM calculations
- Error in Surendra et al. significant at > 1.0 Townsend
- Transport behavior is especially improved for larger reduced electric fields

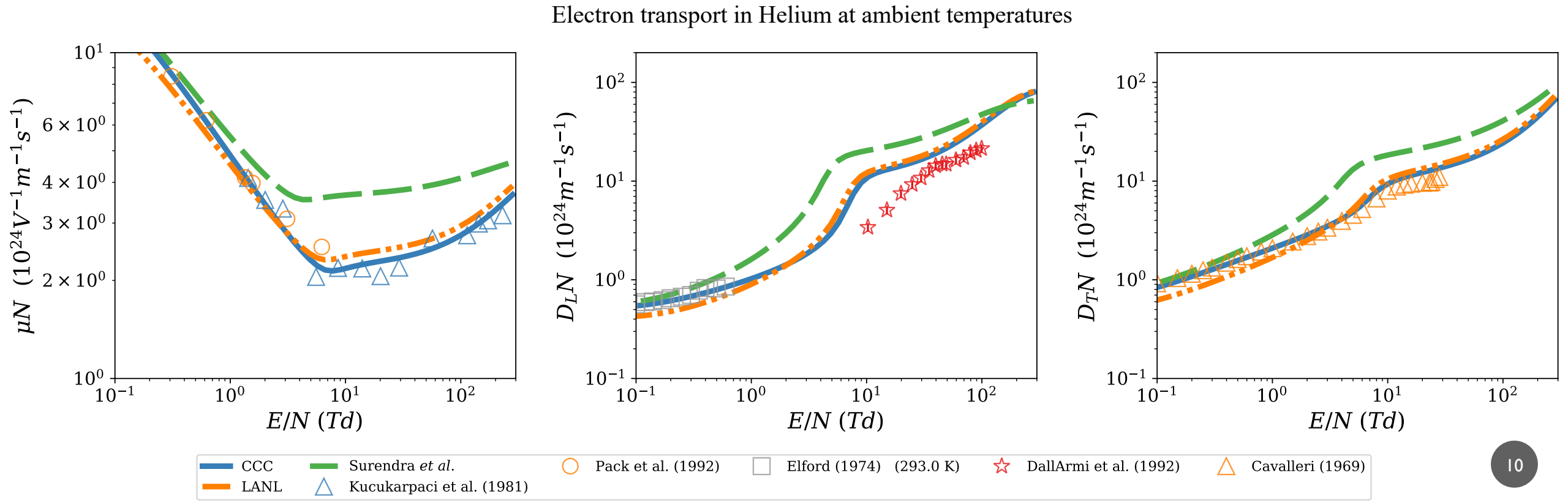

# CONCLUSION

- We have motivated use of the LANL angular distribution in state-of-the-art PIC-MC by demonstrating more accurate transport behavior emergent from a more realistic scattering model
- Currently being implemented in modern PIC codes at LANL
- Plan to make recommendations for the complete range of collision processes that are used in PIC-MC
  - Extend approach to other neutral species such as Nitrogen, Argon, and Xenon
  - Ionization processes (energy sharing and angular distributions)
  - Excitation angular distributions
- This work is in preparation and to be submitted to PSST

Work funded by the Los Alamos National Laboratory (LANL) Laboratory Directed Research and Development program project number 20200356ER.

Los Alamos NATIONAL LABORATORY

# Simulating the Thermodynamic properties of Tungsten Grain Boundaries

T-1 Division: Physics and Chemistry of Materials

By: Quinn Parker, Danny Perez, and Thomas Vogel

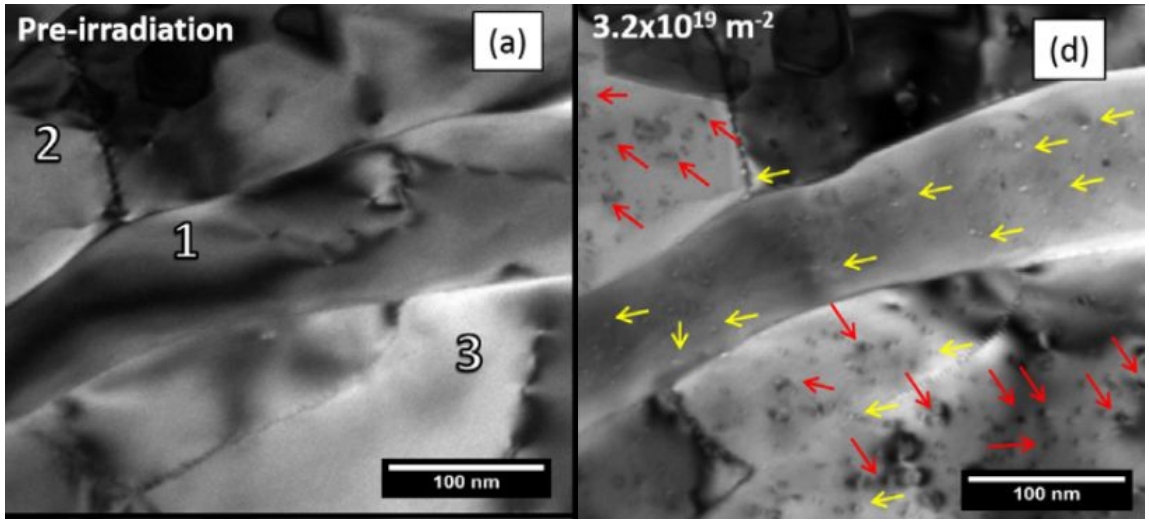


El-Atwani, O., Hinks, J., Greaves, G. *et al.* In-situ TEM observation of the response of ultrafine- and nanocrystalline-grained tungsten to extreme irradiation environments.

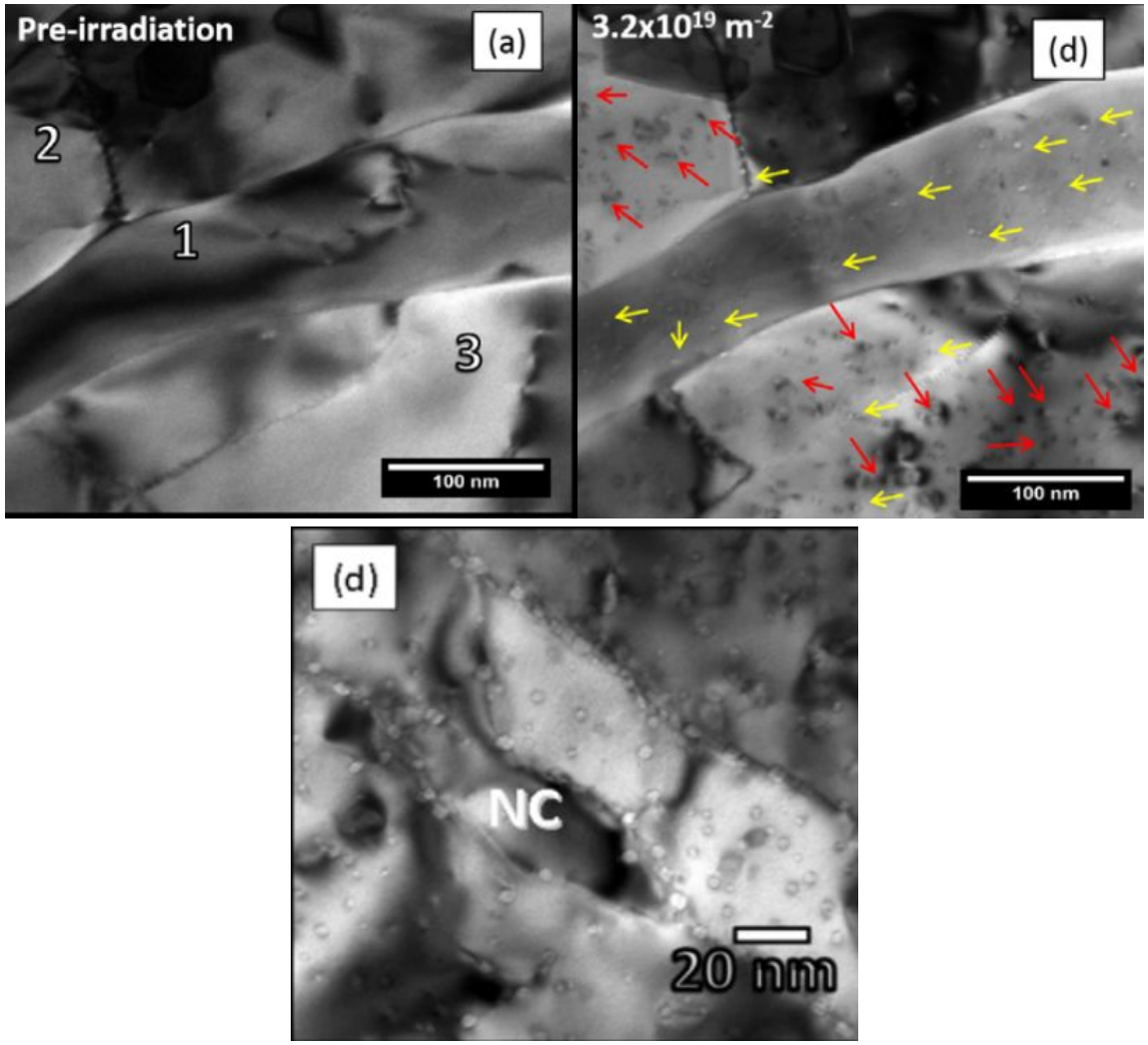


El-Atwani, O., Hinks, J., Greaves, G. *et al.* In-situ TEM observation of the response of ultrafine- and nanocrystalline-grained tungsten to extreme irradiation environments.

# Main Question

How do we predict grain boundary structures within the system?

# Process

We simulate a crystal with degrees of freedom in total particle numbers and with a range of temperatures

1

An Adaptive-Biasing Force scheme iteration runs with each total particle number, N

2

Sample within the whole Grand-Canonical Ensemble, with fixed temperature

# Made up example of free energy landscape

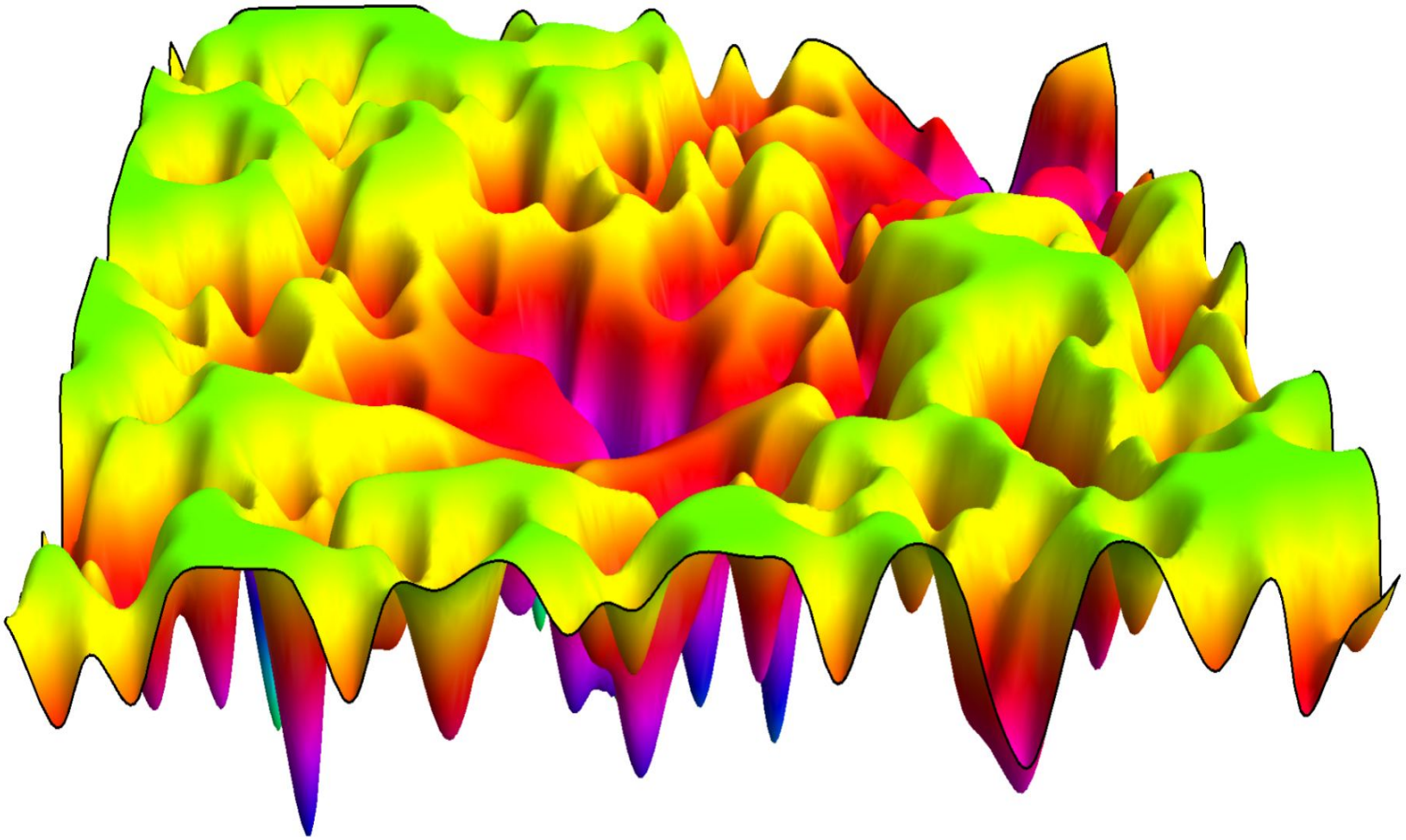

D.J. Wales, Ann. Rev. Phys. Chem., 69 (2017)

# Two body-centered cubic (bcc) Tungsten grain boundaries, seen below in constructed state

[100] tilt GB

Σ5[001] (310)-twist GB

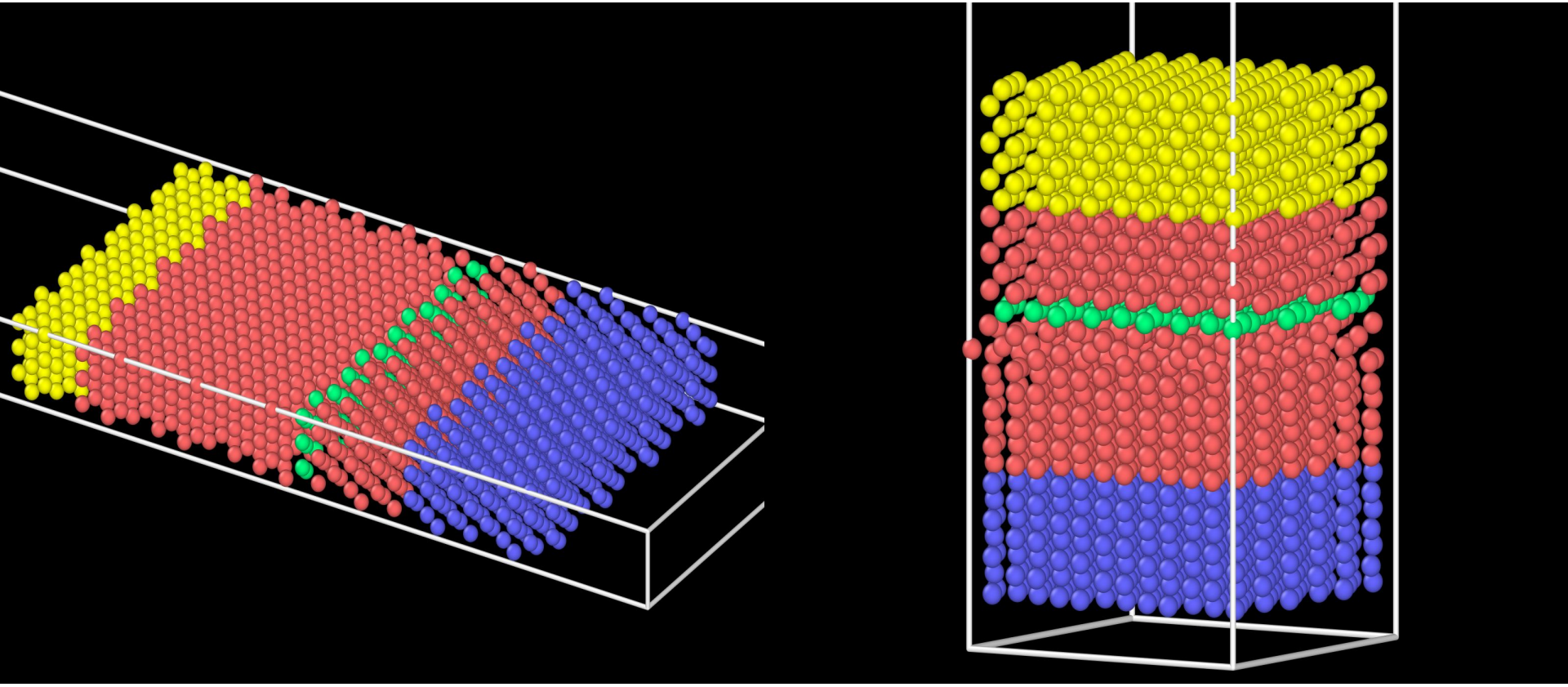

represents fixed Tungsten atoms

represents Tungsten atoms that move during simulation

# Two body-centered cubic (bcc) Tungsten grain boundaries, seen below in constructed state

[100] tilt GB

Σ5[001] (310)-twist GB

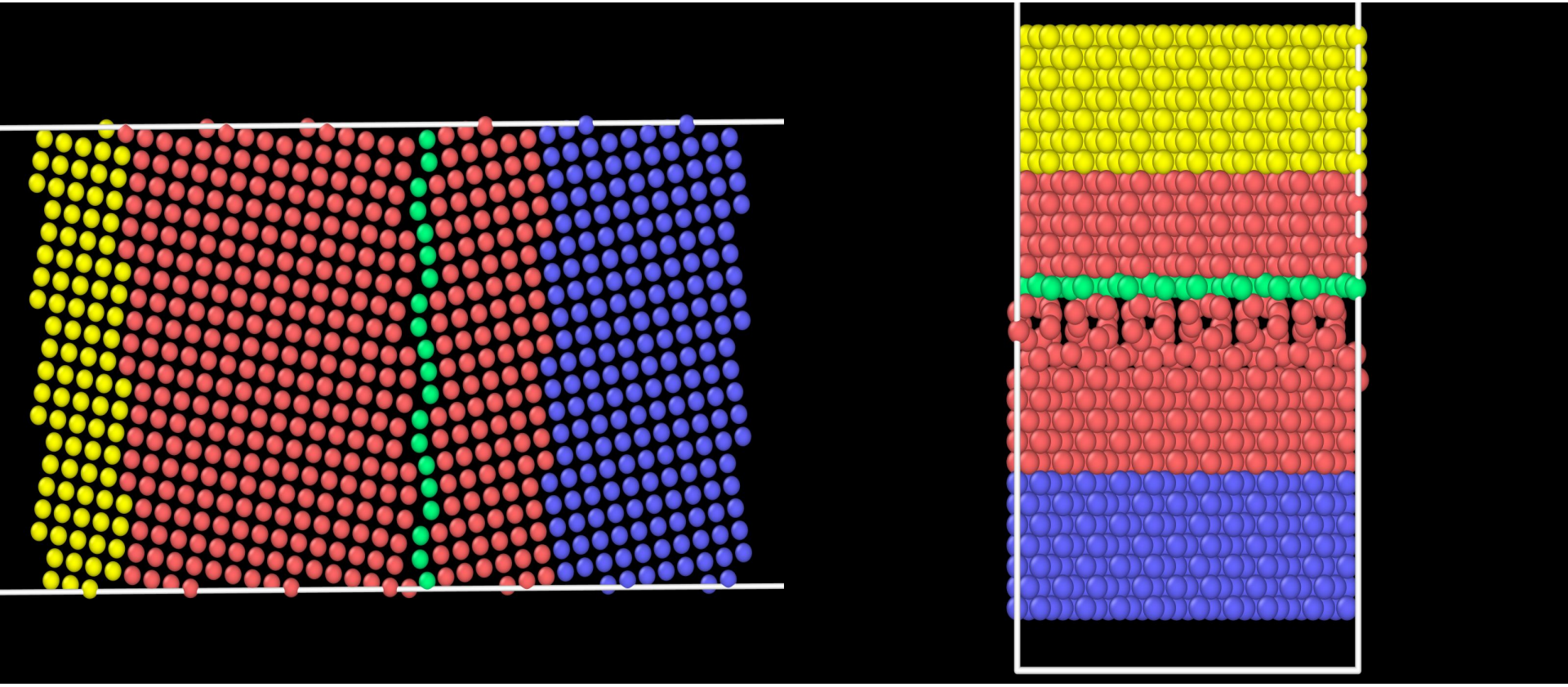

represents fixed Tungsten atoms

represents Tungsten atoms that move during simulation

# Entropy

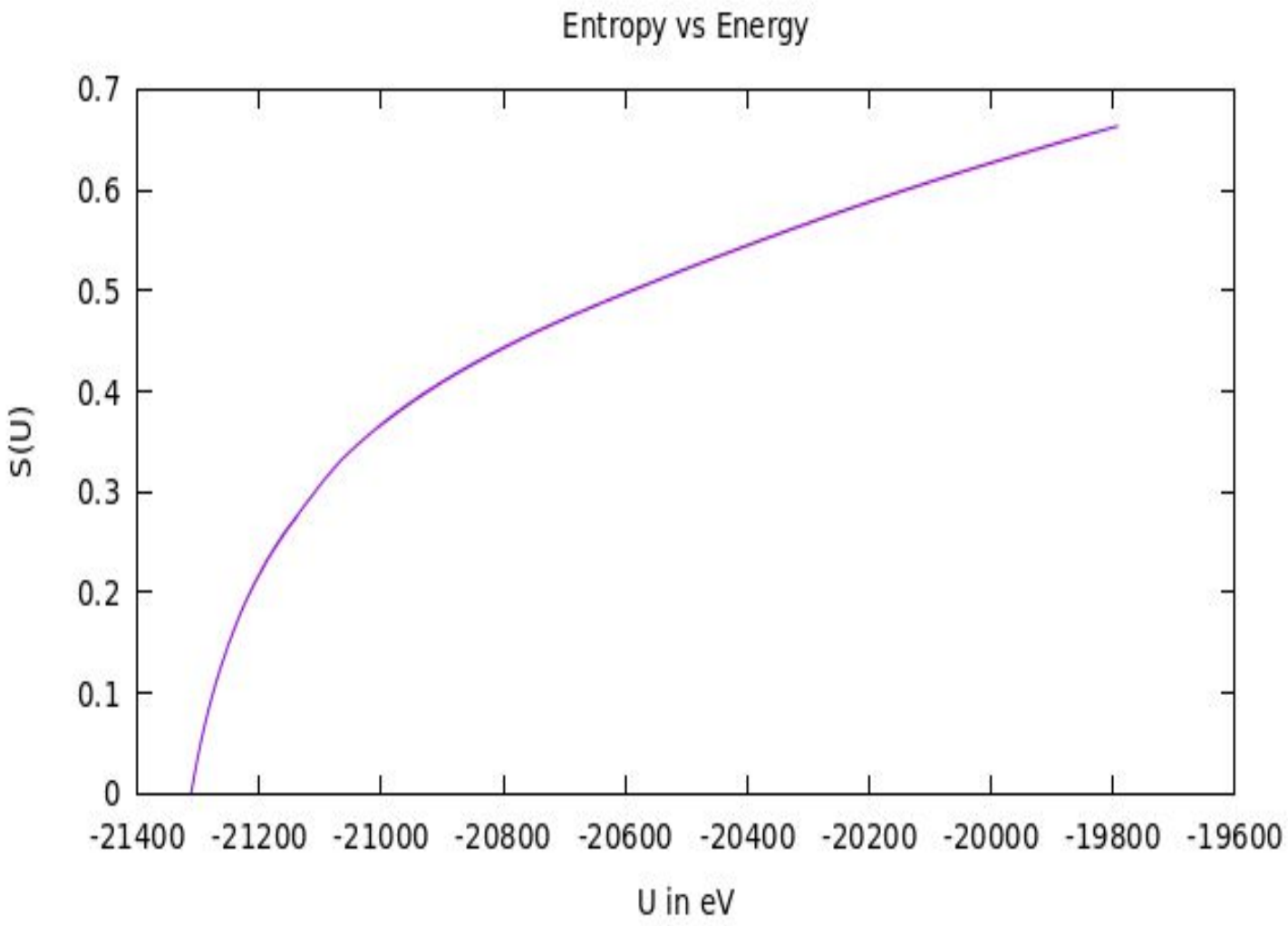
Entropy vs Energy
S(U)
0.7
0.6
0.5
0.4
0.3
0.2
0.1
0
-21400
-21200
-21000
-20800
-20600
-20400
-20200
-20000
-19800
-19600
U in eV

# Derivative and Second Derivative of the Entropy

First derivative

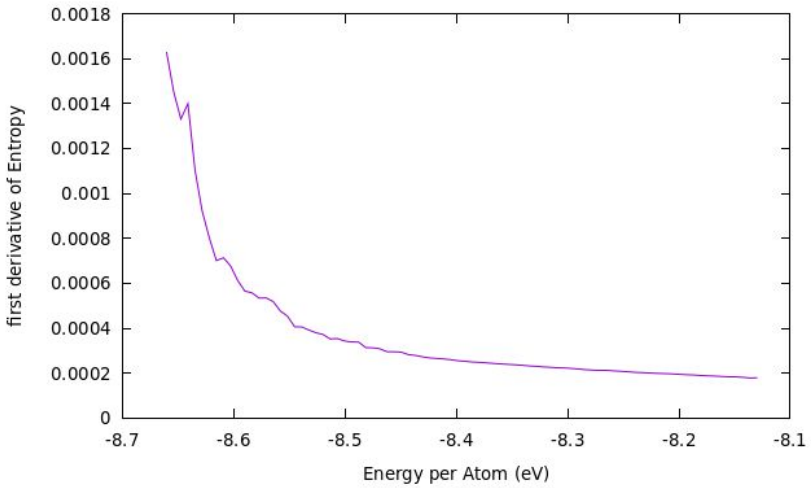


Second derivative

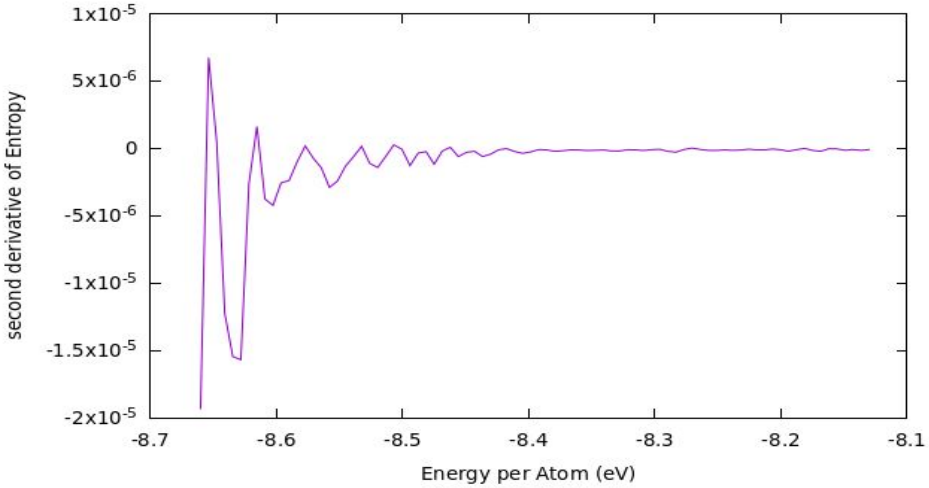

# Derivative and Second Derivative of the Entropy

First derivative

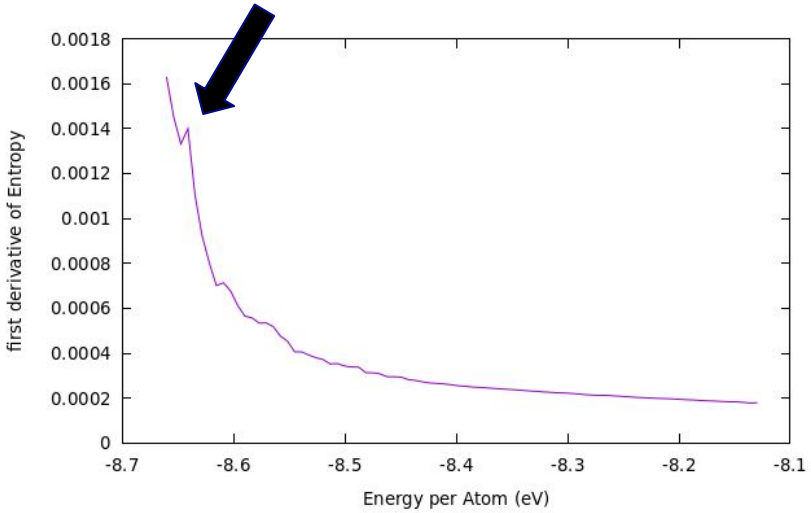


Second derivative

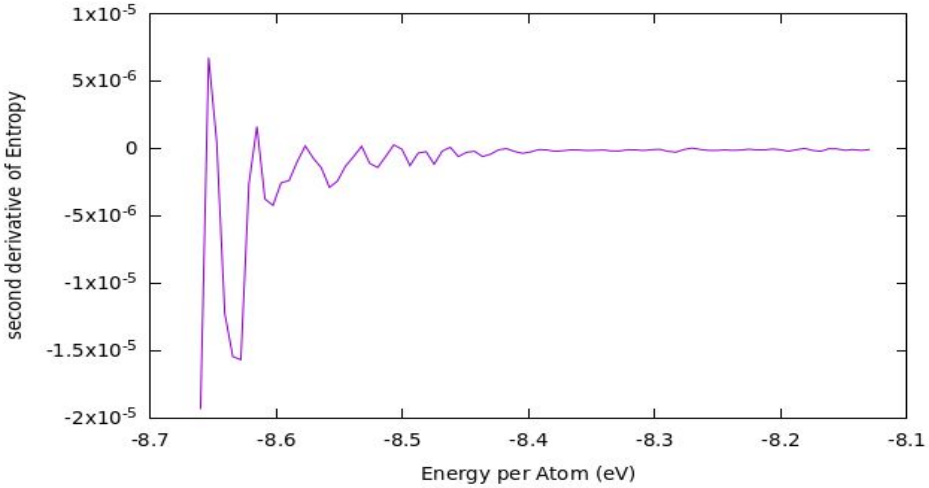

# The derivative of Entropy

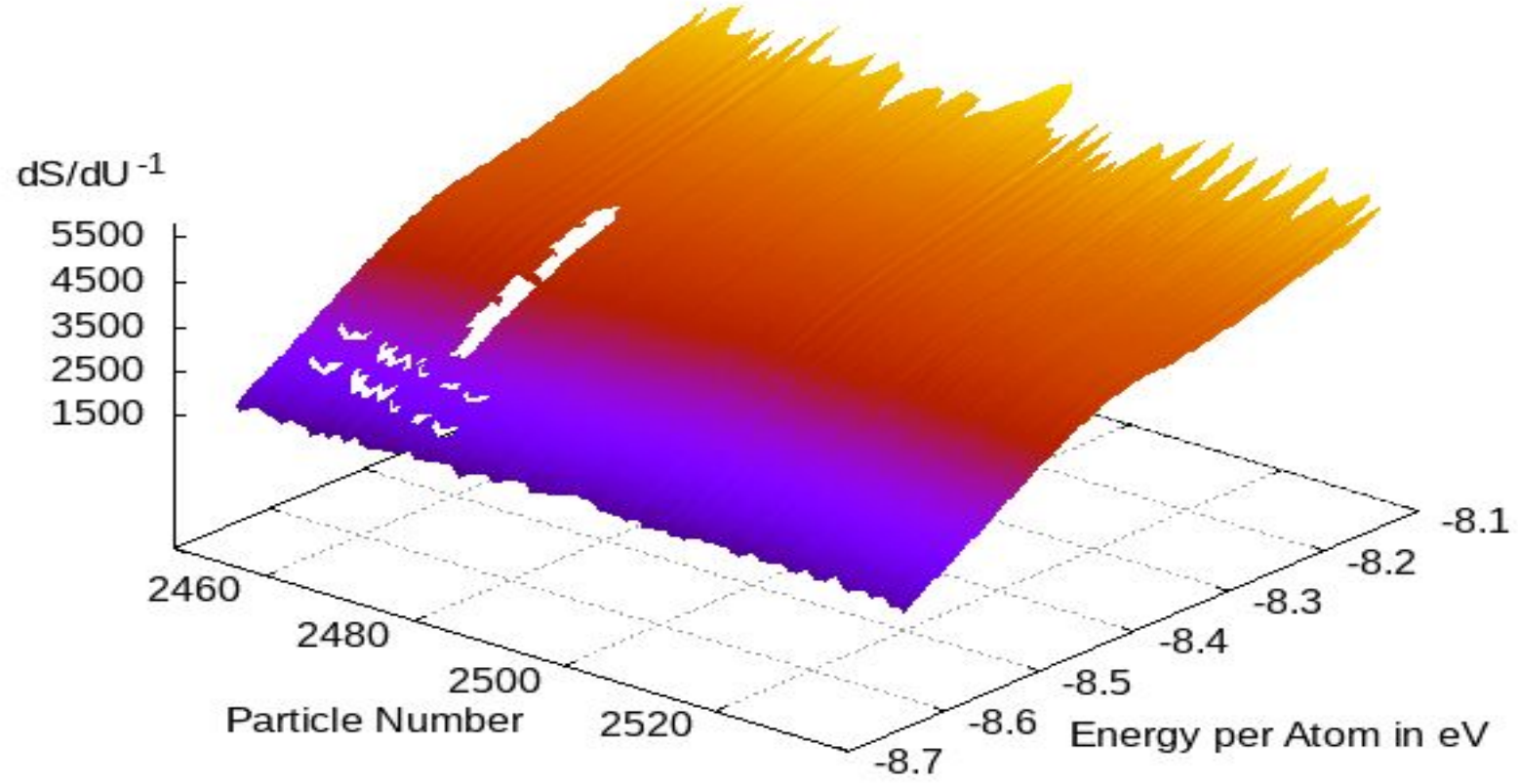

# The derivative of Entropy

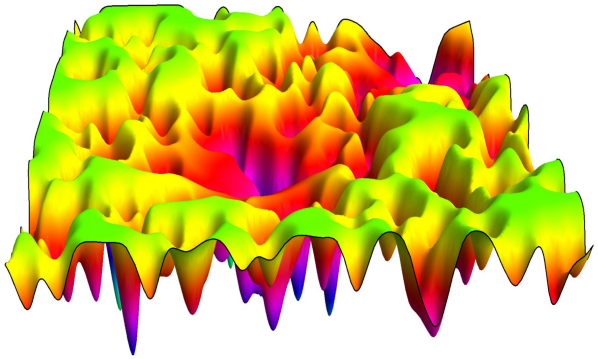

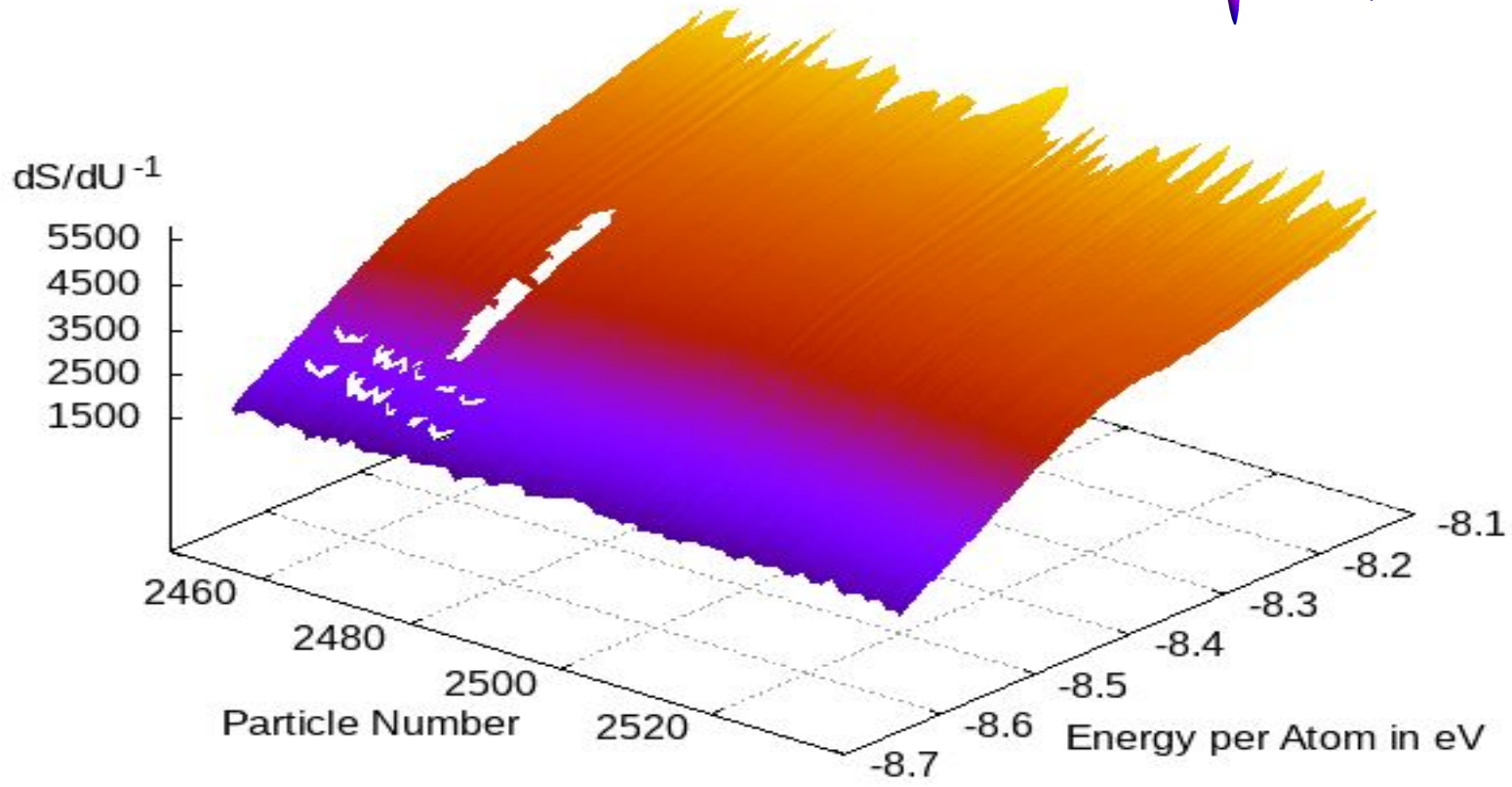

# Take-Home Message and Conclusion

- Don’t look at grain boundaries through a toilet paper roll: experiments suggest a range of temperatures and particle numbers of GBs must be simulated to find minimum free energy structures.

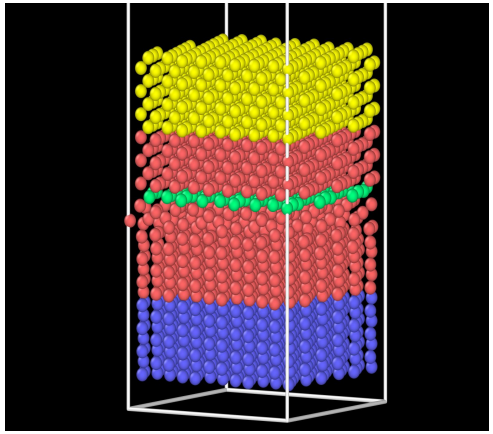

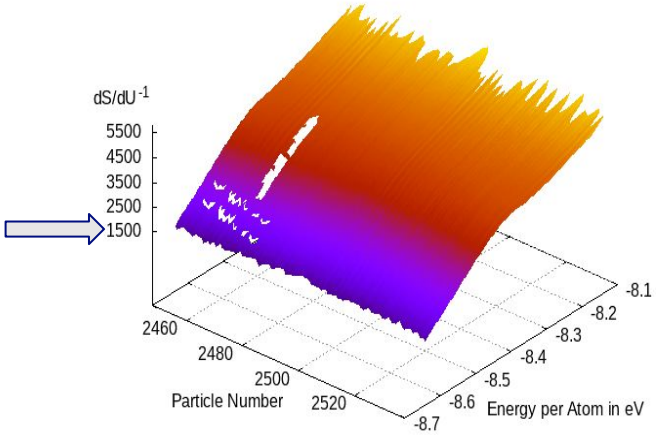


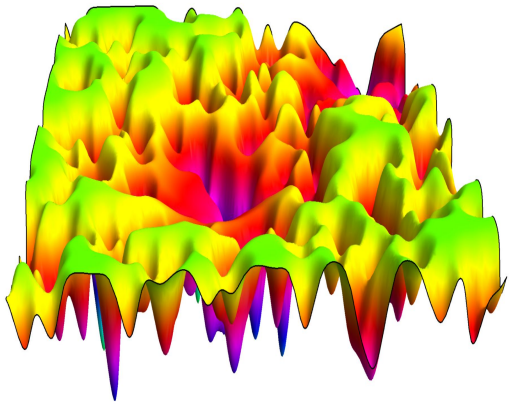

# Take-Home Message and Conclusion

- Don’t look at grain boundaries through a toilet paper roll: experiments suggest a range of temperatures and particle numbers of GBs must be simulated to find minimum free energy structures.

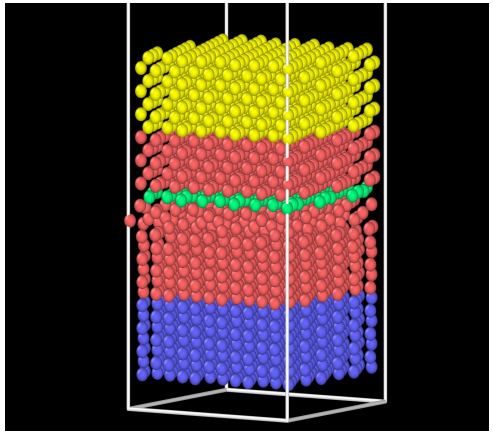

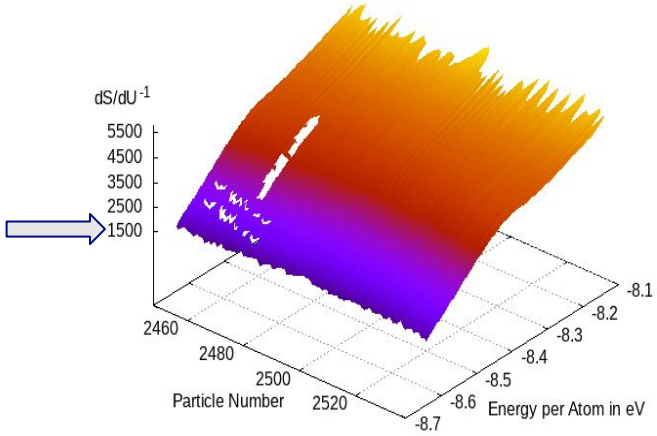


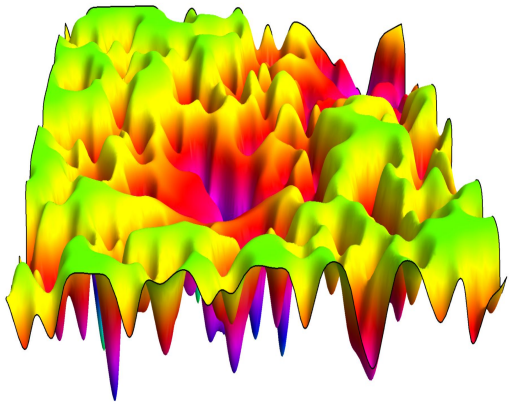

Acknowledgments

Mentors: Thomas Vogel, Danny Perez

Fellow student collaborator: Jacob Spurlock

Thanks to:
Laura Lopes, Peter Hatton, Blas Uberuaga, Nithin Matthews, Jan Janssen, the Scidac group at large, and the DOE’s VFP program

Los Alamos NATIONAL LABORATORY

# Modeling Continua with the Discontinuous Galerkin Method

Kyle Perez

August 17 2021

# Why to Model Continuous Systems Numerically

- These systems display nonlinear behavior that usually lack analytic solutions.
- The dynamics of solids and fluids have important applications in everyday life alongside research performed at LANL.

# Equations of Motion

$$\frac{\partial \rho}{\partial t} + \nabla \cdot (\rho \mathbf{v}) = 0$$

Continuity Equation

$$\rho(\frac{\partial \mathbf{v}}{\partial t} + (\mathbf{v} \cdot \nabla)\mathbf{v}) = \nabla \cdot \sigma + \rho \mathbf{f}$$

Momentum Equation

An Equation of State

Examples

Ideal Gas

$$p = (\gamma - 1)\rho e$$

$$\sigma_{ij} = -p\delta_{ij}$$

Linear Elasticity

$$\epsilon_{ij} = \frac{1}{2}(\frac{\partial u_i}{\partial x_j} + \frac{\partial u_j}{\partial x_i})$$

$$\sigma_{ij} = \sum_{k,l} Y_{ijkl}\epsilon_{kl}$$

# Discontinuous Galerkin Method (DG Method)

Models equations of the form $\frac{\partial q}{\partial t} = \nabla \cdot \mathbf{f} + b$

The function *q* is modeled over *k* subvolumes. *q* in each subvolume is referred to as $q^k$.

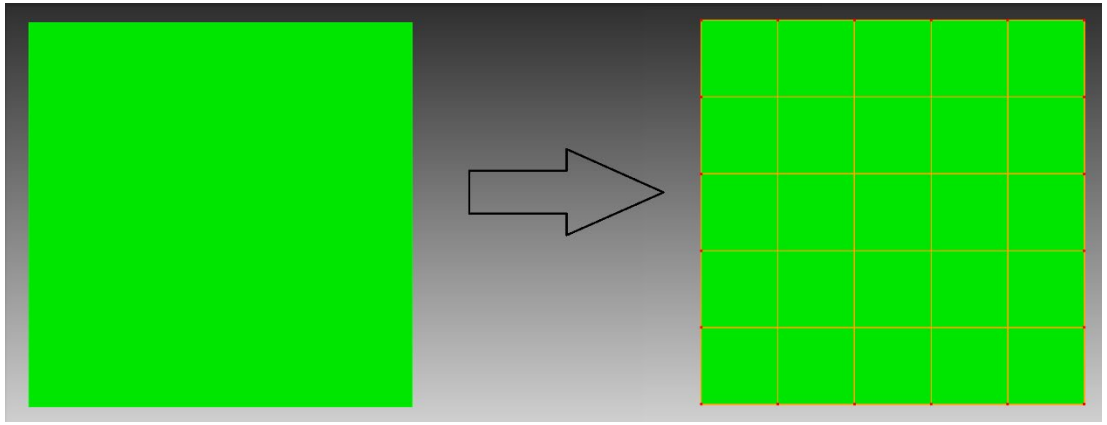

The simulated function gets reassembled as $q(x,t) = \bigoplus_k q^k(x,t)$

# DG Method (cont)

Each $q^k$ is represented as $q^k(x,t) = \sum_i q_i^k(t) S_i^k(x)$

System evolves via

$$\sum_j \frac{\partial q_j^k}{\partial t} \int_{V^k} S_i(x) S_j(x) dV = \int_{\partial V^k} \mathbf{f}^* \cdot \mathbf{n}^k S_i^k(x) dS - \int_{V^k} \mathbf{f} \cdot \nabla S_i^k(x) dV + \int_{V^k} b S_i^k(x) dV$$

Evolves both the Continuity Equation and Momentum Equation

Evolution equation is a matrix equation

# The Surface Integral

The evolution equation contains the term $\int_{\partial V^k} \mathbf{f}^* \cdot \mathbf{n}^k S_i^k(x) dS$

The asterisk captures the effect of neighboring cells on the cell *k*.

Ex: $\mathbf{f}^*(q) = \frac{1}{2}(\mathbf{f}(q^+) + \mathbf{f}(q^-))$

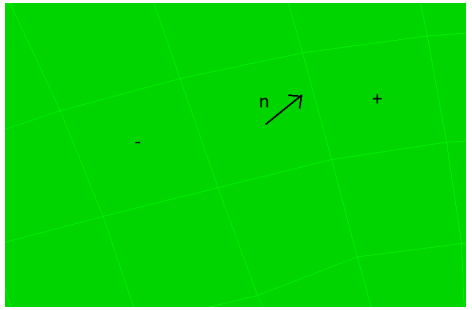


Example: Momentum Equation:

$$\frac{\partial}{\partial t}(\rho \mathbf{v}) = \nabla \cdot (\sigma - \rho \mathbf{v} \otimes \mathbf{v}) + \rho \mathbf{g}$$

We have

$$\mathbf{f}_{ij} = \sigma_{ij} - \rho v_i v_j$$

$$\mathbf{q} = \rho \mathbf{v}$$

And can pick

$$(\mathbf{qv})^* \cdot \mathbf{n}^k = \frac{\mathbf{v} \cdot \mathbf{n}^k}{2}(q^+ + q^-) + |\mathbf{v} \cdot \mathbf{n}^k| \frac{1-\alpha}{2}(q^+ - q^-)$$

$\alpha$ is user-defined

# Computing Integrals

Update rule involves integrals of the form $\int_{\partial V} \mathbf{f} \cdot \mathbf{n} dS$ and $\int_V \phi dV$

Integrals can be done using Gaussian Quadrature:

$$\int_{-1}^{1} f(x)dx = \sum_i w_i f(x_i)$$

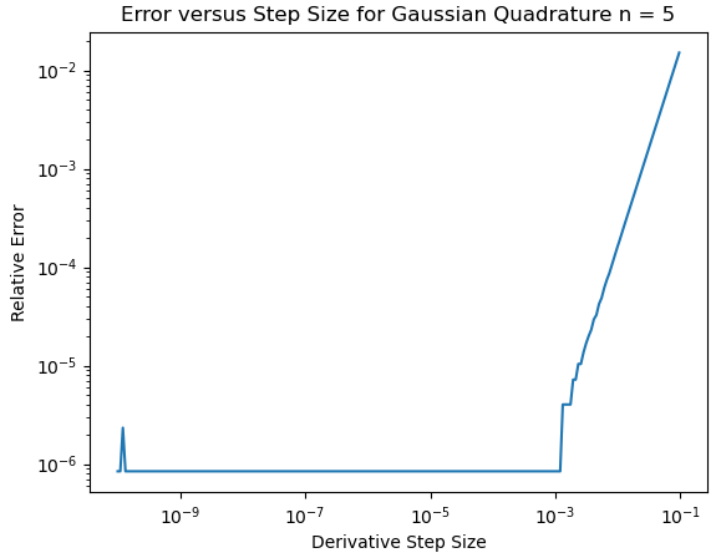


When applied to 3d:

$$\int_V \phi(\mathbf{x})dV = \sum_g w_g \phi(\mathbf{x}(\xi_g))|J(\mathbf{x}(\xi_g))|$$

# Results

In Progress

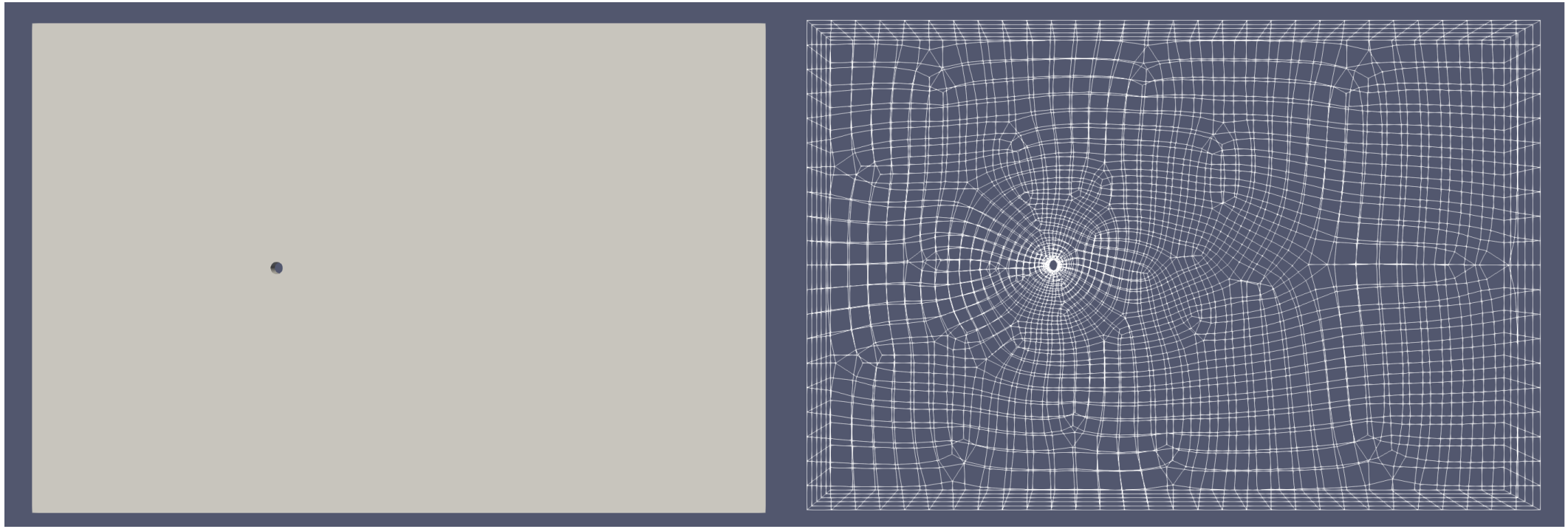

Thank You!

Los Alamos NATIONAL LABORATORY

# Genome-Wide Association Study for Female Infertility

Lillian Petersen, Harvard University
Christina Steadman, LANL Advisor
Liming Liang, Harvard Advisor

August 26, 2021

# Summary

- Female infertility is a rising problem, affecting more than 1 in 10 women
- Infertility is highly heritable
  - Currently very little understanding of genetic risks & biological pathways
- Goal: conduct a Genome-Wide Association Study for female infertility
  - Improve diagnosis, early treatment, fertility outcomes

# Human Genetics: An Overview

3 billion Nucleotides (A, T, G, C) in human genome

99% of nucleotides are identical between all humans

# Human Genetics: An Overview

3 billion Nucleotides (A, T, G, C) in human genome

99% of nucleotides are identical between all humans

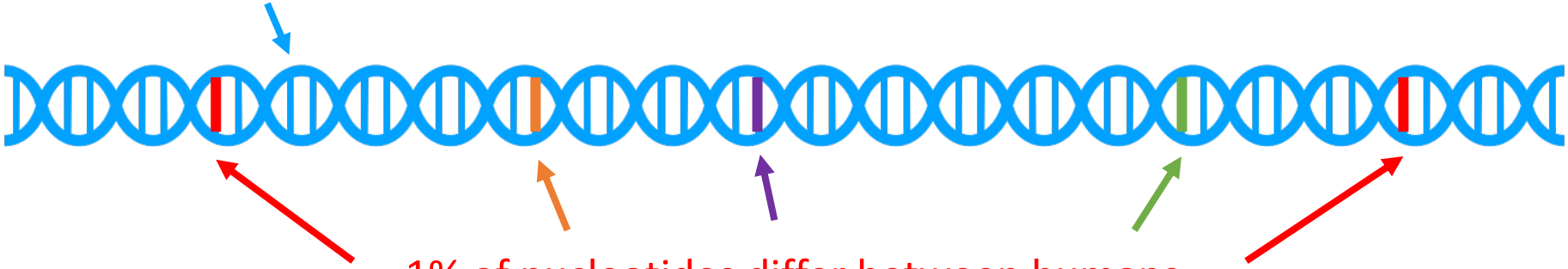

1% of nucleotides differ between humans

**“Single Nucleotide Polymorphism” = “SNP”**

# Human Genetics: An Overview

3 billion Nucleotides (A, T, G, C) in human genome

99% of nucleotides are identical between all humans

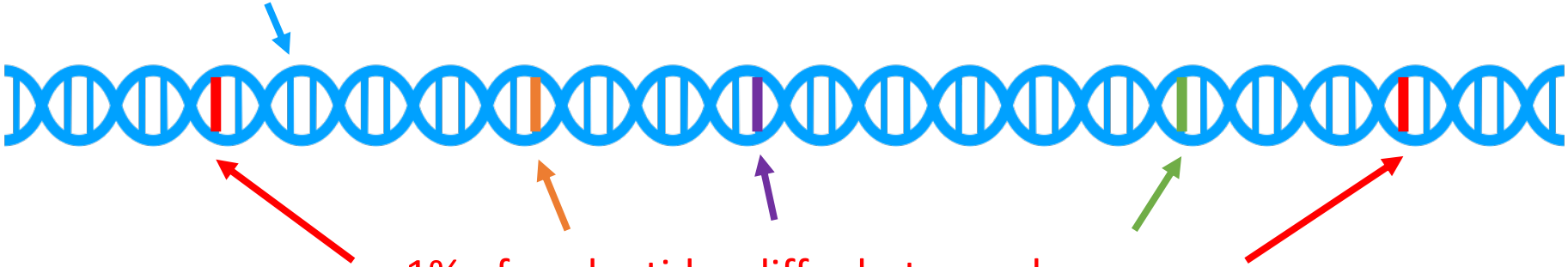

1% of nucleotides differ between humans

**“Single Nucleotide Polymorphism” = “SNP”**

- SNPs cause differences between us
- **Genotyping** identifies the SNPs an individual carries

# Polycystic Ovarian Syndrome (PCOS)

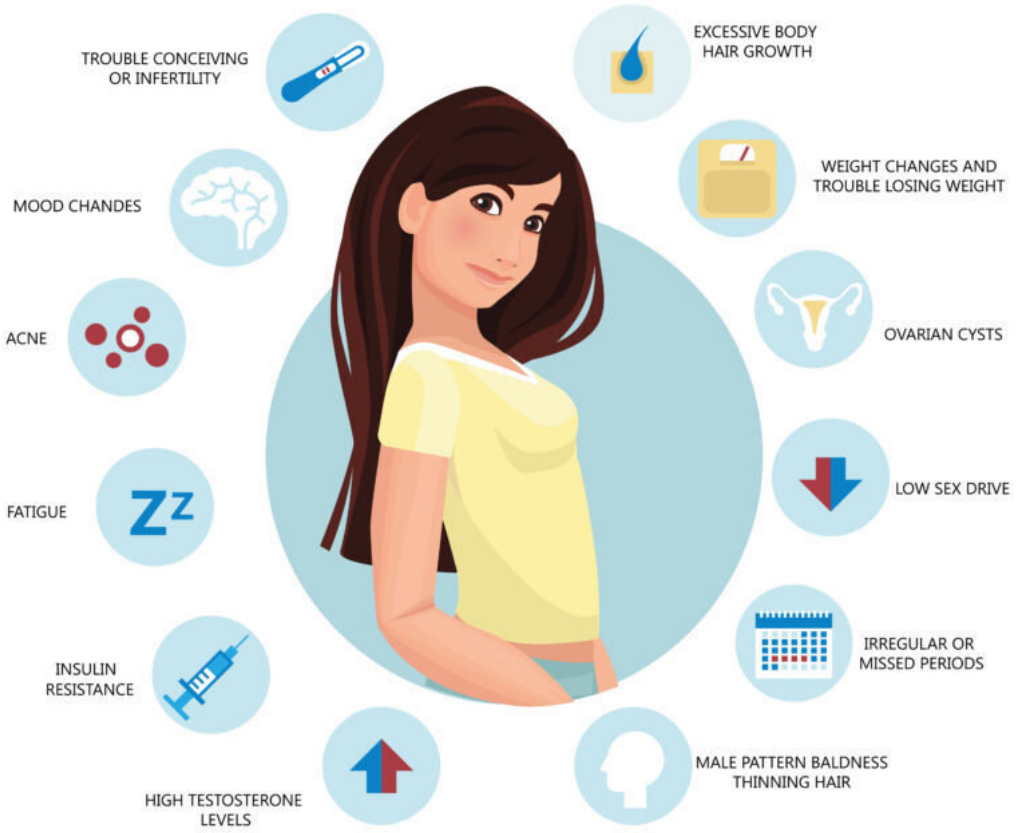


- The leading cause of female infertility
- Affects 1 in 10 women

# Polycystic Ovarian Syndrome (PCOS)

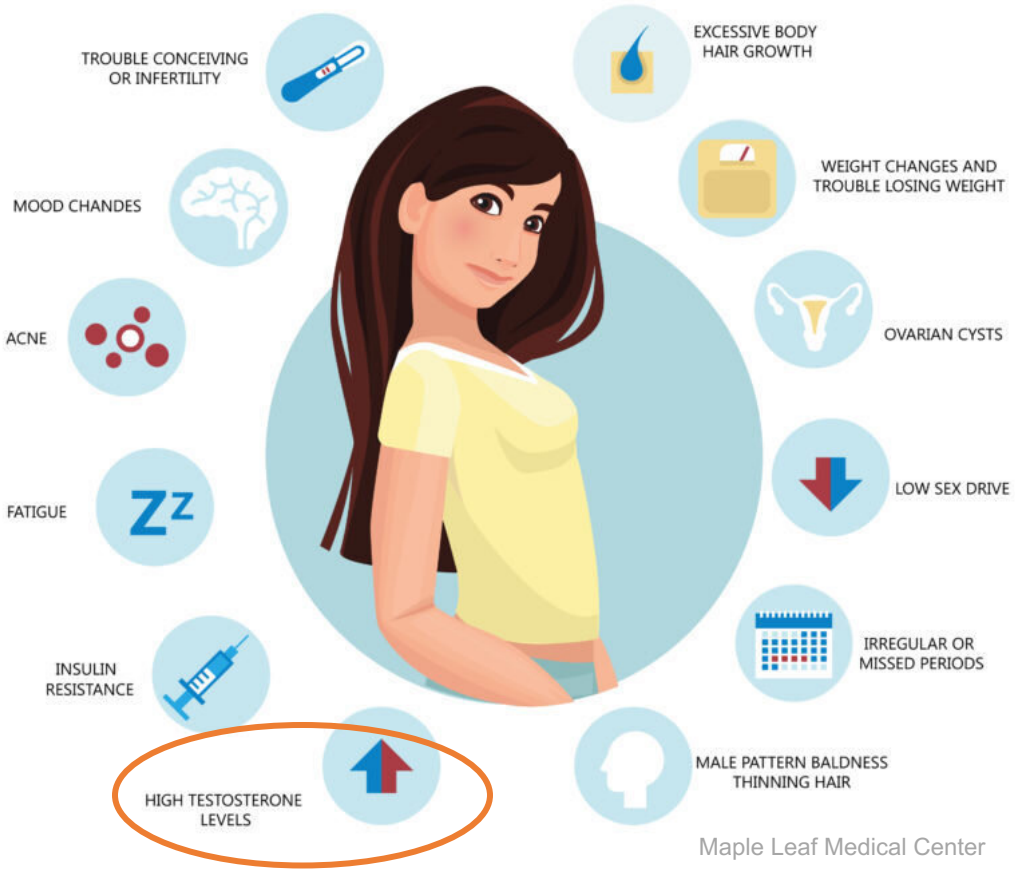


- The leading cause of female infertility
- Affects 1 in 10 women

# Polycystic Ovarian Syndrome (PCOS)

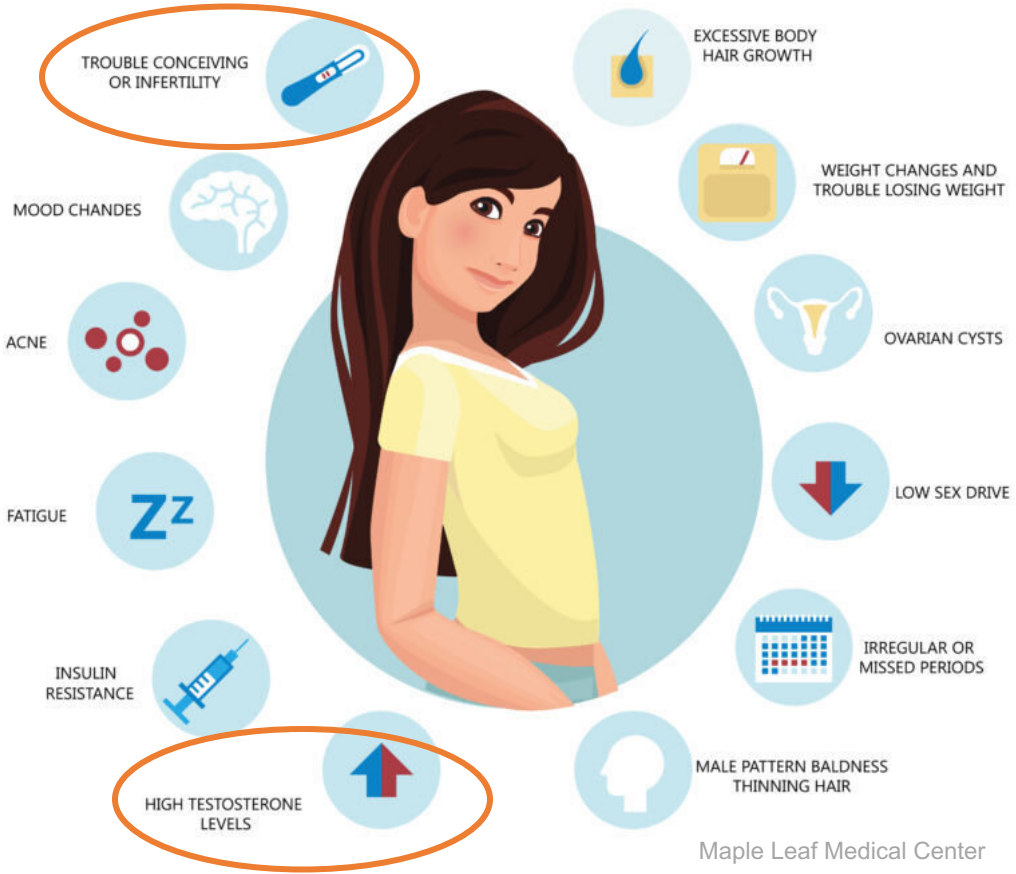


- The leading cause of female infertility
- Affects 1 in 10 women

# Polycystic Ovarian Syndrome (PCOS)

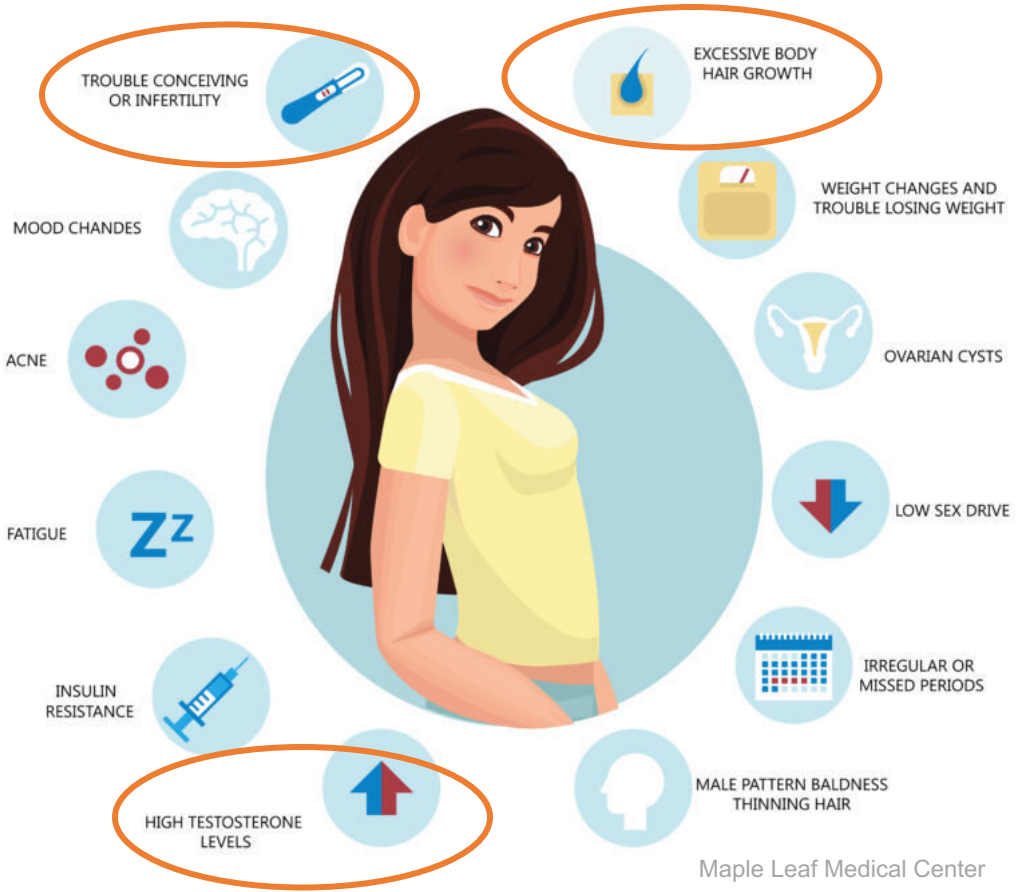


- The leading cause of female infertility
- Affects 1 in 10 women

# Polycystic Ovarian Syndrome (PCOS)


- The leading cause of female infertility
- Affects 1 in 10 women

# Polycystic Ovarian Syndrome (PCOS)

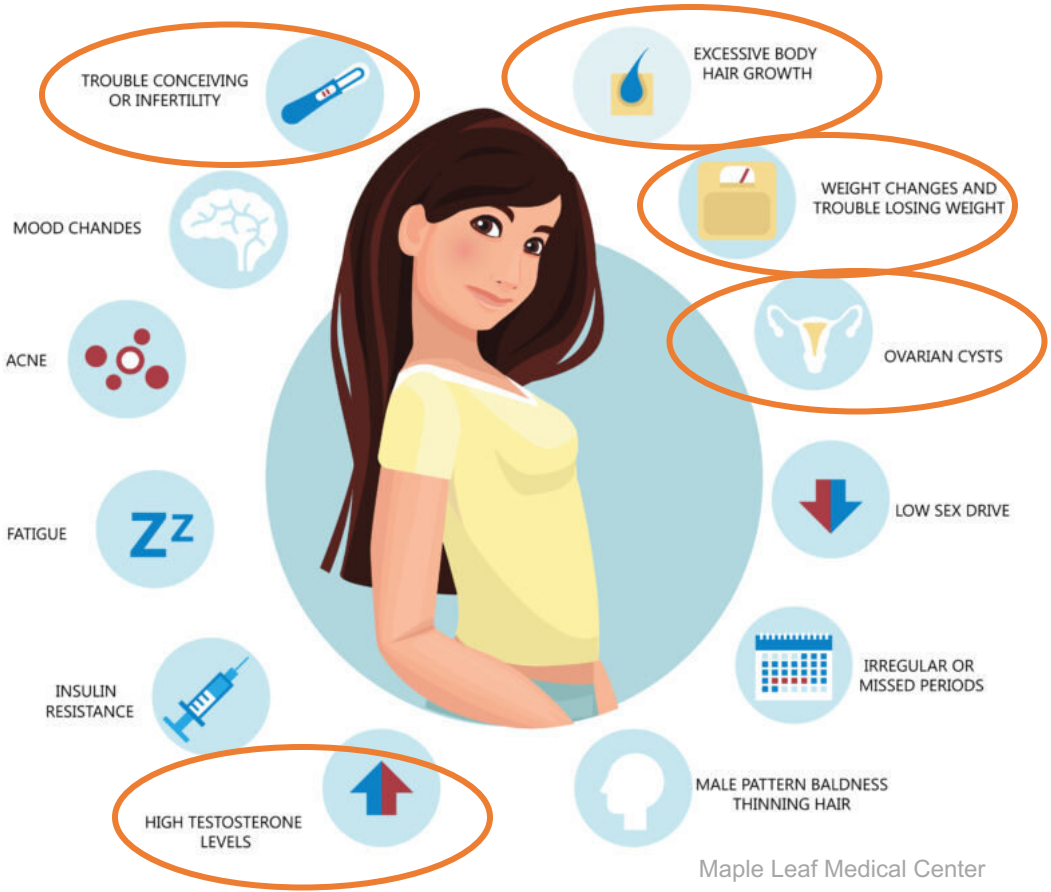


- The leading cause of female infertility
- Affects 1 in 10 women

# Polycystic Ovarian Syndrome (PCOS)


- The leading cause of female infertility
- Affects 1 in 10 women

# Polycystic Ovarian Syndrome (PCOS)


- The leading cause of female infertility
- Affects 1 in 10 women
- Highly heritable (~70%)
- Influenced by thousands of SNPs

# Genome-Wide Association Study (GWAS) of PCOS

Data from UK Biobank: full genotype of 250,000 females

**Problem!** Only 330 females report having PCOS (0.1%)

PCOS has 10% prevalence = 25,000 females

# Genome-Wide Association Study (GWAS) of PCOS

Data from UK Biobank: full genotype of 250,000 females

**Problem!** Only 330 females report having PCOS (0.1%)

PCOS has 10% prevalence = 25,000 females

**Solution:** Predict which females have PCOS from symptoms

# Step 1: Predicting PCOS from Symptoms

Consulted with infertility expert Dr. Mahalingaiah of Harvard Medical School

**PCOS = Excess Androgen + Irregular Menstruation – other disorders**

- Testosterone > 90%
- Facial hair
- Excess acne

- Lack of menstruation
- Excessive menstruation
- Infertility

- Cancer
- Endometriosis
- etc

# Step 1: Predicting PCOS from Symptoms

Consulted with infertility expert Dr. Mahalingaiah of Harvard Medical School

**PCOS = Excess Androgen + Irregular Menstruation – other disorders**

- Testosterone > 90%
- Facial hair
- Excess acne

- Lack of menstruation
- Excessive menstruation
- Infertility

- Cancer
- Endometriosis
- etc

| Before PCOS Prediction | After PCOS Prediction |
| --- | --- |
| • 330 positive cases<br>• Insufficient statistical power | • 1735 positive cases<br>• Higher statistical power |

# Step 1: Predicting PCOS from Symptoms

Consulted with infertility expert Dr. Mahalingaiah of Harvard Medical School

**PCOS = Excess Androgen + Irregular Menstruation – other disorders**

- Testosterone > 95%
- Facial hair
- Excess acne

- Lack of menstruation
- Excessive menstruation
- Infertility

- Cancer
- Endometriosis
- etc

| Before PCOS Prediction | After PCOS Prediction |
| --- | --- |
| • 330 positive cases<br>• Insufficient statistical power | • 1735 positive cases<br>• Higher statistical power |

**This is the first study to predict PCOS for genetic association**

# Step 1: Predicting PCOS from Symptoms

Consulted with infertility expert Dr. Mahalingaiah of Harvard Medical School

**PCOS = Excess Androgen + Irregular Menstruation – other disorders**

- Testosterone > 90%
- Facial hair
- Excess acne

- Lack of menstruation
- Excessive menstruation
- Infertility

- Cancer
- Endometriosis
- etc

# Step 1: Predicting PCOS from Symptoms

Consulted with infertility expert Dr. Mahalingaiah of Harvard Medical School

**PCOS = Excess Androgen + Irregular Menstruation – other disorders**

- Testosterone > 90%
- Facial hair
- Excess acne

- Lack of menstruation
- Excessive menstruation
- Infertility

- Cancer
- Endometriosis
- etc

| Before PCOS Prediction | After PCOS Prediction |
| --- | --- |
| • 330 positive cases<br>• Insufficient statistical power | • 1735 positive cases<br>• Higher statistical power |

# Step 1: Predicting PCOS from Symptoms

Consulted with infertility expert Dr. Mahalingaiah of Harvard Medical School

**PCOS = Excess Androgen + Irregular Menstruation – other disorders**

- Testosterone > 90%
- Facial hair
- Excess acne

- Lack of menstruation
- Excessive menstruation
- Infertility

- Cancer
- Endometriosis
- etc

| Before PCOS Prediction | After PCOS Prediction |
| --- | --- |
| • 330 positive cases<br>• Insufficient statistical power | • 1735 positive cases<br>• Higher statistical power |

**This is the first study to predict PCOS for genetic association**

# Step 2: Validate Genome-Wide Association Study Method

- Compare to accepted results for Body Mass Index (BMI)
- Linear regressions between SNPs of 500,000 individuals and BMI
- Tool: BOLT Linear Mixed Model
- Hundreds of gigabytes of data, processing time ~2 days

# Important Steps in GWAS

- Control for confounding effects
  - Age, sex, assessment center, etc
  - Top principal components (population structure)
- SNP quality control
  - Correlations between nearby SNPs

# Step 2: Validate Genome-Wide Association Study Method

- Fit linear regressions between SNPs and BMI (500,000 individuals)
- Control for confounding variables
- Validated against accepted results

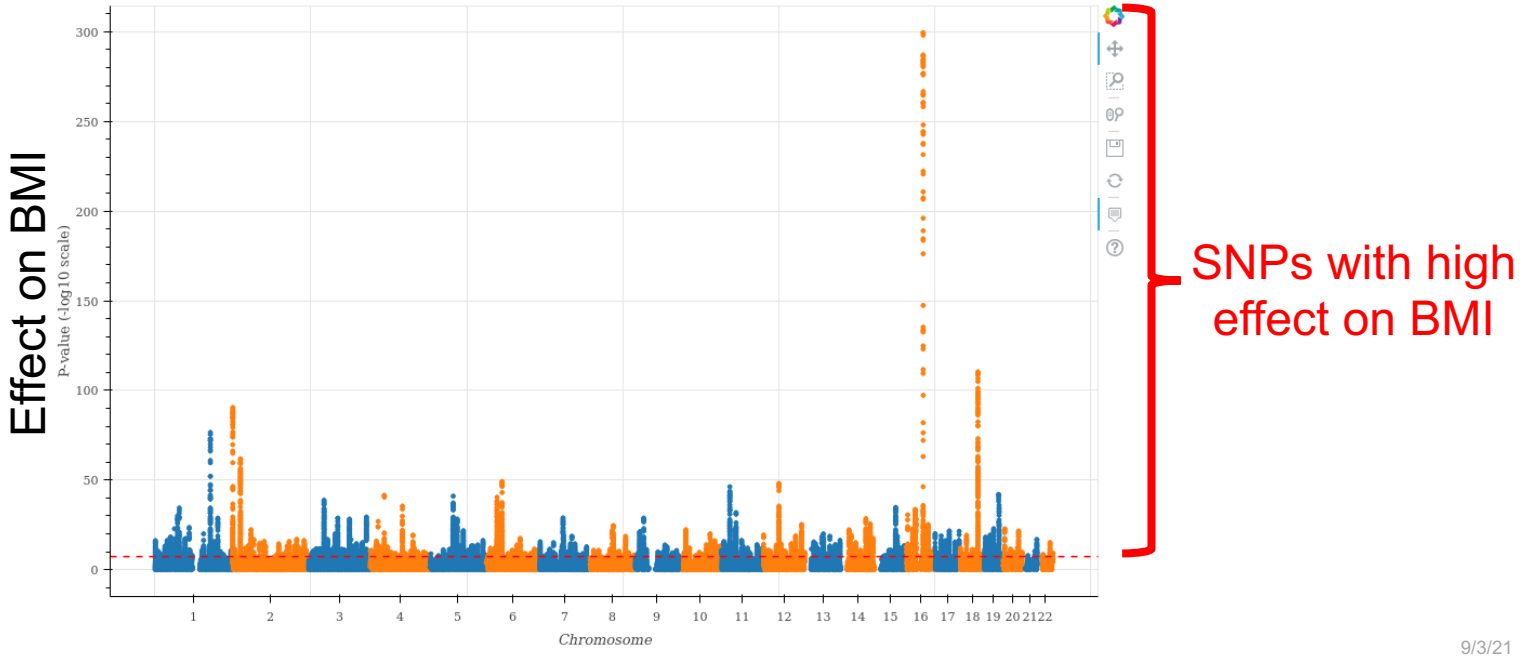

# Step 3: PCOS Genome-Wide Association Study

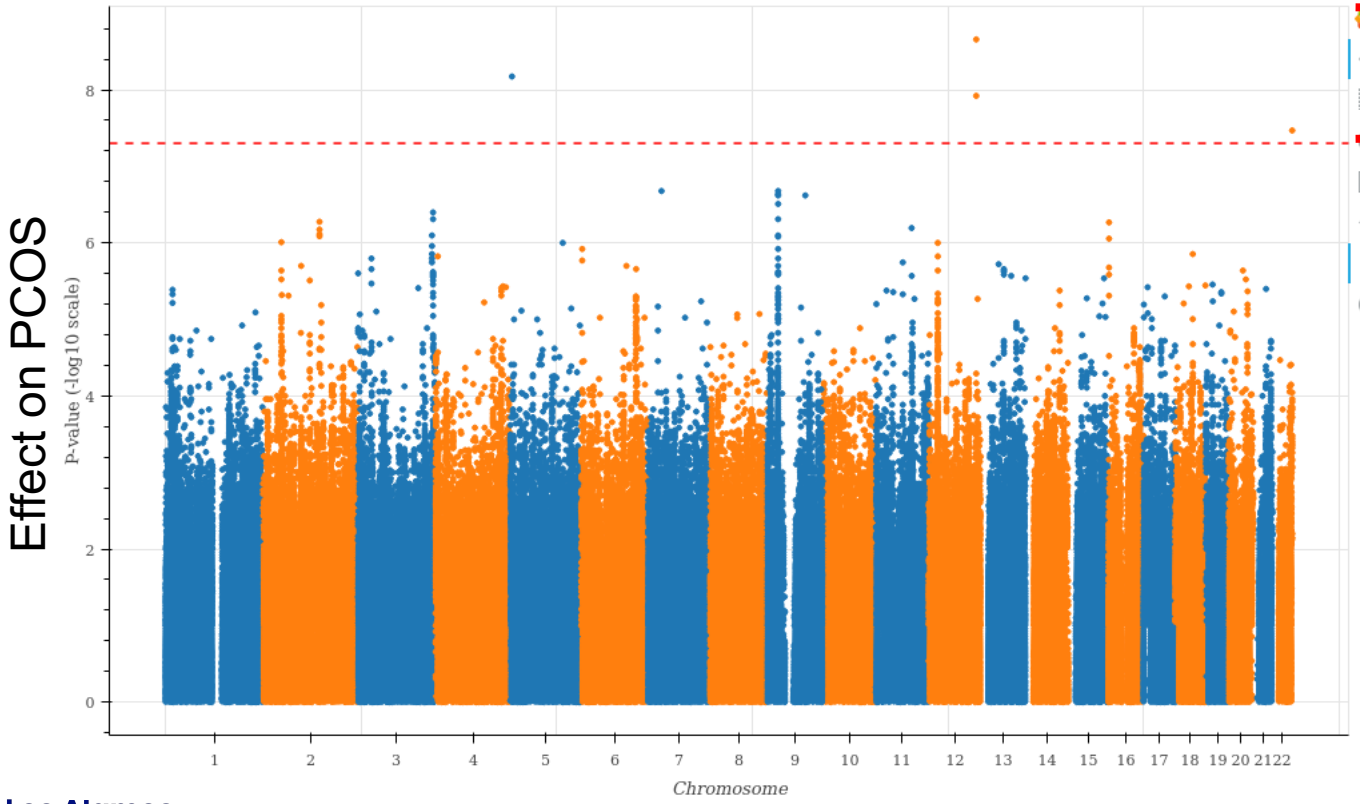


SNPs with high effect on PCOS

SNP Location on each Chromosome

# Current Work

- First study to predict PCOS from symptoms and correlate to genetics
- Importance:
  - Understand biological pathways
  - Predict women's genetic risk of PCOS
  - Improve early diagnosis through genetics

# Future Work

- New genome sequencing methods: whole genome (not just SNPs!)
- Machine Learning for Genetic Association Studies
  - Incorporate gene-gene interactions and non-linear effects
  - Never done before!

Los Alamos
NATIONAL LABORATORY

# Transition Path Search for Light-Driven Molecular Motor

Presenter: Aaron Philip
Mentors: Benjamin Nebgen, Guoqing Zhou

August 26, 2021

# ML Accelerated Approach:

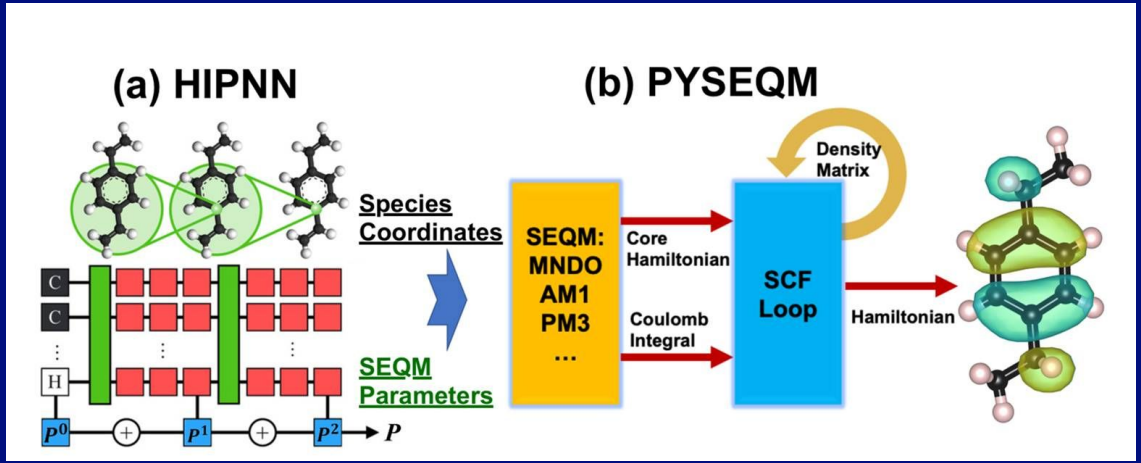


HIPNN produces optimal semi-empirical Hamiltonian parameters for a molecular configuration

Then passed to PYSEQM which solves the Self-Consistent Field equations to determine the orbits of electrons and total molecular energy

# Light-Driven Molecular Motor:

- Synthesized by Feringa et. al. to mimic processes that occur on a microscopic biological level
- Will respond to photochemical and thermal isomerizations to produce unilateral relative rotation
- Double bond between central carbons means most stable states occur at cis and trans configurations.

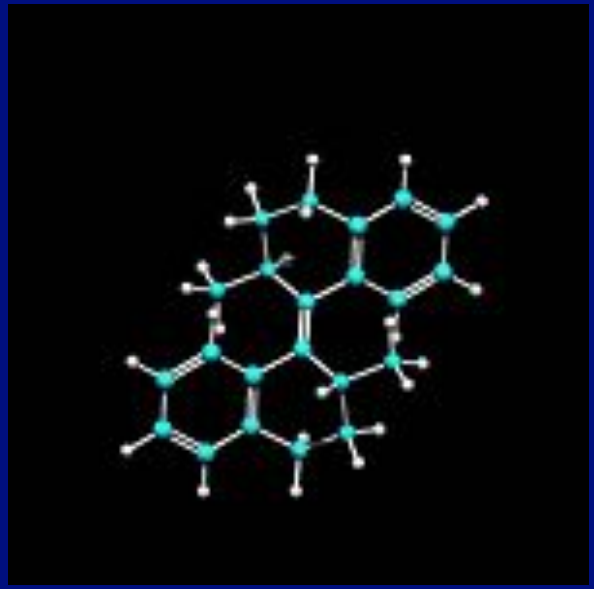

Image Credit:
http://www.benferinga.com/research.php

# Goal:

- To generate a transition path of the rotation with realistic intermediates and a plausible energy barrier

- Note: Rotation through the barrier produced by methyl-methyl proximity was studied -- unique structure of the molecule posed several issues to generating realistic geometries.

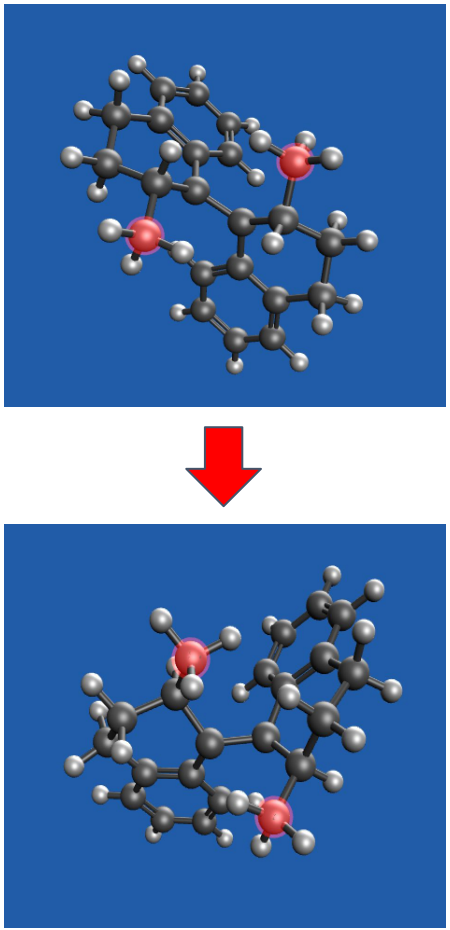

# Execution:

- Ran a Python script on Badger that used the Pytorch-based Semi-Empirical Quantum Mechanics package (PYSEQM)

- This provided both atomization energies and gradients of the structures used to optimize intermediates and output them as xyz files

# Approach: Dihedral Angle Constraint

- Difference in dihedral angle of endpoint molecule guides progression (reaction angle)
- Central carbon atoms and the two attached carbons closer to methyl groups used

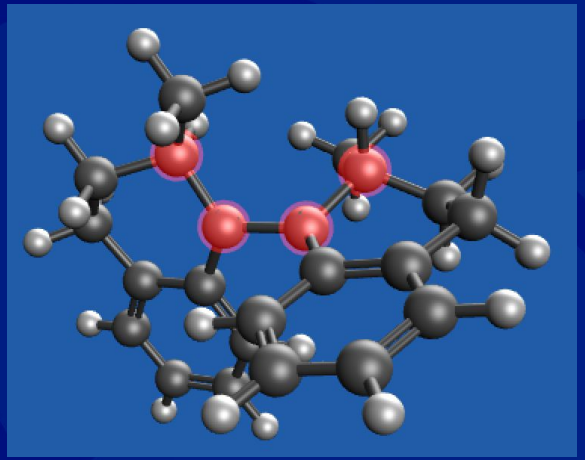

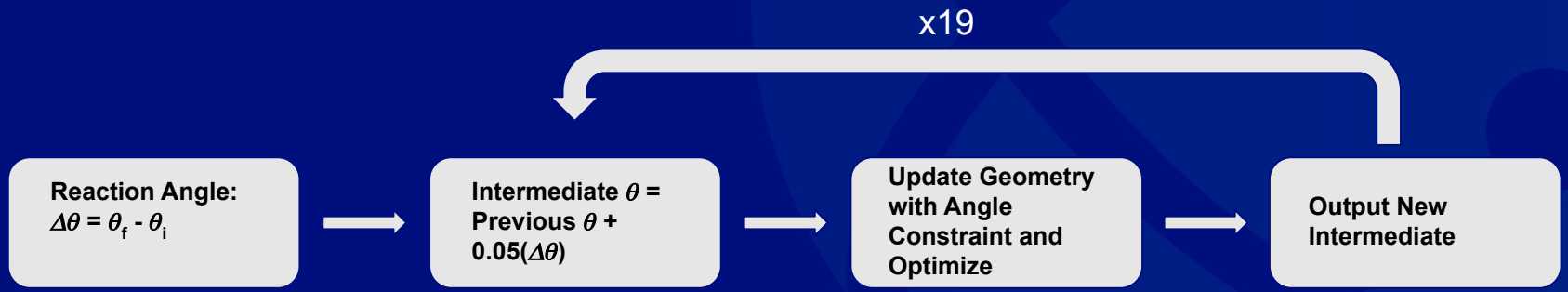

# Results:

## Progression:

- Endpoint was reached
- Barrier was far higher than experimental value
- Additional issue was that the structure used was inconsistent with Feringa's

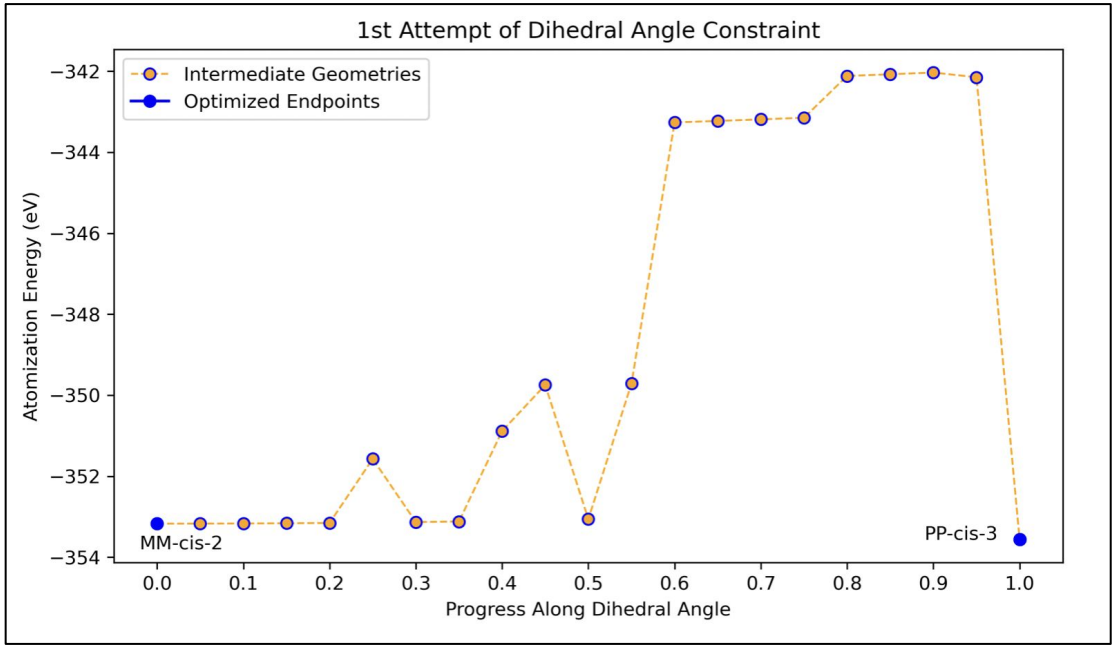

# Visualization:

- Other tests (eg. constrained endpoints, varied atoms in dihedral, multiple dihedral constraints etc.) either destroyed molecule while optimizing or had massive energy barriers
- Due to a few modifications of the molecule being used

Alternate Molecule:

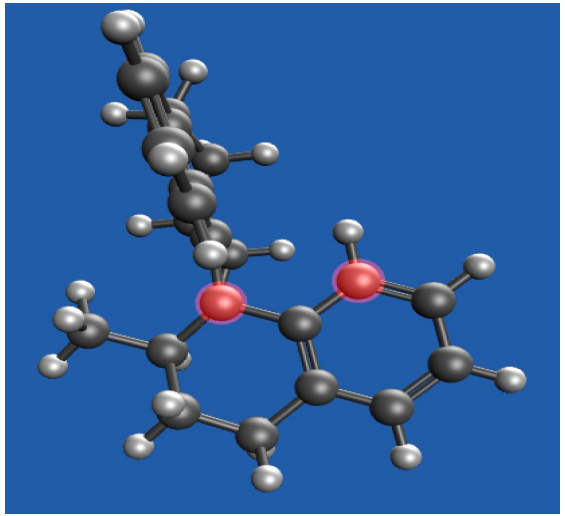

Molecule Initially Used:

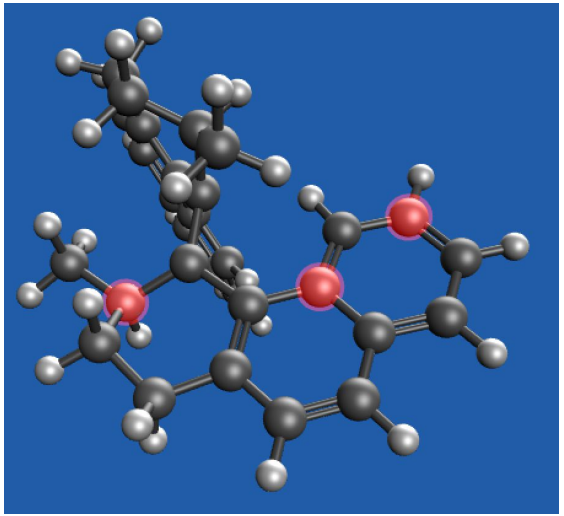

# Approach: Dihedral Angle Constraint

- One constraint would not drive the progression
- Two dihedral angle constraints were sufficient and generated initial guesses for the intermediates
- Barrier was still ~2X too large.

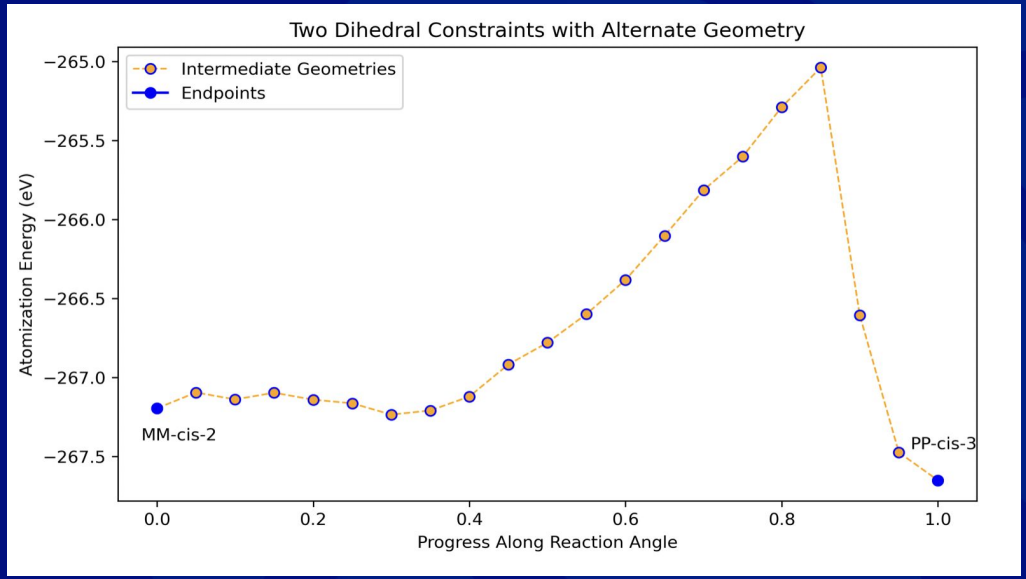

# Approach: Dihedral Angle Constraint

- Used geometries generated with two constraints and optimized each with original single angle constraint
- More probable barrier achieved that reflects the experimental barrier of ~1eV

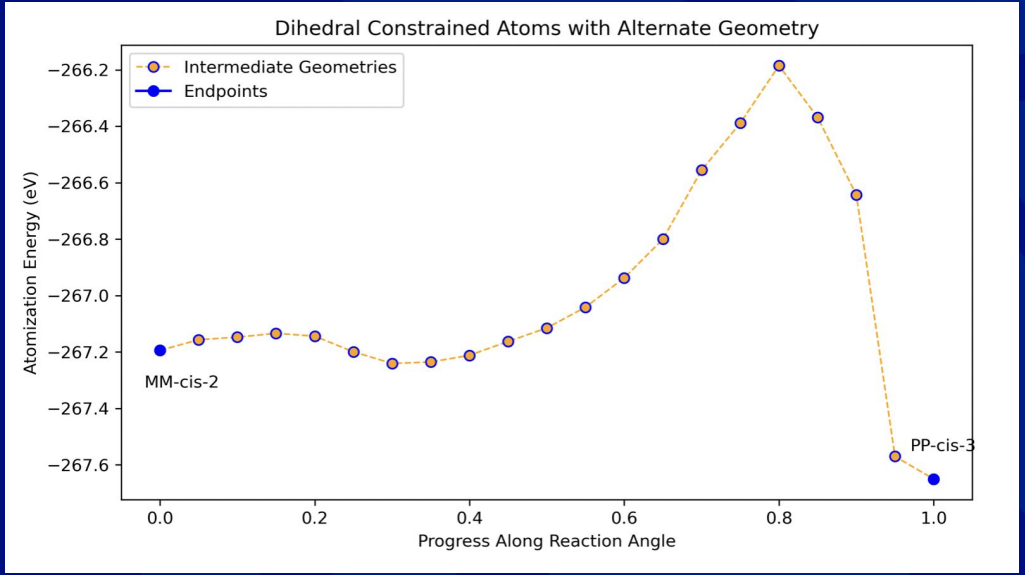

# Visualization: Intermediates of Interest

5% Progress:

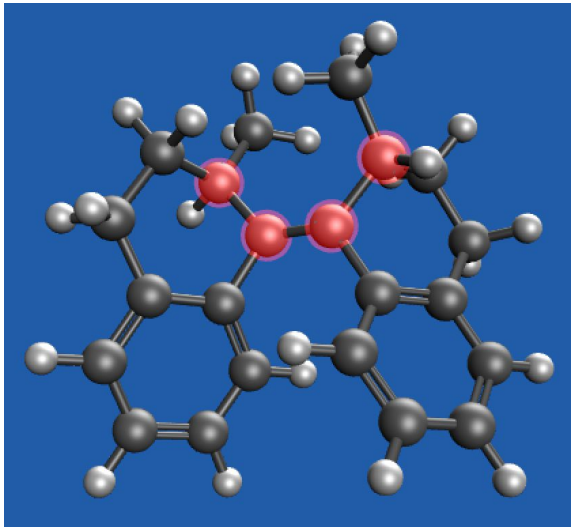

80% Progress:

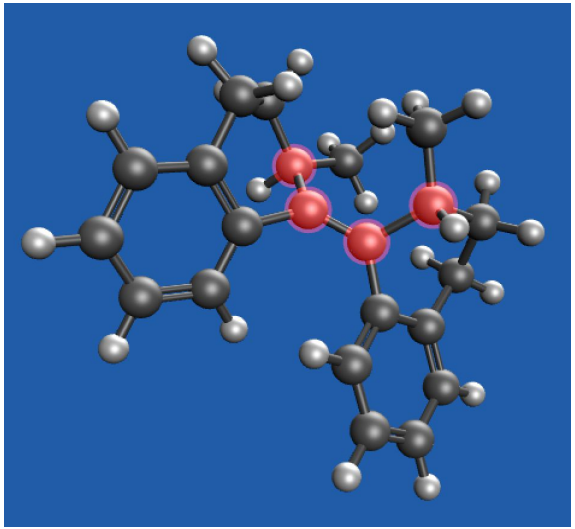

95% Progress:

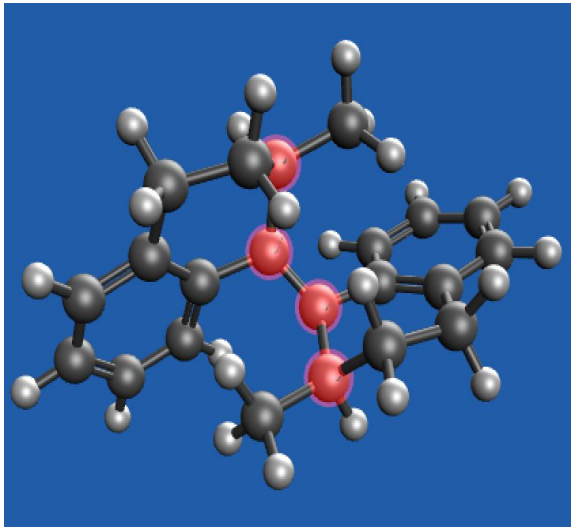

Los Alamos NATIONAL LABORATORY

## Next Steps:

- Repeat process with the other, simpler transitions of rotation
- Generate a smoother path by adding more intermediates between the current 19 intermediates
- Attempt with a different molecule to ensure the efficiency of the method

## Conclusions:

- Machine Learning accelerated Quantum Mechanics method accurately reproduces experimental barrier height, opening possibility for theoretical screening
- Motor proteins carry out dynamic functions on a cellular level by combining several components with specialized molecular function (eg. motor, brake, scissor)
- Continued study and development of synthetic imitations is a huge step forward in nanotechnology

# Example: Molecular Car

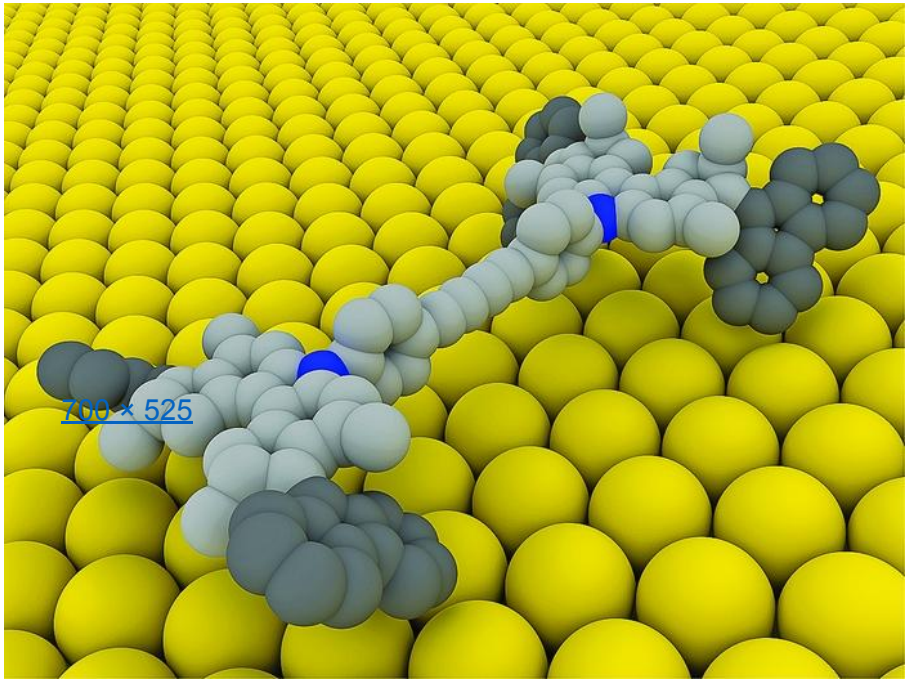


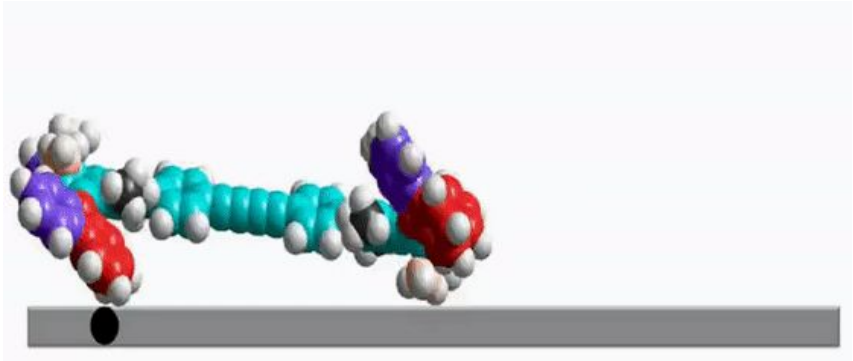

Image Credits: https://cen.acs.org/

# Acknowledgements:

I would like to thank my mentors Dr. Benjamin Nebgen and Dr. Guoqing Zhou for the great project they gave me this summer and all the significant assistance and advice they provided.

Additionally, I thank the T-1 group for allowing me to join this summer and to learn a great deal.


# Questions?

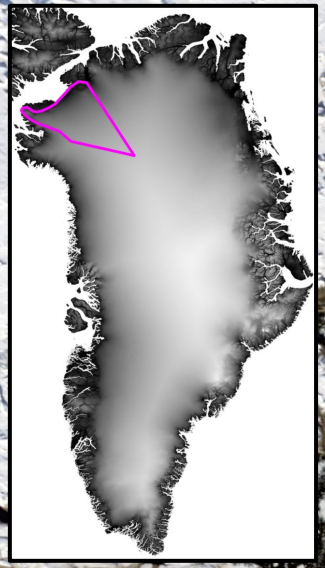

# Characterizing changes in 21st century subglacial hydrology at Humboldt Glacier, north Greenland

Abby Roat[1,2], Trevor Hillebrand[1], Matthew Hoffman[1]
(1) Los Alamos National Lab, (2) Colorado College

NASA Earth Observatory

## Mass Loss From GrIS 1980-2020

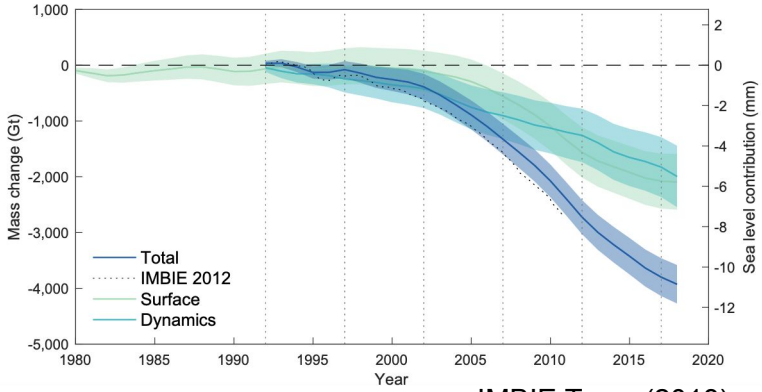


IMBIE Team (2018)

## Humboldt Glacier sea level contribution 21st c.

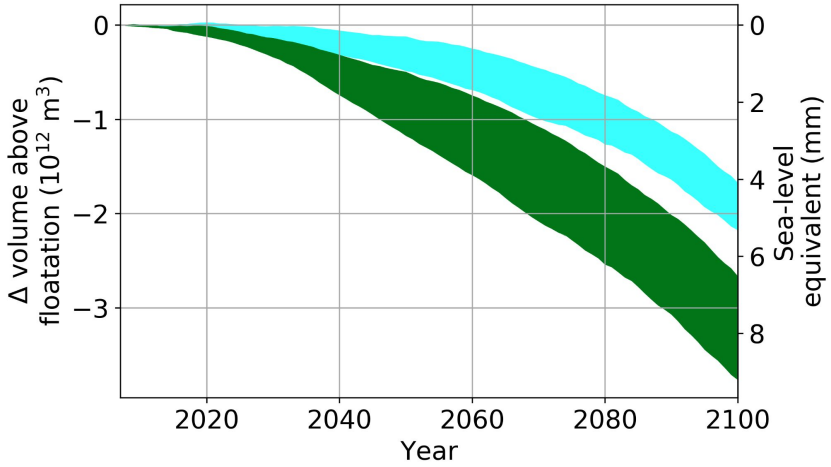


Hillebrand et al. (in prep)

~50% of that mass loss is from surface mass balance
~ 50% is from ice dynamics.

## Negative 21st Greenland surface mass balance

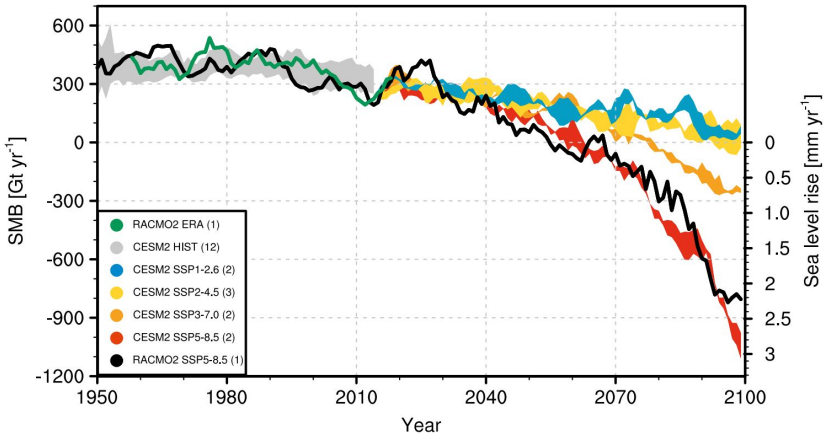


Noël et al. 2021

Large uncertainty in Humboldt glacier sea level contribution through the 21st century

# The subglacial system

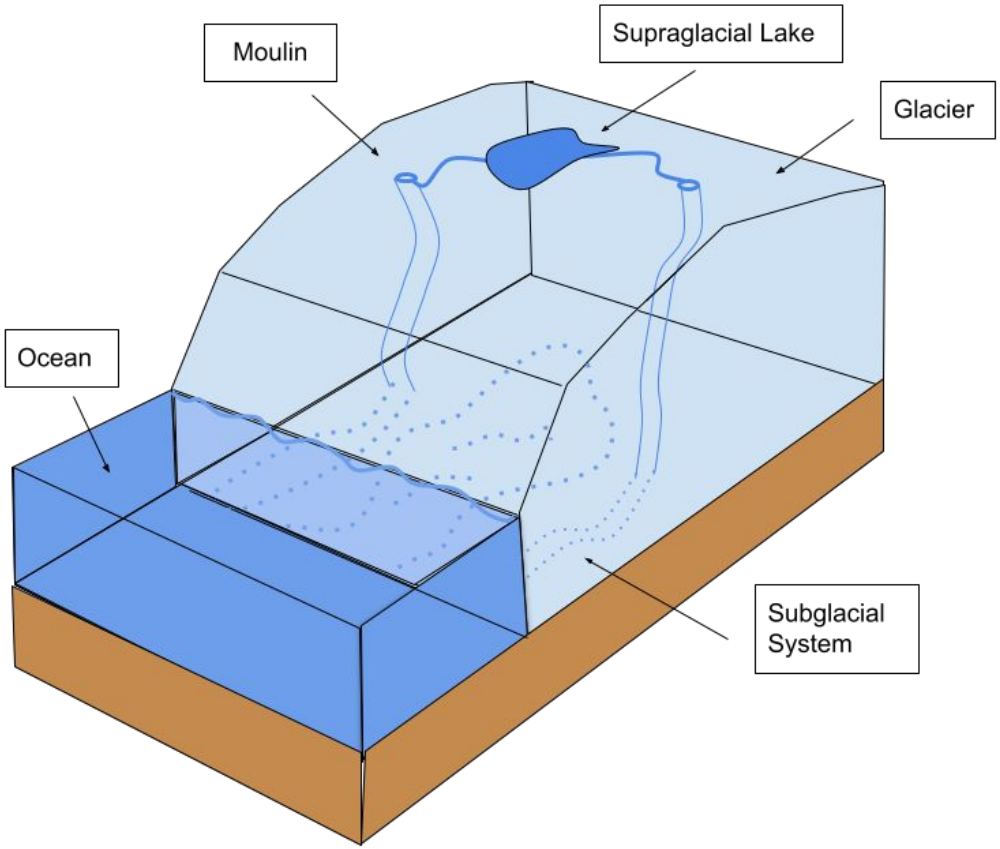


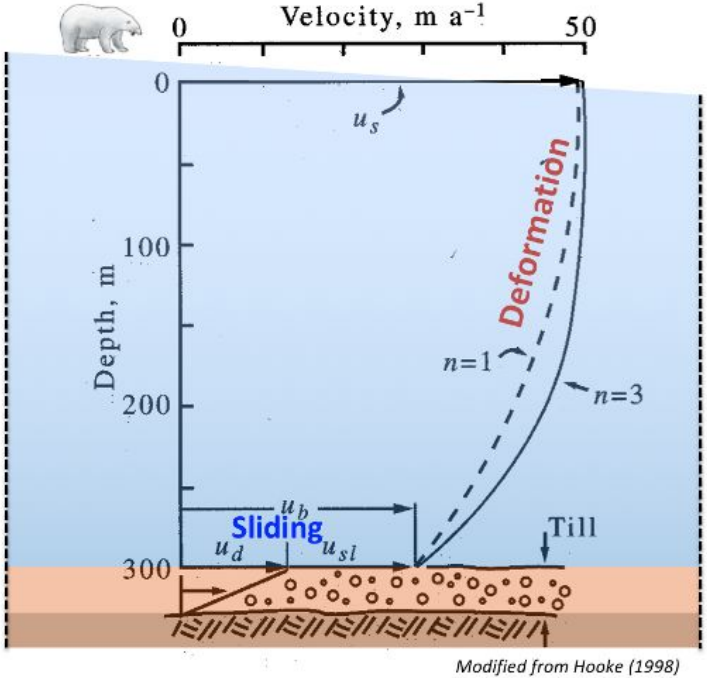


*Modified from Hooke (1998)*

# The subglacial system

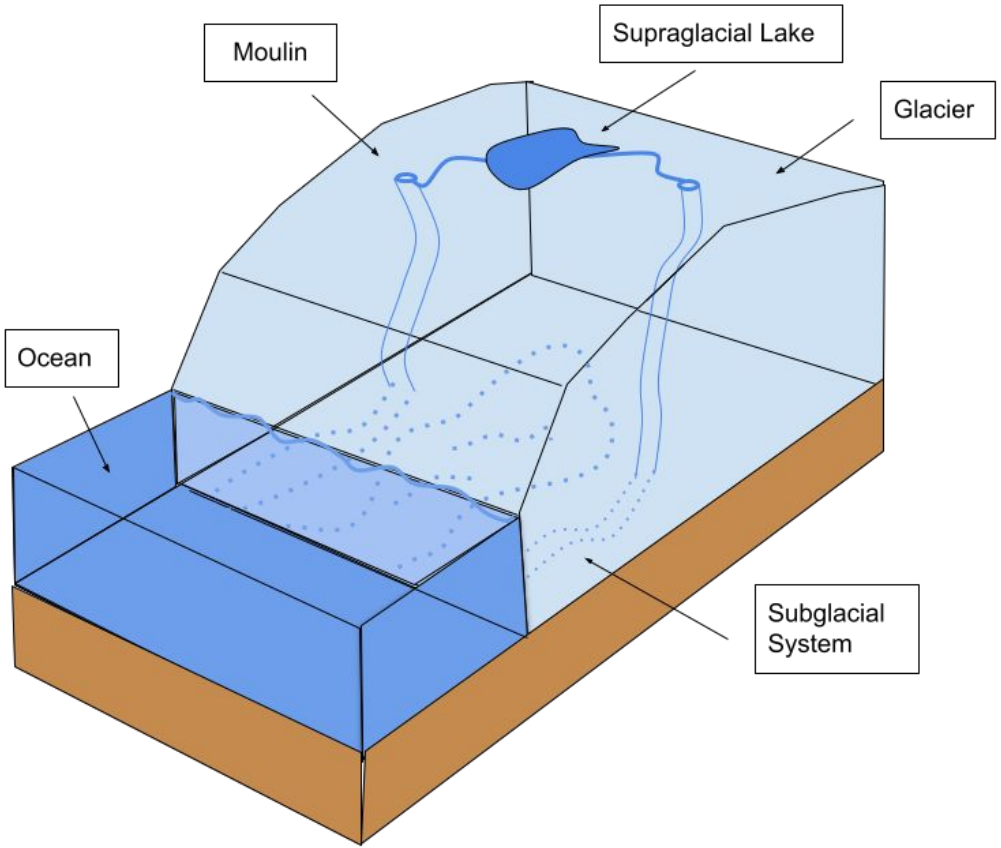


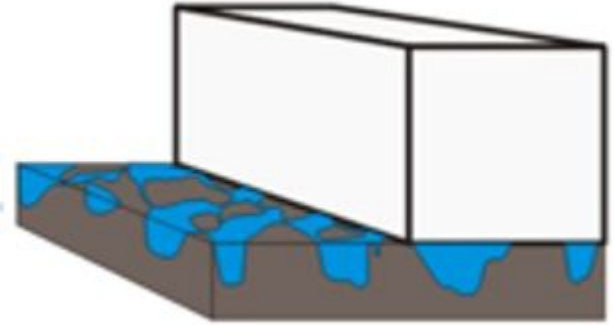

Distributed system (inefficient)

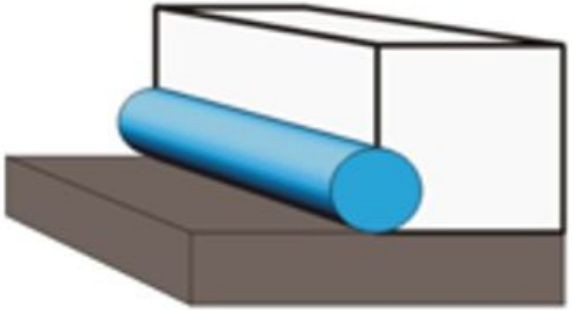

Channelized system (efficient)

# The subglacial system

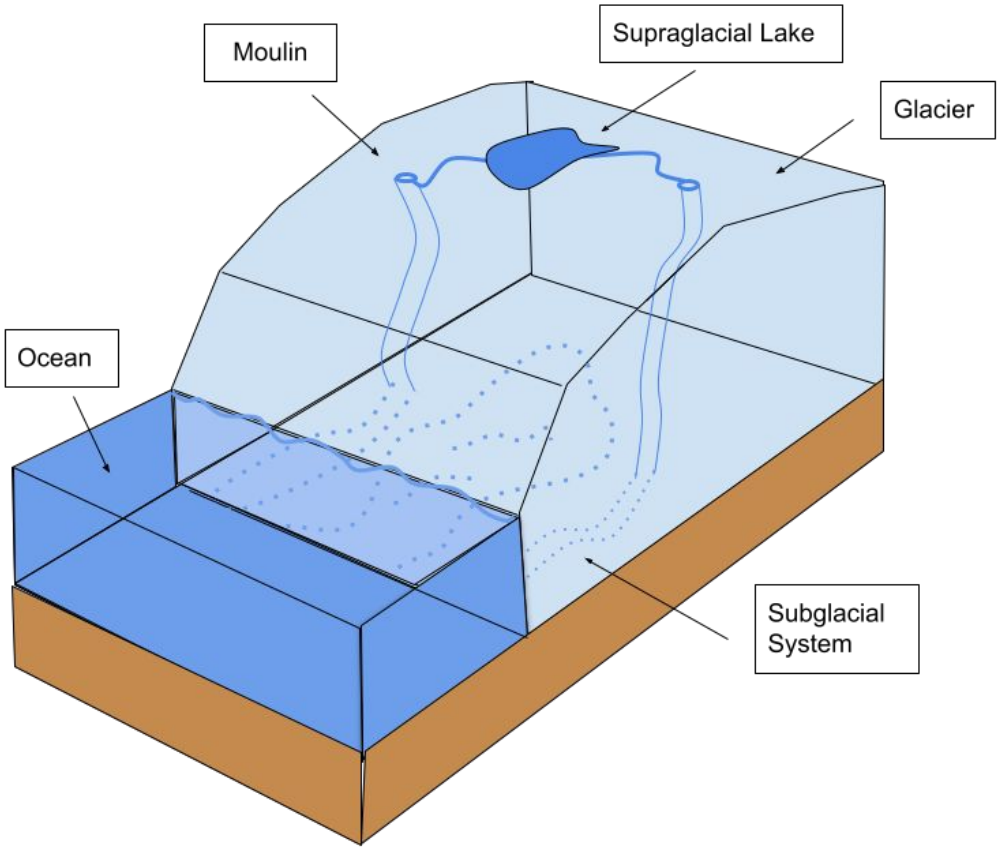


1. Will increased surface melt lead to a change in the character of subglacial drainage?
2. How will that impact subglacial water pressure, and thus, ice dynamics?

# Modeling subglacial drainage

Model: MPAS Albany Land Ice (MALI) Ice sheet model

Solve equations for:

- Mass conservation
- Water flux law
- Cavity space evolution

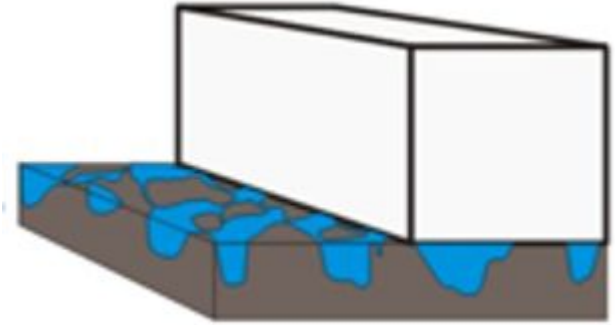

**Distributed Drainage**

- Slow, inefficient
- Cavities open as ice slides over bumps

$$Q \uparrow \Rightarrow P \uparrow$$

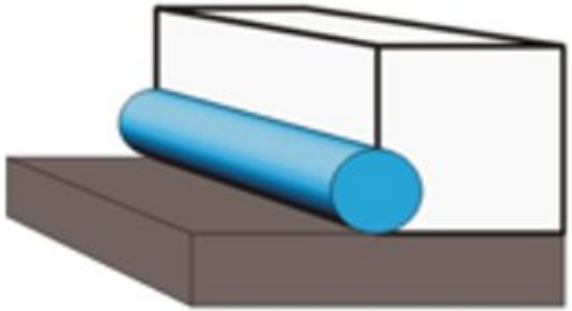

**Channelized Drainage**

- Fast, efficient
- Conduits open by melting from heat dissipation in water flow

$$Q \uparrow \Rightarrow P \downarrow$$

Critical discharge in distributed system leads to channelization

# Experimental Design:

- Model run with daily varying melt from historical and CESM derived RACMO projections from 1990-2100 (ongoing).
- determine extent of channelization and basal water pressure

Inputs:
- Summer surface melt drained to the bed
- Ice sliding velocity (constant)

Outputs:
- Water pressure
- Distributed and channelized:
  - Water volume
  - Water flux

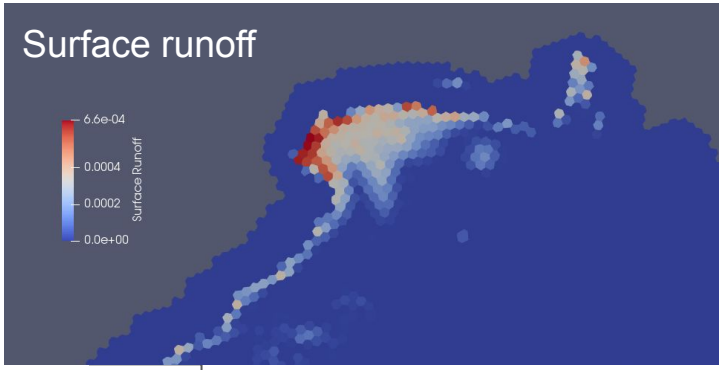


MALI

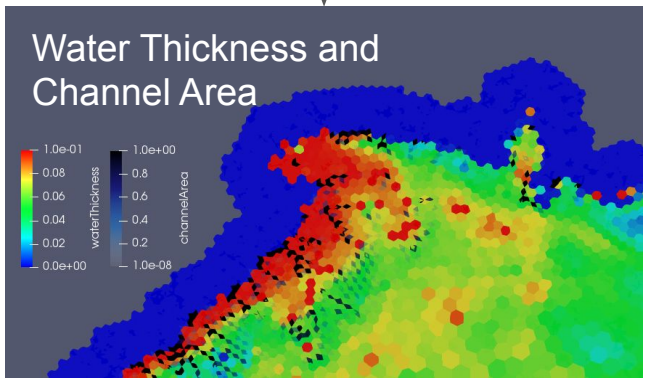

# Results

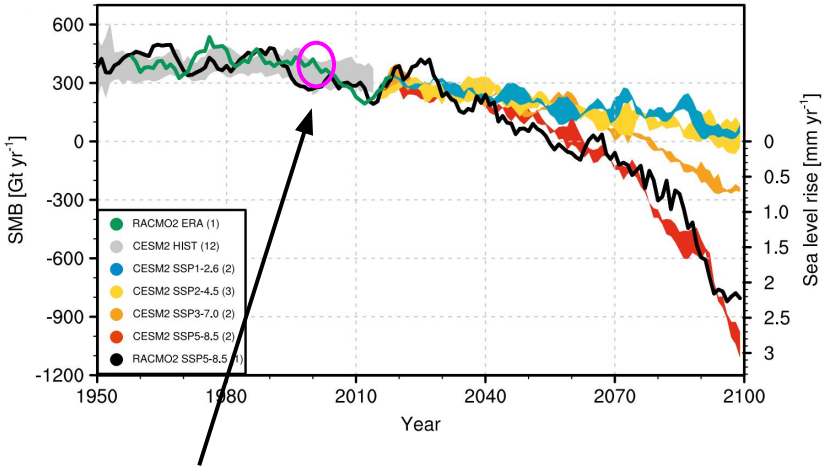


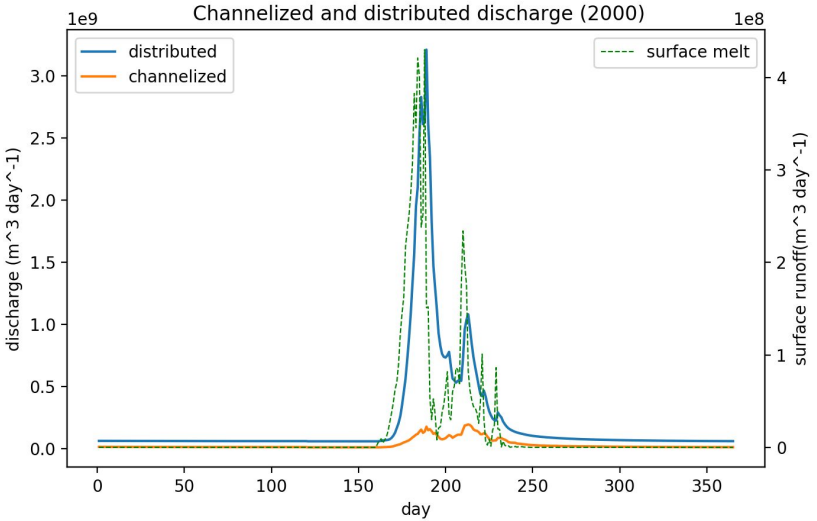


- Large increases in discharge over the summer melt season.
- Distributed discharge is dominant throughout the year, but particularly during the summer.

# Results

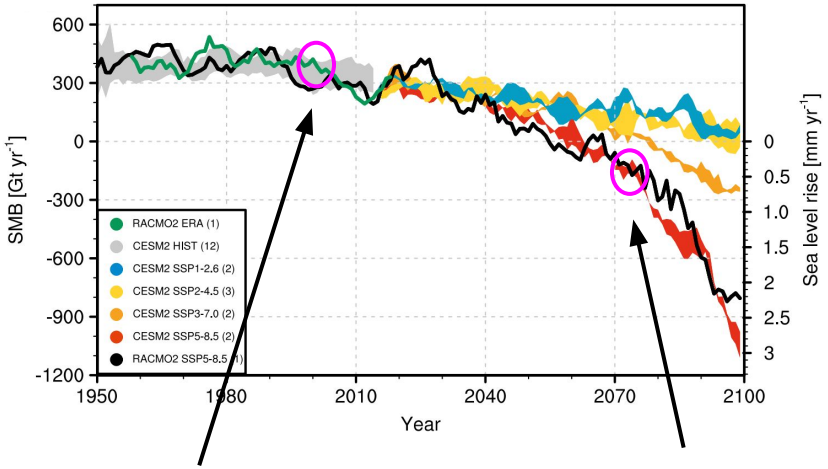


the proportion of channelized drainage increases significantly though the century

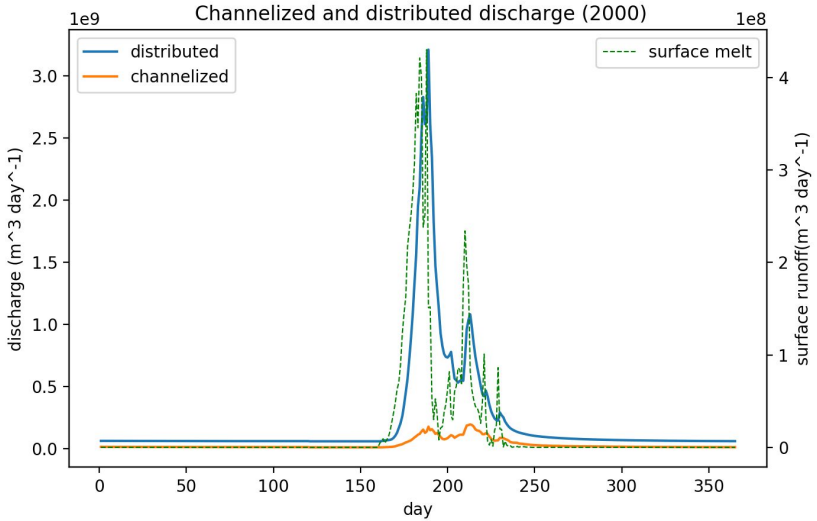


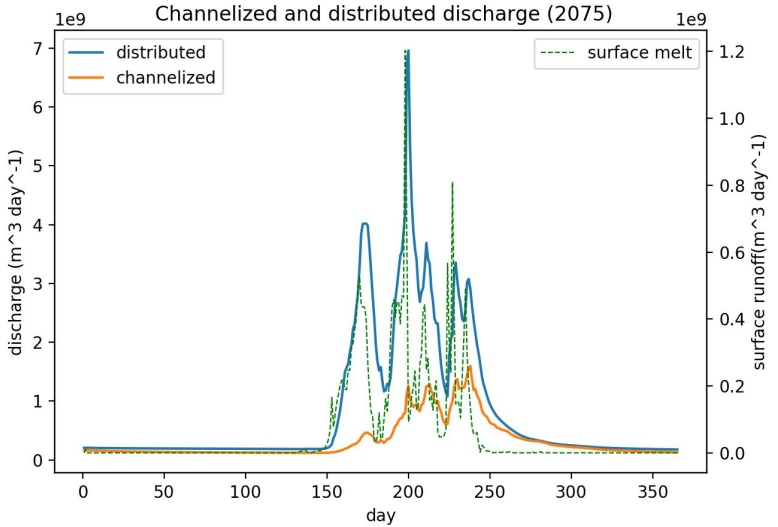

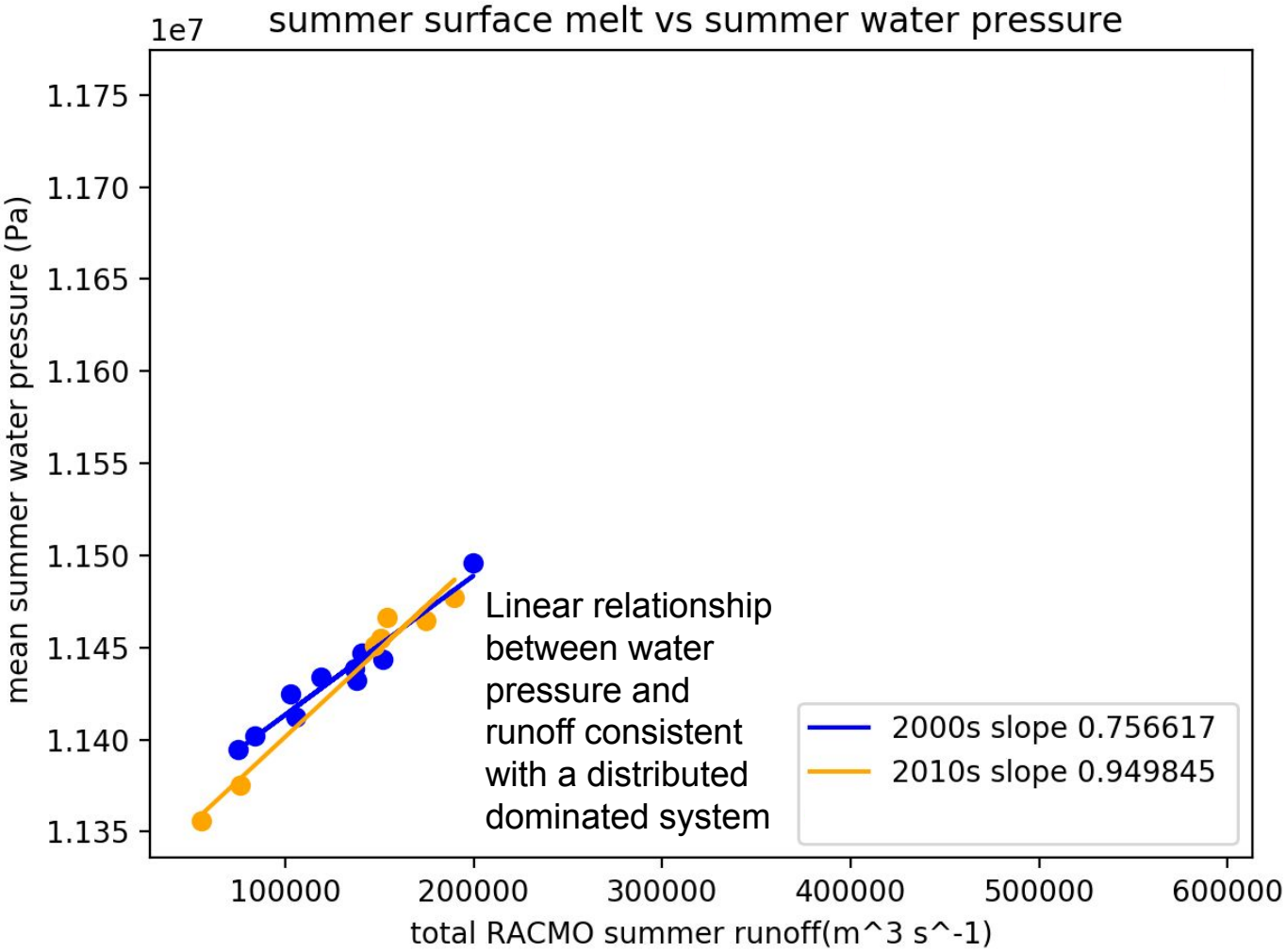
summer surface melt vs summer water pressure
1e7
1.175
1.170
1.165
1.160
1.155
1.150
1.145
1.140
1.135
mean summer water pressure (Pa)
100000
200000
300000
400000
500000
600000
total RACMO summer runoff(m^3 s^-1)
Linear relationship between water pressure and runoff consistent with a distributed dominated system
2000s slope 0.756617
2010s slope 0.949845

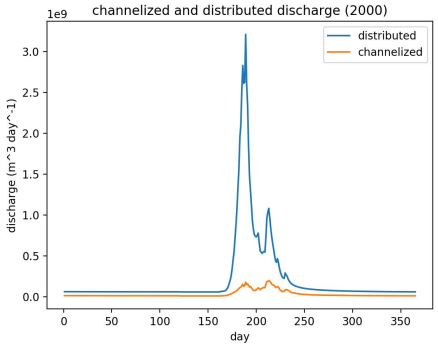
channelized and distributed discharge (2000)
1e9
3.0
2.5
2.0
1.5
1.0
0.5
0.0
discharge (m^3 day^-1)
0
50
100
150
200
250
300
350
day
distributed
channelized

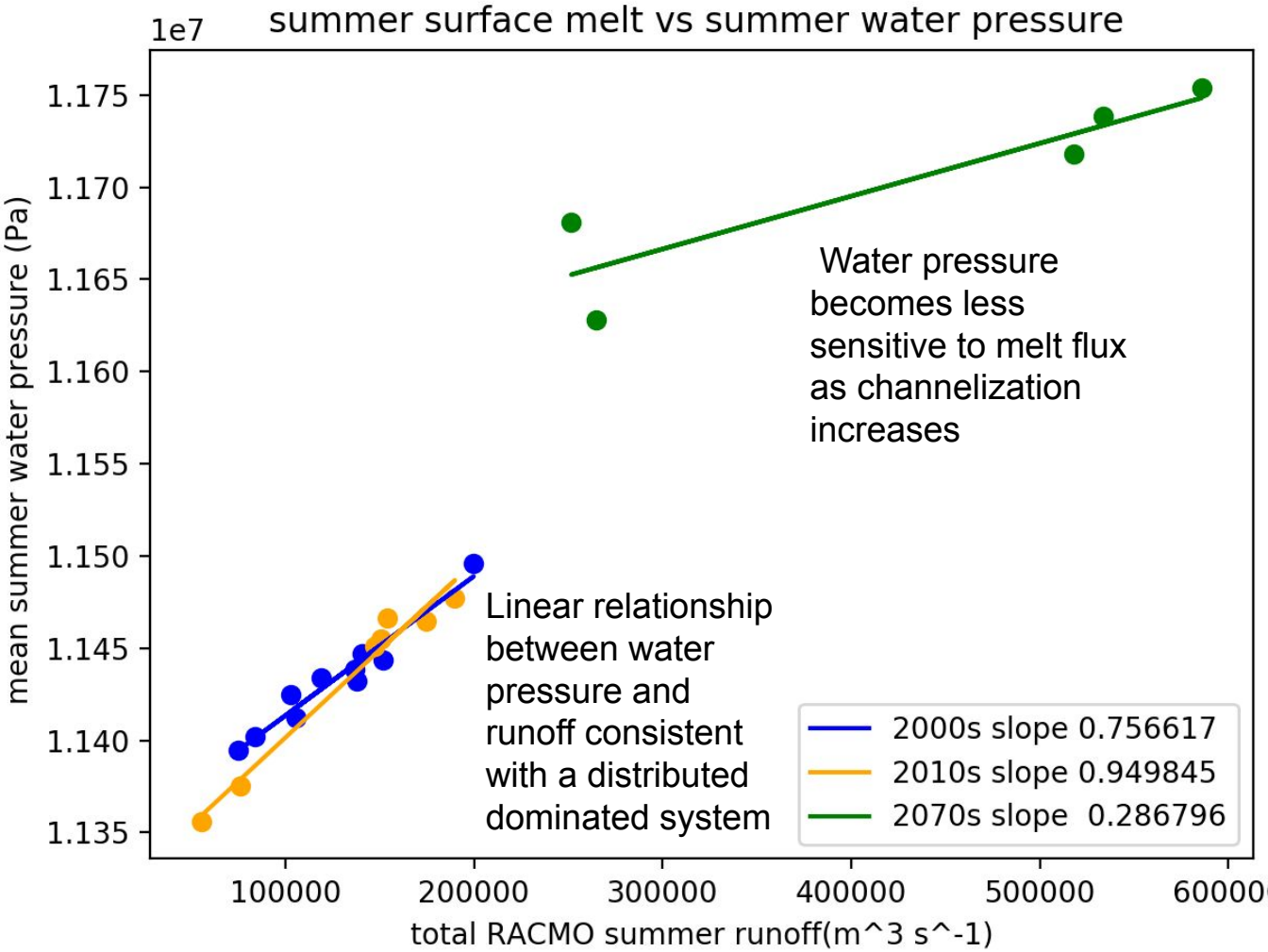
summer surface melt vs summer water pressure
1e7
mean summer water pressure (Pa)
1.175
1.170
1.165
1.160
1.155
1.150
1.145
1.140
1.135
100000
200000
300000
400000
500000
600000
total RACMO summer runoff(m^3 s^-1)
Water pressure becomes less sensitive to melt flux as channelization increases
Linear relationship between water pressure and runoff consistent with a distributed dominated system
2000s slope 0.756617
2010s slope 0.949845
2070s slope 0.286796

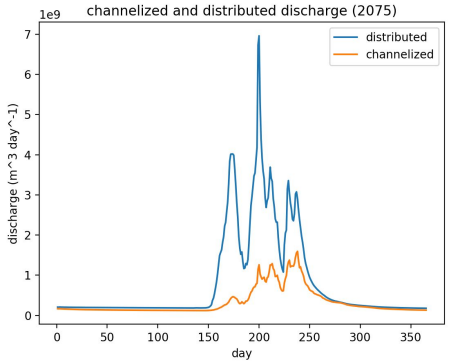
channelized and distributed discharge (2075)
1e9
discharge (m^3 day^-1)
day
distributed
channelized

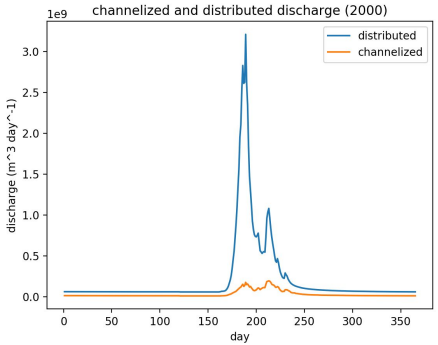
channelized and distributed discharge (2000)
1e9
discharge (m^3 day^-1)
day
distributed
channelized

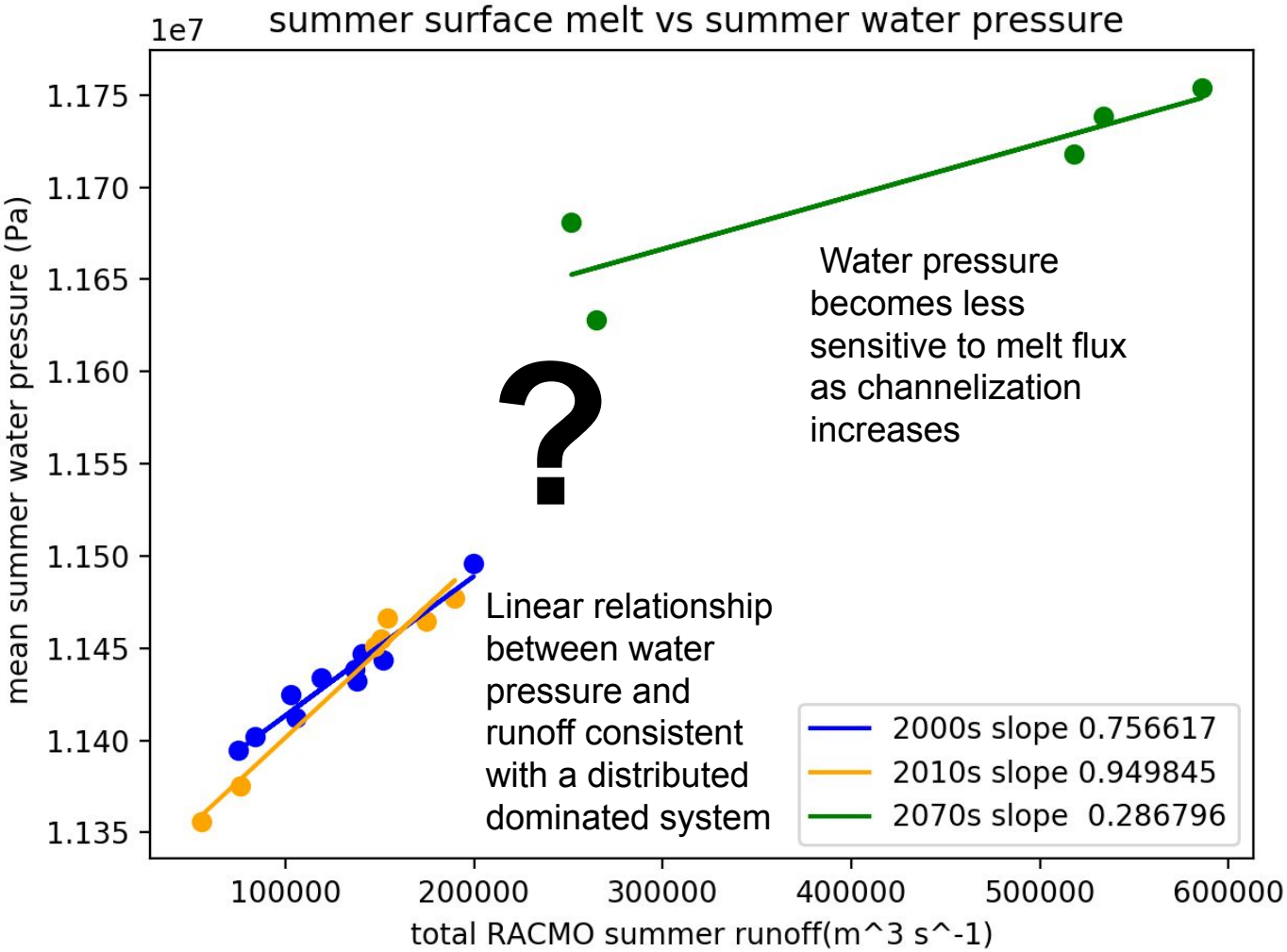
summer surface melt vs summer water pressure
1e7
mean summer water pressure (Pa)
1.175
1.170
1.165
1.160
1.155
1.150
1.145
1.140
1.135
100000
200000
300000
400000
500000
600000
total RACMO summer runoff(m^3 s^-1)
Water pressure becomes less sensitive to melt flux as channelization increases
?
Linear relationship between water pressure and runoff consistent with a distributed dominated system
2000s slope 0.756617
2010s slope 0.949845
2070s slope 0.286796

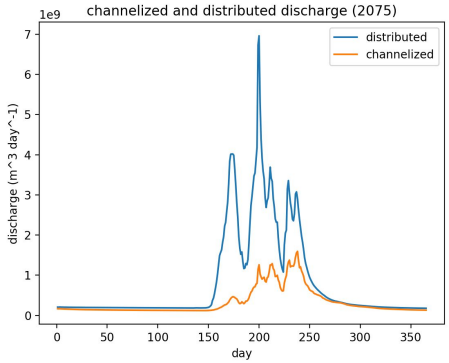
channelized and distributed discharge (2075)
1e9
discharge (m^3 day^-1)
day
distributed
channelized

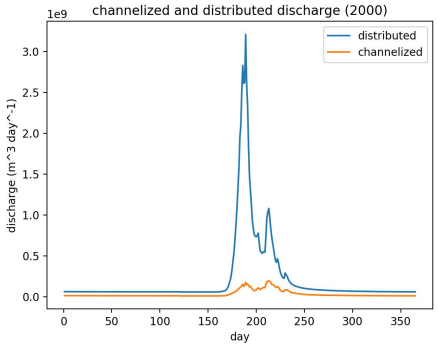
channelized and distributed discharge (2000)
1e9
discharge (m^3 day^-1)
day
distributed
channelized

# Summary and conclusions

- Increasing surface melt has a substantial impact on the character of drainage.
  - Increased channelization has only a slight moderating effect on seasonally-averaged water pressure as surface melt increases.
- This suggests that this increase is insufficient to prevent meltwater-induced speedup of HG in the coming decades.

Future work

- Finishing century scale runs
- Coupling to these subglacial hydrology runs to ice dynamics
- Coupling surface melt and discharge to MPAS-O (and other E3SM models)

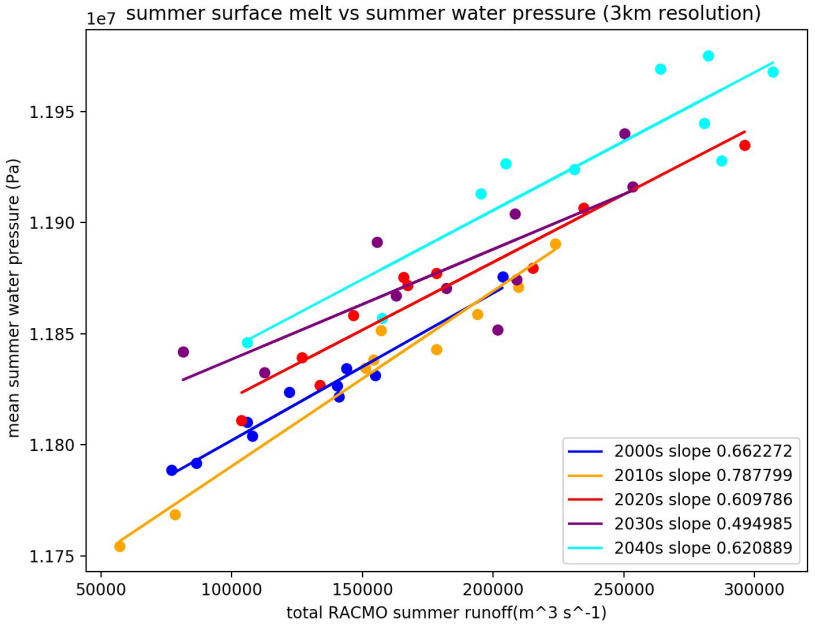

# Thanks

# Creating a genome browser for SARS-CoV-2 visualization.

Elena Romero
Group: T-6
Graduate Student at University of Washington

Mentored by: Brian Foley

# World wide spread of SARS-CoV-2 has generated large amounts of viral diversity.

Variant data from cov.lanl.gov. 06/26/2021 Through 07/26/2021

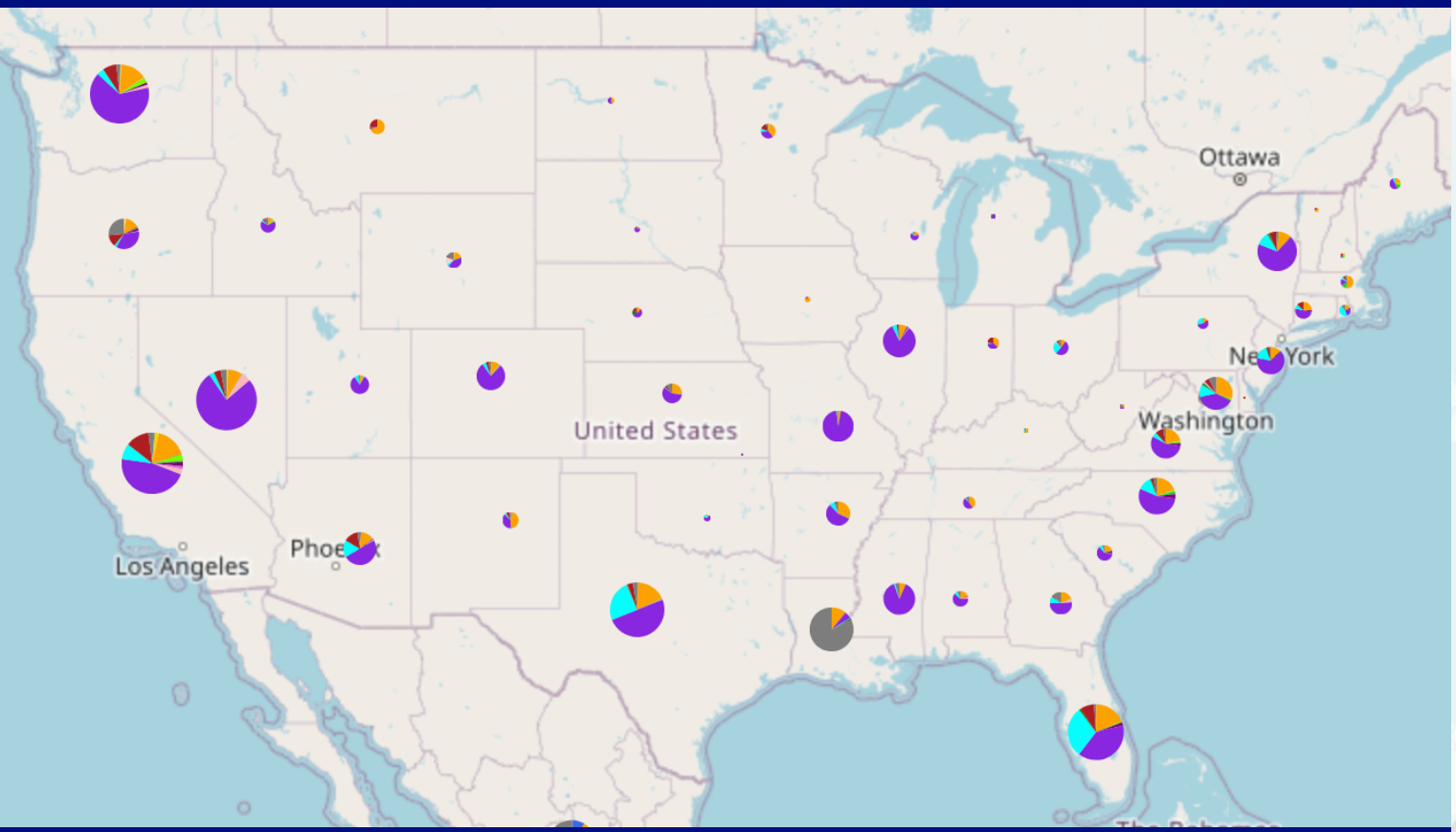


- A.2.5.2
- A.23.1
- A.27
- Alpha+E484K
- Alpha+F490S
- Alpha+T20I
- Alpha+W152R
- Ancestral
- B.1.1.318
- B.1.1.519
- B.1.1.523
- B.1.1.7=Alpha
- B.1.214.2
- B.1.258.17
- B.1.351=Beta
- B.1.429/7=Epsilon
- B.1.525=Eta
- B.1.526.1
- B.1.526.2
- B.1.526=Iota
- B.1.575
- B.1.617.1=Kappa
- B.1.617.2=Delta
- B.1.617.2=Delta+A222V
- B.1.620
- B.1.623

# Not all variants are created equal.

Variant data from cov.lanl.gov. 06/26/2021 Through 07/26/2021

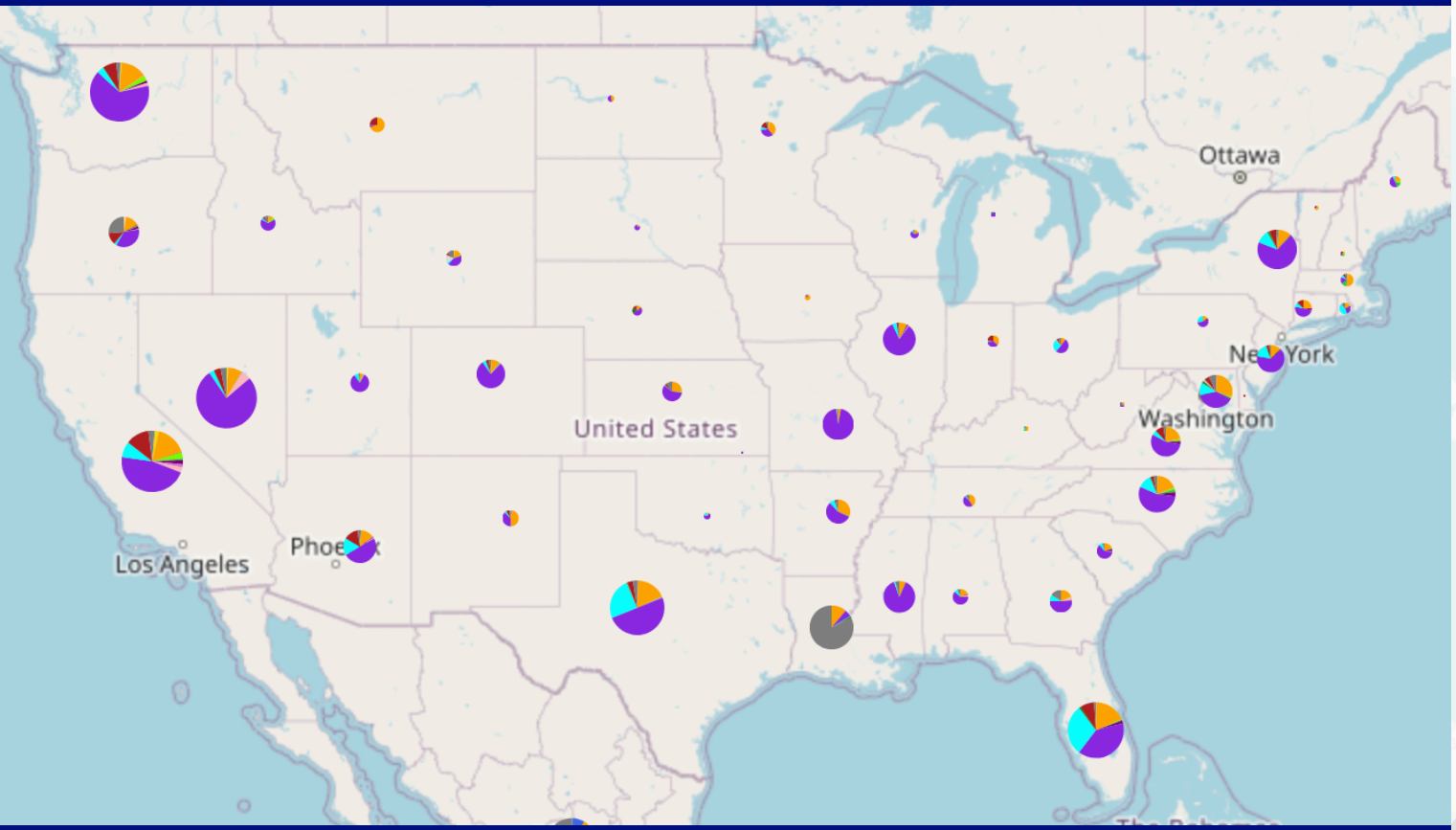


- A.2.5.2
- A.23.1
- A.27
- Alpha+E484K
- Alpha+F490S
- Alpha+T20I
- Alpha+W152R
- Ancestral
- B.1.1.318
- B.1.1.519
- B.1.1.523
- B.1.1.7=Alpha
- B.1.214.2
- B.1.258.17
- B.1.351=Beta
- B.1.429/7=Epsilon
- B.1.525=Eta
- B.1.526.1
- B.1.526.2
- B.1.526=Iota
- B.1.575
- B.1.617.1=Kappa
- B.1.617.2=Delta
- B.1.617.2=Delta+A222V
- B.1.620
- B.1.623

# How can researchers assess what variants present further threats?

# How can researchers assess what variants present further threats?

- They can perform in vitro experiments.
- They can collect and analyze data such as outcomes for patients who have contracted the variant.

# How can researchers assess what variants present further threats?

- They can perform in vitro experiments.
- They can collect and analyze data such as outcomes for patients who have contracted the variant.


# The SARS-CoV-2 Genome Browser helps provide detailed information about specific variants.

# The SARS-CoV-2 Genome Browser helps provide detailed information about specific variants.

- This information can be used to identify what variants are likely to have the biggest impact.

# Specific proteins and annotations of their regions are included in the browser.

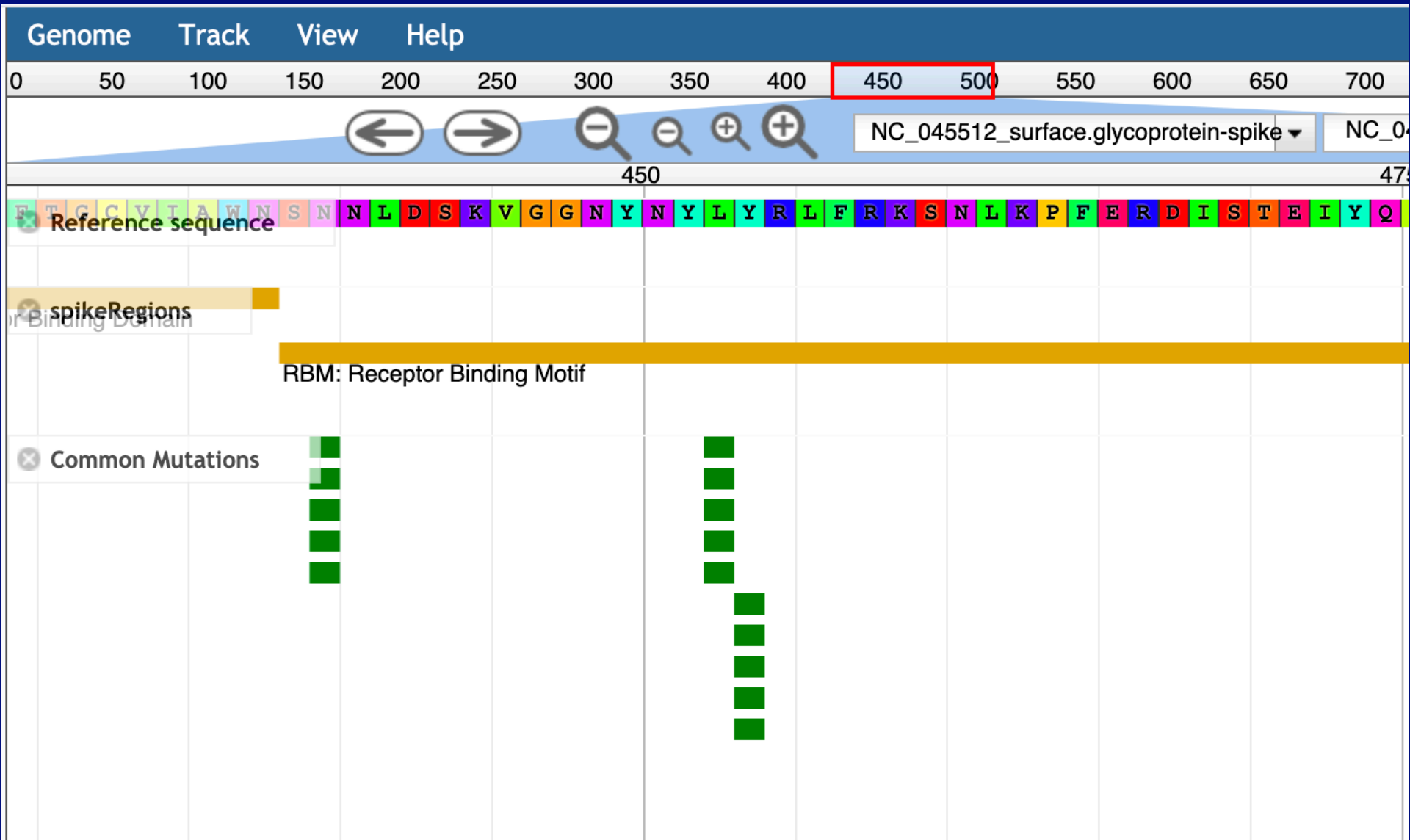

# The Genome Browser includes information about common mutations in selected proteins.

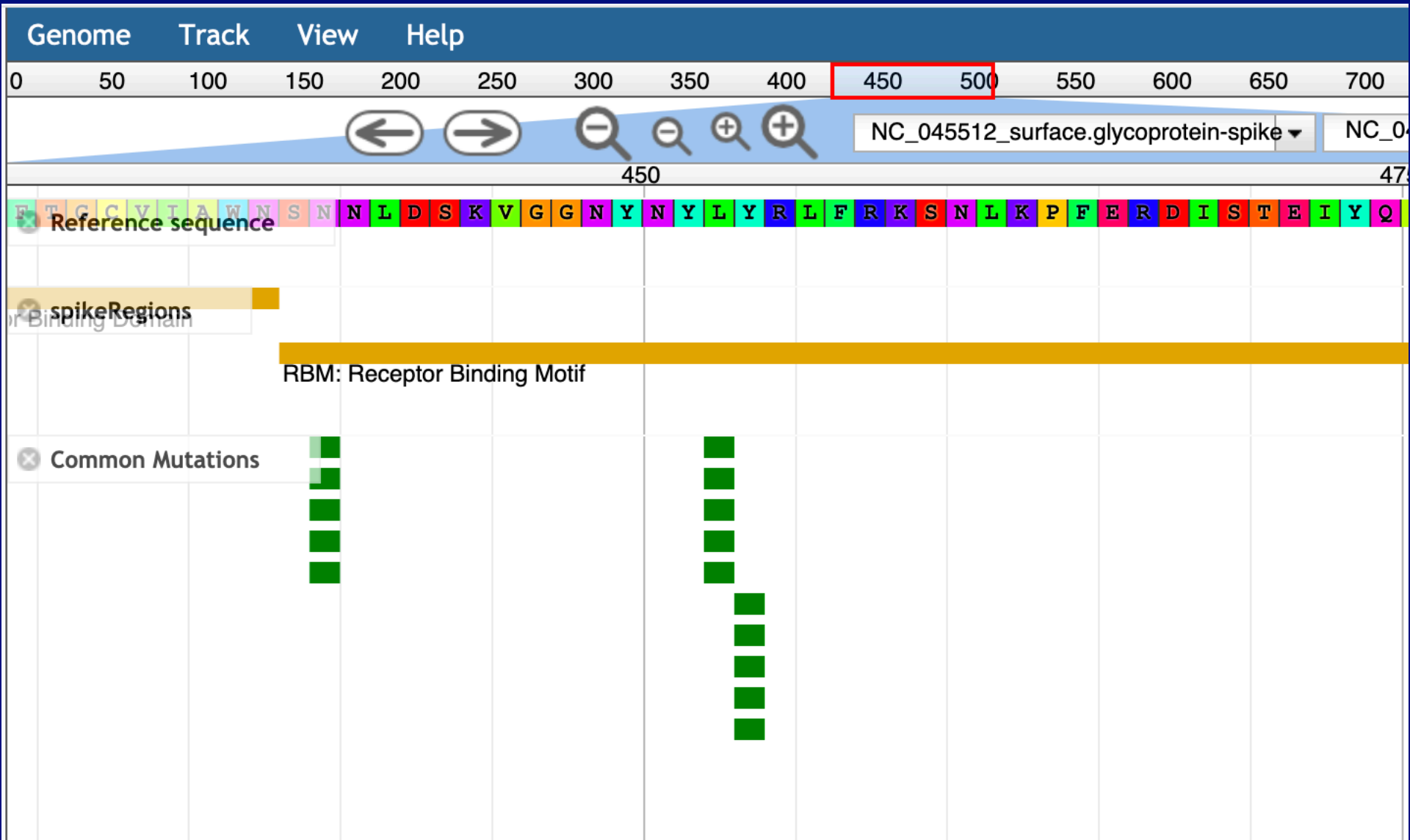

# These common mutations are often relevant to variants such as the delta variant.

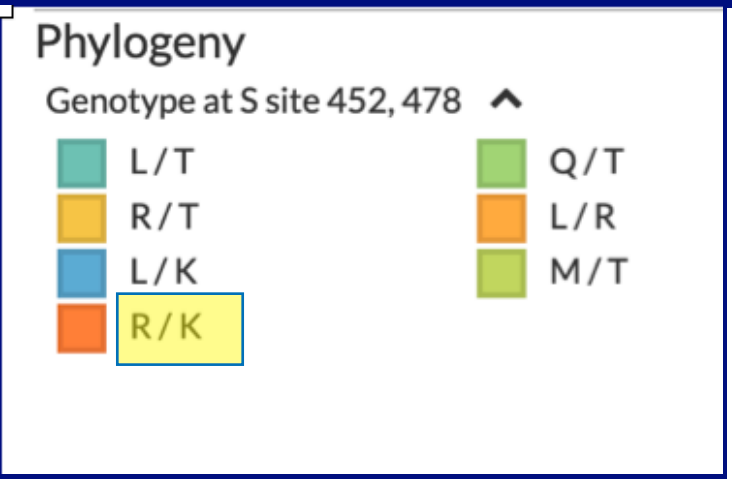


Tree from nextstrain.org

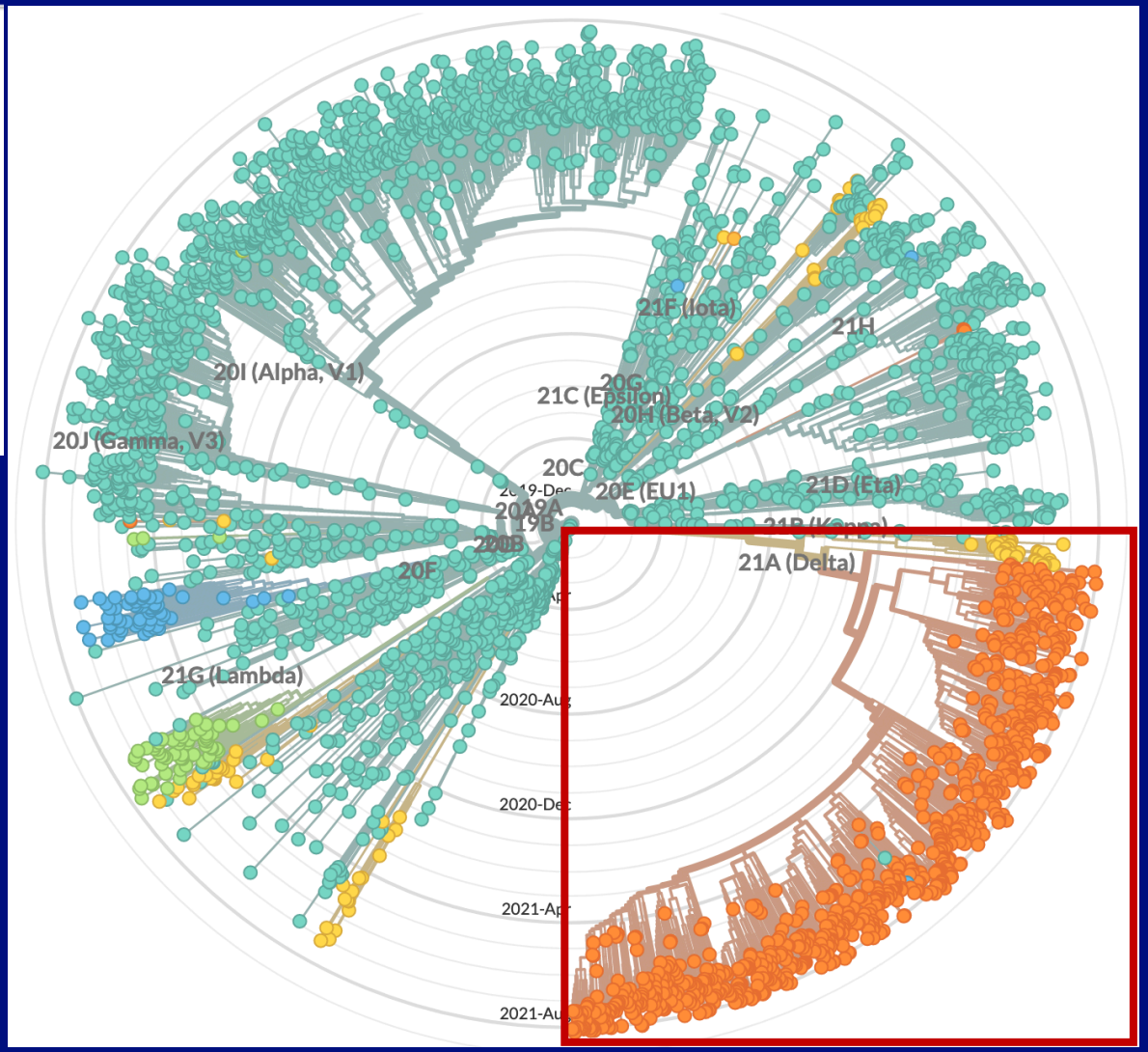


Los Alamos NATIONAL LABORATORY

# The genome browser includes information about common mutations in selected proteins.

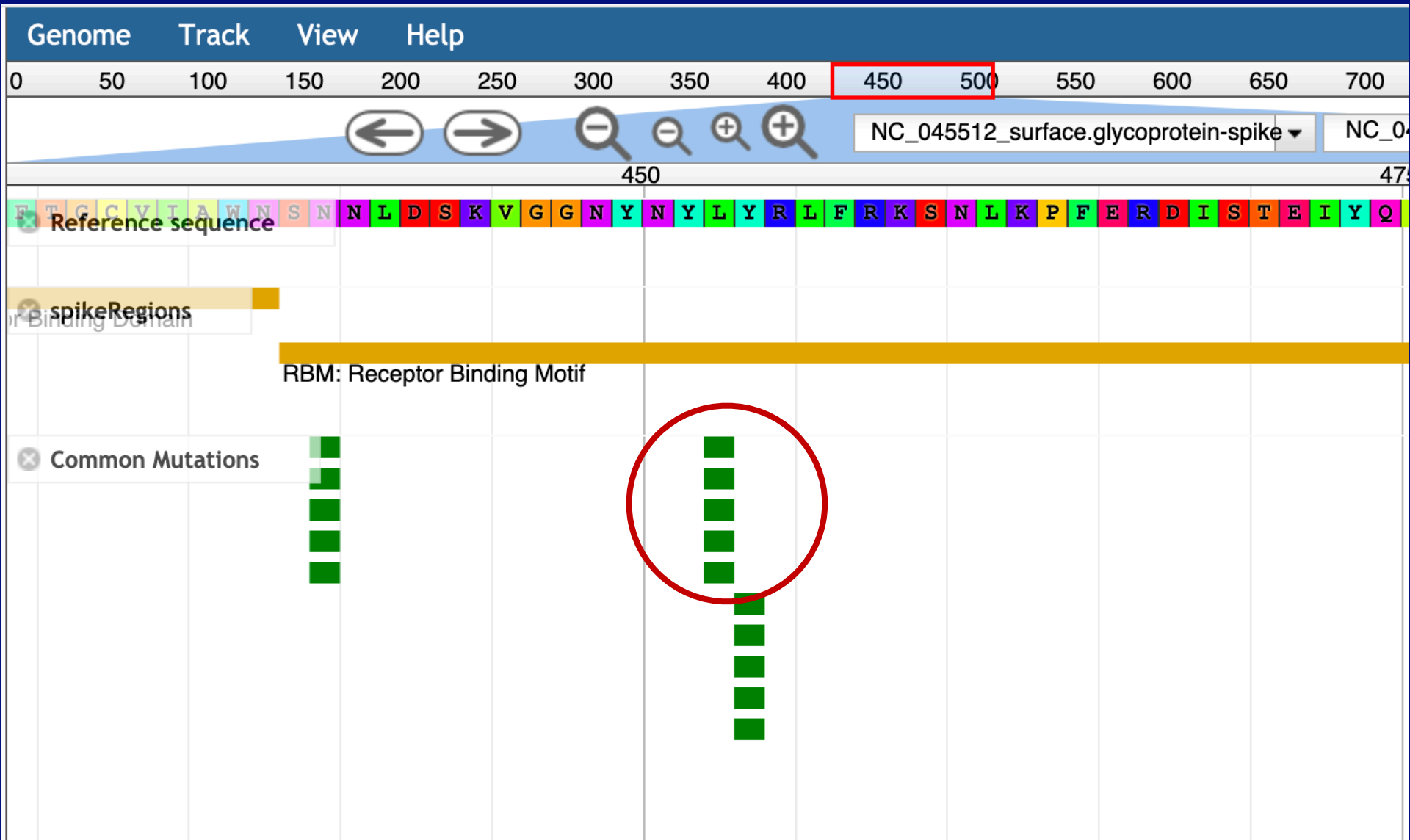

# Each site of interest in the genome has a link to more information about that site.

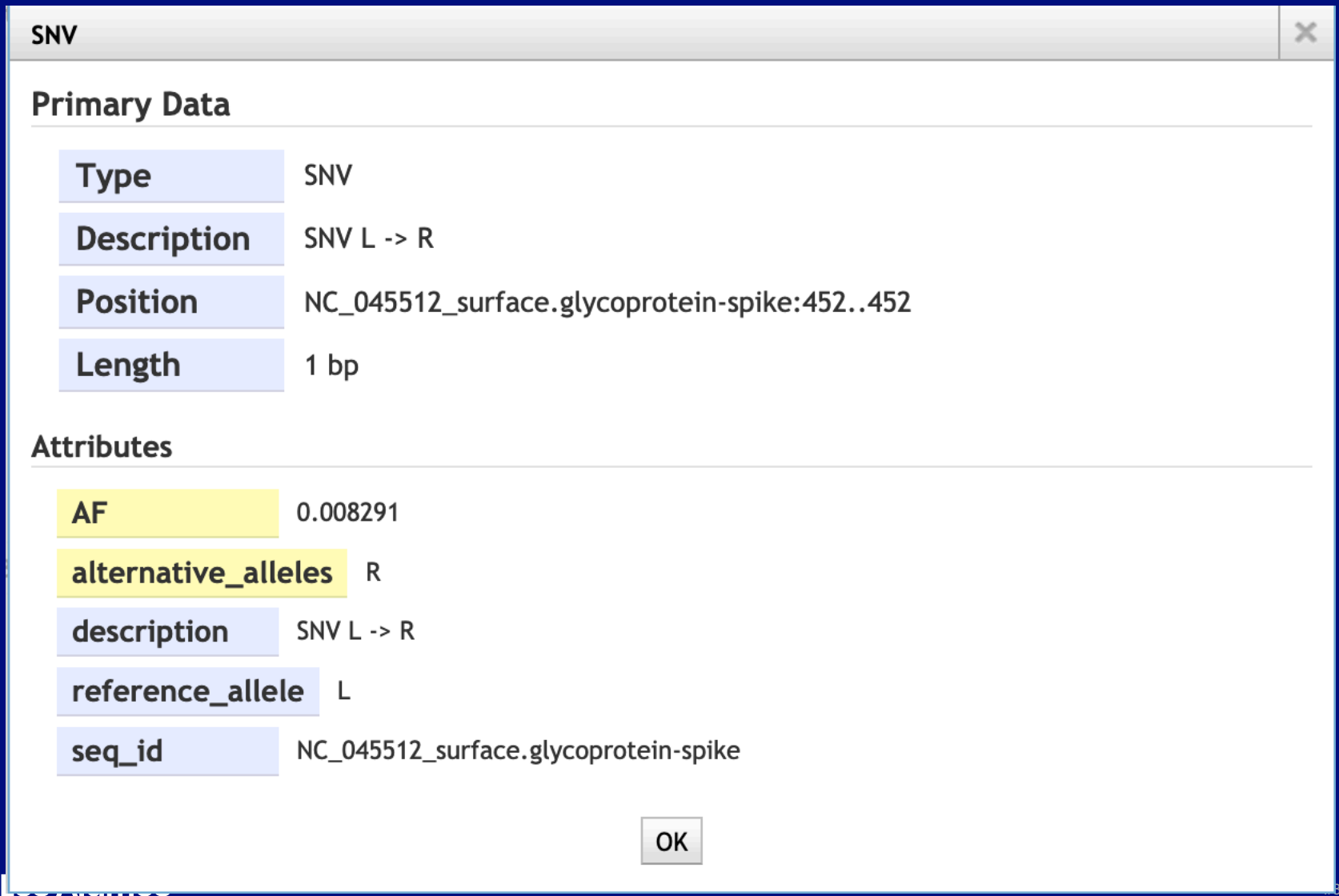

# Variants' mutations can also be viewed alongside the protein annotations.

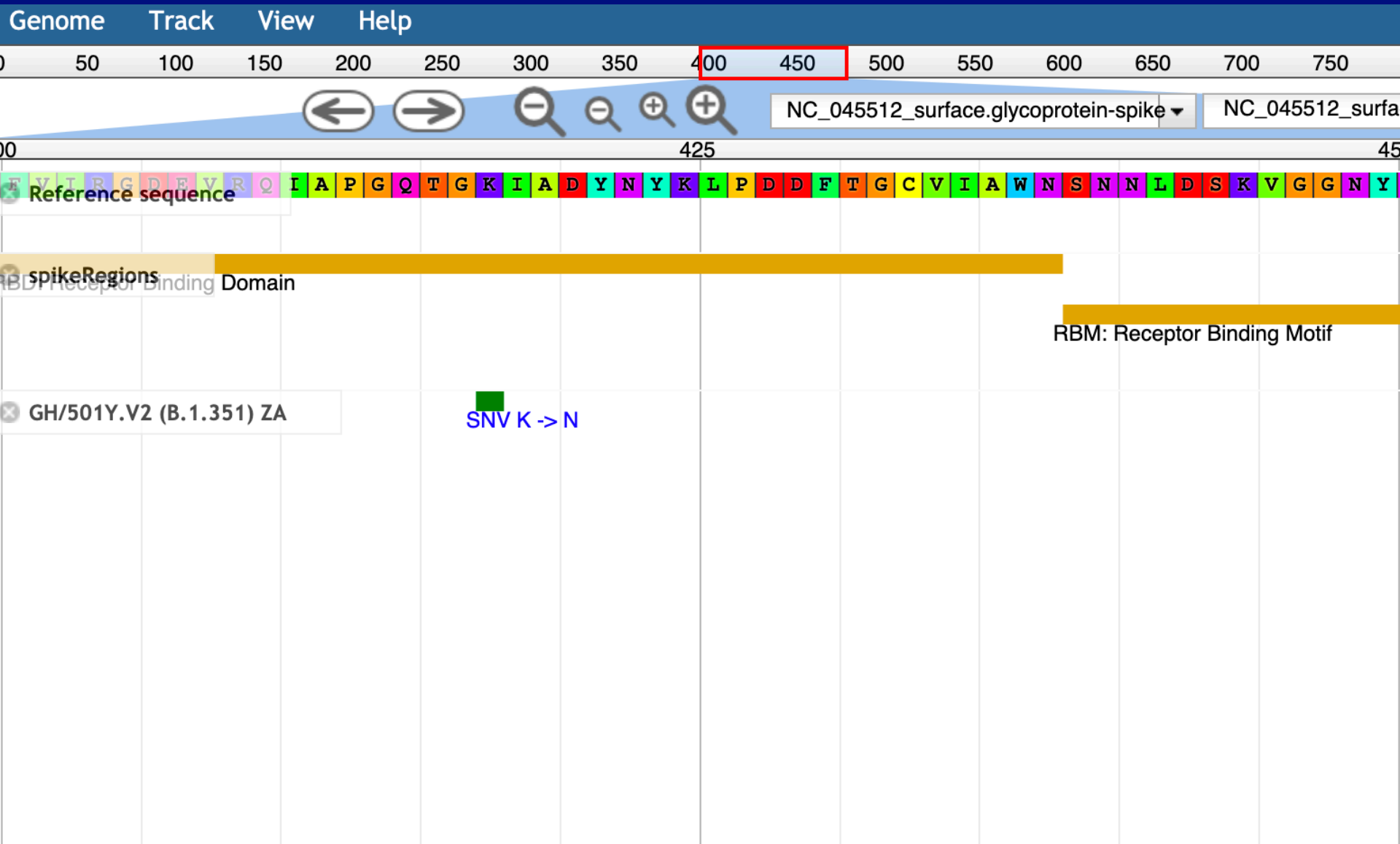

# Researchers can also utilize the whole genome nucleotide view to see the bigger picture.

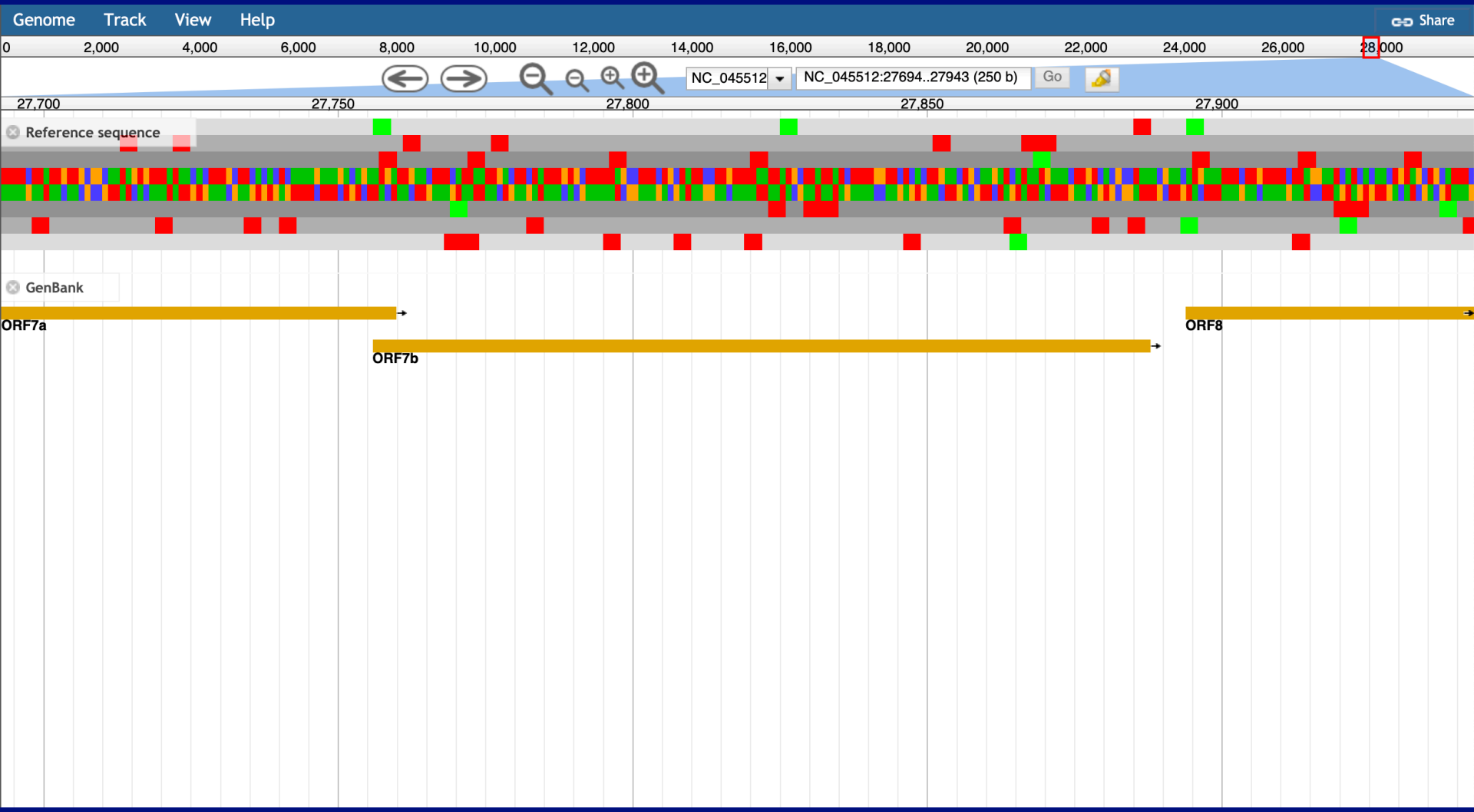

# Conclusions

- The Genome Browser provides:
  - A nucleotide view of the Sars-Cov-2 Genome
  - Protein views of major genes and open reading frames
- On top of these views, annotations of key regions and common mutations help provide researchers with a quick way to assess new variants.

# Conclusions

- The Genome Browser provides:
  - A nucleotide view of the Sars-Cov-2 Genome
  - Protein views of major genes and open reading frames
- On top of these views, annotations of key regions and common mutations help provide researchers with a quick way to asses new variants.

# Acknowledgements


- Brian Foley, Werner Abfalterer, James Szinger, Elizabeth Fung, Will Fischer, Bette Korber, Hyejin Yoon, Shihai Feng
- Funding: NIAID

# Anti-corrosion 2D Surface Coatings for Uranium Dioxides Studied with Density Functional Theory

*Lightning Talk*

Geeta Sachdeva
T1, Theoretical Division, LANL
Mentors- Dr. Ping Yang, Dr. Gaoxue Wang

08/24/2021

# Outline

- Background
- Spent nuclear fuels- prevention from corrosion
- Anti-corrosion coatings for $UO_2$ surface
- Results and Discussions
- Summary

# Background

Nuclear power plant

Spent fuel

Storage and disposal

## Nuclear Fuel Process

Fresh fuel

Conversion and Enrichment

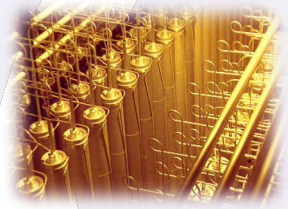

Mining and milling

# Spent nuclear fuels

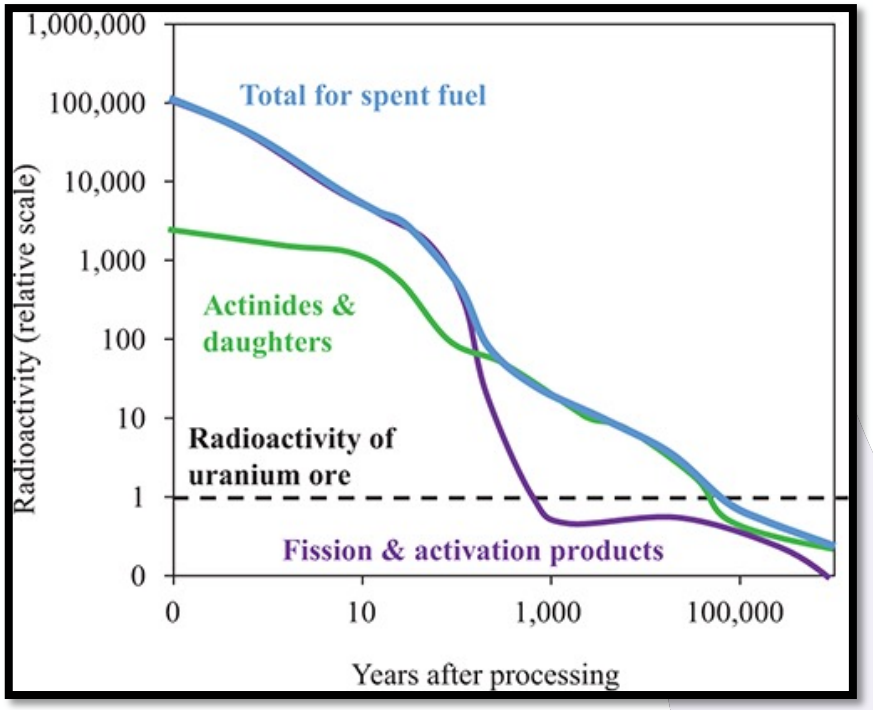


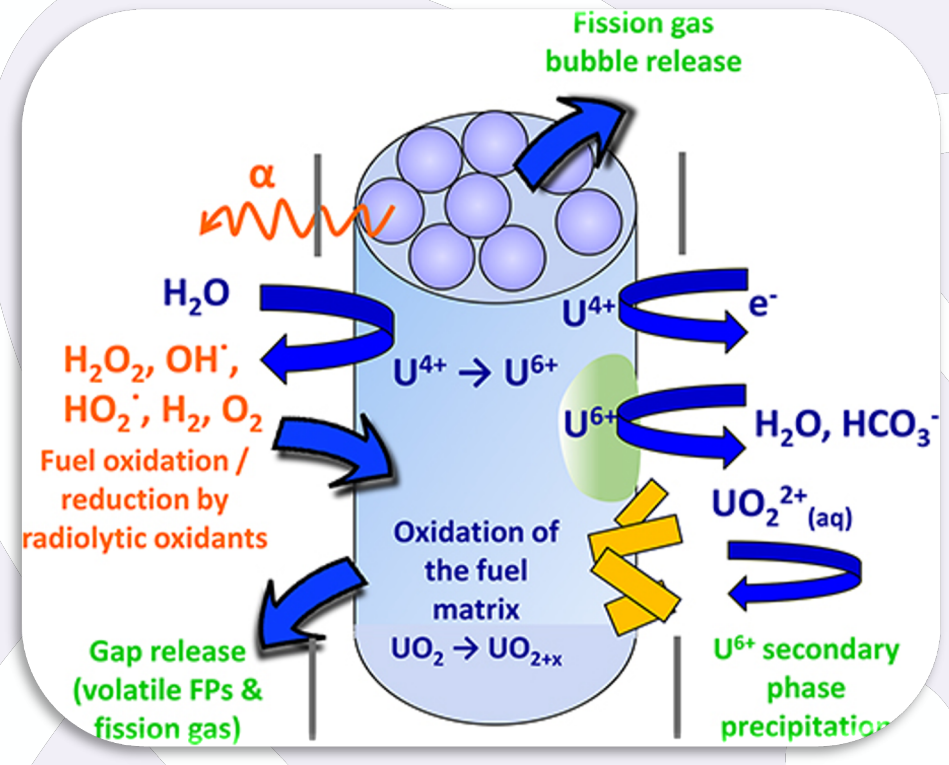


- **The corrosion of $UO_2$ is a persistent problem** for their safe usage and long-term storage.

Corkhill et al., IOP Publishing, 2018
Tanjil et al.,*Coatings* 9, no. 2 (2019): 133.

# 2D Materials as Anti-corrosion Coating

- Advantages: **atomic thickness, inert and impermeable to common gases, excellent thermal and mechanical properties**
- Synthetically achievable
- Used as coatings for photocathodes

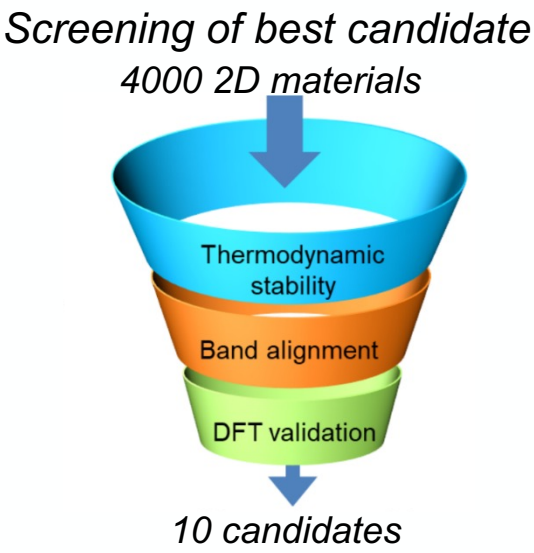


Wang, Gaoxue, Ping Yang, and Enrique R. Batista, Physical Review Materials 4, no. 2 (2020): 024001.

# 2D Materials as Anti-corrosion Coating

- ❑ Binding strength of 2D nanomaterials on nuclear materials
- ❑ Driving forces for the interaction
- ❑ The change of surface properties after coating with 2D materials

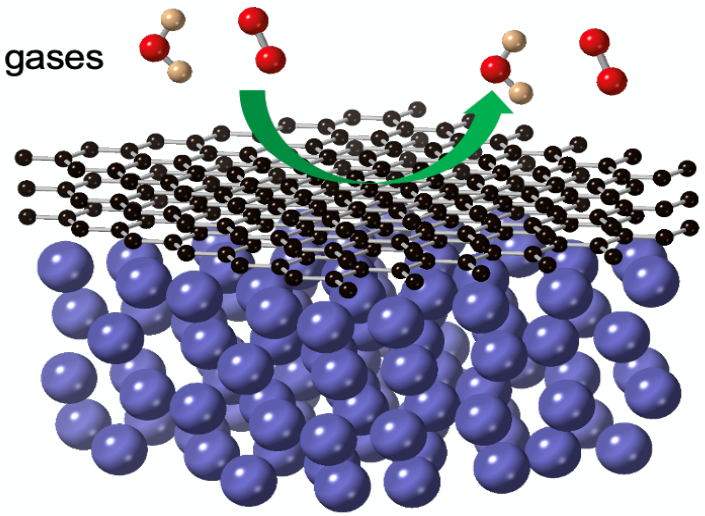


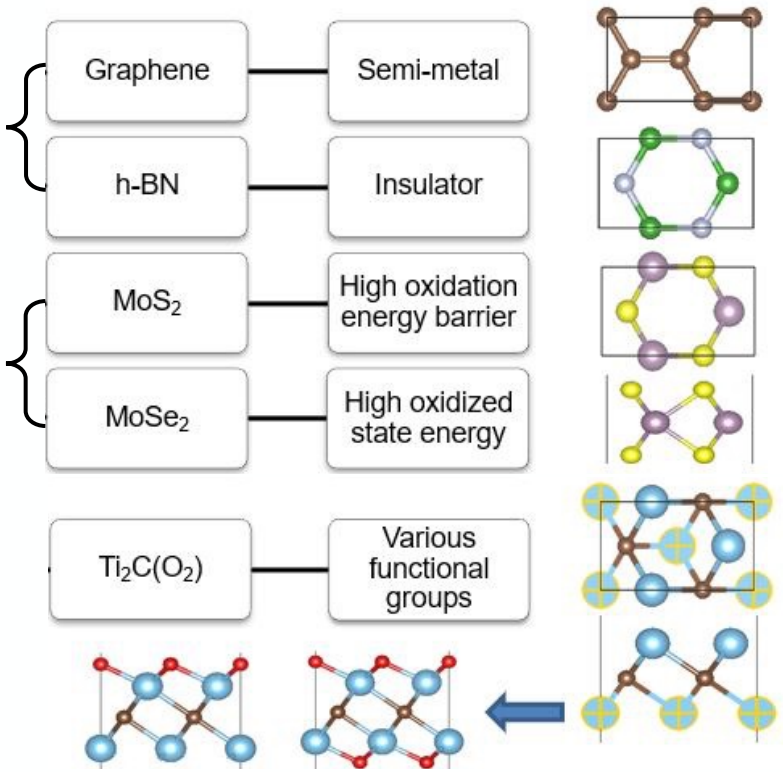




Guo et al., *ACS Applied Nano Materials* 4, no. 5 (2021): 5038-5046

# Methodology

Uranium dioxide - $UO_2$ (fluorite structure)

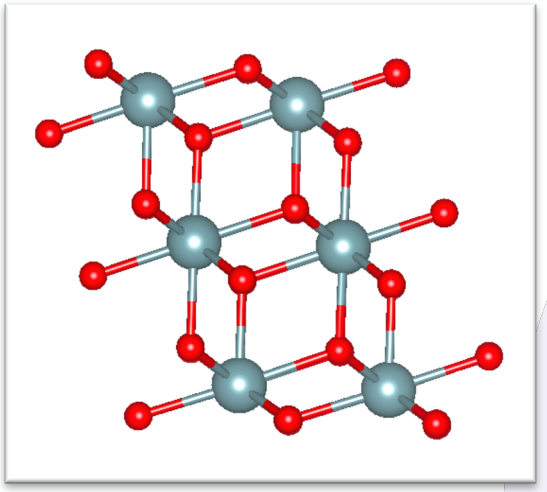

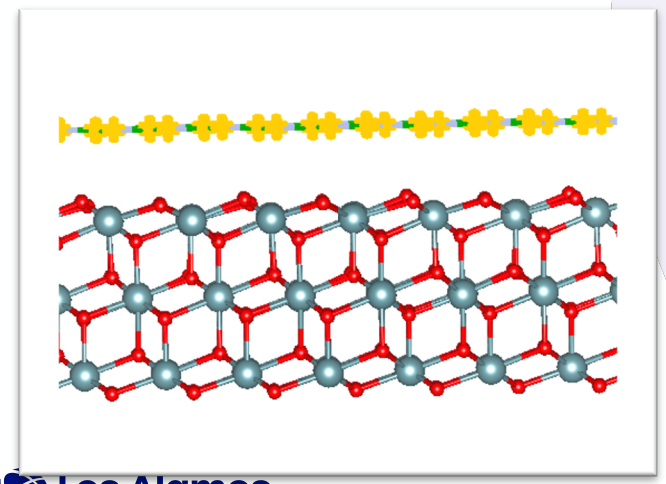

- Electronic structure calculations based on density functional theory (DFT)
- Perdew-Burke-Ernzerhof (PBE+U) exchange-correlation functional with a Hubbard U
- Spin polarized calculations

Density functional theory (DFT)- VASP

Binding Energy, Density of states, Bader's charge transfer etc.



Guo et al., *ACS Applied Nano Materials* 4, no. 5 (2021): 5038-5046

# Results: Comparison of various 2D materials coatings

## Binding strength

| | BE/A ($J/m^2$) | Bader's charge transfer (e) | Interlayer distance (Å) |
|---|---|---|---|
| UO2/BN | -0.38 | 0.03 | 3.4 |
| UO2/Graphene | -0.37 | 0.03 | 3.4 |
| UO2/MoSe2 | -0.94 | 0.3 | 3.1 |

$$E_b = \frac{E_{U/2D} - (E_U + E_{2D})}{A}$$

$UO_2$/BN $UO_2$/Graphene $UO_2$/MoSe2

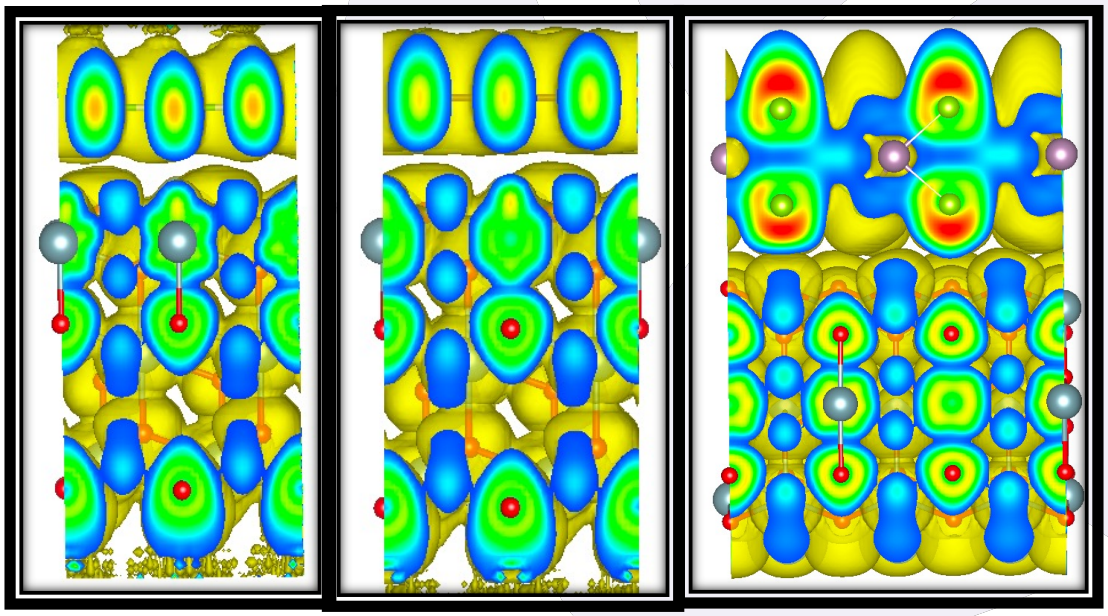

Electron localization function (ELF)

# Effect on the structure

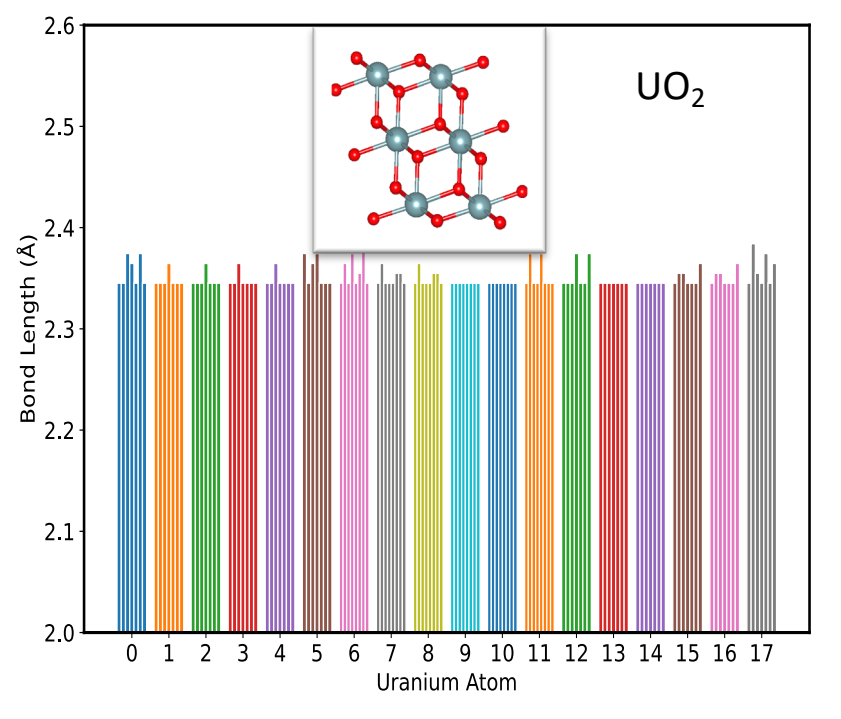


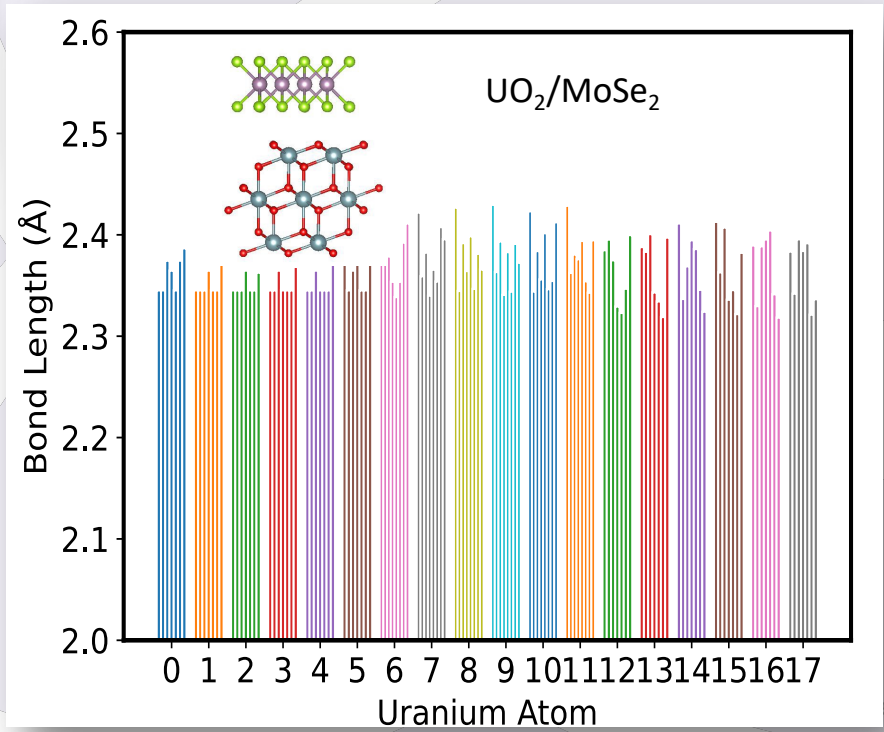

# Electronic Density of States

$UO_2$/BN

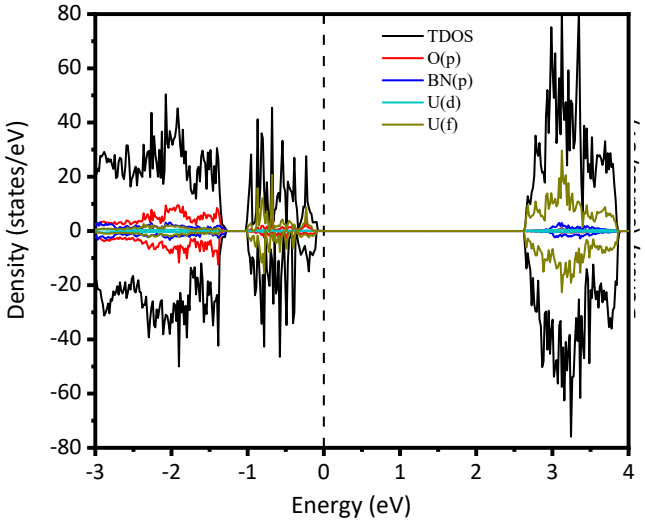


$UO_2$/Graphene

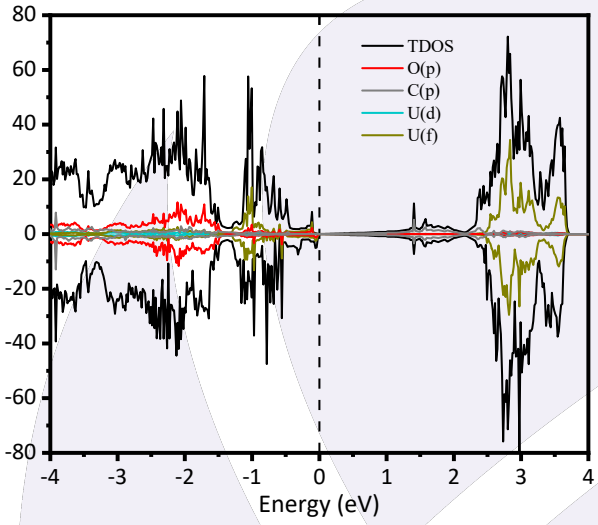


$UO_2$/MoSe2

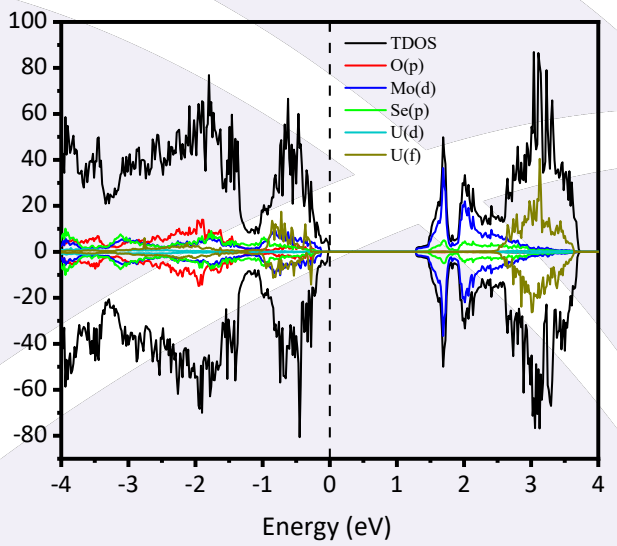


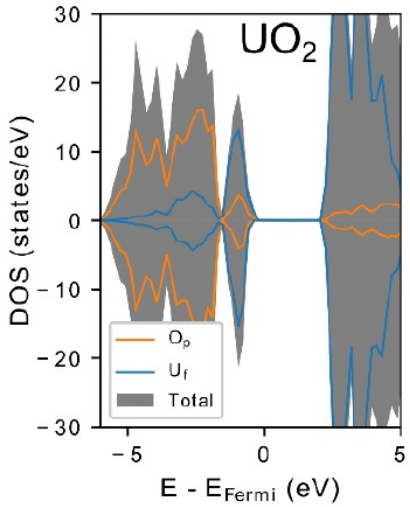


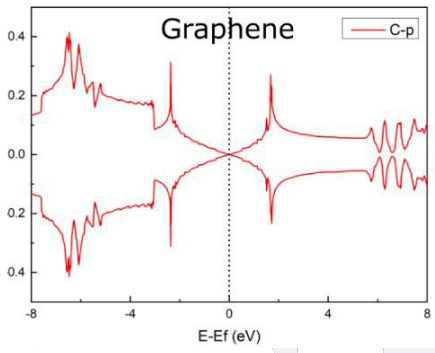


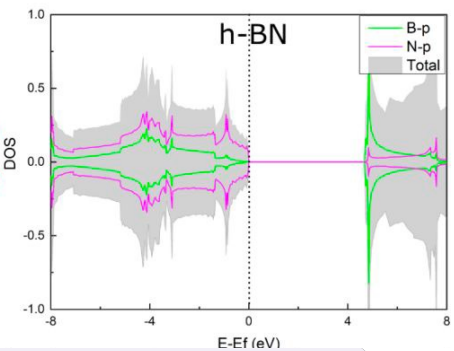


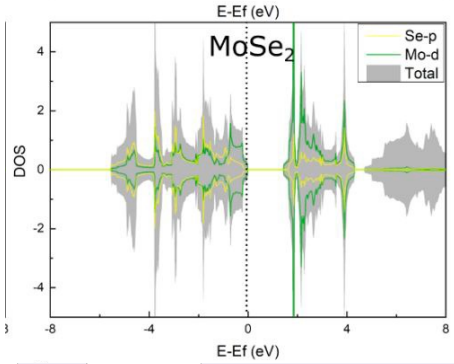


Hybridization between coating and $UO_2$ orbitals can be seen



Wang et al.,*Journal of Physical Chemistry C* 123, no. 50 (2019): 30245-30251.
Guo et al., *ACS Applied Nano Materials* 4, no. 5 (2021): 5038-5046

# Summary

- Interfacial properties including atomic configuration, electronic structure, charge transfer, and binding strength of representative 2D coatings (graphene, *h*-BN, $MoS_2$, $MoSe_2$, $Ti_2CO_2$ and $Ti_2CO$ ) on $UO_2$ surfaces were studied.

- Stronger binding energy reflects stronger protection to $UO_2$ surface. Graphene and BN have smaller binding energies, while $MoSe_2$ has much stronger binding strength on $UO_2$ surface.

- Orbital hybridization is observed between the 2D nanomaterials and $UO_2$ surface represents interaction between the surface and the coating.

# Acknowledgements


- ❑Mentors
- ❑Funding
  - G. T. Seaborg research fellowship
- ❑Computational resources
  - Superior at Michigan Tech, Slurm at LANL


Ping Yang (T-1)

Gaoxue Wang (T-1)

Enrique R. Batista (T-CNLS)

# Thank you!

# Unraveling the Thermodynamics of Copper Grain Boundaries in the Grand-Multi-Canonical Ensemble via Adaptive Biasing Force Simulations

By: Jacob Spurlock, Dr. Thomas Vogel, and Dr. Danny Perez

# Introduction

- What am I analyzing?
- What is a Grain Boundary?
- Why do GB matter?

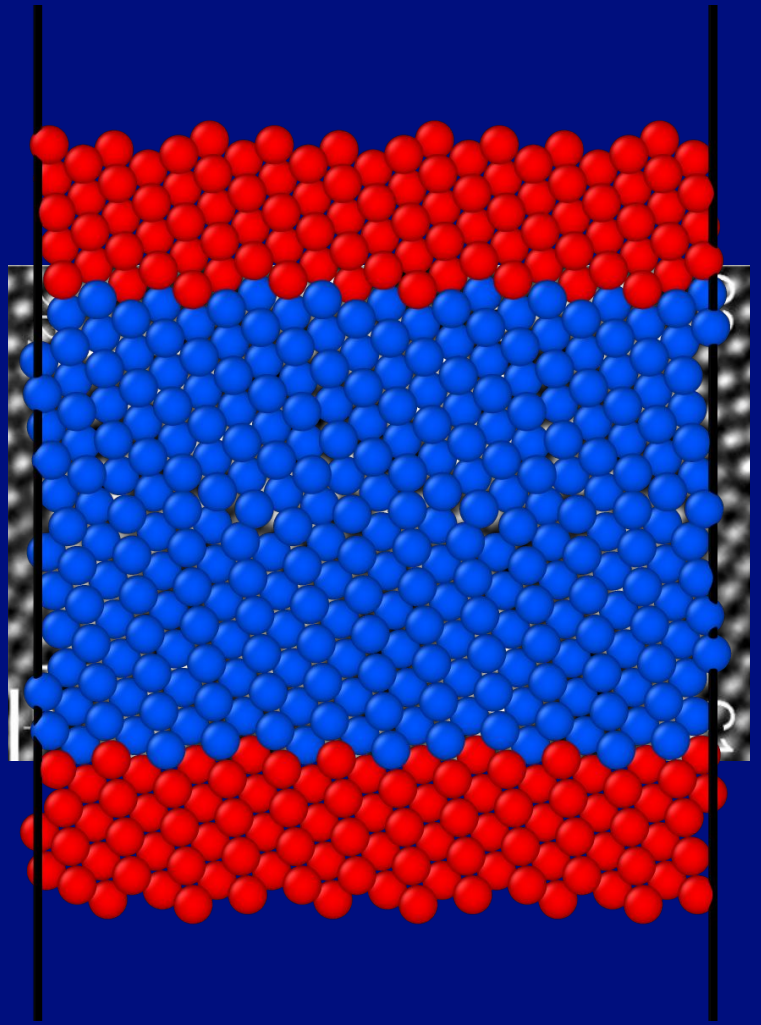

O. Hardouin Duparc et al. / Acta Materialia 55 (2007)

# Introduction

- What am I analyzing?
- What is a Grain Boundary?
- Why do GB matter?

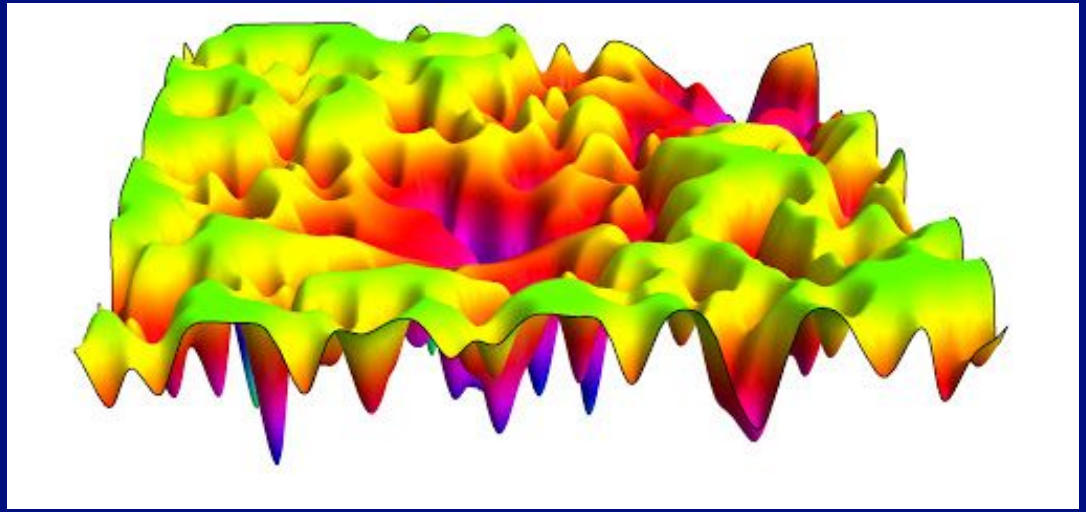

D.J. Wales, Ann. Rev. Phys. Chem., 69 (2017).

# Introduction

- What is the process?
- Multi-Canonical vs Grand-Canonical?

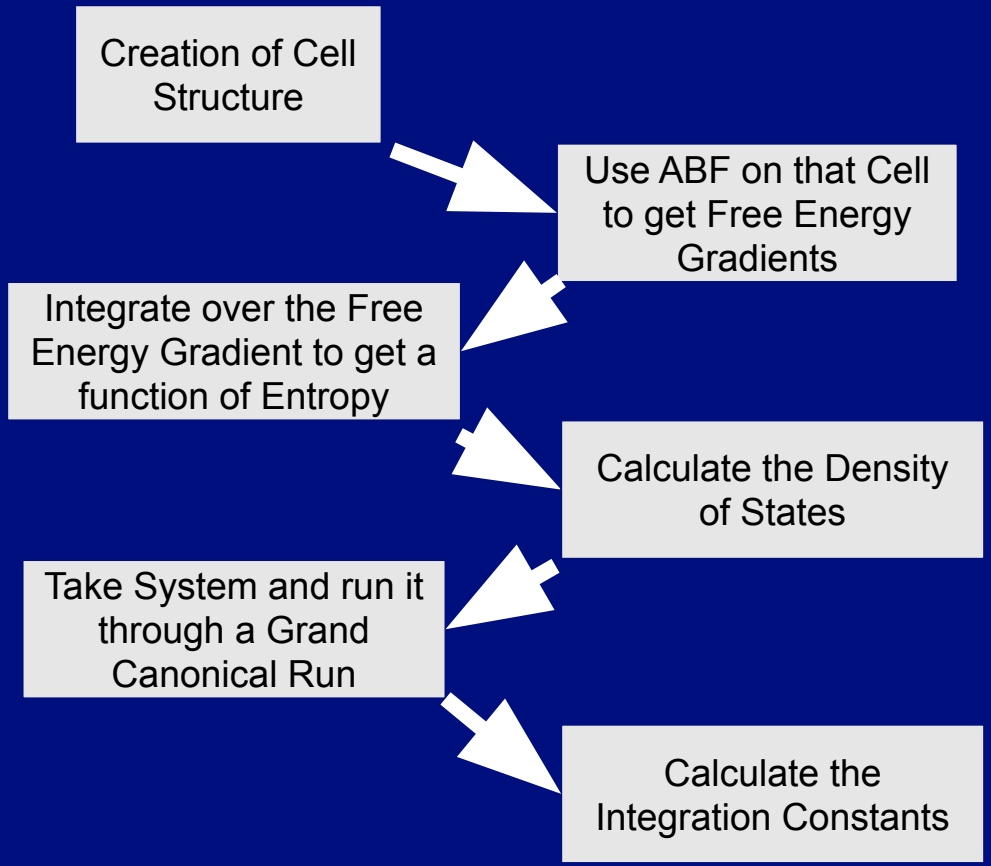

# Background

Simulation type - Adaptive Biasing Force(ABF)

How does it work?

Free Body Diagram:

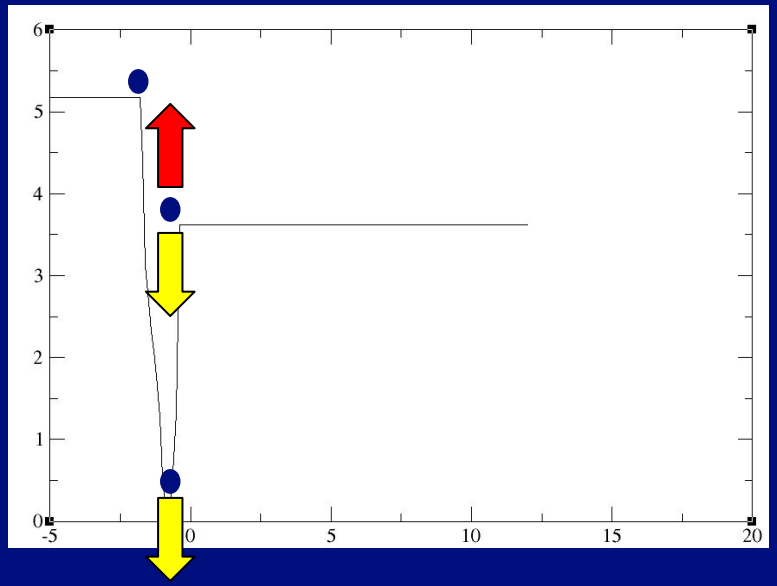

# Σ11 Asymmetric Tilt Grain Boundary

- System size varies from 2265 - 2385 particles
- Runs are done for each system size

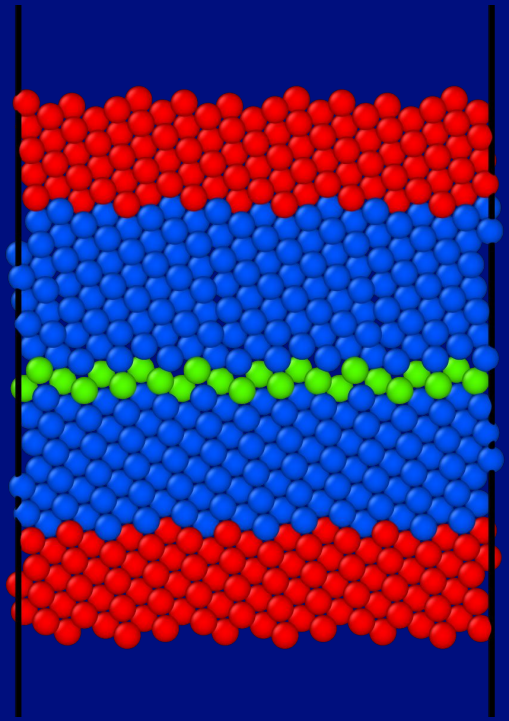

# Σ45 Asymmetric Tilt/Twist Grain Boundary

- System size varies from 2370 - 2460 particles
- Runs are done for each system size

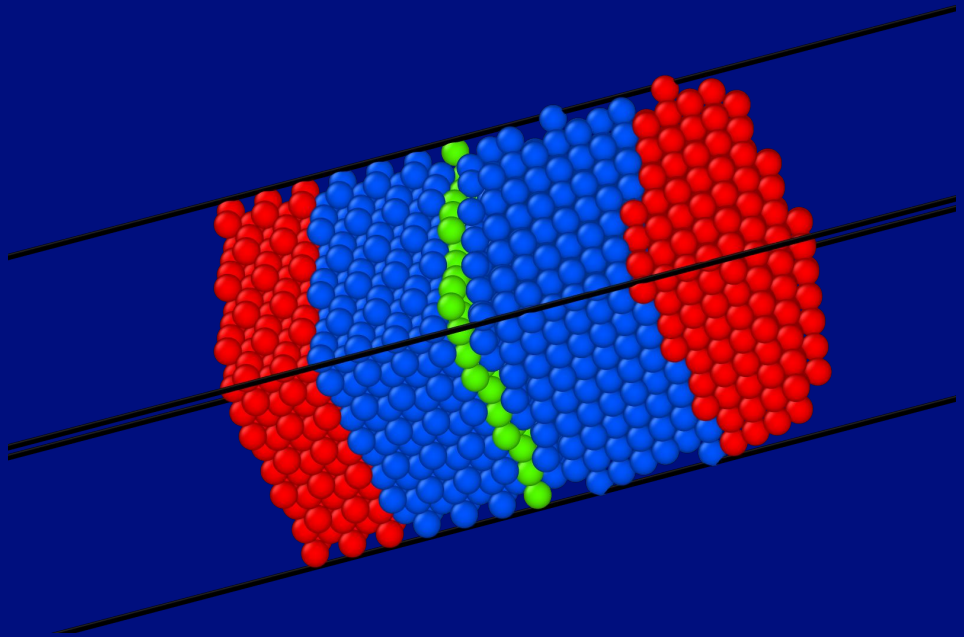

# Raw Data

- The Machine outputs raw noisy data(top)
- We can adjust the y-axis to represent temperature(bottom)
- This data is then sent into a python code to be processed

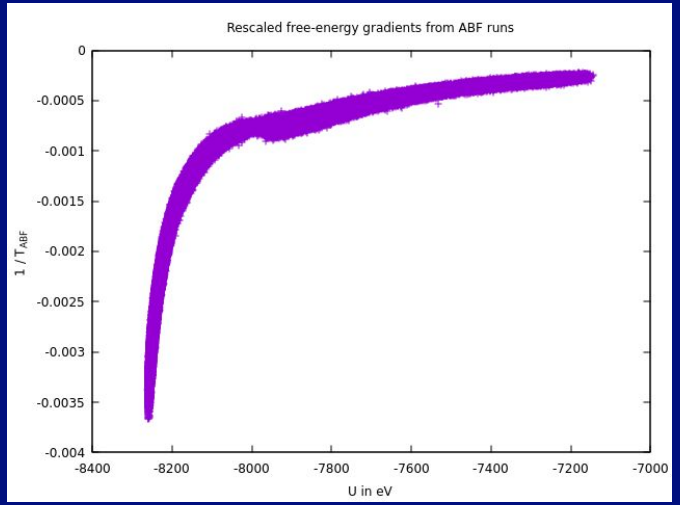


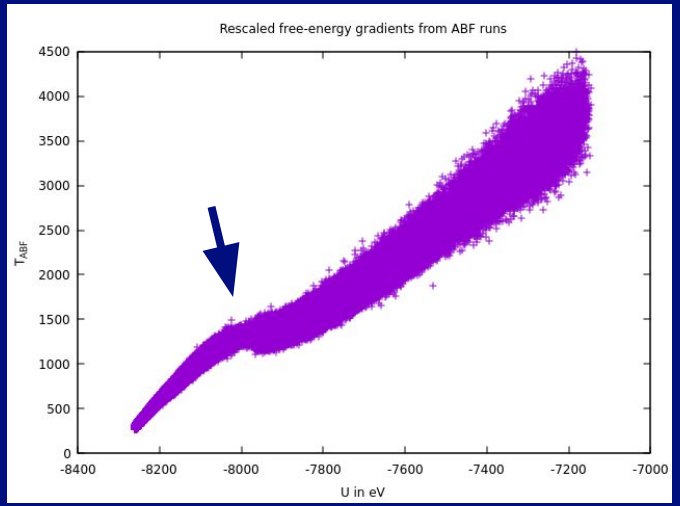

# Integral of the Data - Entropy

- The python code then integrates over the data cumulatively
- The result is the Entropy of the system

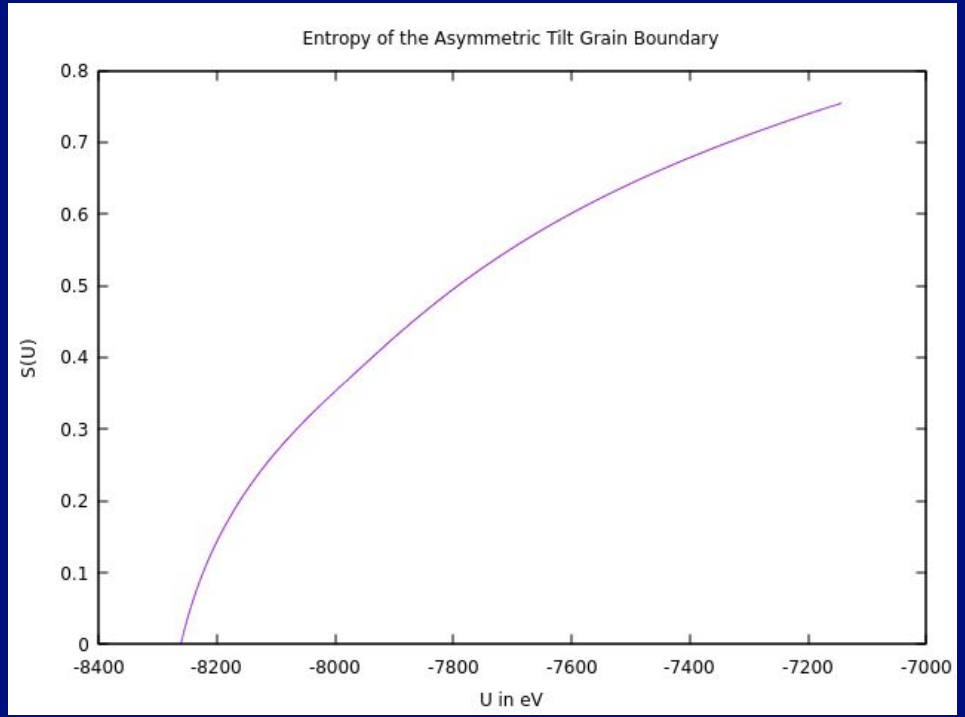

# First and Second Derivative of the Entropy

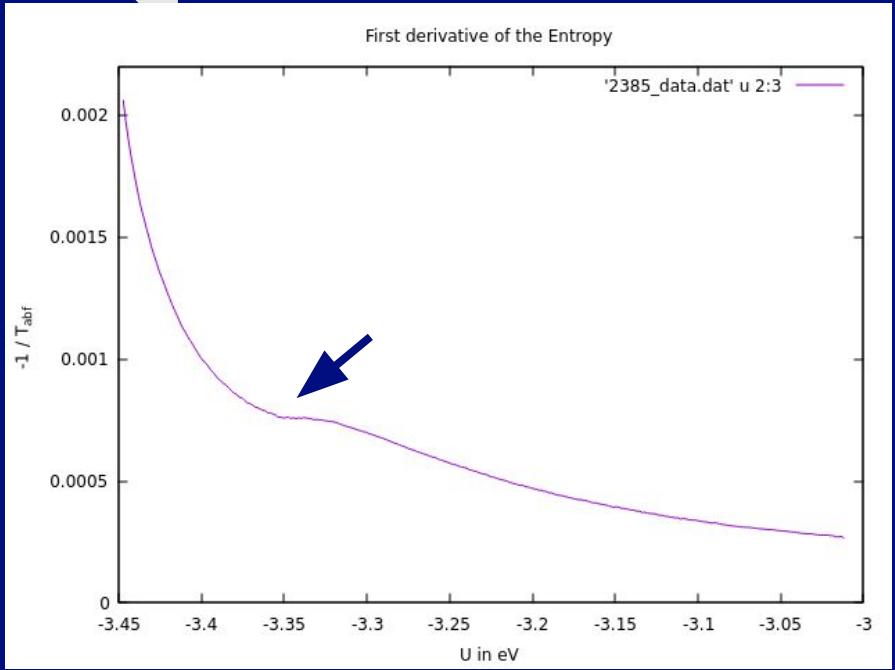


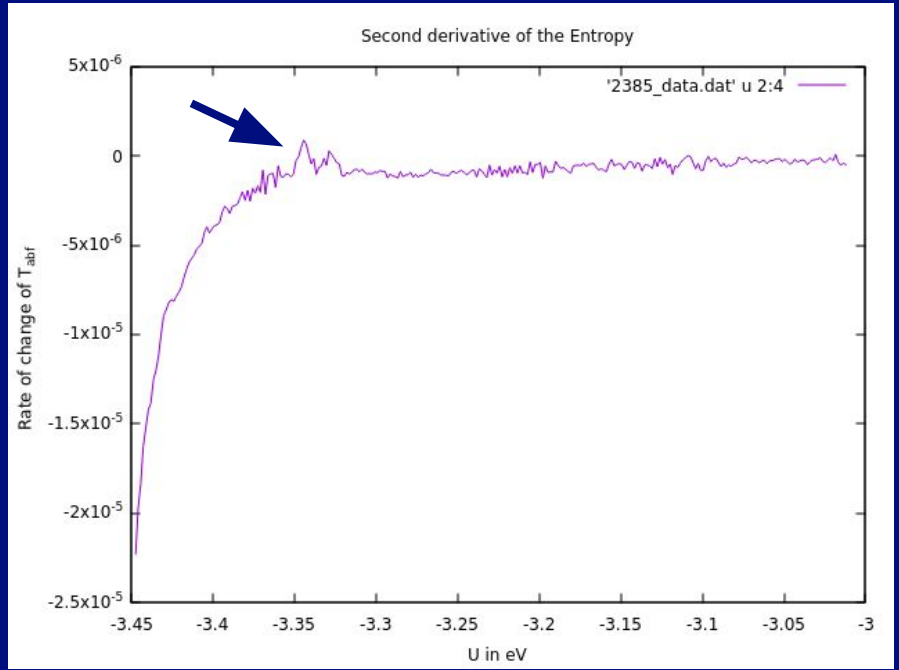

# Entropy of the Systems

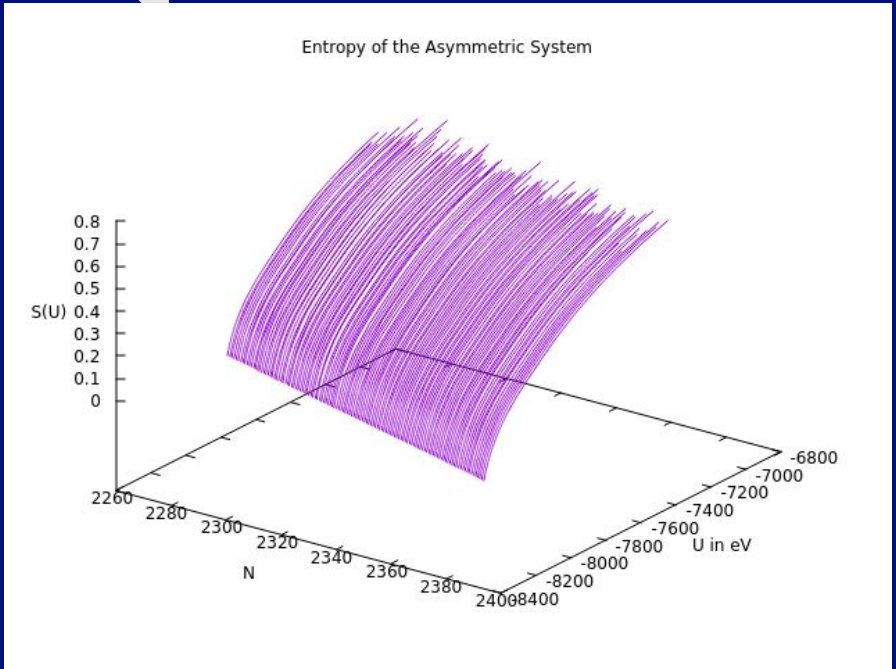


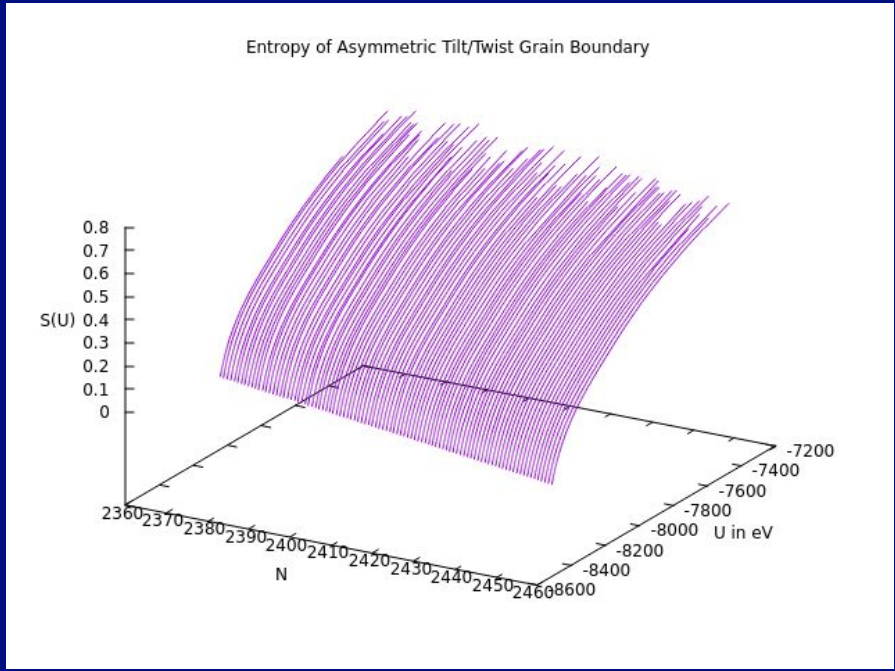

# Data: Asymmetric vs Sutton

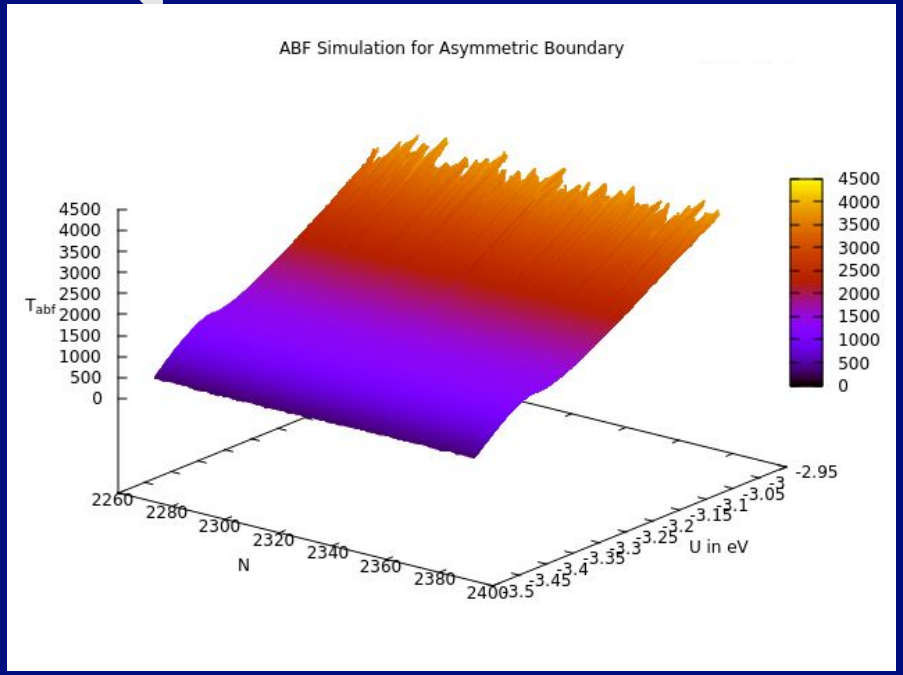


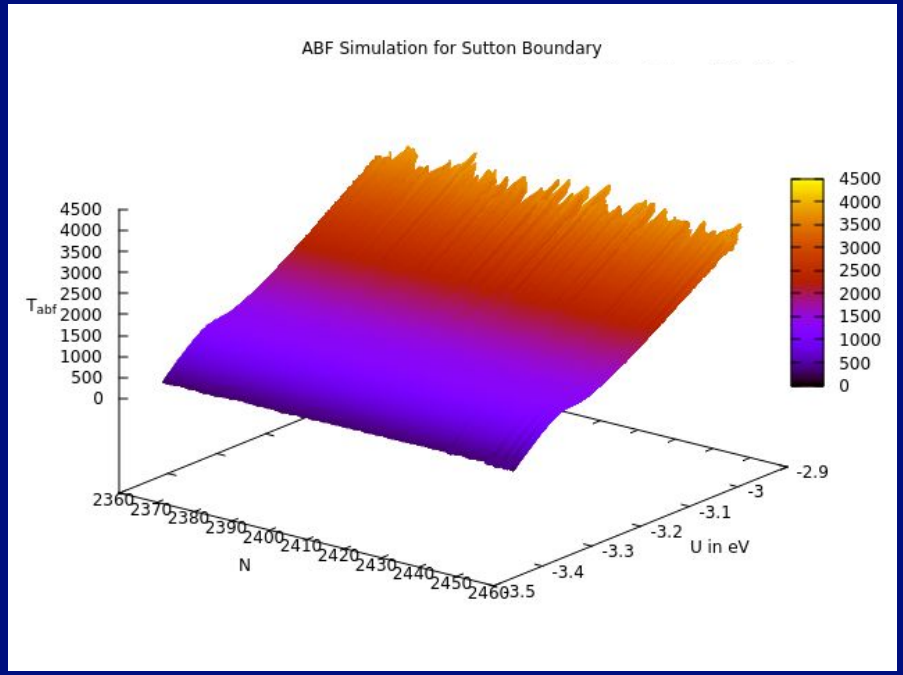

# Zoomed into the transition

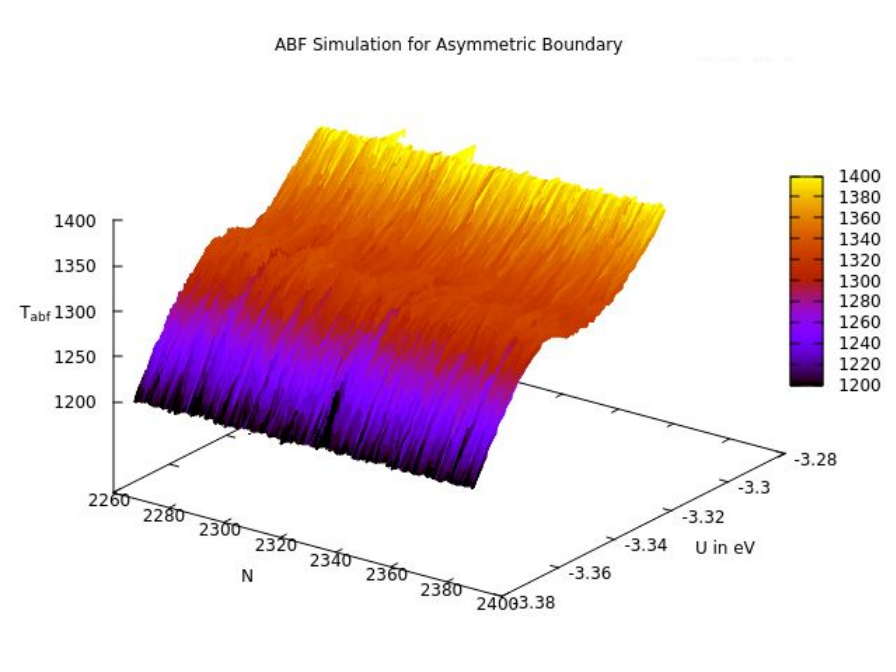


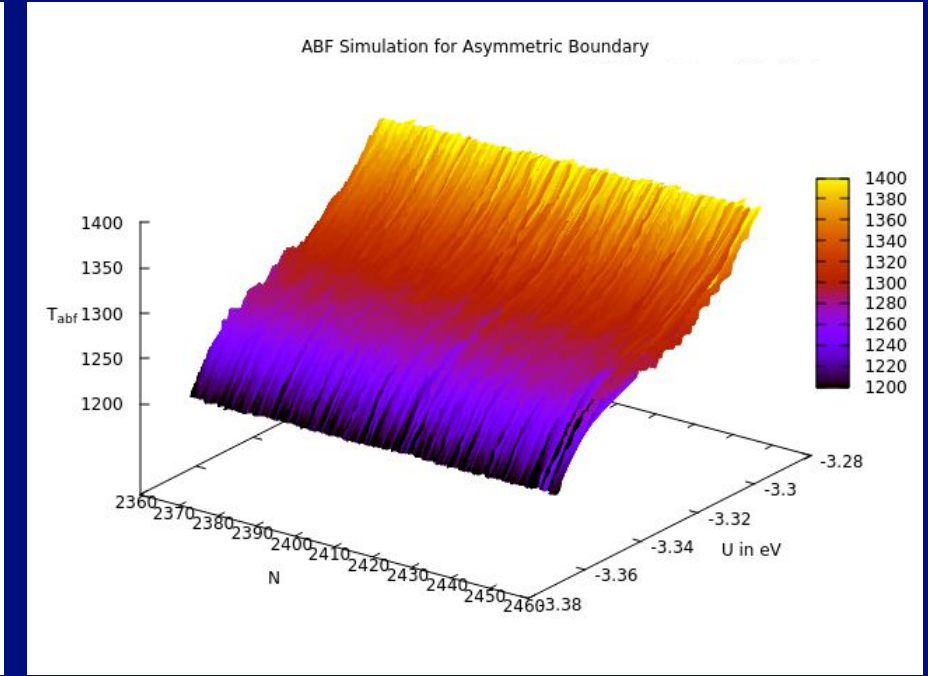

# Results

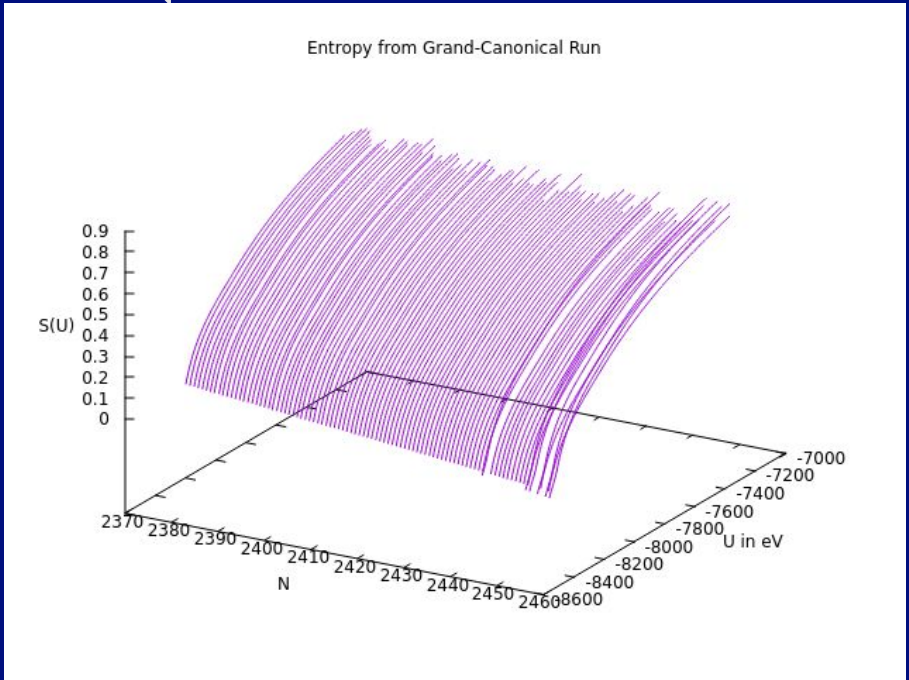
Entropy from Grand-Canonical Run
S(U)
0.9
0.8
0.7
0.6
0.5
0.4
0.3
0.2
0.1
0
2370
2380
2390
2400
2410
2420
2430
2440
2450
2460
N
-7000
-7200
-7400
-7600
-7800
-8000
-8200
-8400
-8600
U in eV

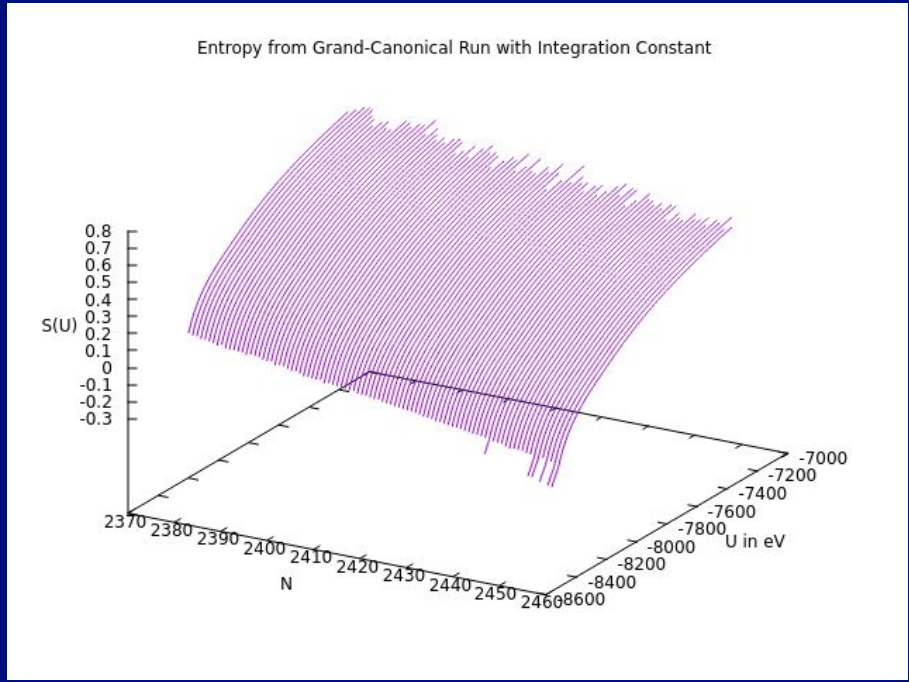
Entropy from Grand-Canonical Run with Integration Constant
S(U)
0.8
0.7
0.6
0.5
0.4
0.3
0.2
0.1
0
-0.1
-0.2
-0.3
2370
2380
2390
2400
2410
2420
2430
2440
2450
2460
N
-7000
-7200
-7400
-7600
-7800
-8000
-8200
-8400
-8600
U in eV

# Results

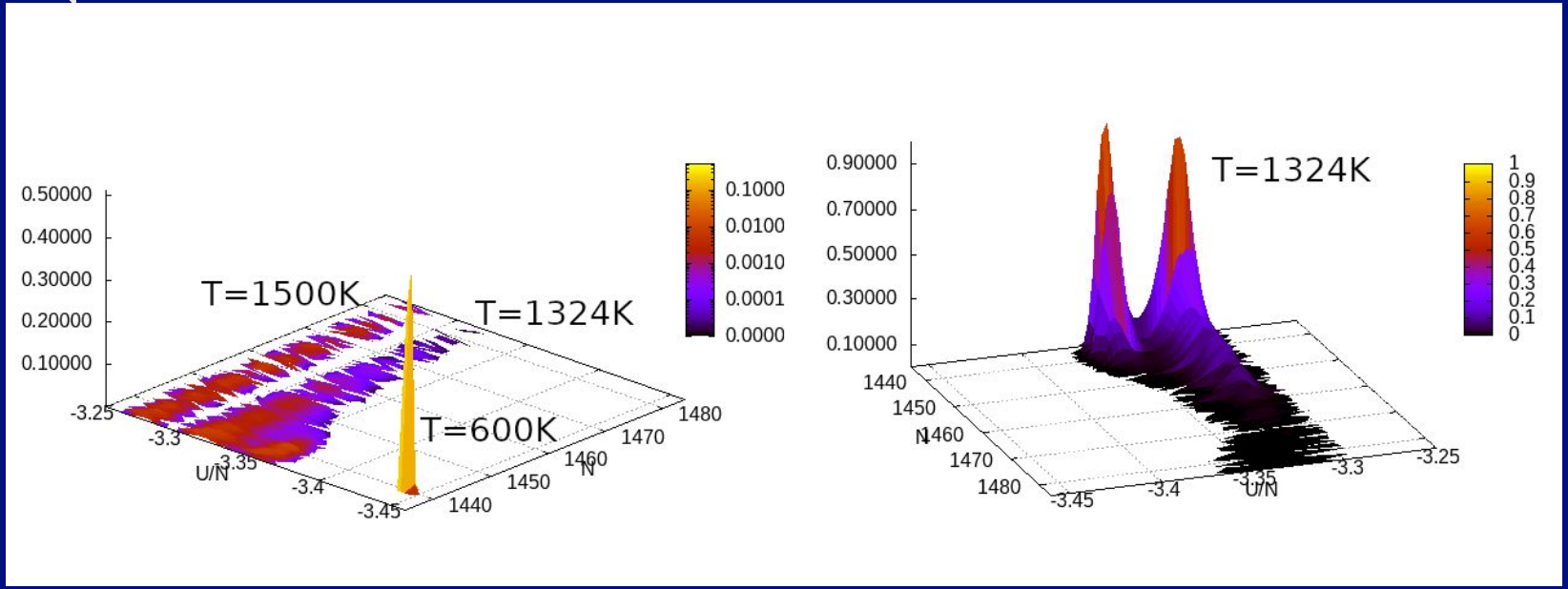
0.50000
0.40000
0.30000
0.20000
0.10000
T=1500K
T=1324K
T=600K
0.1000
0.0100
0.0010
0.0001
0.0000
-3.25
-3.3
-3.35
-3.4
-3.45
U/N
1440
1450
1460
1470
1480
N
0.90000
0.70000
0.50000
0.30000
0.10000
T=1324K
1
0.9
0.8
0.7
0.6
0.5
0.4
0.3
0.2
0.1
0

# What lies ahead

- Further analysis of data at wider temperature ranges
- More boundaries to explore

## Special Thanks To:


- Dr. Blas Uberuaga
- Dr. Danny Perez
- Dr. Thomas Vogel
- Quinn Parker
- T-1 & Scidac Group
- VFP Program

# Eavesdropping on the Decohering Environment: Quantum Darwinism, Amplification, and the Origin of Objective Classical Reality

**Akram Touil**

9/02/2021

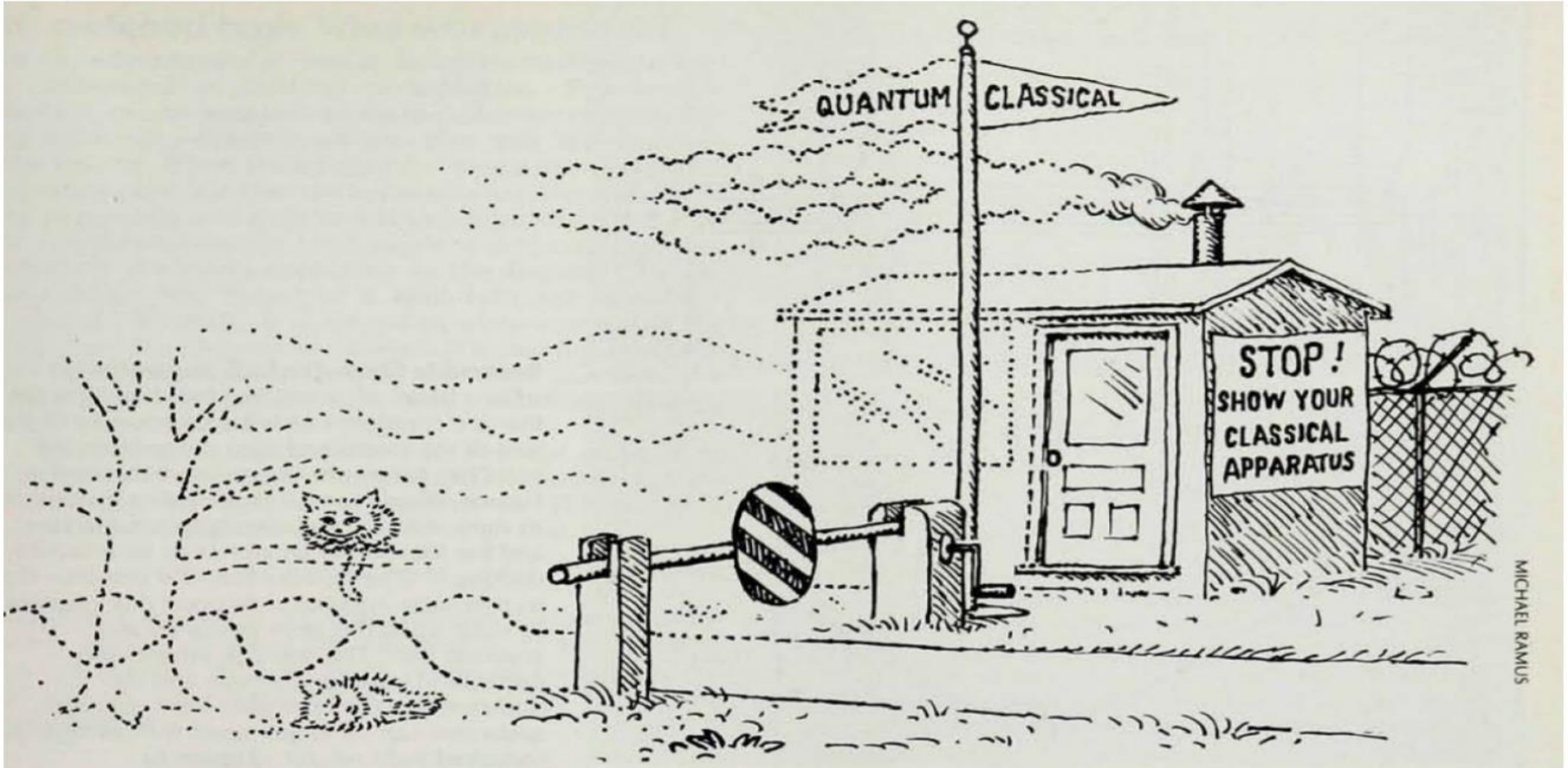


**Delineating the border** between the quantum realm ruled by the Schrödinger equation and the classical realm ruled by Newton's laws is one of the unresolved problems of physics.

W. H. Zurek, Physics Today, Oct. 1991

# Decoherence Theory

- Decoherence is the basis dependent process of loss of quantum coherence.

- We consider a quantum system $\mathcal{S}$ interacting with an environment $\mathcal{E}$ ( $\rho_{\mathcal{SE}}$ pure) .

$$\frac{\partial \rho_{\mathcal{S}}}{\partial t} = -\frac{i}{\hbar}[H(t), \rho_{\mathcal{S}}] + \mathcal{D}(\rho_{\mathcal{S}}).$$

**von Neumann term**

$\mathcal{S}$ - $\mathcal{E}$

- **Environment as a sink for information.**

# Quantum Darwinism

- Environment as a witness $\Longrightarrow$ e.g. Photon environment
- Observers eavesdrop on **fragments** of the environment "$\mathcal{F}_m$"
- **Objective:** Quantifying information that can be obtained **from the environment**

$$\mathcal{I}(\mathcal{S}:\mathcal{F}_m) \quad \& \quad D(\mathcal{S}:\check{\mathcal{F}}_m) \quad \& \quad J(\mathcal{S}:\check{\mathcal{F}}_m)$$

**Vs.**

$$\mathcal{I}(\mathcal{S}:\mathcal{F}_m) \quad \& \quad D(\check{\mathcal{S}}:\mathcal{F}_m) \quad \& \quad J(\check{\mathcal{S}}:\mathcal{F}_m)$$

# Quantum Darwinism

- **Big picture:**

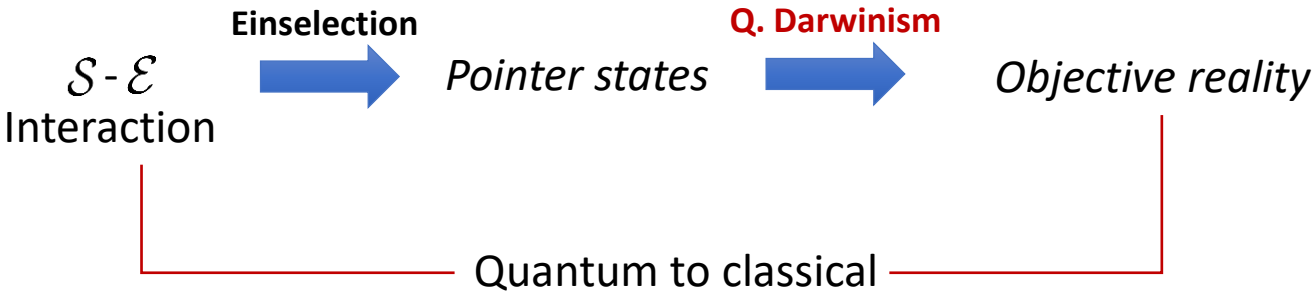


- **Pointer states & einselection:** States robust to decoherence.

- **Objective reality:** Independent observers agree on their measurements.

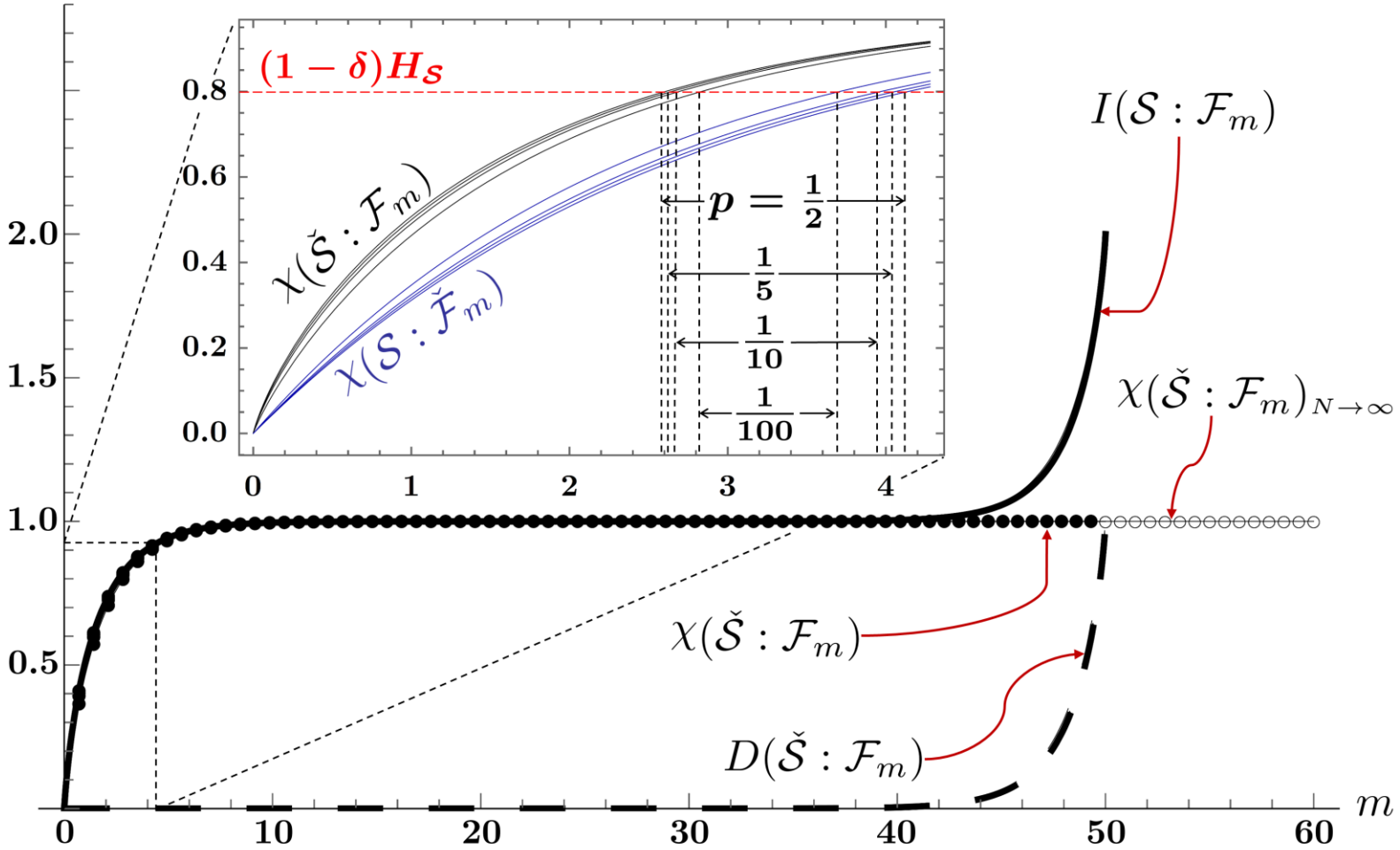


Qubit $\mathcal{S}$ interacting with a many-qubit environment $\mathcal{E}$

# Take-home message

- Quantum mutual information and discord quantify quantum to classical transitions
- Environment as a witness (through the quantities $D(\mathcal{S}:\check{\mathcal{F}}_m)$ and $J(\mathcal{S}:\check{\mathcal{F}}_m)$)
- Universal rise of the mutual information and the Holevo bound

U.S. DEPARTMENT OF ENERGY

Office of Science

Center for Nonlinear Studies

LDRD LABORATORY DIRECTED RESEARCH & DEVELOPMENT

Dr. Bin Yan

Dr. Davide Girolami

Dr. Sebastian Deffner

Dr. Wojciech Zurek

**arXiv:2107.00035** **LA-UR-21-25646**

# Non-adiabatic Dynamics Simulations of Single-Walled Carbon Nanotubes with Topological $sp^3$-hybridization Defects

**Braden M. Weight**, GRA (PhD-track)
University of Rochester, Rochester, NY 14627
Theoretical division (T-1)
Center for Integrated Nanotechnologies (CINT)

August 12, 2021

# Motivation

- SWCNTs are quasi-one-dimensional structures
- Highly tunable diameter ( 0.5 – 2 nm )
- Each chirality is labeled by (n,m) which determine all properties:
  - Diameter (D)
  - Chiral Angle
  - Emission Energy (i.e, $E \sim 1/D^2$)

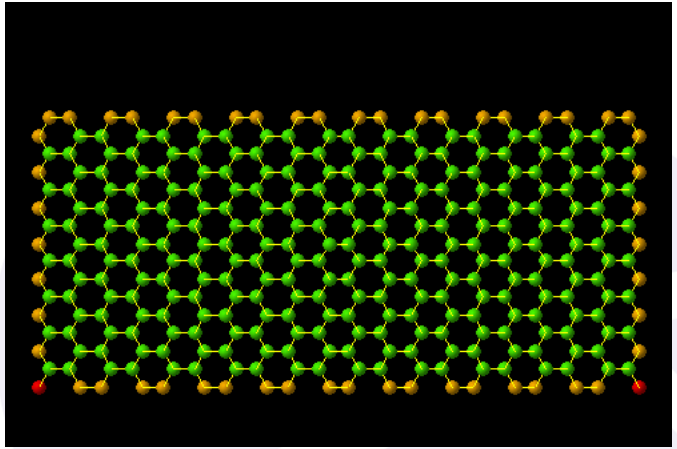

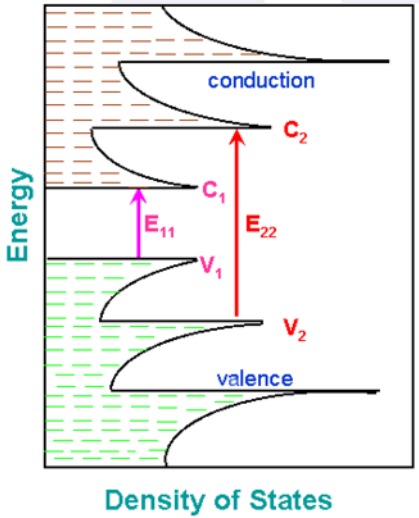


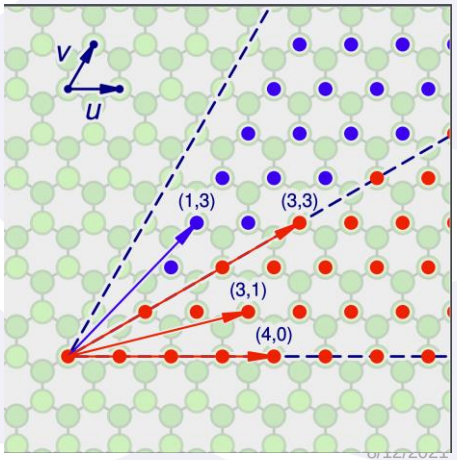

# Motivation

- Pristine SWCNTs exhibit low PL due to symmetry-disallowed low-energy states

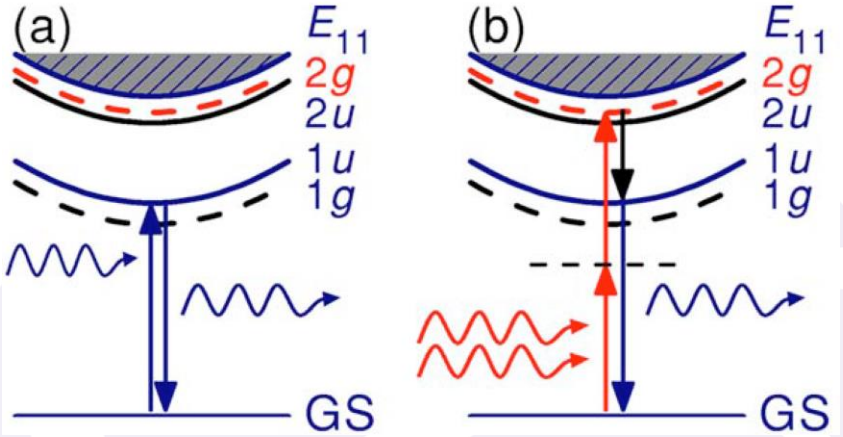


*Phys. Rev. B* 2005, **72**, 241402(R)

# Motivation

- Pristine SWCNTs exhibit low PL due to symmetry-disallowed low-energy states
- Covalent surface functionalization breaks this symmetry and provides new, bright low-energy states
- Configuration and chemical composition of defects can further tune the emission energy of the system by up to 300 meV

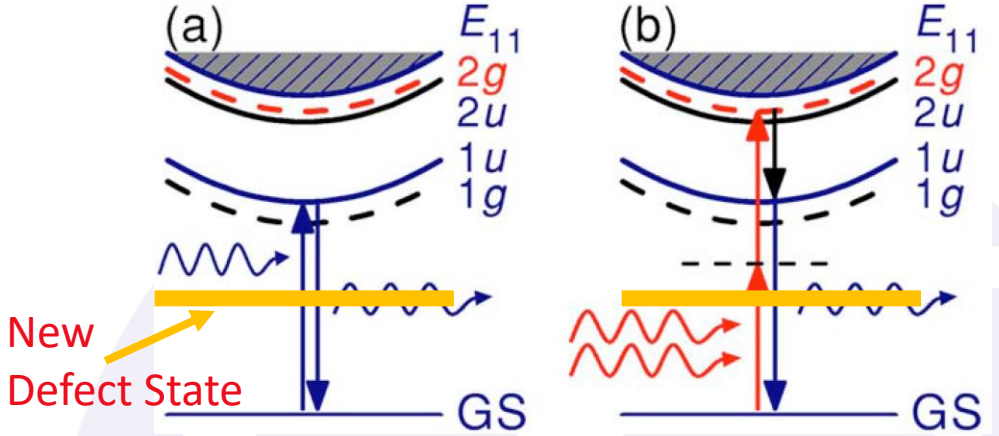


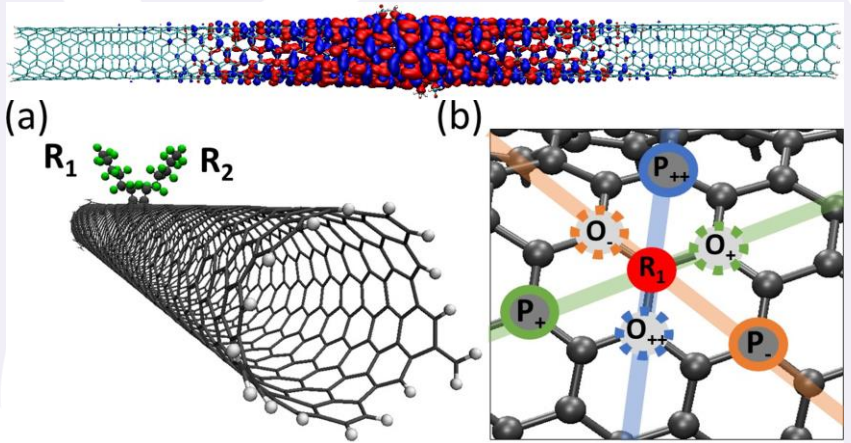




*Phys. Rev. B* 2005, **72**, 241402(R)

# Methodology

- *Hamiltonian:*
  - Semi-empirical AM1
- *Excited States:*
  - RPA Equations in CIS Approximation
  - Solutions for transition density matrices provided by the collective oscillator (CEO) method
- *Non-adiabatic Molecular Dynamics:*
  - NEXMD Package
  - Fewest Switches Surface Hopping (FSSH)
  - Instantaneous Decoherence Corrections
  - Unavoided Crossing Detection
  - Linear Response Solvation
  - Microcanonical Ensemble (NVE)

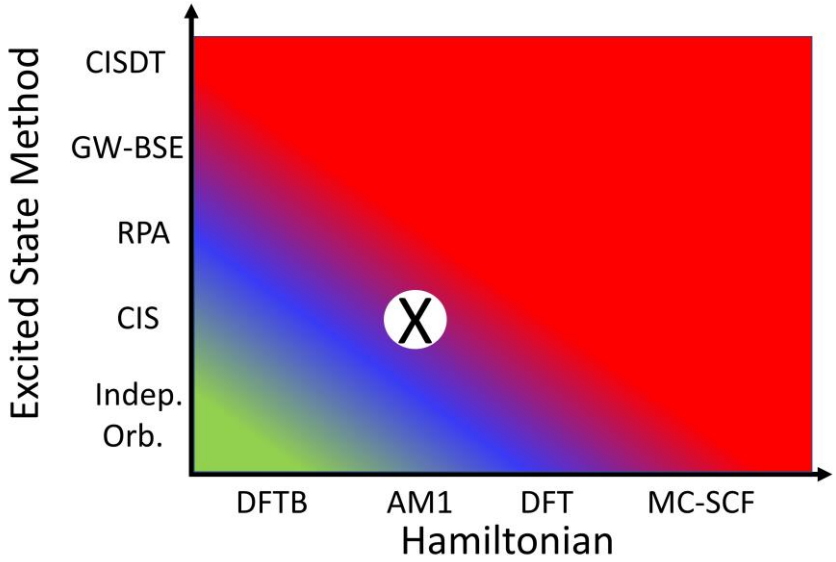


| Chirality | Diameter (nm) | Length (nm) | # Atoms |
|---|---|---|---|
| (6,2) | 0.57 | 2.93 | 236 |
| (11,0) | 0.86 | 2.70 | 354 |
| (6,5) | 0.75 | 3.94 | 394 |

# Initial Conditions

- Nuclear wavepacket sampled from ground state dynamics trajectory
  - NVT Ensemble, T = 300 K
  - 300 trajectories
- Initial Electronic Configuration
  - $\hat{\rho}_{el.} = |k><k|$ , k = 2
- Initial Wavefunction:
  - $\hat{\rho}_o = \hat{\rho}_R \otimes \hat{\rho}_{el.}$

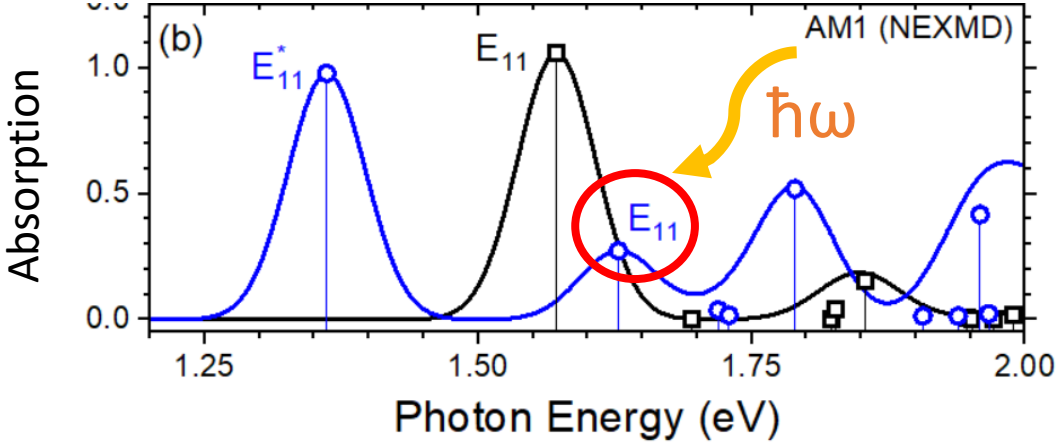


0.0 fs Active State S2

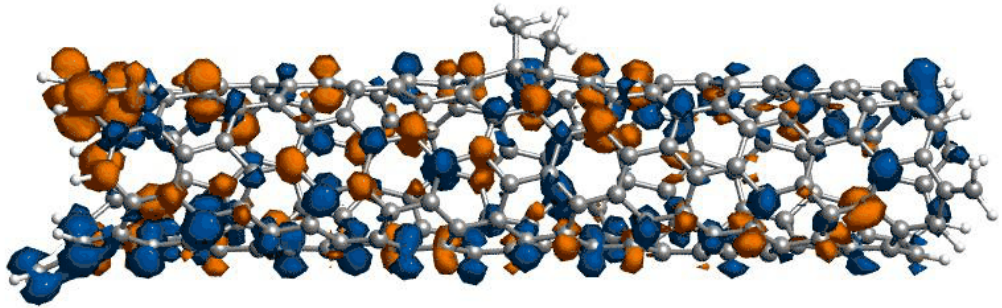

# Population Dynamics (Chirality/Configuration)

$$|\Psi(\mathbf{R}(t))\rangle = \sum_{\alpha} c_{\alpha}(t)|\alpha(\mathbf{R}(t))\rangle$$

$$\dot{c}_j = -ic_jE_j - \sum_k c_k\dot{\vec{R}}\cdot\vec{d}_{jk}$$

$$P_j(t) = \rho_{jj}(t) = |c_j(t)|^2$$

Single-exponential Fit: $S_2(t) \sim \exp[-t/\tau_{12}]$

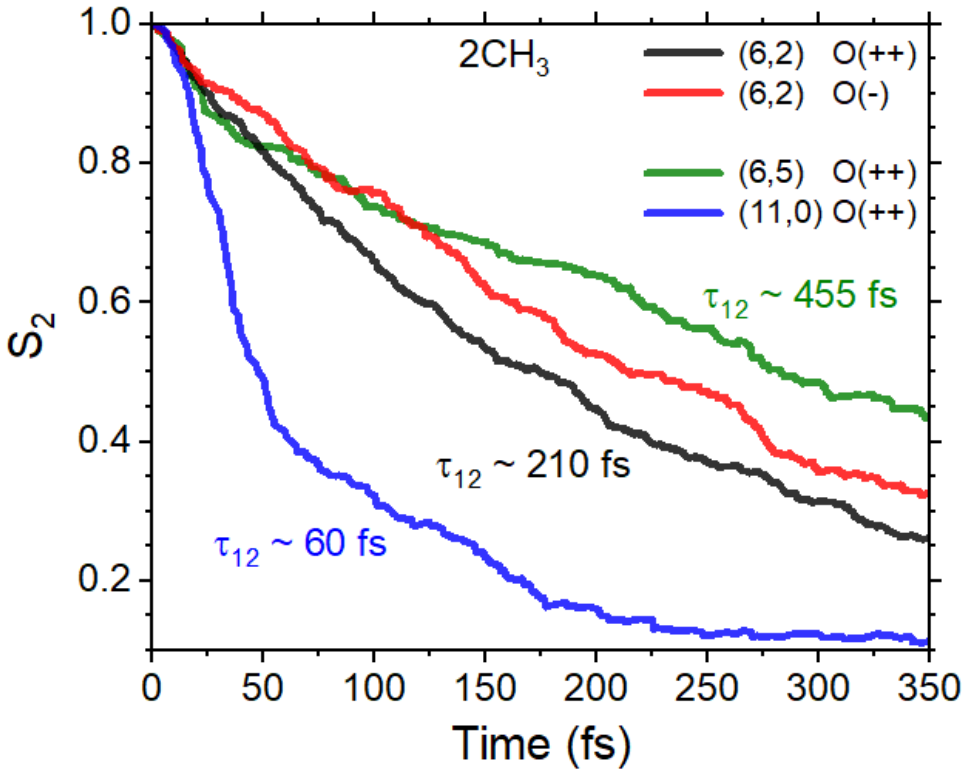


- Population dynamics are strongly chirality-dependent
  - (11,0) shows uniquely fast relaxation

# Population Dynamics (Configuration/Composition)

$$|\Psi(\mathbf{R}(t))\rangle = \sum_{\alpha} c_{\alpha}(t)|\alpha(\mathbf{R}(t))\rangle$$

$$\dot{c}_j = -ic_jE_j - \sum_k c_k\dot{\vec{R}}\cdot\vec{d}_{jk}$$

$$P_j(t) = \rho_{jj}(t) = |c_j(t)|^2$$

Single-exponential Fit: $S_2(t) \sim \exp[-t/\tau_{12}]$

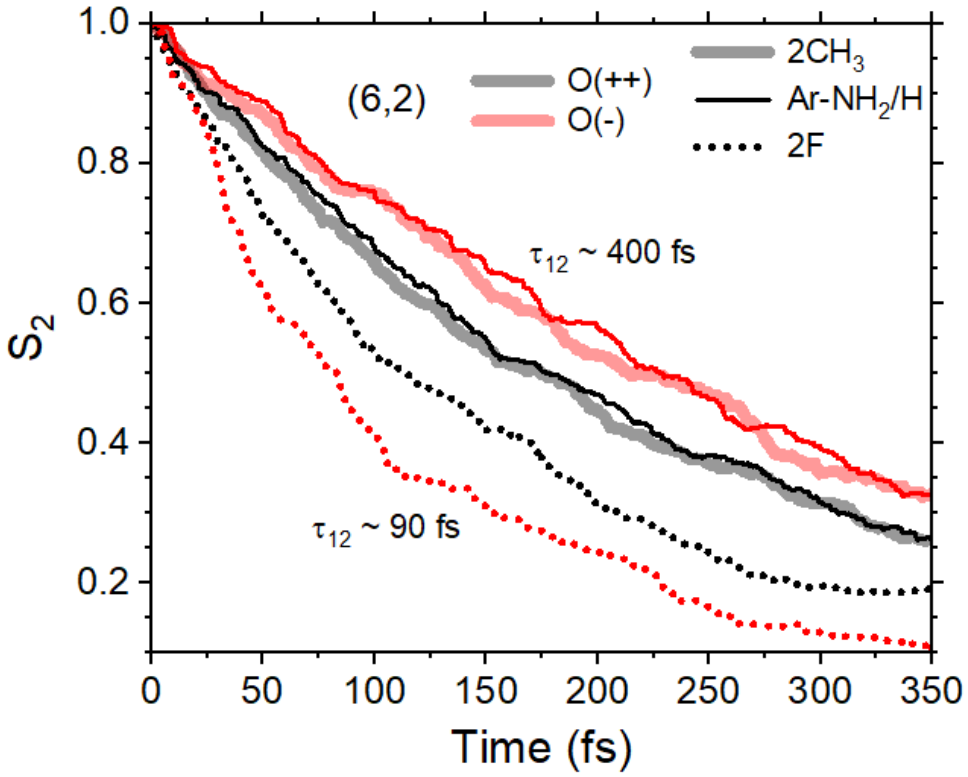


- Population dynamics strongly dependent on chemical composition
  - Alkyl and Aryl defects act similarly
  - Halide attachment produces fast relaxation
  - Ortho(-) coupled with halide produces largest change from alkyl/aryl rate

# Rate of Relaxation

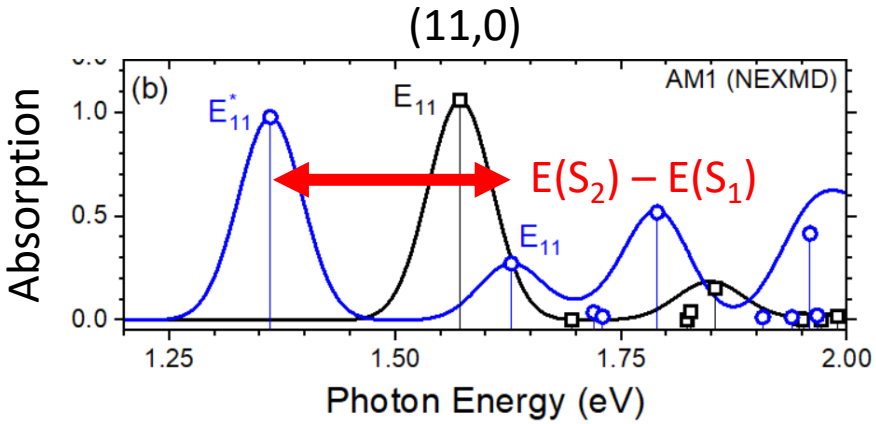


$S_2(t) \sim \exp[ - t/\tau_{12} ]$

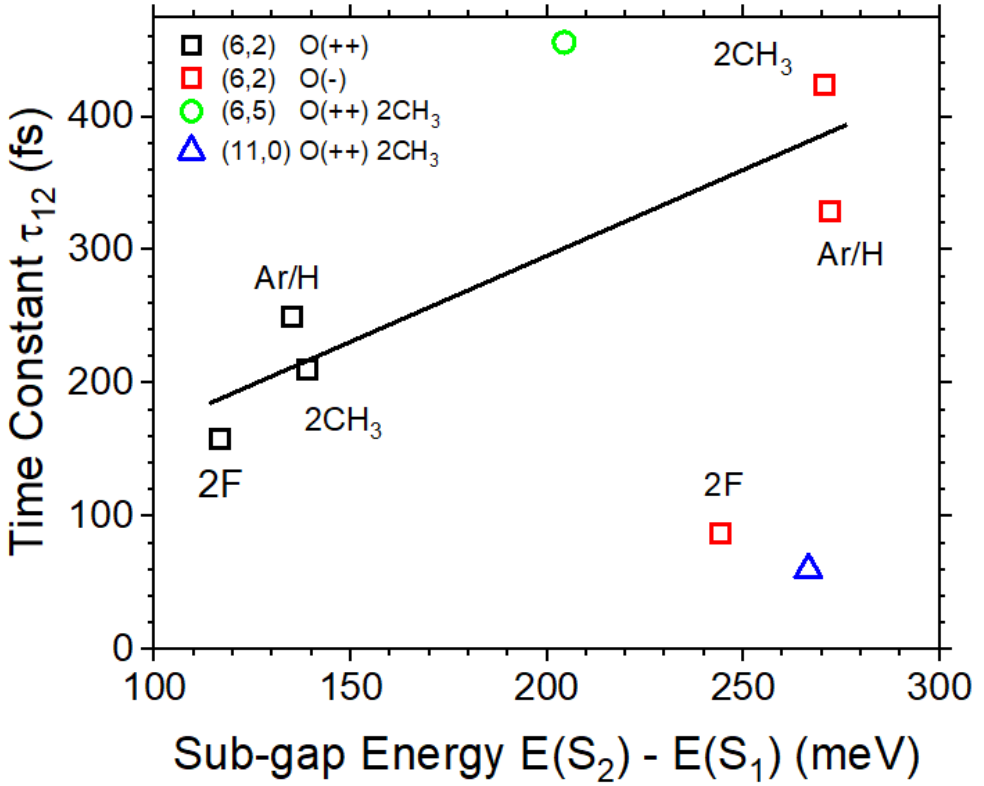


- Time constant ~ $E(S_2) - E(S_1)$ (sub-gap energy)
- (6,2) Ortho(-) 2F shows a strong deviation from this trend
- Chirality-dependent change in time-constant cannot be explained by diameter or chiral angle

# Conclusions and Future Work

- Using a semi-empirical Hamiltonian at the CIS level, we have investigated non-adiabatic molecular dynamics of SWCNT systems of 300+ atoms
- The population dynamics of these model systems are well-approximated by a single exponential function during the simulated time scale
- The gap law is roughly satisfied for alkyl/aryl-type defects
  - Direct halide attachment produces deviations from this hypothesis. Why?
- Chirality-dependent relaxation rates are not well understood and do not stem from diameter or chiral angle

# Acknowledgements


- Sergei Tretiak
- Brendan Gifford
- Andrew Sifain
- Los Alamos National Laboratory (LANL) Directed Research and Development Funds (LDRD)
- LANL Institutional Computing